M.Eng. Chaiyaporn Lothongkam

Dielectric strength behaviour and mechanical properties of transparent insulation materials suitable to optical monitoring of partial discharges

BAM-Dissertationsreihe · Band 120
Berlin 2014

Die vorliegende Arbeit entstand an der BAM Bundesanstalt für Materialforschung und -prüfung.

Impressum

Dielectric strength behaviour and mechanical properties of transparent insulation materials suitable to optical monitoring of partial discharges

2014

Herausgeber:
BAM Bundesanstalt für Materialforschung und -prüfung
Unter den Eichen 87
12205 Berlin
Telefon: +49 30 8104-0
Telefax: +49 30 8112029
E-Mail: info@bam.de
Internet: www.bam.de

Layout: BAM-Referat Z.8

ISSN 1613-4249
ISBN 978-3-9816380-9-7

Dielectric strength behaviour and mechanical properties of transparent insulation materials suitable to optical monitoring of partial discharges

Von der Fakultät für Elektrotechnik und Informatik
der Gottfried Wilhelm Leibniz Universität Hannover
zur Erlangung des akademischen Grades

Doktor-Ingenieur

Dr.-Ing.

von

M. Eng. Chaiyaporn Lothongkam

geboren am 14.05.1972 in Bangkok, Thailand

Promotionsausschuss:

Vorsitzender:	Prof. Dr.-Ing. habil. Lutz Hofmann
Referent:	Prof. Dr.-Ing. Ernst Gockenbach
Korreferent:	Prof. Dr.-Ing. Ronald Plath, TU Berlin
Gutachter:	Dr.-Ing. Wolfgang R. Habel, BAM Berlin (Teilgebiet Mess- und Versuchstechnik)

Tag der wissenschaftlichen Aussprache: 25. Juli 2014

Berlin 2014

D 89

This thesis book is dedicated to the memory of my parents,
my brothers and my sisters,
my teachers,
and my peers.

Dielectric strength behaviour and mechanical properties of transparent insulation materials suitable to optical monitoring of partial discharges

Key words: silicone rubber, dielectric strength, tensile strength, elongation at break, Weibull distribution, dielectric breakdown test, IEC 60243-1, fluorescent silicone rubber

Abstract

A novel optical detection method for partial discharge in HV/EHV cable terminations has been proposed. Optical sensor fibres integrated into the HV equipment provide high sensitivity as well as immunity to electromagnetic interference and enable therefore on-line monitoring in electromagnetically noisy environment. The availability of optically transparent silicone rubbers that meet strict dielectric and mechanical criteria is a crucial prerequisite for the implementation of this method. The optically transparent silicone rubbers can be applied for the fabrication of a modern rubber stress cone as well as for the development of a new optical sensing element sensitive to PD activities. In this thesis, AC dielectric strength behaviour and mechanical properties of three types of commercially available silicone rubbers were investigated. One of the characterized silicone rubbers was a translucent type whereas the two others were optically transparent types, however with different chemical curing reactions.

The measurements of tensile strength and elongation at break were carried out according to the ISO 37 standard. For investigation of the dielectric strength E_b behaviour of the virgin and modified silicone rubbers, a new methodology was developed. It is, at the same time, highly reliable and efficient, saves time and reduces material consumption in comparison to previously reported methodologies. The key component of this methodology is a specifically developed test facility. Furthermore, the methodology comprises determinations for easy preparation and handling of high-quality test specimens. This test method provides various advantages over other methods that have previously been used for measurement of the fundamental quantity E_b value of silicone rubbers. Both technical and economic demands are satisfied. The new facility also enables cost-effective routine tests in material research laboratories. The high quality of the obtained test results was verified by statistical analysis based on the 2-parameter Weibull distribution function.

The investigations revealed that the virgin translucent silicone rubber has a large elastic region with an acceptable plastic deformation and also provides an AC 50 Hz dielectric strength of approximately 24 kV/mm for 0.5 mm thickness. These values enable considering the tested translucent silicone as replacement material for an opaque elastomer that is currently used for a rubber stress cone of HV cable accessories. Unfortunately, its optical transmittance is poor compared to optically clear transparent silicone rubbers. On the other hand, the mechanical properties of virgin transparent silicone rubbers do not comply with those demanded from push-on stress cones. In particular, their elongation at break is considered too low for that application. However they provide the AC dielectric strength values in either 28 kV/mm or 29 kV/mm for 0.5 mm thickness, which are higher than those of the translucent type. Moreover, it was found that the post-curing process does not provide

a positive impact on the ultimate elongation of silicone rubbers. Hence, the elongation at break of virgin transparent silicone rubbers must be improved before they can be used as insulating material for a rubber stress cone. In addition, the influence of mechanical tensile stress on the dielectric strength of the virgin translucent silicone rubber was investigated. The results show that mechanical tensile stress does not negatively influence on dielectric strength of such silicone rubber, so it can be well-operated under combined electrical and mechanical stresses.

Beside the improvement of optical PD detection performance in the translucent silicone insulation materials, the influence of fluorescent dye's modification was investigated. The results indicate that the commercially available fluorescent dyes of 0.02 wt. % mixed into the translucent silicone polymer do not negatively influence on the E_b value of such silicone material. So an optically compatible silicone rubber is perfectly suitable for the fabrication of novel fluorescent silicone optical fibres, which can be integrated into the modified transparent rubber stress cones of HV cable terminations.

The final outcomes of this investigation are experimentally substantiated recommendations for future revision of IEC 60243-1, especially the chapter dealing with the determination of AC dielectric strength of silicone rubbers. Recommendations and suggestions for further investigations are addressed in the final chapter of this thesis.

Dielektrische Festigkeit und mechanische Eigenschaften transparenter Isolierstoffe, tauglich für das optische Monitoring von Teilentladungen

Schlagworte: Silikonelastomer, dielektrische Festigkeit, Reißdehnung, Weibull-Verteilung, Durchschlagtest, IEC 60243-1, fluoreszierendes Silikonelastomer

Kurzfassung

Eine neue Methode zur optischen Detektion von Teilentladungen in Hoch- und Höchstspannungs-Kabelgarnituren wird vorgeschlagen. Optische Fasern, integriert in die Hochspannungseinrichtung, können hochempfindlich messen und sind gegenüber elektromagnetischen Feldern immun. Sie ermöglichen somit ein Online-Monitoring in Bereichen hoher elektromagnetischer Felder. Diese optische Detektionsmethode kann in transparenten Silikonelastomer-Isolierstoffen, die sowohl dielektrische als auch mechanische Anforderungen erfüllen und für moderne Feldsteuerteile zum Einsatz kommen, zur Früherkennung von Teilentladungen genutzt werden.

In dieser Arbeit werden das dielektrische Festigkeitsverhalten und die mechanischen Eigenschaften dreier kommerziell verfügbarer Silikonelastomere unter Wechselspannungsbeanspruchung untersucht. Ein Silikonmaterial war transluzent, zwei andere waren transparent, jedoch mit unterschiedlichen Vernetzungsbedingungen.

Die Messung der Reißdehnung bzw. Zugfestigkeit erfolgte gemäß Standard ISO 37. Zur Untersuchung der dielektrischen Festigkeit E_b der unmodifizierten und modifizierten Silikonelastomere wurde eine neue Untersuchungsmethodik entwickelt. Gegenüber bisherigen Methodiken erlaubt dieses Prüfverfahren Untersuchungen mit geringem Materialverbrauch bei minimalem Zeitaufwand und ist gleichermaßen zuverlässig und effizient. Kernstück dieses Untersuchungsverfahrens ist eine speziell entwickelte Prüfeinrichtung. Darüber hinaus ermöglicht diese Prüfmethode eine einfache Präparation und Handhabung hochwertiger Prüflinge. Diese sowohl technischen als auch ökonomischen Vorteile können bei der Bestimmung des für Silikonelastomere wichtigen Wertes der elektrischen Festigkeit E_b ausgenutzt werden. Wegen der kostensparenden Prüfmethodik kann diese Prüfeinrichtung auch vorteilhaft für statistische Untersuchungen in Laboratorien eingesetzt werden. Die Untersuchungsergebnisse werden mittels Weibull-Verteilung statistisch analysiert und bewertet.

Die Untersuchungen zeigten, dass das transluzente unmodifizierte Silikonelastomer einen großen Elastizitätsbereich mit akzeptabler plastischer Deformation besitzt; für Prüflinge mit einer Dicke von 0,5 mm wurde für 50 Hz Wechselspannung eine dielektrische Festigkeit von annähernd 24 kV/mm gemessen. Diese Festigkeitseigenschaften des transluzenten Silikonelastomers lässt die Schlussfolgerung zu, dass dieses Material die gegenwärtig für Feldsteuerteile in Hochspannungsgarnituren genutzten lichtundurchlässigen Elastomere ersetzen können. Die Lichtdurchlässigkeit des transluzenten Materials ist allerdings gering im Vergleich zu optisch klaren (transparenten) Silikonelastomeren. Andererseits erfüllen die mechanischen Eigenschaften der unmodifizierten transparenten Silikonelastomere nicht die Anforderungen, die an Aufschiebe-Feldsteuerteile gestellt werden; ihre Reißdehnung wird als zu gering eingeschätzt. Sie erreichen jedoch einen Wert

für die Wechselspannungsfestigkeit von 28 kV/mm bzw. 29 kV/mm (0,5 mm Probendicke), der höher ist, als der für den transluzenten Typ. Es wurde des Weiteren herausgefunden, dass ein Nachvernetzen der Silikonelastomere keinen positiven Einfluss auf ihre Reißdehnung hat. Aus diesem Grund muss die Reißdehnung unmodifizierter transparenter Silikonelastomere verbessert werden, bevor sie als Isoliermaterial in Feldsteuerteilen verwendet werden können.

Zusätzlich wurde auch in der Arbeit der Einfluss der Dehnungsbeanspruchung auf die dielektrische Festigkeit unmodifizierter transluzenter Silikonelastomere untersucht. Es konnte gezeigt werden, dass eine Dehnungsbeanspruchung derartiger Silikonelastomere die dielektrische Festigkeit nicht negativ beeinflusst; diese Materialien können somit unter kombinierter mechanischer und elektrischer Beanspruchung eingesetzt werden.

Neben der Verbesserung der optischen Teilentladungsdetektion in transluzenten Silikonelastomer-Isolierstoffen wurde auch der Einfluss ihrer Modifikation mit Fluoreszenzfarbstoffen untersucht. Die Ergebnisse zeigen, dass das Modifizieren transluzenter Silikonpolymere mit 0,02 Gew.-% kommerziell erhältlicher Fluoreszenzfarbstoffe die dielektrische Festigkeit dieser Werkstoffe nicht negativ beeinflusst. Somit eignet sich ein optisch kompatibles Silikonelastomer sehr gut für die Herstellung neuartiger fluoreszierender Silikonfasern, die dann in modifizierte transparente Silikonelastomer-Aufschiebekörper für Hochspannungskabel-Endverschlüsse zum Zwecke der Teilentladungsdetektion integriert werden können.

Im Ergebnis der Untersuchungen können experimentell verifizierte Empfehlungen für die Revision des IEC-Standards 60243-1 gegeben werden, insbesondere für die Bestimmung der Wechselspannungsfestigkeit von Silikonelastomeren. Empfehlungen für weiterzuführende Untersuchungen werden im abschließenden Kapitel dieser Arbeit gegeben.

Acknowledgements

This dissertation work is based on experimental and theoretical work carried out at the Federal Institute for Material Research and Testing (BAM) in collaboration with the Institut "Prüffeld für elektrische Hochleistungstechnik" GmbH (IPH-CESI Group) in Berlin. This research work was conducted under the supervision of Prof. Dr.-Ing. Ernst Gockenbach from Schering-Institut, Leibniz Universität Hannover. It was supported by the PhD research programme of BAM in the time period from 2010 until 2013. I truly appreciate Prof. Dr.-Ing. Thomas Böllinghaus, Vice-President of BAM, for getting this support and for giving me this big chance in my life. My sincere gratitude is also extended to the Mahanakorn University of Technology (MUT), Bangkok, Thailand, for their financial support. I also give my warm thank to the BAM division heads Dr.-Ing. Werner Daum and Dr.-Ing. Katerina Krebber for their great supports to complete my work.

I would like to express my deepest gratitude my supervisor Prof. Dr.-Ing. Ernst Gockenbach for his advice and continuous involvement in this work. Productive discussions and comments received from him have shown me the right way. I wish to express my sincere gratitude to my second supervisor, Prof. Dr.-Ing. Ronald Plath from Technische Universität Berlin, for his useful advice and carefully reviewing this thesis. I would also like to thank Prof. Dr.-Ing. habil. Lutz Hofmann, the chairman of my thesis defense committee, for his carefully reviewing this thesis. I would like to express my sincere gratitude to Dr.-Ing. Wolfgang Habel (BAM) for his support throughout my work as well as his help to improve my skills in writing the thesis. His encouragement has always inspired me with confidence to complete my graduate education.

I also like to express my sincere gratitude to Dr. rer. nat. Gerd Heidmann (IPH) for his suggestions and sincere gratitude is also extended to IPH-CESI Group for providing testing facilities for all experiments in this work. My special thanks go to all staff members of the HV laboratory at IPH in particularly Mrs. Karin Fink and Mrs. Silvia Küchler for all their helps. A number of investigations were supported by Wacker Chemie AG, Germany, which provided sample materials.

I would like to acknowledge the co-authors of my publications for their valuable contributions. I am also grateful to my colleagues at BAM and friends, Dr. rer. nat. Daniel Siebler and Dr. rer. nat. Philipp Rohwetter, and also to Dr. rer. nat. Marek Hoehse (currently at Sartorius Stedim Biotech GmbH) for all the important scientific discussions and encouragements. I include in my thank Mr. Harald Kohlhoff and Miss Jessica Erdmann from BAM for their support with all mechanical works, and finally, I thank all my colleagues at BAM division 8.6 for their collective responsibility and their team spirit. I have learnt a lot during my work at BAM; this experience will be transferred to the students in Thailand.

Last but not least, my sincere gratitude and respect to my parents, my brothers, my sisters, my teachers and my best friends in Thailand for their continuous love and great support during my study far away from my home country.

Berlin, 2014

Table of Contents

1 Introduction……..……..... 1
1.1 Innovative research for PD on-line monitoring in HV cable termination…… 1
1.2 The thesis work motivation…….. 4

2 State-of-the-art silicone rubbers for HV applications…… 7
2.1 Silicone rubber…….. 7
2.1.1 History……..... 7
2.1.2 Products and processing technology for silicone elastomers…….. 8
2.1.3 Chemical structure…….. 10
2.1.4 Curing or cross-linking reaction…….. 10
2.1.5 Fillers……... 13
2.2 General properties of silicone rubbers…….. 15
2.2.1 Physicochemical properties……..... 15
2.2.2 Hydrophobic recovery property…….. 15
2.2.3 Heat and cool resistance…….. 16
2.2.4 Electrical properties……..... 16
2.2.5 Weatherability…… 18
2.2.6 Mechanical properties…… 18
2.2.7 Optical properties……..... 18
2.2.8 Flame Retardancy……..... 18
2.3 Silicone rubbers in medium- and high-voltage applications……..... 19
2.4 Silicone rubbers as power cable insulation……... 21
2.5 Silicone rubbers for optical partial discharge (PD) detection..... 24
2.5.1 The influence of embedded polymeric-optical sensor element into the rubber stress cone of HV cable accessories…….. 25
2.5.2 Fluorescent silicone optical fibre as sensor element……... 27
2.5.3 Modification of siloxane insulation material…….. 28
2.6 Conclusions……... 29

3 Theoretical background…… 31
3.1 Electrical field distribution and breakdown strength of insulating materials……..... 31
3.2 Fields in homogeneous, isotropic materials…….. 34
3.2.1 Coaxial cylindrical fields……..... 35
3.2.2 Sphere-to-plane electrode configuration……..... 36
3.3 Breakdown in solid dielectrics…….. 37
3.3.1 Intrinsic breakdown……..... 39
3.3.2 Streamer breakdown…… 42

Table of Contents

3.3.3 Electromechanical breakdown……..... 42
3.3.4 Edge breakdown and treeing…….. 43
3.3.5 Thermal breakdown……..... 45
3.3.6 Erosion and electrochemical breakdown……..... 49
3.3.7 Tracking……... 52
3.4 Mechanism of electrical degradation and breakdown in polymers……... 53
3.4.1 Low level degradation in polymers……..... 53
3.4.2 Electrical treeing…….. 56
3.4.3 Electroluminescence under electric field……..... 58
3.4.4 Deterministic models of breakdown in polymeric materials……... 60
3.5 Partial discharges……... 63
3.6 Dielectric polarization and permittivity…… 67
3.6.1 Polarization mechanisms……..... 67
3.6.2 Dielectric permittivity……..... 68
3.6.3 Complex permittivity and dielectric loss ($\tan\delta$)……..…….. 70
3.6.4 Factors influencing dielectric properties…… 73

4 Development of the breakdown test facility for silicone rubbers…….. 75
4.1 State-of-the-art review of dielectric breakdown testing methods for silicone rubbers……..... 75
4.2 Steps in test cell construction for dielectric breakdown test of silicone rubbers……... 81
4.2.1 The test cell configuration with five embedded sphere electrodes……. 81
4.2.2 The test cell configuration with single embedded sphere electrode…… 82
4.2.3 Summary……..... 83
4.3 Development of a new efficient methodology to measure dielectric strength of silicone rubbers…… 84
4.4 Conclusions……... 88

5 Experimental details……... 91
5.1 Description of the materials used…….. 91
5.2 Preparation of the test specimen…… 94
5.2.1 A silicone sheet specimen……... 94
5.2.2 A small test cell with embedded sphere electrode…….. 95
5.3 Experimental setup……..... 96
5.3.1 Calibration of partial discharge measuring system……. 98
5.3.2 Method of voltage application……..... 98

Table of Contents

5.4 Methodology for statistical analysis of dielectric breakdown results……... 99
5.4.1 The Weibull distribution for dielectric breakdown data…… 99
5.4.2 Plotting of the Weibull function…….. 101
5.4.3 Plotting the experimental data into the Weibull probability diagram……..... 102
5.4.4 Parameter estimation for the Weibull distributed data……..... 103
5.4.5 Estimation of confidence intervals for the Weibull function…….. 105
5.4.6 Tests with increasing voltage…….. 105

6 Experimental results and discussions……... 107
6.1 Mechanical properties of the optically compatible silicone rubbers……. 107
6.1.1 Mechanical properties of ESA 7250 silicone rubber……... 109
6.1.2 Mechanical properties of LSR 7665 silicone rubber……... 111
6.1.3 Mechanical properties of LSR 3003/30 silicone rubber…….. 113
6.1.4 Discussion and conclusion……..... 115
6.2 Dielectric strength of silicone rubbers……..... 118
6.2.1 The reliability of measurements…….. 118
6.2.2 The dielectric strength value of optically compatible silicone rubbers…..... 121
6.2.3 The influence of specimen thickness on dielectric breakdown measurements……..... 124
6.2.4 The influence of voltage increase rate on breakdown test results of silicone rubber……..... 126
6.3 Dielectric strength behaviour of silicone rubber under mechanical tensile stress…….. 130
6.4 Dielectric strength behaviour of fluorescent silicone rubbers……... 132
6.5 Dielectric strength behaviour of silicone rubber with embedded sphere electrode……..... 135

7 Conclusions……... 139
7.1 A novel methodology for dielectric breakdown test of silicone rubbers…….. 139
7.2 Mechanical properties and dielectric strength behaviour of optically compatible silicone rubbers……... 140
7.2.1 Mechanical properties 140
7.2.2 AC 50 Hz dielectric strength behaviour 141
7.3 Observations 142

References……..... 143

List of publications……. 157

List of Figures

Figure 1.1: Electric field distribution in HV cable termination and the position of highest electric field……. 2

Figure 1.2: The fibre-optic sensor application concept for PD monitoring in high-voltage cable termination……. 4

Figure 2.1: Schematic of the production of silicone elastomers…… 9

Figure 2.2: Products and processing technology for silicone elastomers…….. 9

Figure 2.3: Chemical structure of a linear methy/vinyl siloxane polymer……. 10

Figure 2.4: Curing or cross-linking reaction to form silicone rubbers……... 11

Figure 2.5: Peroxide curing reaction…….. 11

Figure 2.6: Platinum-catalysed addition curing reaction……... 12

Figure 2.7: Layered silicate (LS) nanofillers improve tensile strength and elongation at break in the RTV silicone rubber……. 14

Figure 2.8: Variation of dielectric constant value of polydimethylsiloxanes as a function of degree of polymerization (DP), measured at 1000 Hz and 25 ºC…….. 17

Figure 2.9: Dielectric loss factors (ε_r and $\tan\delta$) of an electronics grade silicone elastomer as a function of frequency and temperature…… 17

Figure 2.10: Dielectric loss factor of silicone rubber filled with fumed silica as a function of temperature compared with several typical silicone rubbers……. 21

Figure 2.11: Dielectric constant ε_r and dielectric loss tangent ($\tan\delta$) at various frequencies for typical silicone rubbers filled with fumed silica for cable insulation…… 22

Figure 2.12: Current carrying capacity of silicone rubber insulated cable is compared with that of conventional thermoplastic insulated cable……. 22

Figure 2.13: Percentage of light transmission compared to the spectrum of PD light emission in the commercially available transparent silicone rubber with a thickness of 10 mm……... 24

Figure 2.14: The stress-cone rubber part of HV cable accessories wrapped with the optical fibre sensor to detect PD activity inside such device……... 25

Figure 2.15: No influence of embedded silicone fibres into the transparent silicone rubber RTV 604 used as insulating material under high electrical stress…… 26

Figure 2.16: Surface tracking on the PMMA fibres caused by PD activities after the embedment of such fibres into the transparent silicone rubber RTV 604….... 26

Figure 2.17: Scheme of the platinum-catalysed cross-coupling reaction of modified vinyl, hydridosiloxanes and respectively of a functionalized fluorescent dye (green sphere) with hydridosiloxanes……... 28

Figure 2.18: Absorption and emission spectra of coumarin modified FlSiOF over the spectrum of PD light emission in transparent silicone rubber……. 28

Figure 2.19: Light transmission in the optically compatible silicone rubbers (a) and influence of SiO_2 nanofillers on percentage of light transmission in transparent silicone rubber (b)……. 29

List of Figures

Figure 3.1: Rod-to-plane electrode configuration with different electric field factor η… 32

Figure 3.2: Breakdown and corona inception voltage for the electrode arrangement of Figure 3.1 in atmospheric air (normal conditions) with d = 10 cm, for positive and negative DC voltage (η see Equation (3.1))…… 33

Figure 3.3: Cross-sections of coaxial cylinders a), and an XLPE coaxial cable b); the electric field varies in the radial direction of the coaxial cable c)……... 35

Figure 3.4: The sphere-to-plane electrode system…….. 36

Figure 3.5: Mechanisms of failure and variation of breakdown strength in solids with time of stressing……... 38

Figure 3.6: Electrode arrangement used for measuring intrinsic breakdown in solids….. 39

Figure 3.7: Schematic energy level diagram for an amorphous…… 40

Figure 3.8: The average rate of energy gain $A(E, T, W_e)$ from an applied field for various field strengths and the average rate of energy loss to lattice $B(W_L, T)$……... 41

Figure 3.9: Rate of energy gain and loss for high temperature intrinsic breakdown model…… 41

Figure 3.10: Breakdown channels in transparent polymer between point-plane electrodes…….. 42

Figure 3.11: Breakdown of solid specimen due to ambient discharge-edge effect…….. 44

Figure 3.12: Breakdown channels in plexiglass between point-plane electrodes. Radius of point = 0.01 in; thickness 0.19 in. Total number of impulses = 190. Number of channels produced = 16; (n) point indicates end of n^{th} channel. Radii of circles increase in units of 10^{-2} in…… 45

Figure 3.13: Thermal stability or instability under different applied fields…… 45

Figure 3.14: Cubical specimen – Heat flow…… 46

Figure 3.15: Arrangement for testing a dielectric for minimum thermal breakdown voltage…….. 48

Figure 3.16: Temperature–time relationship for slow thermal stressing under various applied voltages……... 49

Figure 3.17: Electrical discharge in cavity and its equivalent circuit……... 50

Figure 3.18: Sequence of cavity breakdown under alternating voltages…….. 51

Figure 3.19: Lifetime (t) versus stress relationship of polyethylene medium-voltage cables determined by different manufacturers…… 52

Figure 3.20: Propagation states of electrical treeing until breakdown……. 57

Figure 3.21: Physical ageing model of polymeric insulating materials…… 59

Figure 3.22: Mechanism of EL during each cycle of the AC voltage…….. 60

Figure 3.23: Various partial discharge phenomena…….. 63

Figure 3.24: Mechanisms of dielectric polarization……. 67

List of Figures

Figure 3.25: Dielectric permittivity spectrum over a wide range of frequencies; ε′ and ε″ denote the real and the imaginary part of the permittivity. Various polarization mechanisms are labelled on the image……. 71

Figure 3.26: A capacitor with losses can be represented at any given frequency either by capacitance C_s and resistance R_s in series, or by capacitance C_p and resistance R_p (or conductance G_p) in parallel……. 73

Figure 4.1: Electrode arrangements for tests on silicone sheet perpendicularly to the surface…….. 76

Figure 4.2: Test sample embedded with the equal-diameter opposing cylinder electrodes……. 77

Figure 4.3: Problems with electrodes in dielectric breakdown tests of silicone rubbers 78

Figure 4.4: Various types of the test cells used for the measurement of dielectric strength in silicone rubbers…….. 80

Figure 4.5: The test cell configuration using five embedded sphere electrodes……. 81

Figure 4.6: The test cell configuration with embedded single sphere electrode…… 82

Figure 4.7: Sphere electrode and accessories……. 82

Figure 4.8: Voltage distribution (equi-potential lines) between test electrodes (R-Z plane)…… 83

Figure 4.9: The efficient electrode arrangement to measure the dielectric strength of SiRs…… 84

Figure 4.10: Test arrangement with silicone sheet specimen……... 85

Figure 4.11: The new accessories for breakdown test of elastomeric materials…….. 86

Figure 4.12: Schematic test diagram for investigation of the dielectric strength behaviour of silicone elastomers when loaded in tension……. 86

Figure 4.13: Special tool for loading silicone rubber sheets in tension…… 86

Figure 4.14: A small test cell with embedded sphere electrode for the specific breakdown test…… 87

Figure 4.15: New apparatus for the dielectric breakdown test of silicone rubbers…….. 88

Figure 5.1: Examples of the transparent silicone sheet specimens…….. 94

Figure 5.2: Examples of the translucent and the RTV-2 silicone sheet specimens…… 95

Figure 5.3: Cross-sectional views of the casting mould and the small test cell with embedded sphere electrode…….. 95

Figure 5.4: Test cells with embedded sphere electrodes for specific breakdown test…… 96

Figure 5.5: Experimental setup……... 96

Figure 5.6: Experimental setup in the high-voltage laboratory (CESI-IPH Berlin)……... 97

Figure 5.7: Calibration of PD measuring system before every test…… 98

Figure 5.8: Example of voltage profile with the 60 s step-by-step test procedure…… 98

Figure 5.9: Examples of the two-parameter Weibull distribution functions with $\alpha = 650$ and $\beta = 1$, 2.5, 5 and 30. Note that $\beta = 1$ equals to exponential distribution function……. 101

List of Figures

Figure 6.1: Dimensions of a dumb-bell test pieces Type 2 according to ISO 37:2011….. 108
Figure 6.2: Examples of the transparent silicone test pieces…….. 108
Figure 6.3: Examples of the experimental setup in the testing laboratory of CESI-IPH Berlin…… 108
Figure 6.4: Tensile strength TS_b test results for ESA 7250 silicone rubber under different curing processes…… 109
Figure 6.5: Elongation at break of ESA 7250 under different curing conditions; the error bars represent the 90 % confidence intervals of data for the *i*-th Weibull percentiles…….. 110
Figure 6.6: Tensile strength TS_b test results for LSR 7665 silicone rubber in case of normal- and post-curing conditions……..... 111
Figure 6.7: Elongation at break of LSR 7665 in case of normal- and post-curing conditions……...…….. 112
Figure 6.8: Tensile strength TS_b test results for LSR 3003/30 silicone rubber in case of normal- and post-curing conditions……..…..... 113
Figure 6.9: Elongation at break of LSR 3003/30 in case of normal- and post-curing conditions……...…….. 114
Figure 6.10: Comparison of tensile strength properties of the optically compatible silicone rubbers (ESA 7250, LSR 7665 and LSR 3003/30) and the electrical grade silicone rubber (PowerSil 600)……..... 115
Figure 6.11: Comparison of elongation at break of the transparent types (ESA 7250 and LSR 7665), the translucent type (LSR 3003/30) and the electrical grade (PowerSil 600) silicone rubbers……... 116
Figure 6.12: Experimental evaluation of tensile strength at break for silicone rubbers compared to reference values from silicone producers…… 116
Figure 6.13: Experimental evaluation of elongation at break for silicone rubbers compared to reference values from silicone producers…… 117
Figure 6.14: Stress-strain characteristics of the investigated silicone rubbers……. 117
Figure 6.15: Comparison of the AC 50 Hz dielectric strength values measured from five different silicone sheets made from the same type of silicone rubber……..... 119
Figure 6.16: The results of statistical evaluation of the AC 50 Hz dielectric strength value of LSR 7665 silicone rubber sheet when tested with larger sample size (n = 60)…… 120
Figure 6.17: AC 50 Hz dielectric strength values of the optically compatible silicone rubbers compared to the E_b value of the electrical grade RTV-2 silicone rubber…….. 122
Figure 6.18: Comparison of the dielectric strength values of silicone rubbers evaluated from experimental data and the values given in the data-sheets from silicone producers…….. 123
Figure 6.19: Effect of specimen thickness on AC 50 Hz dielectric breakdown measurements of silicone rubber sheets……... 124

List of Figures

Figure 6.20: Variation of the AC 50 Hz dielectric strength of silicone rubber as a function of the thickness of test specimens in the range of small thickness (less than 1.0 mm)…… 125
Figure 6.21: The influence of voltage increase rate on dielectric strength measurements of silicone rubber…… 127
Figure 6.22: The influences of modes of increasing voltage on AC 50 Hz dielectric strength measurements of the silicone rubber…….. 128
Figure 6.23: AC 50 Hz dielectric strength behaviour of silicone rubber under the influence of mechanical tensile stresses…….. 130
Figure 6.24: Variation of the dielectric strength values and the thicknesses of silicone rubber sheet under the influence of elongation strains…… 131
Figure 6.25: Examples of the fluorescent silicone rubber (FlSiR) sheets with different commercially available dyes by 0.02 wt. %..... 132
Figure 6.26: Examples of the inspected results to see uniformity of fluorescent particles in silicone rubber sheet using 2D digital microscope (1000x); there were no perceivable inhomogeneities…… 133
Figure 6.27: AC 50 Hz dielectric strength behaviour of the fluorescent silicone rubbers with different commercially available dyes by 0.02 wt. %..... 133
Figure 6.28: Influence of fluorescent dye on dielectric strength behaviour of the optically compatible silicone rubber……... 134
Figure 6.29: Statistical evaluations for AC 50 Hz dielectric strength of the virgin LSR 7665 silicone rubber tested with and without embedded sphere electrode….. 136
Figure 6.30: AC 50 Hz dielectric strength behaviour of the ESA 7250, LSR 7665 and LSR 3003/30 silicone samples tested with and without embedded sphere electrode (the thickness of test specimens = 0.5 mm and 60 s step-by-step test)……... 136
Figure 7.1: Definition of breaking point in stress-strain characteristics of the optically compatible silicone rubbers compared to the electrical grade silicone rubber, according to results shown in Figure 6.14……... 141

List of Tables

Table 2.1: Physicochemical characteristics of bond length, bond strength and ionic character between Si − X bonds in silicones and C − X bonds…….. 15
Table 2.2: Silicone rubbers in medium- and high-voltage applications…….. 20
Table 3.1: The specific features of non-conventional PD detection methods……. 65
Table 3.2: Comparison of conventional and non-conventional methods…… 66
Table 4.1: Review of E_b measurement techniques for silicone rubbers……. 79
Table 5.1: The values of some physical properties of the selected silicone rubbers……... 92
Table 5.2: Mechanical properties of the selected silicone rubbers, which are guided by the silicone producers……. 93
Table 5.3: Electrical properties of the selected silicone rubbers, which are guided by the silicone producers……. 93
Table 6.1: Recommended curing conditions for the silicone rubber samples……... 107
Table 6.2: Estimates of the 90 % confidence intervals of the Weibull parameters for tensile strength at break results of ESA 7250 from Figure 6.4…….. 109
Table 6.3: Estimates of the 90 % confidence intervals of the Weibull parameters for the elongation at break results of ESA 7250 from Figure 6.5……. 110
Table 6.4: Estimates of the 90 % confidence intervals of the Weibull parameters for tensile strengths at break results of LSR 7665 from Figure 6.6……. 112
Table 6.5: Estimates of the 90 % confidence intervals of the Weibull parameters for the elongation at break results of LSR 7665 from Figure 6.7…….. 112
Table 6.6: Estimates of the 90 % confidence intervals of Weibull parameters for tensile strength at break results of LSR 3003/30 from Figure 6.8……. 114
Table 6.7: Estimates of the 90 % confidence intervals of Weibull parameters for the elongation at break results of LSR 3003/30 from Figure 6.9……. 114
Table 6.8: Estimates of the 90 % confidence intervals of the Weibull parameters for AC dielectric strength measurements from five silicone sheets as shown in Figure 6.15……. 119
Table 6.9: Estimates of the 90 % confidence intervals of the Weibull parameters for experimental results with larger sample size ($n = 60$) as shown in Figure 6.16……. 121
Table 6.10: Estimates of the 90 % confidence intervals of the Weibull parameters for AC dielectric strength values of the investigated silicone sheets as shown in Figure 6.17……. 121
Table 6.11: Estimates of the 90 % confidence intervals of the Weibull parameters for the distribution functions of the results in Figure 6.19…… 125
Table 6.12: Estimates of the 90 % confidence intervals of the Weibull parameters for the distribution functions of the results in Figure 6.21…… 127
Table 6.13: AC 50 Hz dielectric strength and time to breakdown for the translucent silicone rubber measured with different test procedures……... 129
Table 6.14: Estimates of the 90 % confidence intervals of the Weibull parameters for the distribution functions of the results in Figure 6.23…… 131

List of Tables

Table 6.15: Estimates of the 90 % confidence intervals of the Weibull parameters for the distribution functions of the results in Figure 6.27…… 134
Table 6.16: The estimated Weibull parameters for the E_b test results of the silicone samples with and without embedded sphere electrode…….. 137

Abbreviations and symbols

AC	Alternating current
BD	Breakdown
CV	Continuous vulcanisation
CBM	Condition based maintenance
DC	Direct current
DGA	Dissolved Gas Analysis
ES	Electric strength
EL	Electroluminescence
EM	Electromagnetic
EHV	Extra high-voltage
FlSiR	Fluorescent silicone rubber
FlPOF	Fluorescent plastic optical fibre
FlSiOF	Fluorescent silicone optical fibre
HV	High-voltage
HCR	High consistency rubber
HTV	High temperature vulcanising
I	Ionisation
LV	Low-voltage
LR	Liquid rubber
LDPE	Low density polyethylene
LSR	Liquid silicone rubber
NC	Normal curing
PC	Post curing
PD	Partial discharge
PE	Polyethylene
PVC	Polyvinyl chloride
PDMS	Polydimethyl siloxane
PMMA	Polymethylmethacrylate
PRPD	Phase resolved partial discharge
RTV, RT	Room temperature vulcanising, Room temperature
SiR	Silicone rubber
SD	Standard deviation
TS_b	Tensile strength at break
XLPE	Cross-linked polyethylene
i.e.	id est “that is, in other words”
e.g.	exempli gratia “for example”
et al.	et alii “and others”
etc.	et cetera “and so forth”

Abbreviations and symbols

A	Area, m^2
C	Capacitance, F
C_h	Specific heat capacity of the polymer dielectric, kJ/(kg·K)
C_p	Capacitance in the equivalent parallel circuit, F
C_s	Capacitance in the equivalent series circuit, F
C_v	Thermal capacity of the dielectric material at constant volume, kJ/(kg·K)
d	Thickness of specimen *or* the shortest gap distance between the electrodes
d_0	Initial thickness of the specimen
$d_1 \dots d_n$	Thickness of the dielectric media 1 … n
d_f	Fractal dimension of the electrical tree
$\boldsymbol{D}$	Electric flux density (or electric displacement field) vector
DF	Dissipation factor
$\boldsymbol{E}$	Electric field vector
E_b	Dielectric strength *or* Breakdown field strength
E_c	Critical field strength
E_{max}	Maximum value of electric field
E_{mean}	Mean value of electric field
$\hat{E}_{b,p\,\%}$	Estimated breakdown field strength E_b for the breakdown p-th percentile
ΔE	Electron release energy, eV
f	Electrical frequency, Hz
F_E	Electrically developed compressive stress
F_m	Mechanical compressive stress
$F(x)$	Weibull cumulative probability of failure at the measured variable x
G_p	Conductance in the equivalent parallel circuit, Mho
h	Planck's constant (6.6261×10^{-34} J.s *or* 4.1357×10^{-15} eV.s)
I_g	Energy for ionization of a macromolecule in the gaseous phase, eV
$\boldsymbol{J}$	Current density vector
k	Boltzmann's constant (1.3806×10^{-23} J/K *or* 8.6173×10^{-5} eV/K)
K	Thermal conductivity
L	Electrical tree length, µm
L_b	Unit increment in electrical tree length due to the jointing of a secondary tree. It is approximately equal to the average length of the secondary tree, µm
n	Sample size
n_D	Refractive index
N	Factor which describes the sample size increase
N_d	Number of electric dipoles per unit of volume Δv
$\boldsymbol{p}_t$	Total dipole moment vector
$\boldsymbol{p}_{av}$	Average electric dipole moment vector per polarized entity

Abbreviations and symbols

$\boldsymbol{P}$	Electric polarisation vector
p %	Given probability of failure or the p-th Weibull percentile
P	Energy for polarisation of the polymer by a unit charge, eV
P_i	Calculation of the i-th cumulative probability corresponding to the i-th failure event
Q	Storage charge, C
Q/l	Charge per unit length
r	Value of correlation coefficient
r_1 and r_2	Inner and outer radii of the coaxial cylindrical conductors, respectively
R	Radius of sphere electrode
R_p	Resistance in the equivalent parallel circuit, Ω
R_s	Resistance in the equivalent series circuit, Ω
S_0	Size of the submicroscopic void
t	Time
t_b	Time of breakdown
t_c	Critical time
T	Temperature
T_c	Critical temperature
T_e	Electron temperature
T_L	Lattice temperature
U_0	Activation energy of the breakdown process in physics
U_μ	Intrinsic property of the polymer dielectric
V	Applied voltage
V_b	Breakdown voltage
V_s	Start voltage
V_ws	Withstand voltage
w_i	Weightings for each data point X_i and Y_i
W_e	Energy of the electrons
W_L	Energy loss
W_μ	Barrier energy
X	Number of submicroscopic trees that have formed the electrical tree
X_i	X axis breakdown field strength value for each probability of failure
$\bar{X}$	Weighted average of X_i
Y	Young's modulus of the dielectric
Y_i	Y axis breakdown probability value for each breakdown field strength data
$\bar{Y}$	Weighted average of Y_i

Abbreviations and symbols

α	Weibull scale parameter
$\hat{\alpha}$	Estimated Weibull scale parameter α
α_{m}	Property of the material, which represents the activation area in the direction of the applied electric field
α_{lower}	Lower limit value of the scale parameter α for 90 % confidence intervals
α_{upper}	Upper limit value of the scale parameter α for 90 % confidence intervals
β	Weibull shape parameter
$\hat{\beta}$	Estimated Weibull shape parameter β
β_{lower}	Lower limit value of the shape parameter β for 90 % confidence intervals
β_{upper}	Upper limit value of the shape parameter β for 90 % confidence intervals
γ	Weibull location parameter
δ	Dielectric loss angle
$\tan\delta$	Dielectric loss or dielectric loss factor
ε	Dielectric permittivity ($\varepsilon = \varepsilon_0\varepsilon_{\mathrm{r}}$)
ε_0	Permittivity of free-space (8.854×10^{-12} F/m)
ε_{r}	Relative permittivity of dielectric *or* dielectric constant
$\varepsilon_{\mathrm{r}}'$	Real part of dielectric constant
$\varepsilon_{\mathrm{r}}''$	Imaginary part of dielectric constant
η	Electric field factor
λ	Wavelength, nm
ρ	Density of dielectric
σ	Electrical conductivity
σ_0	Conductivity at ambient temperature
χ	Dielectric susceptibility (dimensionless quantity)
ω	Angular frequency, rad
$\varnothing$	Diameter

1 Introduction

Today's cable manufacturers are able to provide innovative and customized solutions for the modern state-of-the-art power transmission industry. Underground high-voltage (HV) and extra high-voltage (EHV) cables are equipped with new design features, such as real-time monitoring, which make them an effective and reliable alternative to overhead lines. The modern underground power cables are powering a changing world. This is due to their state-of-the-art technology, reliable service performance, lower maintenance costs than overhead lines and least impact on the environment. In fact, power cable systems can fail over time for a number of reasons e.g. external interference or damage, overheating, moisture ingress, poor accessory insulation and incorrect installation, cable or accessory defects, interface problems between its insulation and semiconducting layer. All of them can lead to electrical failure or breakdown of the primary insulation [1-6]. Moreover, during normal operation the polymeric insulation of power cables and their accessories are not only subjected to electrical stresses, but also to other stresses that can cause degradation and ultimately lead to insulation failure [7-9]. Insulation failure caused by partial discharge (PD) is a major cause of cable accessories damage [10-12]. Failure of the insulation system of such components often leads to costly power interruptions to customer disturbances that could be prevented if the actual conditions of the insulation system are known. Due to the great impact of an insulation failure in the service life of HV power cable transmission systems, therefore, PD detection is an important condition monitoring tool for new power cable systems. This is consistent with the concept of CBM (Condition Based Maintenance) [9]. Partial discharges monitoring in power cable systems is the most effective method that is able to monitor long-term aging mechanism of electrical insulations caused by electrical and thermo-mechanical stresses under operating conditions. Therefore, new concepts for modern HV cable terminations and cable joints that contain integrated non-electrical sensors for on-line PD health monitoring are in the focus. They enable assessing insulation deterioration and finally to avoid insulation failures. The alternative methods i.e. optical PD detection with highly sensitive fibre-optic sensors, have a distinct advantage of being immune to electrical interference. It is possible to use them for PD on-line monitoring in such devices.

1.1 Innovative research for PD on-line monitoring in HV cable termination

The interconnecting points between overhead lines and underground cables in power transmission systems need a high-voltage cable termination. With regard to failure rate, cable terminations are the most critical part of power transmission interconnection lines. A defect in insulation system of high-voltage (HV) cable terminations is the major cause of its failure and led to electrical blackout in the past. For example, failures of the 220 kV and 380 kV interconnection lines in Berlin, in January 2008 and in December 2009 respectively, were caused by explosions of the HV outdoor terminations (*source: 50Hertz Transmission GmbH*). The interfaces of the XLPE cable insulation and the silicone rubber (SiR) stress-cone which is susceptible to long-term degradation when subjected to high electric-field stresses are potentially weak points of HV cable terminations. The breakdown of the HV cable terminations is preceded by electrical partial discharge (PD) activity generated in the interfaces. There are many factors that have an influence on interface reliability particularly thermal expansion coefficients of two different materials at the interfaces. Imperfection of interface can be caused by thermal change due to the variation of load current in power transmission system. Moreover, the interfaces in such components frequently run partly parallel to the electrical field. The tangential electric field along the interface increases

proportionately to the increased cable stress. The design of highest tangential electric field stresses in termination is in the range of lower than 1 kV/mm (typically from 0.4 kV/mm to 0.7 kV/mm) depending on surface smoothness. But in case of imperfections at the interface, the tangential electric field may run from 1 kV/mm to 5 kV/mm, which then approximately equals the intrinsic strength of the interface [5, 13-14]. As a rule of thumb, the electrical strength at the interface of two insulating materials is usually weaker than that of each individual bulk insulator. This is the reason that problems arises at interfaces of such components. Obviously, the interfaces need to be handled with care and adverse influences must be suppressed adequately.

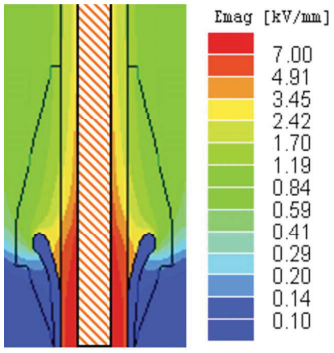

a) Magnitude of electric field distribution (source: Südkabel GmbH)

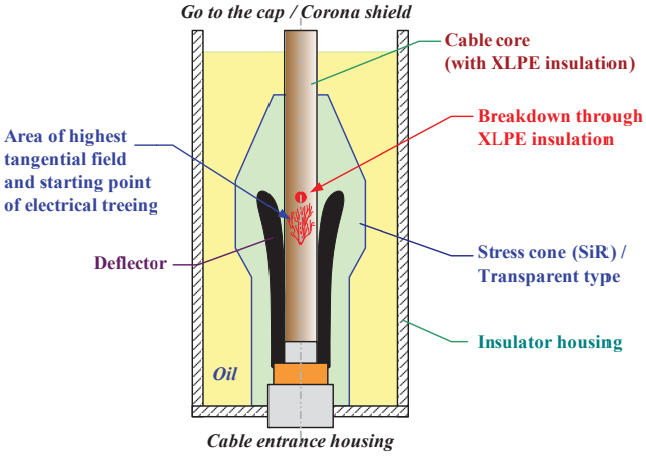

b) Position of highest electric field

Figure 1.1: Electric field distribution in HV cable termination and the position of highest electric field

Figure 1.1 a) shows the magnitude of electric field distributions and the area of the highest electric field in typical high-voltage cable terminations. Electrical trees as shown in Figure 1.1 b) are often found in the interface shortly before its failure. It is noteworthy that the electrical treeing can be started at the interfaces without any direct connection to any of the electrodes. Moreover, high electric fields caused by temporary and transient overvoltages

also excite the electrical treeing mechanism and increase the treeing channels. In fact, the marks of the electrical treeing at the interface in HV cable termination that take place during service in a matter of days or months rather than minutes, a breakdown ultimately follows the discharging activity at the interface [5]. This means, there is enough time to detect arising electrical treeing in such components and could be taken it out of service before breakdown.

As mentioned above, insulation failure in HV cable termination is preceded by discharge activity between the interfaces. This also gives the possibility of pre-breakdown warnings. PD on-line monitoring program must be set up in order to enable timely replacement and prevent outages. In this application field for PD on-line monitoring of HV outdoor cable termination, two main ways are being investigated in the BAM division 8.6:

(i) Detection of the light signals emitted from PD activity as a result of various ionization, excitation and recombination processes, which are caused by the discharges inside the HV cable termination [15-17]. They are detected in optically-clear insulating materials using fluorescent probes and fluorescent optical fibre sensors, which transmit the discharge light signals to the detector. These special signals can be used to switch off the corresponding circuit.

(ii) Detection of occurring acoustic wave signals during growing of PD activity inside cable joints and terminations [15, 17-18]. They can be detected by acousto-optic sensors with interferometric optical method. Acousto-optic sensors have shown high sensitivity and good accuracy for measurement of physical parameters [17]. For the range of ultrasonic frequencies, the acoustic pressure on the fibre is axisymmetric and uniform along the fibre, and hence producing a uniform radial pressure on the fibre. The pressure sensitivity of fibres is governed by elasto-optic coefficients of the glass fibre and the elastic coefficients of the fibre coatings.

Due to the complicated structure of cable accessories, the integration of fibre-optic sensors for PD on-line monitoring needs to be checked. This contribution is mainly focused on new ways and opportunities to enable the early PD detection. The research concept is shown in Figure 1.2. In all these activities, among the development of the appropriate sensor design and the application of the fibre sensing features, the specification of these sensors to be integrated in high-voltage equipment is an important scientific detail.

Optical PD detection with a highly sensitive fibre-optic sensors has a distinct advantage in view of practical applications such as possibility of fabricating small and passive components, high reliability and low cost. The inside into the housing of HV cable termination enables a night vision under low light conditions caused by partial discharges activity. The whole measurement system is galvanically isolated. There is no electromagnetic influence so that the optical PD detection is nearly immune against environmental noise signals. Therefore, it is possible to use the optical sensors for PD on-line monitoring in HV cable termination because there are high noise level and high electromagnetic interference in HV sub-stations. The optical detection of PD activity requires optically clear insulating materials. One of the possible ways to be improvement of high efficient optical PD detection is the modification of the rubber stress-cone part with transparent silicone. The transparent insulation materials enable transmitting light emitted from electrical treeing between the critical interface areas. Therefore, modification of transparent or translucent silicone rubbers is needed. In order to expand the application to higher voltages, the dielectric performance of silicone rubbers, i.e. the electric strength or breakdown field strength E_b and their technical

characteristics, should be investigated. Hence, the objective of this thesis is focused on the investigation of new elastomeric materials based on transparent and translucent types of commercially available silicone rubbers and their possible uses in HV cable accessories.

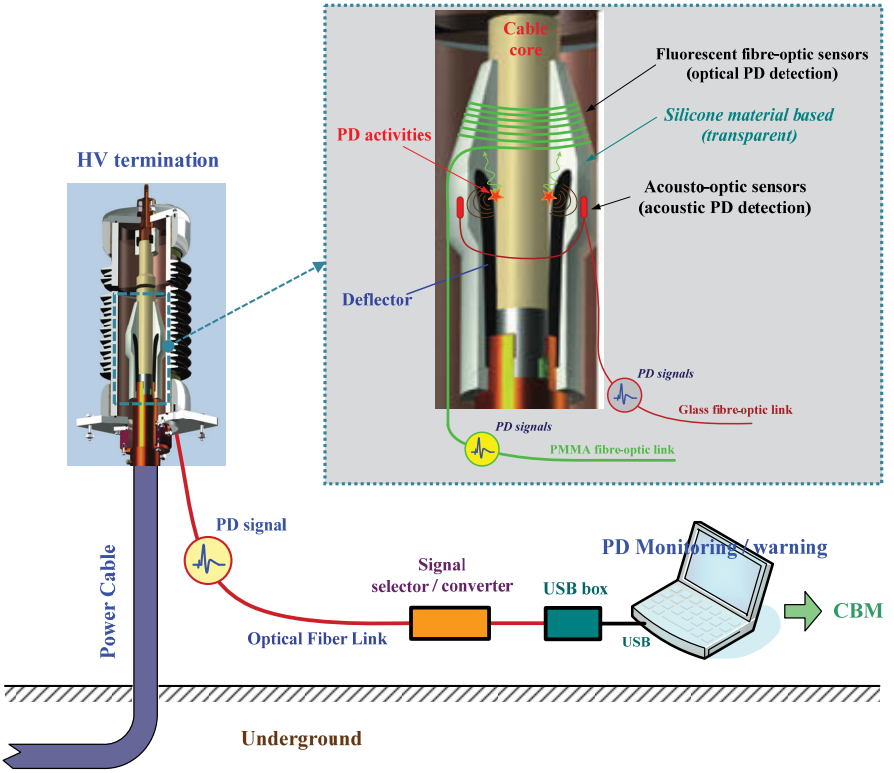

Figure 1.2: The fibre-optic sensor application concept for PD monitoring in high-voltage cable termination

1.2 The thesis work motivation

The use of elastomeric insulating materials for high-voltage (HV) engineering has significantly increased over recent decades. Elastomeric materials, particularly silicone rubbers, are well suited to such applications as the material demonstrates excellent dielectric, thermal, chemical and mechanical resilience whilst remaining economically attractive. It has excellent inherent resistance to degradation when exposed to ultraviolet (UV) radiation. Silicone rubber (SiR) is not a unique material, but consists basically of a base polymer, inorganic fillers and across linking agent. Moreover, in the last years silicone rubber is increasingly used also in cable joints and terminations. The optical detection of PD activity requires optically clear insulating materials. Previous research in the literature [15] showed that silicone fibres offer great potential for PD detection when embedded into the stress cone part of HV cable termination. Electrical stress does not lead to a significant electrical ageing of a silicone rubber. There are two possible ways to improve the efficiency of optical PD

detection. The first method is the development of fluorescent silicone fibre (sensor probe) with high UV absorption and high coupling efficiency of light. The second technique is modification of rubber stress-cone part with the transparent silicone rubbers to make it optically clear and do not impede light emitted from PD sources and transmitted between the critical interface areas. This is the reason why the transparent or translucent types of silicone rubbers need to be modified. Both types of silicone rubbers are commercially available. Unfortunately, they are not designed as an insulating material for HV application. Therefore, electrical properties (i.e. dielectric strength value, volume resistivity, dielectric constant and dissipation factor) as well as mechanical properties (i.e. tensile strength and elongation at break) of the focused silicone rubbers must be investigated.

The dielectric strength values E_b of transparent or translucent silicone rubbers have not yet been investigated with except of special types of silicone rubbers previously presented in literature [19], [20], [21] and [22]. These are the typical products for HV applications but unfortunately not optically clear. Different test set-ups and test methodologies were used, thus, the measured results of dielectric strength show quite different values. In fact, the measured dielectric strength value of elastomeric materials depends on a variety of parameters, e.g. material-related factors (molecular structure, purity, fillers etc.), the geometry of the electrodes, their surface quality and the stressed volume [23]. Therefore, the evaluation of dielectric strength behaviour of the commercially transparent or translucent silicone rubbers is of research interest because the true value for them is not really known. Furthermore, the comparison of E_b value of silicone rubbers before and after modification must be clarified by a standard test method.

However, critical reading of the IEC standard 60243-1 [24] shows that it does not give recommendations for the measurement of dielectric strength value of silicone rubbers. Specific recommendations for moulded thermoset polymers and thermoplastic materials are only provided in sub-clause 4.1.6 of that standard. Due to a lack of specific recommendations for elastomeric materials, often the procedure according to sub-clause 4.1.6 is used for silicone rubbers [22, 25]. This situation strongly motivated the research described in this thesis.

This thesis also deals with the development of a new methodology to measure dielectric strength of elastomeric materials especially silicone rubbers. Results achieved should be useful for the development of a standard test method to determine the dielectric strength property of silicone rubbers. Dielectric strength behaviour and mechanical properties of new elastomeric materials based on transparent and translucent types of commercially available silicone rubbers are described, and their possible uses in HV cable accessories are also presented. Results including evaluation are discussed as well as suggestions for transfer of the results into the cable industry are given.

2 State-of-the-art silicone rubbers for HV applications

Silicone elastomers are widely used in industry and in the field of engineering and scientific applications, for examples: wires and cables (especially heat proof cables), transmission and distribution, electronic industries, automotive applications, food appliance, and mould making. Silicone elastomer differs from other elastomers in its unparalleled property range. Of particular interest are the characteristics resulting not from additives or surface treatment but from the polymer and filler structure. These are inherent properties of silicone polymer. Silicone rubber is generally non-reactive, resistant to extreme environments and while still maintaining its useful properties, high thermal stability, biocompatibility, hydrophobic nature and a good balance of electrical and release properties. When silicones are cross-linked to form a silicone rubber their characteristic properties are still prevalent. Siloxane polymer is normally transparent material and therefore, they can be used for optical applications, i.e. optical sensor and sensing element for HV applications.

This chapter deals with the state-of-the-art in silicone rubbers for HV applications. The chemical structure of silicone and its desirable features regarding electrical engineering aspects are briefly addressed.

2.1 Silicone rubber

Silicone rubbers are often one- or two-part polymers which generally contain only three additional substances, i.e. crosslinker, fillers and additives. During manufacture, heat may be required to vulcanise (or cure) the silicone into its rubber-like form. This is normally carried out in a two stage process at the point of manufacture into the desired shape, and then in a prolonged post curing process. Silicone rubber can be processed in a variety of ways. The main processes include extrusion, compression moulding and injection moulding. The property of silicone rubber is mostly stable over a wide temperature range. Silicone rubber has relatively high bond dissociation energy; especially the high binding energy of the silicon-oxygen bond it the reason for its high chemical stability even at high temperatures. Currently due to its great features, silicone rubber is used for electrical insulating materials in medium- and high-voltage applications, wherever high operational safety and long service lives are required. Knowledge of dielectric properties from these materials thus becomes important for future equipment designs.

2.1.1 History

The first silicone elastomers were developed as better insulating materials for electric motors and generators. Resin-impregnated glass fibers were the state-of-the-art materials at this time. The glass was very heat resistant, but the phenolic resins would not withstand the higher temperatures that were being encountered in new smaller electric motors. Chemists at Corning Glass Works (Corning Incorporated) and General Electric were investigating heat-resistant materials for use as resinous binders when they synthesized the first silicone polymers, demonstrated that they worked well and found a route to produce polydimethylsiloxane commercially.

Corning Glass in a joint venture with Dow Chemical formed Dow Corning in 1943 to produce this new class of materials [26]. The first product was manufactured in 1944 [27]. As the unique properties of the new silicone products were studied in more detail, their potential

for broader usage was envisioned, and GE opened its own plant to produce silicones in 1947. Wacker Chemie [28] also started the production of silicones in Europe in 1947. The Japanese company Shin-Etsu Chemical [29] began mass production of silicone in 1953. The companies mentioned above are now still the silicone market.

2.1.2 Products and processing technology for silicone elastomers

The nomenclature classifies silicone elastomers by their curing mechanism and curing conditions. Silicone rubbers are essentially divided into two groups of materials, i.e. room temperature vulcanising (RTV) and high temperature vulcanising (HTV) silicones. RTV systems are able to cure at room temperature (RT) and HTV systems at temperatures above 100 °C. A number in the name indicates the number of components that upon mixing will form a curable composition, e.g. RTV-2. HTV rubbers mainly have very high viscosity in the uncured state and appear as solids. This behaviour has also led to the creation of the term 'High Consistency Rubber (HCR)'.

Approximately 37 years ago a new group of materials appeared that was intended for processing in injection moulding machines. Because of their low viscosity and paste-like behaviour they were named 'liquid silicone rubbers (LSR)' or simply liquid rubbers (LR). The abbreviation LSR or LR are commonly used instead of HTV. However, they can be cured at high temperatures same as in the case of solid silicone rubbers.

Normally LSR materials consist of 2 components which cure after mixing and at elevated temperatures. In summary the silicone industry uses the terms RTV-1, RTV-2, LSR or LR, HTV or HCR. These refer to the material categories as follows:

- RTV-1; Room temperature vulcanising with one component,
- RTV-2; Room temperature vulcanising with two components,
- HTV; High temperature vulcanising (both liquid or solid silicone rubber),
- HCR; High consistency rubber, one component solid silicone rubber, and
- LR or LSR; Liquid rubber, liquid silicone rubber (which is also cured at high temperatures).

Among all silicone elastomers, LSR exhibits the highest growth rate and HTV solid silicone rubbers have the highest portion of the global market especially in the electrical power industry, i.e. HV insulators.

In most cases RTV systems are cured by a condensation reaction. The curable composition is formed by two-component mixing, while in the case of one component systems (RTV-1) it will cure after its application out of the packaging. The major part of the curing system is a polydimethyl siloxane (PDMS) polymer with terminal hydroxyl groups and reinforcing filler. As additives it contains a crosslinker, usually a functional silane, and a catalyst, in many cases a tin complex [30].

The curing systems are classified by the chemical nature of the split products formed during the condensation process, when the functional silane is incorporated into the polymer network splitting off the condensation products. Such systems cure in the presence of air moisture. As they form split products during their cure, such materials exhibit shrinkage with increasing degree of curing.

The complex chemistry and versatile properties of silicones are built on sand, as shown in Figure 2.1. A schematic overview of the processing and product groups for silicone elastomers are shown in Figure 2.2.

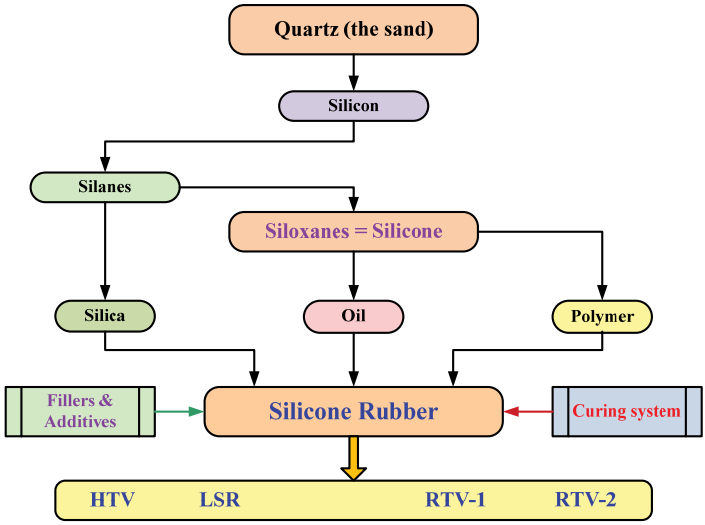

Figure 2.1: Schematic of the production of silicone elastomers [30]

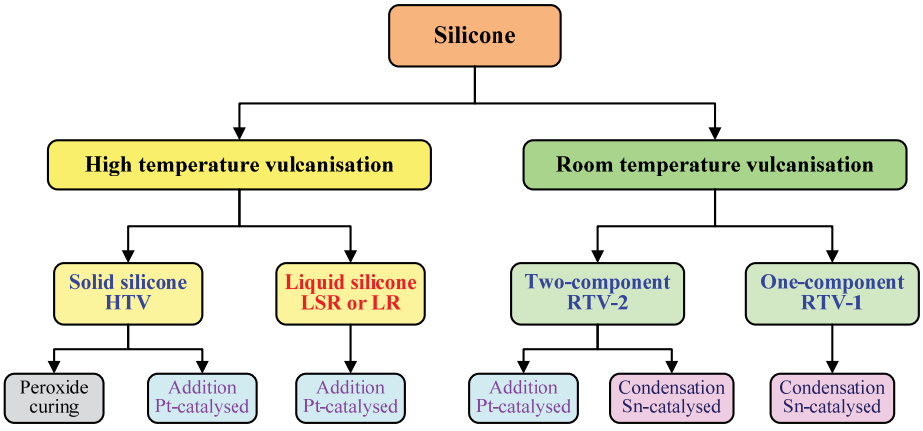

Figure 2.2: Products and processing technology for silicone elastomers [30]

2.1.3 Chemical structure

In fact, silicone is an inorganic polymer, and the technically correct term for the various silicone rubbers is polysiloxanes or polydimethylsiloxanes. Silicones, by contrast, are "semiorganic materials". Silicones have a similar structure to organically modified quartz. They consist of a backbone comprising alternating silicon (Si) and oxygen (O) atoms. The high binding energy of the silicon-oxygen backbone gives silicones a high chemical stability.

The chemical structure of a polydimethylsiloxane (PDMS) is

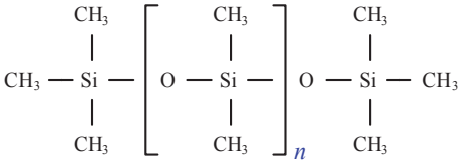

If n is several thousand, highly viscous fluids of siloxane gum like consistency are obtained, which are suitable for making silicone rubbers. The chemical structure of a linear silicone polymer is shown in Figure 2.3 [28].

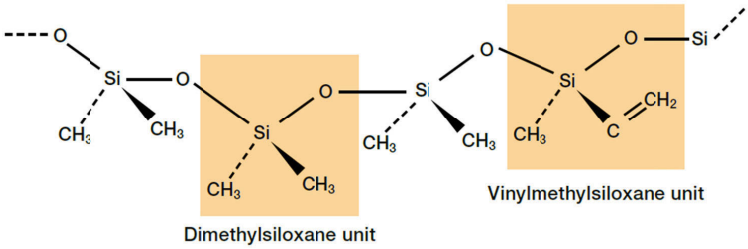

Figure 2.3: Chemical structure of a linear methy/vinyl siloxane polymer [28]

Silicone polymer formulations consist essentially of an intimate mixture of a siloxane gum, fillers, crosslinkers and additives. Fillers are used to reinforce the elastic silicone network. A crosslinker is required to convert the raw rubber into an elastomeric material. Silicone rubber requires few additives because the essential properties are determined by the siloxane polymer used.

2.1.4 Curing or cross-linking reaction

To become an elastomeric material, raw silicone rubber has to be cured. This can be done either by peroxide or addition curing. They decompose to form highly reactive radicals which chemically crosslink the polymer chains as shown in Figure 2.4 [28]. The result is a highly elastic, three-dimensional network.

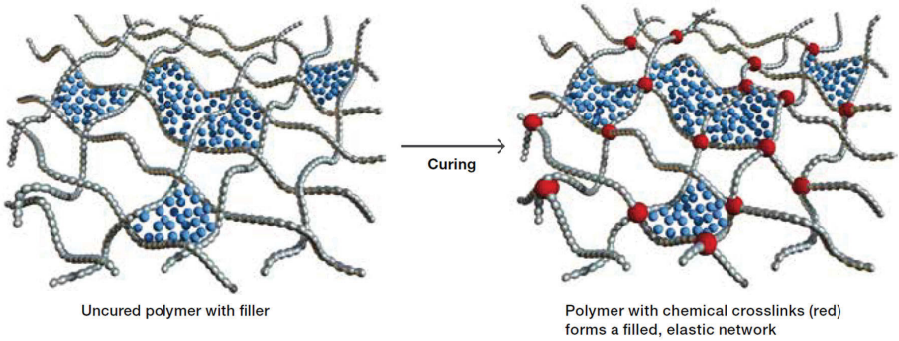

Figure 2.4: Curing or cross-linking reaction to form silicone rubbers [28]

a) Heat-curing process

When a methy/vinyl siloxane gum is heated with a curing agent (e.g. benzoyl peroxide), cross-linking occurs between siloxane polymer chains, principally by the formation of ethylene bridges [27]:

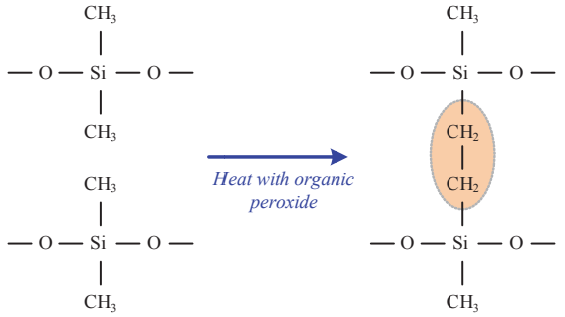

Peroxide curing is a time-tested and technically mature process. This curing technique involves the use of organic peroxides. Generally, the peroxide crosslinkers are offered in paste or powder form. At elevated temperatures, they decompose to form highly reactive radicals which chemically crosslink the polymer chains.

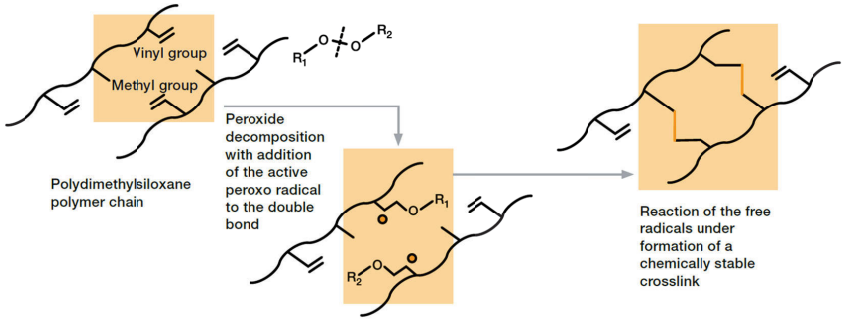

Figure 2.5: Peroxide curing reaction [28]

Improved curing characteristics can be obtained if some of the methyl groups ($-CH_3$) are replaced by vinyl groups ($-CH=CH_2$), which are more chemically reactive, and, when cured with peroxide catalyst, give vinyl-vinyl or vinyl-methyl linkages, as shown in Figure 2.5. The inclusion of vinyl groups reduces compression set of the cured silicone rubber, and enables thick sections to be cured without gaseous-void formation, since peroxide concentrations and hence volatile by-products can be reduced.

Associated with these, the platinum-catalysed addition curing can be used. Unlike peroxide-curing, they have many advantages such as fast curing process and the curing speed can be controlled via temperature. During platinum-catalysed addition curing, the crosslinker's Si – H groups react with the vinyl groups of the polymer to form a three-dimensional network, as shown in Figure 2.6. It is important to note that Platinum-catalysed grades may start crosslinking even at room temperature; therefore it is important to avoid exceeding the shelf life.

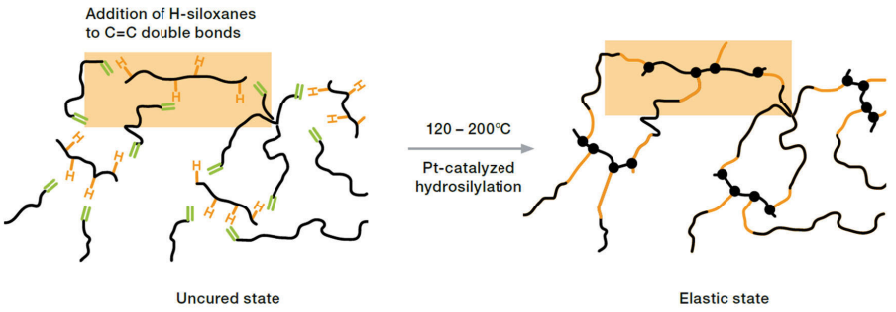

Figure 2.6: Platinum-catalysed addition curing reaction [28]

b) Room temperature curing process

This basic curing process is a condensation reaction between hydroxyl groups ($-OH$) and alkoxy groups ($-RO$) attached to silicon atoms of siloxane chains, under the influence of a catalyst such as an organometallic compound (e.g. Pt or Sn). The typical reaction is shown below [27].

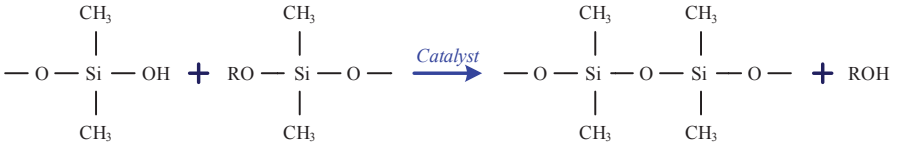

Since this reaction takes place in a relatively short time (about 1 h), materials of this sort are normally made and supplied in two parts, which when stored separately are quite stable, but on mixing react to form elastomers. In some cases, this mixing process is inconvenient and therefore the single-component silicone rubbers have been developed [28-29]. They are stable in the absence of air, but, on exposure to the atmosphere, react with moisture and set at room temperature to form elastomers. These are usually made by replacing the hydroxyl group with the acetoxy group ($-OCOCH_3$), which is stable in the presence of an organometallic catalyst already incorporated in the elastomer [27]. On exposure to atmospheric moisture, the acetoxy group is liberated, leaving a hydroxy group,

which then reacts by the normal cold-curing silicone-rubber mechanism described above. This type of chemical reaction is shown below [27].

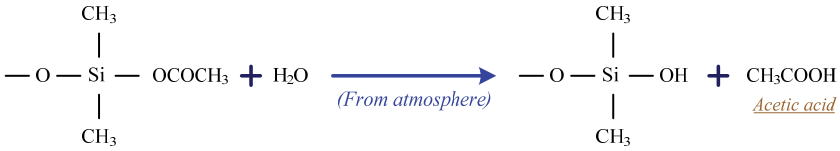

c) UV-cure silicone rubber

New UV-cure technology offers the possibility to produce parts and combinations that were previously difficult to manufacture, since heat curing processes limit the use of temperature sensitive ingredients. And, this technology can help save energy. UV-cure silicone rubber belongs to a new class of rubber that offers high cure speed at low temperatures. UV light initiates cross-linking through a photochemical reaction. The rubber can be processed via injection moulding with special moulds or via extrusion without additional heat cure.

2.1.5 Fillers

The high and reversible deformability of elastomers is of great industrial importance. Typically however, the initial modulus and durability of pure silicone are low, and an additional reinforcing phase is required for practical use. For commercially available silicone rubbers, similar amounts of fillers are used in general. All silicone elastomers typically contain filler content up to 40 %. The bulk of this is fumed silica with surface areas between 150 m^2/g and 300 m^2/g. Fillers are normally responsible for better mechanical and flow properties [30].

The final properties of silicone rubbers are dependent on the type and amount of fillers compounded into the polymer. Various types of fillers in silicone rubber have been investigated for outdoor HV insulation applications [31-39]. The most common fillers used for improvement in mechanical and electrical properties are listed and discussed in [40]. The filler used in the first commercial compounds was titanium dioxide (TiO_2). These rubbers had fair physical and electrical properties but their electrical properties were adversely affected by moisture [41]. Silicon dioxide fillers were the next to receive attention because they are less affected by water. Silicone rubbers compounded with silica in the form of diatomaceous earth have been used in large quantities. These rubbers are characterized by excellent handling properties, fair physical and good electrical properties. In general, they can be extruded in conventional rubber extruders at rates comparable to those obtained with organic rubbers.

Over the past 19 years, polymer nanocomposites revealed a great important idea of the polymer/nanofiller interface [42]. Polymer nanocomposites present a series of unique properties, such as electrics [43-45], mechanics [46-47] and optics [48], due to nanoparticles with a giant specific surface area, quantum size effect and the special interface between particles and polymer matrix. In contrast to conventional filled polymers, nanocomposites are composed of nanometer-sized fillers (nanofillers) which can be homogeneously dispersed within the polymer matrix. The extent of property improvement depends on filler concentration, filler morphology, such as particle size and structure, the degree of dispersion and orientation in the matrix, and also the degree of adhesion with the polymer chains. To

improve particle dispersion, several techniques other than mixing are listed and discussed in [49-50]. This includes the surface modification of the micro/nanoparticles (micro/nanofillers) by physical and chemical methods using surfactants. The chemical nature of the surface of nanofillers is important, and various chemical treatments have been developed, resulting in greatly improved properties of silicone rubbers [28-29].

Some improvement in the mechanical properties is given by certain types of filler, including fumed silica, ground silica, silicon dioxide (SiO_2), titanium dioxide (TiO_2), carbon nanotubes, calcium carbonate ($CaCO_3$), and alumina tri-hydrate ($Al(OH)_3$) [27, 40, 51]. However, for commercially HTV and LSR silicone rubbers, reinforcing fillers are fumed silica. Ground silica has only slight reinforcing properties, but, if silica is prepared by a chemical process, such as burning silicon tetrachloride ($SiCl_4$), which yields silica in the form of finely divided particles of very large surface area, much greater reinforcement is possible. Apart from that, the recent research reported by Dangke *et al*. [31] reveals that layered silicate (LS) nanotechnique provides good improvement in tensile strength and elongation at break in the RTV silicone rubber for outdoor insulators. These results are shown in Figure 2.7.

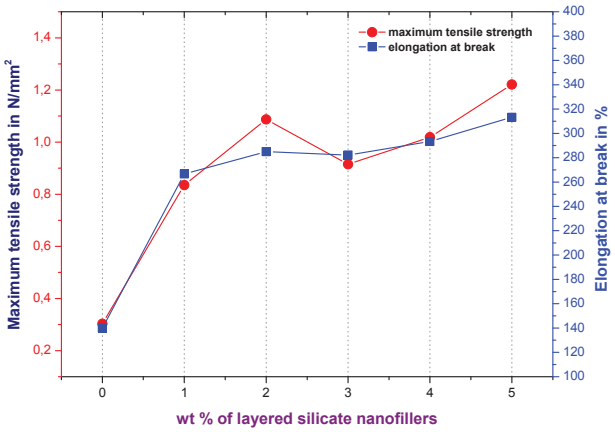

Figure 2.7: Layered silicate (LS) nanofillers improve tensile strength and elongation at break in the RTV silicone rubber [31]

Electrical properties may also be modified by the addition of fillers; for example, permittivity can be increased by the addition of several types of fillers, e.g. silicon carbide (SiC), titanium dioxide (TiO_2), zinc oxide (ZnO), barium titanate ($BaTiO_3$) [40, 52-53]. This type of silicone rubbers is usually used as stress grading materials for cable terminations. Electrical conductivity can be enhanced by the addition of carbon-black particles or carbon nanotubes or graphite or zinc oxide filler as well as metallic powders [40]. Aluminiumoxide (Al_2O_3), alumina tri-hydrate (ATH) and silica based fillers (i.e. silicon dioxide and fumed silica) are typically used for improvement in erosion and anti-tracking for outdoor HV insulators [32-34, 36-38, 40]. Dielectric strength E_b of silicone rubbers may be improved by the addition of alumina or silica fillers [50, 52].

The improvement in physical properties can also be obtained by the addition of fillers; for example, aluminiumoxide and silicon dioxide fillers can improve thermal conductivity. Hydrophobicity and flame-retarding can get better by adding calcium carbonate fillers [40].

There are other fillers, so-called "*inactive fillers*". Inactive fillers do not reinforce the elastic silicone network. They are widely used in order to improve certain chemical or thermal properties. Examples of such fillers are ground quartz, diatomaceous earth and chalk. Too high levels of such inactive fillers result in the loss of the excellent mechanical properties of most silicone elastomers. Of course, a high degree of filling results in very high densities and thus a high weight per part. Their specific properties related to desired features in electrical engineering aspects are briefly addressed as follows [27, 30, 40].

2.2 General properties of silicone rubbers

Special features of silicone runners are originated from its unique molecular structure that they carry both inorganic and organic properties unlike other organic rubbers. The following is a summary of general properties of silicone rubbers.

2.2.1 Physicochemical properties

Silicones have a similar structure to organically modified quartz. They consist of the backbone comprising alternating silicon and oxygen atoms. The high binding energy of the siliconoxygen backbone ($Si-O-Si-O$) gives silicones a high inorganic stability. The physicochemical characteristics of bond length, bond strength and ionic character between $Si-X$ bonds in silicones and $C-X$ bonds are shown in Table 2.1. It shows that siloxane bond ($Si-O$) has greater capacity and stability. As a result, silicone rubber has better heat resistance and chemical stability than any other ordinary organic rubbers. Siloxane bond's energetic stability is secured due to sharp difference in terms of electro-negativity between Si (1.9) and O (3.44) making $Si-O$ to be closest to ionic bond. Hence, silicones are more stable than polymers with a carbon ($C-C$) backbone, for example Ethylene-Propylene Diene Monomer (EPDM) rubber.

Table 2.1: Physicochemical characteristics of bond length, bond strength and ionic character between Si - *X* bonds in silicones and C - *X* bonds [54-56]

Element *X*	Bond length in Å		Bond strength in kJ/mol		Ionic character in %	
	$Si-X$	$C-X$	$Si-X$	$C-X$	$Si-X$	$C-X$
C	1.88	1.54	240-340	346	12	-
H	1.47	1.07	318	411	2	4
O	1.63	1.42	452	358	50	22
Si	2.34	1.88	222	240-340	-	12

The bond energy of $C-C$ is 346 kJ/mol, as opposed to 452 kJ/mol for $Si-O$. Shortwave sunlight (300 nm) has an energy content of about 6.2×10^{-22} kJ (app. 398 kJ/mol) and can therefore cleave $C-C$ bonds, whereas the $Si-O$ bond remains stable. Thus, silicone rubbers are not prone to chalking or cracking caused by UV radiation from sunlight. This is a desired feature for outdoor HV insulators in electrical power transmission systems.

2.2.2 Hydrophobic recovery property

Compared to other materials, silicones show very good water repellency, also known as hydrophobic surface. With its coil shaped spiral structure and low intermolecular force, silicone rubber has outstanding water repellency and contact resistance. As methyl groups CH_3 are located in the outside of coil spiral structure, they are free to rotate on its own. In the

case of PDMS the Pauling electronegativity index difference of 1.81 between silicon and oxygen atoms confers a 50 % polar or ionic character on the siloxane bond. Its consequent sensitivity to hydrolysis at extremes of pH is the most significant difference between silicones and organic polymers [57]. The reaction between water and siloxane is shown below.

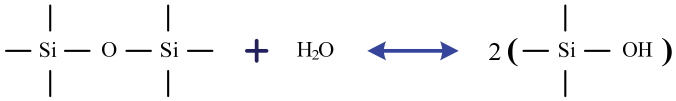

This is an equilibrium that results in a redistribution of siloxane linkages known as the equilibration of siloxanes. Normally, the water-insoluble nature of PDMS keeps this equilibrium well to the left by mass action effects. The hydrophobic recovery property may be attributed at least in part to the transfer of low molecular weight (LMW) from bulk to surface. A hydrophobic surface is a highly-desirable property for outdoor electrical insulations to protect the HV substation equipment from environmental effects such as water and to minimize the leakage current on insulator surface as well as to reduce energy loss.

2.2.3 Heat and cool resistance

Heat resistance of silicone rubber is one of the most excellent properties and provides the basis for its creation. Silicone rubber is far better than organic rubbers in terms of heat resistance. At 150 ºC, almost no alteration in properties take place that it may be used semi permanently. Furthermore, silicone rubber withstands use for over 10,000 consecutive hours even at 200 ºC and, if used for a shorter term, it may also be used at 300 ºC as well. Boasting this excellent heat resistance, silicone rubbers are widely used to manufacture rubber components and parts used in high-temperature places [28-30, 58].

Cold resistance of silicone rubber is the finest among organic rubbers. It provides a critical reason behind the creation of silicone rubbers. Natural and ordinary rubbers demonstrate significant changes in formation depending on temperatures. They become soft at high temperatures and hard at low temperatures so that they may not be used any more. While other organic rubbers may only be used up to -20 ºC or -30 ºC, silicone rubber maintains its elasticity between -55 ºC and -70 ºC. Some silicone products can even withstand temperatures as low as -100 ºC [28-30, 58].

2.2.4 Electrical properties

One of the key properties of silicone polymers is good electrical properties. These are influenced to a large extent by the grade, purity and type of fillers. As with other insulating materials, dielectric strength E_b depends on several factors, including the thickness of the sample and shape of the test electrodes. Silicone rubber is extensively used for electrical insulation materials at high temperature with its superior insulation properties. It is particularly known for good properties over a wide range in temperature and volume resistance between 10^{14} Ω-cm and 10^{16} Ω-cm [28-30, 58]. Silicone rubber experiences lowest change in dielectric performance under wet condition.

The dielectric constant ε_r of commercial PDMS increases with the degree of polymerization (DP) of the siloxane backbone before quickly reaching a plateau value as shown in Figure 2.8 [59]. This effect is related to the siloxane-to-methyl-groups ratio, which

quickly increases, particularly in the shortest DP. At higher DP, adding one more unit has little impact on the permittivity of the media, which explains the plateau region. However, typical values of dielectric constant ε_r for a commercial silicone rubber are in the range of 2.6 to 3.5 (at 25 °C and 50 Hz). This property can be increased up to 150 by the use of suitable fillers [60].

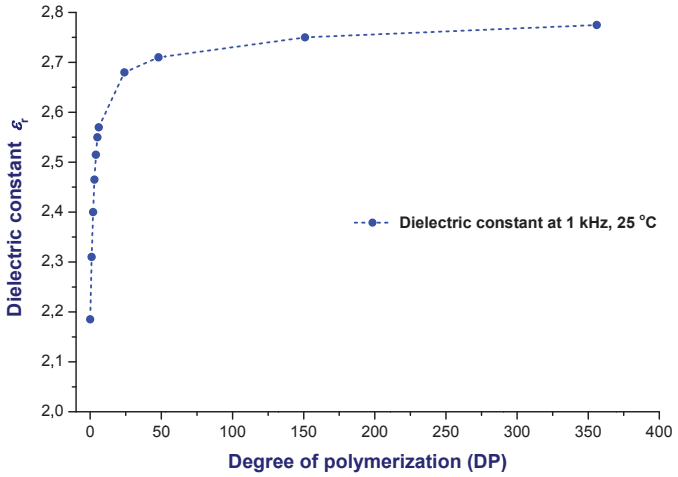

Figure 2.8: Variation of dielectric constant value of polydimethylsiloxanes as a function of degree of polymerization (DP), measured at 1000 Hz and 25 ºC [59]

The dielectric loss factors (ε_r and $\tan\delta$) of an electronic grade silicone elastomer have been investigated in the frequency range of 0.1 Hz to 1 MHz and the temperature range of -150 ºC to 100 ºC [61]. The measured results are illustrated in Figure 2.9.

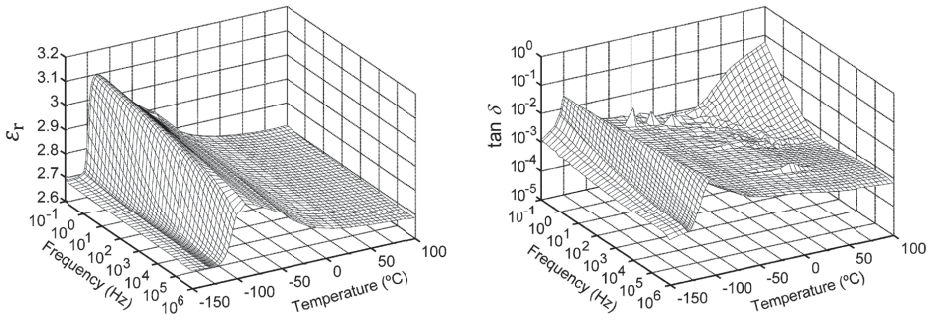

a) Dielectric constant ε_r *b) Dielectric loss (*tan δ*)*

Figure 2.9: Dielectric loss factors (ε_r and $\tan\delta$) of an electronics grade silicone elastomer as a function of frequency and temperature [61]

Silicone rubbers exhibit extremely low electrical aging compared to other insulating materials. They can strongly resist against corona discharge compared to others, while being widely used for insulation purposes in HV environments. No elastomeric material is currently found to match the electric properties of silicone rubber over 200 ºC. By adding special

conductive fillers, e.g. silicon carbide (SiC), conductive silicone rubbers can also be manufactured. Such modified materials are utilized to avoid stress concentrations in HV/EHV applications such as HV/EHV cable accessories and end windings of HV rotating machines. Conductive silicone rubber is also being used for keyboard interfaces, anti-electrostatic parts, and shield materials for high voltage power cables. [28-29, 53, 58]

2.2.5 Weatherability

Silicone rubber has superb ozone resistance. Due to corona-discharged ozone, other organic rubbers become deterioration (weaken) at a higher rate, but silicone rubber is rarely affected. Furthermore, even long-term exposures to UV rays, winds, or rain its physical properties will not be changed substantially.

2.2.6 Mechanical properties

With its coil shaped spiral structure and low intermolecular force, silicone rubber is highly elastic and compressible. The excellent elastic properties of silicone rubbers provide the best fit for used as a rubber stress cone of HV/EHV cable terminations. A silicone polymer with low molecular weight will make a paste suitable for knife coating onto fabric or for caulking voids in electrical equipment. Silicone rubbers can provide excellent stress-strain characteristics as well as high tear strength. These are influenced to a large extent by the grade and type of fillers as well as the degree of cross-linking. Typical values for tensile strength are in the range of 5 N/mm^2 to 12 N/mm^2 and typical values for elongation at break are in the range of 110 % to 1,100 %. A high-elasticity silicone rubber facilitates installation and allows novel installation techniques, e.g. cold shrinking on cables. In contrast to other elastomers, silicone elastomers have a permanent elasticity when cross-linking process is stable. They maintain their elasticity down to -70 °C [28-29, 58].

2.2.7 Optical properties

The colour and appearance of silicone rubber is determined by the fillers used in the respective compound. In the visible spectral range (400 nm to 760 nm), thin layers of unfilled materials are almost 100 % transparency. They only become opaque in the UV range below 200 nm. Their refractive index n_D is between 1.41 and 1.44 [60].

2.2.8 Flame Retardancy

Silicones in general have lower heat release rates, toxic gas emission and smoke output in comparison with most organic polymers [62-63]. Silicone rubber does not burn easily when it is in contact with a flame, but it would burn out consistently once ignited. However, by adding a small amount of flame retardant, it may become flame retardant and self-extinguisher. Flame retardant silicone rubbers presently in use would scarcely produce toxic gas during combustion since they do not contain organic halogen compounds discovered in organic polymers. Modern ceramifying silicone formulations are used to construct fire safety cables economically [64]. Flame retardant silicones and silicones for safety cables not only provide more safety to human in case of severe fire in a building but also help to slow down fire spreading. Furthermore they produce only small amounts of smoke and toxic fumes. All these products are also halogen free.

2.3 Silicone rubbers in medium- and high-voltage applications

These applications cover the transmission and distribution of electric power. Special silicones are the best choice for medium- and high-voltage cable accessories and insulators for high-voltage transmission lines and substations. The key advantage of silicones are their high volume resistivity, good trip-off properties, resistance to environmental degradations and to long-term electrical aging as well as their hydrophobicity, which results in lower assembly and maintenance costs [28, 58, 65].

Historically, the transmission and distribution applications for silicones developed from normal porcelain insulators which were covered with silicone grease in order to achieve hydrophobicity. Later, silicone rubber dispersions were used to cover porcelain with a rubbery and hydrophobic layer. Today, after 30 years of development, insulators tend to consist entirely of special silicone rubbers. Most of them contain special fillers allowing for more enhanced electrical properties. The technology of silicone rubber pellets is also available for these special grades resulting in processing advantages.

The most important properties are based on the electrical parameters of silicone rubbers, such as dielectric strength (around 18 kV/mm to 20 kV/mm), volume resistivity (10^{15} Ω-cm) and surface resistance (10^{13} Ω) [30]. These properties are the reason for the suitability of silicone rubbers for electrical applications. A further advantage of silicones is their hydrophobic behaviour which is of importance in many outdoor transmission and distribution electrical systems. As a result of their hydrophobic nature, silicone insulators show much smaller leakage currents than porcelain or EPDM offsets. Even in cases of bad environment with electrically conductive contaminated silicone insulators will remain hydrophobic along their surface. Silicone elastomers are capable of turning deposits from their environment hydrophobic, e.g. dust, sea salt, etc. This is due to the small amount of siloxanes bleeding out of the elastomer surface, covering the deposit and rendering it hydrophobic. Even after cleaning the insulators with detergents the hydrophobic behaviour will remain or return in due course. This is called hydrophobic transfer and regeneration [30]. Insulators in outdoor applications often are in contact with moisture. This is why tracking resistance is of utmost importance, special silicone grades [65] for outdoor HV applications provide a tracking resistance of up to 4.5 kV (typically ≈ 2.5 kV) according to IEC 60587 [66]. Should flashovers take place special silicone elastomers also exhibit excellent resistance to electric arc. Needless to say that silicone elastomers have relatively low changes of properties over time and temperature they are very suitable for long-term applications and for varying conditions. UV and ozone resistance complement the spectrum of properties. These are the key properties of silicone rubbers for medium- and high-voltage applications.

Recently, specially formulated silicones have been developed to smooth the electrical field distributions within the connection end and to ensure long-term performance. This is achieved in composite cable terminations either using some electrically-conductive silicone rubbers or, in more modern and smaller accessories, shaped deflectors made from silicone rubbers with medium electrical permittivity.

For performance reasons silicones are increasingly used in these areas as ceramics and organic rubbers do not show the same degree of performance, particularly in medium- and high-voltage applications. Table 2.2 gives a list of key applications and the silicone elastomer type used.

Table 2.2: Silicone rubbers in medium- and high-voltage applications [30, 65]

Applications	Type of silicones	Key properties	Key benefits
Long-rod insulators *with a silicone elastomer sheath*	– HCR – RTV-2 – LSR	• Resistance to UV radiation • Hydrophobic nature • Tracking resistance	○ High pollution-flashover voltage ○ Low leakage current ○ Lightweight ○ Low maintenance costs ○ Long service life
Hollow-core insulators *with a silicone elastomer sheath*	– HCR – RTV-2 – LSR	• Resistance to UV radiation • Hydrophobic nature • Tracking resistance	○ High pollution-flashover voltage ○ Low leakage current ○ Lightweight ○ Low maintenance costs ○ Long service life
Surge arresters	– HCR – RTV-2 – LSR	• Reliability with respect to overloading and low flammability • UV and tracking resistance (housing)	○ Greater safety ○ Long service life
Cable terminations	– HCR – RTV-2 – LSR	• Permanent elasticity • High dielectric strength • Tracking resistance	○ Long service life ○ Less or no maintenance costs
Cable joints	– HCR – RTV-2 – LSR	• Stability of the important electrical and mechanical properties in the temperature range used in applications	○ Long service life ○ Less or no maintenance costs

Long life, resistance to severe conditions and other properties make silicone elastomers suitable material for electric insulators in transmission and distribution applications. This is particularly of importance where electric energy must be distributed in desert or coastal areas, where the most severe conditions occur.

For HV cable accessories, modern materials allow pre-assembly and thus avoid problems associated with the use of molten casting material or mistakes made during manual assembly on the construction site. Today cable accessories are completely built at the supplier. Typically they consist of rubber terminations made of different insulating silicone rubbers. Two types of design are [65]:

- Push-on technique where a PE ring acts as a space holder until placement, and using silicone rubbers with hardness from 35 to 50 Shore A
- Cold shrink technique using softer silicone rubbers with hardness from 25 to 35 Shore A.

Modern cable accessories are produced by rubber injection moulding using a silicone High Consistency Rubber (HCR) or by liquid injection moulding using a two-part liquid silicone rubber (LSR) [30]. The integration of sensitive sensor element for online health monitoring into such devices is possible, particularly for PD detection in the critical interface area, which are often occurs and lead to electrical failures.

2.4 Silicone rubbers as power cable insulation

The first shipments of silicone rubber to power cable manufacturers were made in 1945 [41]. Early in the development of silicone rubbers it was recognized that the polymer determined the inherent stability of the rubber, while fillers determined to a great extent the physical and electrical properties of the cured rubber. These properties can be modified to a certain extent by changes in the polymer.

The properties of silicone rubbers are dependent on the type and amount of fillers compounded into the polymer. Recently, improvements in physical and electrical properties obtained with *fumed silica* nano-fillers stimulated further interest in silicone materials [36-37, 40]. This silica material is the basis for a series of new silicone rubbers that are of special interest to the cable manufactures and their end users. Because of the physical nature of the fumed silica, tough, tear resistant silicone rubbers are obtained. By varying the amount of silica in the formulation, rubbers with varying degrees of hardness can be made. Besides, fumed silica filled silicone rubbers with very low dielectric losses can be produced. An outstanding property of silicone rubbers filled with fumed silica is the stability of electrical properties over a wide temperature range. Figure 2.10 displays the dielectric loss factor of silicone rubber filled with fumed silica as a function of temperature compared with several typical filled silicone rubbers [41]. Dielectric constant ε_r and dielectric loss $\tan\delta$ at various frequencies for silicone rubbers filled with fumed silica are shown in Figure 2.11.

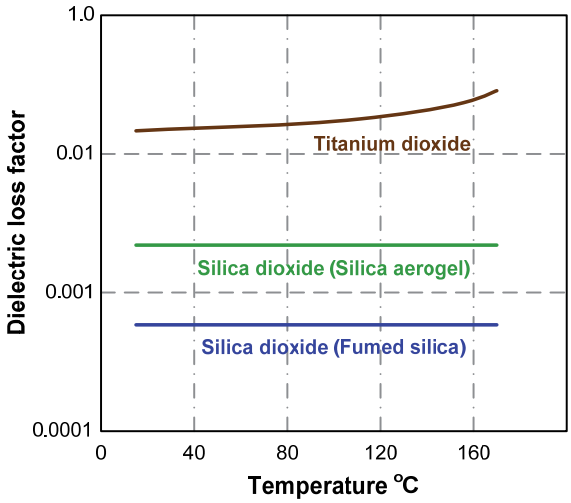

Figure 2.10: Dielectric loss factor of silicone rubber filled with fumed silica as a function of temperature compared with several typical silicone rubbers [41]

Dielectric constant ε_r and dielectric loss $\tan\delta$ of silicone rubbers filled with fumed silica do not change appreciably with frequency between the ranges of power frequencies up to 1 MHz. However, at higher frequencies, the dielectric loss increases with frequency and peaks at a frequency greater than 100 MHz. This increase in dielectric loss $\tan\delta$ at the higher frequencies is due to the polarity of the silicone-oxygen linkage in the silicone rubber polymer as mentioned before. It is characteristic of all silicone rubbers.

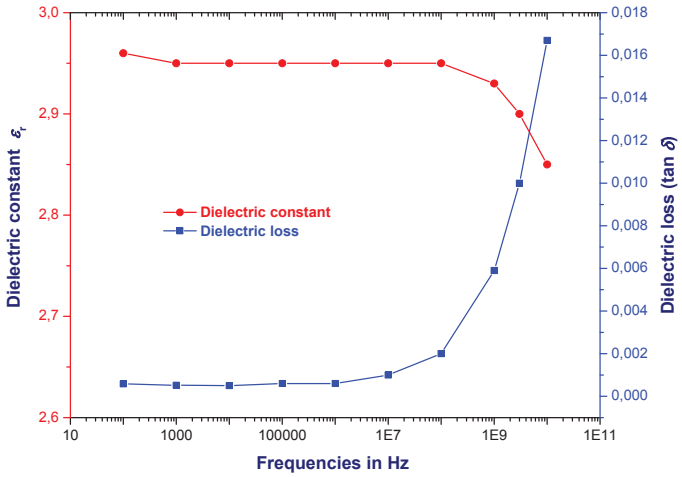

Figure 2.11: Dielectric constant ε_r and dielectric loss $(\tan\delta)$ at various frequencies for typical silicone rubbers filled with fumed silica for cable insulation [41]

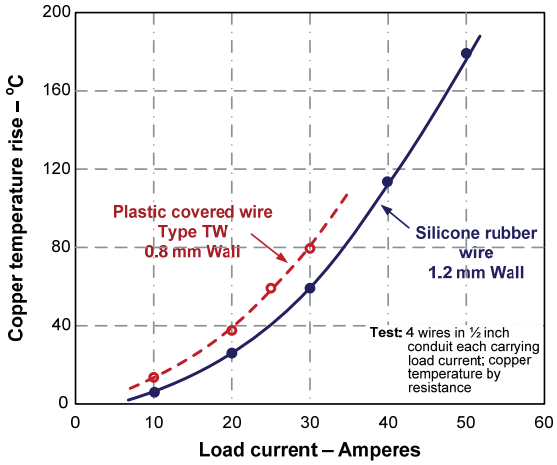

Figure 2.12: Current carrying capacity of silicone rubber insulated cable is compared with that of conventional thermoplastic insulated cable [41]

The high thermal conductivity of many silicone rubbers is another property of special interest in power cable applications. In Figure 2.12 the copper core temperature rise of silicone rubber insulated cable is compared with that of conventional thermoplastic insulated cable at various load currents. The temperature of the copper was determined from its change in resistance. The copper temperature rise of the plastic insulated cable was about 40 % higher than that of the silicone rubber cable at a load current of 10 amperes and 33 % higher at 30 amperes. Not only can the silicone rubber cable operate at much higher temperatures than the plastic covered wire, but the silicone rubber cable will be significantly cooler at the same load.

The thermal stability of silicone rubber insulated cable is difficult to define since its lifetime at high temperatures will depend greatly upon the application. One test of thermal stability is to age lengths of cable at various temperatures and periodically measure the dielectric strength of the cable insulation. Evaluations of this type test and several years field experience indicate that silicone rubber insulated cables can be operated continuously at temperatures in the range 150 ºC to 200 ºC with a life expectancy equal to that of organic insulated cables at their respective operating temperatures [41].

However, the temperature is increased above 150 ºC, some decrease in flexibility of the cable will occur. If flexing is a requirement of the application at these higher temperatures, some decrease in life must be expected. But, unlike most organic insulating materials, silicone rubbers do not lose their insulating qualities after aging at high temperatures. When silicone rubbers are completely decomposed by burning, the remaining ash retains its insulating properties. This fact is used to advantage in military control cables that must remain operative after several hours in an open flame [41].

The specific requirements for silicone elastomers that are used in cables develop from the requirements of cable manufacturers and their end users. Today, high consistency rubber (HCR) stocks can be made from higher molecular weight polymers. These rubber stocks are suitable for injection moulding and extruding. Improvement in these polymers has resulted in stocks that can be handled by conventional wire covering techniques. HCR solid silicone rubbers are now easy to mill under temperature control. They can be extruded uniformly and cross-linked in continuous vulcanisation (CV) lines by heating. Heating is usually by means of pressurized steam. The line is usually fed with steam at a high pressure (4 bars to 20 bars). The vulcanisation time depends on the length of the zone, the temperature, and the wall thickness of the cable insulation. As a manufacturer of silicone rubber insulated cables, the silicone material must be easily extruded and qualitatively for mass production. Adhesion or release from the wire can be controlled by treating the wire. The use of primers for a good adhesion is also possible [28-30, 58, 65].

Besides, in case of low- and medium-voltage systems, the use of silicone rather than PVC or other thermoplastic and elastomeric materials, has been boosted by safety discussions after recent fire accidents in which most of the damage was unfavourably attributed to the contribution of the PVC sleevings to smoke toxicity and density as well as cable function. Silicone cables burn at a much slower speed and their combustion products have low toxicity. During combustion silicone degrades to silica, hence, most of the silicone forms an electrically insulating ash. This prevents short circuits and their consequences. The accidents referred to above gave rise to the rapid development of so-called “safety cables”. Such cables will maintain the integrity of the electric circuit over a certain period of time in the case of a fire. Today, silicone technology enables cable manufacturers to produce a safety cable which will maintain circuit integrity over 90 minutes at temperatures higher than 1,000 °C even if they are quenched with water. This technology is based on the fact that ceramics are electrical insulators. A further competitive advantage of these safety cable materials is the fact that they can be extruded at very high speeds (of up to 400 m/min) whereas more traditional safety cable technology allows only a few metres per minute (m/min). For example, mica tape safety cables have a production rate of 12 m/min [30, 64].

2.5 Silicone rubbers for optical partial discharge (PD) detection

Fibre-optic sensors for high-voltage facilities are already known because of their advantageous non-electrical functional principles. Their components can be made from dielectric material and do not need any electrical power supply. Such components are immune to high-voltage and electromagnetic interference. Their tiny size and compactness enable integration into high voltage equipment, for example: power transformers, generators, power circuit breaker, gas insulated switchgears and cable accessories. Some more properties make fibre sensors interesting: capability of taking measurement signals along the optical fibre over up to several kilometres, capability of recording highly accurate digital information with high signal bandwidth and dynamic range. Commonly, fibre-optic sensors can be easily installed and do not require extensive maintenance.

Modern optical partial discharge (PD) detection based on fibre-optic sensors for PD on-line monitoring in high-voltage (HV) or extra high-voltage (EHV) cable systems necessarily requires optically transparent or translucent insulation materials. The optically compatible silicone rubbers are the key to facilitate such innovative technology. Percentage of optical transmission compared to the spectrum of PD light emission during electrical tree propagation in the commercially available transparent silicone rubber with a thickness of 10 mm is illustrated in Figure 2.13. The transmission is about 90 % over a broad spectral range (approximately 350 nm up to 850 nm), being more or less similar for all transparent silicone rubbers. Thus, the detection of PD light emission during electrical tree propagation in transparent rubber stress cones is promising, assuming that the PD emits either directly in this optical range of such silicones or the optical wavelength range of the emission can be shifted towards it.

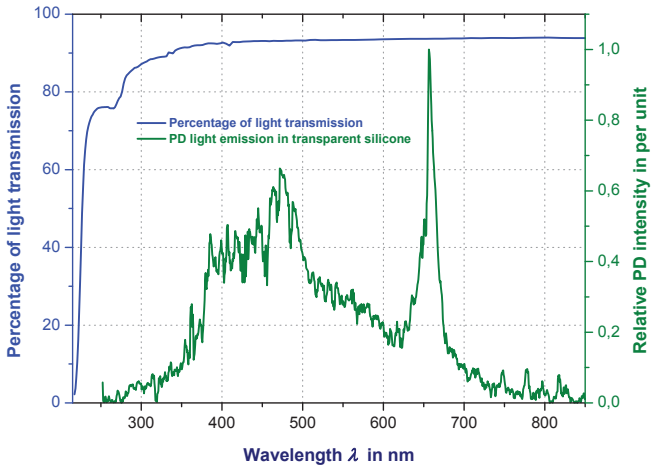

Figure 2.13: Percentage of light transmission compared to the spectrum of PD light emission in the commercially available transparent silicone rubber with a thickness of 10 mm

Besides the strong emission of Hydrogen at 656.28 nm, the broad continuum (approximately 350 nm till 700 nm) can be exploited for PD detection. The low optical transmission loss of transparent silicone insulation is ensured as the emission occurs in the optical range of the investigated silicone materials.

One of the possible ways to increase the sensitivity of optical PD detection in HV cable termination is the integration of an optical sensor element (i.e. optical fibres or optical probes) on/into the stress-cone rubber part. Figure 2.14 illustrates the stress-cone rubber part of HV cable accessories wrapped with the optical fibre sensor to detect PD activity at the critical interface area inside such a device. The results achieved by optical measurements were compared with that of electrical measurements. The measurement systems recorded and visualised optical and electrical pulses as phase resolved partial discharge (PRPD) pattern. The comparison of electrical and optical patterns for a small channel on a metallic tip showed a nearly identical visualisation as reported in [15-16] and [67-68]. Thus, the detection of optical PD in transparent silicone insulations by integrated optical fibres opens very efficient monitoring and diagnostic opportunities.

Figure 2.14: The stress-cone rubber part of HV cable accessories wrapped with the optical fibre sensor to detect PD activity inside such device [16-68]

2.5.1 The influence of embedded polymeric-optical sensor element into the rubber stress cone of HV cable accessories

In order to establish this new optical detection technology fully available for commercial use, some properties of the optical sensor elements in the HV environment must be clarified. The influences of embedded optical sensor elements into the transparent silicone rubber under high electrical stress have been investigated. Figure 2.15 and Figure 2.16 show two different types of sample fibres, i.e. fabricated silicone fibres and PMMA optical fibres, being hit by PD activities and the associated microscope pictures of the fibres after being exposed to PD. In contrast to silicone fibre samples (Figure 2.15), PMMA fibres are destroyed by electrical treeing (Figure 2.16). The damage is clearly visible by the red laser light shining through the broken cladding in such PMMA optical fibres.

Silicone fibres provide great potential for embedment into silicone insulation material because there are quite similar electrical properties. It does not seem to negatively influence the electric field distribution in the bulk dielectric system. It would be possible to embed silicone fibres as an optical sensor element in a region of moderate to high electrical stress near the critical interface area between the rubber stress cone of cable accessories and the

power cable core. Unfortunately, silicone optical fibres are currently not commercially available. Hence, the use of silicone polymers as an ideal basis for the development of new optical sensor and sensing elements as well as new elastomeric insulating material for a modern rubber stress cone has to be considered. All of these may lead to technology changes for PD on-line health monitoring in HV/EHV cable accessories in the future.

a) Silicone fibres being hit by PD activities in silicone cube specimen

b) Inspection of damages on test specimens using microscope (200x)

Figure 2.15: No influence of embedded silicone fibres into the transparent silicone rubber RTV 604 used as insulating material under high electrical stress [15]

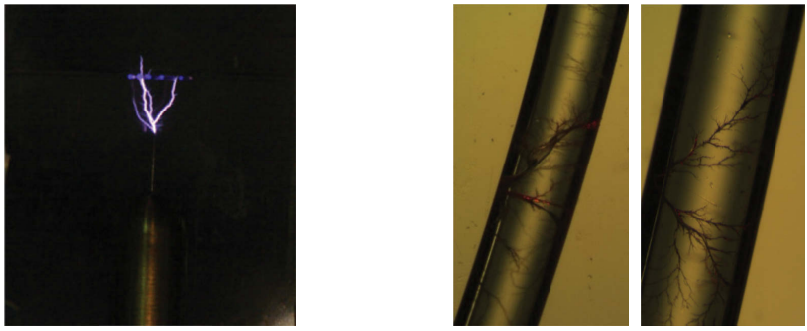

a) PMMA fibres being hit by PD activities in silicone cube specimen

b) Inspection of damages on test specimens using microscope (200x)

Figure 2.16: Surface tracking on the PMMA fibres caused by PD activities after the embedment of such fibres into the transparent silicone rubber RTV 604 [15]

The dielectric behaviour of the transparent RTV-2 silicone rubber under the influence of embedded PMMA optical fibre has been investigated and published in [15]. Under highly non-uniform electric fields, it could be seen that no significant difference occurred either in PD inception voltage or in breakdown voltage between samples with or without embedded fibre. This demonstrates the ability of safe operation of optical fibres for PD detection.

However there is currently no report regarding the effects of embedded silicone fibres. Thus, after successful development of new silicone optical fibres, the influence of their embedment on dielectric strength E_b behaviours of the bulk optically compatible silicone insulation system has to be investigated to avoid damage in HV/EHV equipment.

2.5.2 Fluorescent silicone optical fibre as sensor element

The optical recognition of PDs is based on the detection of light emitted during excitation, ionization and recombination processes. Generally the optical PD intensity is much lower in solids than in gas insulation medium. In order to achieve optimal detection of PD, the optical sensor elements shall be satisfactory designed to match various aspects. Practically, the position of PD origin cannot be identified hence PD emission cannot be detected by the front surface of a single fibre. One alternative method is the coupling of light via the fibre surface which requires the avoidance of light absorption by the fibre coating and/or cladding. In this case, the effect of total reflection does not impede the light transfer into the fibre. Due to little differences in the refractive index of core and cladding (max. 0.1), the critical angle for light coupling into the fibre is very low. Thus, most parts of the light emission will pass the undoped optical fibre without being transported via total reflection. Fluorescent fibres improve the light coupling efficiency and the differences in the refractive index Δn_{D} of core and cladding materials still remains important [69]. The fluorescent dye absorbs light independently of the angle of incidence and emits fluorescence into all directions in space. Consequently, a higher percentage of light fulfils the requirements relating to total reflection, and is guided to the detector. The coupling efficiency is improved with increasing amounts of fluorescent dye then the attenuation characteristic of the fibre is decreased. Therefore the fluorescent optical fibres are beneficial for effective coupling of light into the fibres. Unfortunately, commercially available fluorescent plastic optical fibres (FlPOFs) are not compatible when embedded into the silicone rubber insulation system as mentioned in the previous section. Silicone optical fibres seem to be suitable for this application. But, unluckily, the fluorescent silicone optical fibres (FlSiOFs) are not currently commercially available. Hence, a new fluorescent silicone optical fibre has to be developed and fabricated.

For integration of fibre-optic PD sensors into the real rubber stress cones a high flexibility of the fibre-optic material is necessary because an expansion of at least 10 % of the rubber stress cone perpendicular to the fibre axis is performed during the installation in cable accessories. Again, commercially available fluorescent plastic optical fibres do not meet this demand. In contrast siloxane is a flexible polymer with good properties for the application as elastomeric optical fibre material. Siloxane materials are highly transparent, have low optical attenuation and good mechanical as well as electrical properties. Silicones are well known for their high gas permeability and outstanding UV stability. Moreover, their refractive index can be tuned within a relatively wide range ($n_{\mathrm{D}} \approx 1.38$ to 1.58) by modifying the base polymers. Hence, transparent siloxanes would be appropriate for the development of a new FlSiOF [69].

The major disadvantage of mixing a fluorescent dye into the polymer is the migration of the dyes to the adjacent insulation material. Colour bleeding is an unacceptable phenomenon for long-term operation of FlSiOF sensing elements embedded into insulation materials. Thus, covalent bonding is necessarily required to prevent the migration of the fluorescent dye. Transparent silicone rubber is normally formed by platinum-catalysed hydrosilylation of two liquid siloxane components (cross-coupling), one carrying vinyl groups and the other consisting of hydrido-functionalized siloxane. Therefore, the main idea is that the vinyl modified dyes can be covalently bound to the siloxane polymer matrices by hydrosilylation reaction with hydridro substance silicone. These can be taken advantage of the platinum-catalysed cross-coupling reaction during the curing process of the siloxane network, as shown in Figure 2.17. To reach this goal, novel fluorescent silicone rubbers are being developed at BAM division 8.6 [69].

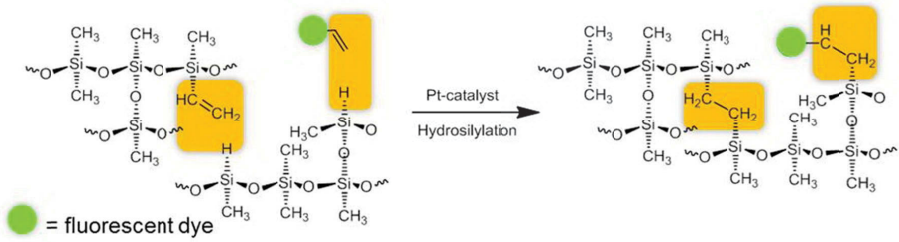

Figure 2.17: Scheme of the platinum-catalysed cross-coupling reaction of modified vinyl, hydridosiloxanes and respectively of a functionalized fluorescent dye (green sphere) with hydridosiloxanes

Fluorescent dyes of the coumarin family are known to fulfil most of these requirements. Several coumarin dyes were functionalized with unsaturated hydrocarbon groups. The optical properties of the dyes in the siloxane matrices and their photophysical properties were examined as illustrated in Figure 2.18 [69].

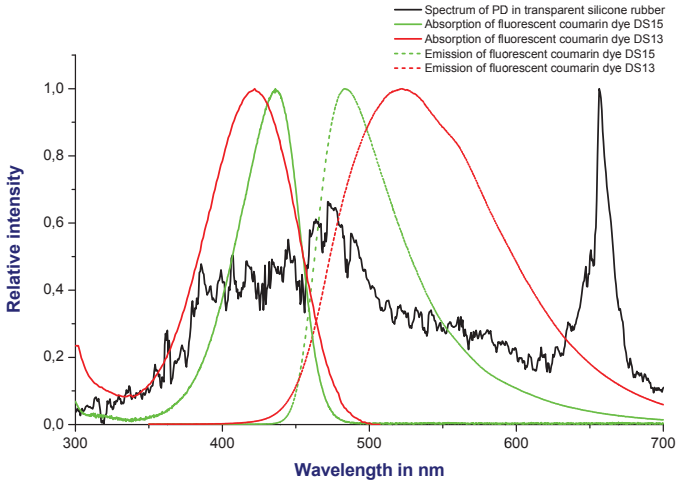

Figure 2.18: Absorption and emission spectra of coumarin modified FlSiOF over the spectrum of PD light emission in transparent silicone rubber

However, the influences of fluorescent modification on dielectric strength behaviour of silicone rubber need to be investigated. Because of such material will be operated under high electrical stress. It should not negatively influence the dielectric performance of the original rubber stress cone.

2.5.3 Modification of siloxane insulation material

For the establishment of the optical PD detection method in HV/EVH cable terminations it is necessary to use highly transparent rubber stress cones. However the current rubber stress cones used are translucent elastomers. Percentage of optical transmission in the translucent silicone rubbers is for sure poorer than that in the transparent types, as shown in Figure 2.19 a). This causes loss or distortion of the signals as well as a reduction of sensor

sensitivity. Unfortunately, the values of tensile strength and elongation at break of the transparent silicones are normally low. In order to improve such a poor mechanical strength, the addition of reinforcing fillers (mostly fumed silica) can be used but such fillers must not degrade optical properties of the rubber itself. To further enhance the transparency one possibility is to use hydrophobic nanoparticles as fillers. These fillers are much smaller than the wavelength of visible light and reduce the proportion of light being scattered at the interface of nanoparticles and matrix. The influence of nanofiller dispersion in silicone rubber matrix must be considered. A high concentration of surfactant in the matrix material can lead to reduced adsorption properties. Indeed silica nanoparticle filled siloxanes maintain highly transparent in the visible regime between 400 nm and 800 nm even at a weight load of 15 % as shown in Figure 2.19 b). Further investigations on the mechanical properties of nanoparticle filled silicone rubber at a lower filling grade will be elucidated by covalently linking nanoparticles to the silicone network. Therefore surface modification of commercial silica nanoparticles will be performed in the future.

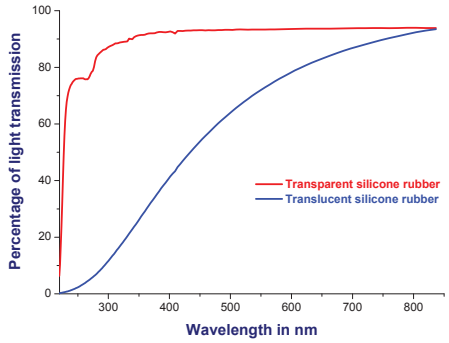

a) Light transmission in transparent and translucent silicone rubbers

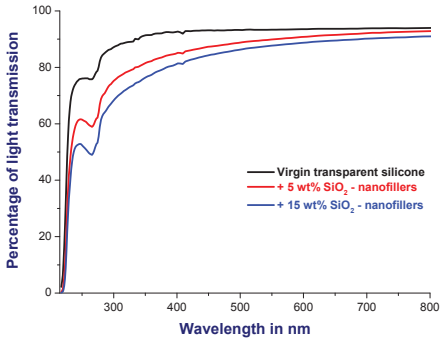

b) Light transmission in transparent silicone rubber with different wt% of silica nanofillers

Figure 2.19: Light transmission in the optically compatible silicone rubbers (a) and influence of SiO_2 nanofillers on percentage of light transmission in transparent silicone rubber (b)

2.6 Conclusions

Silicone rubbers and their specific properties related to desirable features in electrical engineering are reviewed. The final properties of silicone rubbers can be modified by addition of fillers. For their performance reasons silicone rubbers are increasing used as elastomeric insulation material for electrical engineering applications such as insulators, cable accessories, LV safety cables and silicone rubber insulated cables. Due to their molecular structure, silicone rubbers are also a promising solution for insulating applications in the transmission and distribution systems. Improvements in their useful properties for HV/EHV applications have been made in recent years. Transparent siloxane materials provide good performance for development of a new fluorescent silicone optical fibre used as optical sensing elements for optical PD detection technology in HV/EHV cable terminations are being developed at BAM. The preliminary results are presented in chapter 2.5. Indications are that new silicone rubber types for electrical and optical applications will continue to be developed.

3 Theoretical background

As a response to an increasing demand for electrical energy, transmission voltage levels have increased considerably over the last decades. Designers are therefore forced to reduce the size and weight of high-voltage electrical equipment in order to remain competitive. The high-voltage insulation must work satisfactorily as part of a complex system in high-voltage electrical equipment. There is an increased need for insulation to perform satisfactorily after it has been subjected to high electric fields followed by a period of electro-thermo-mechanical stresses in an aggressive environment. In designing the system's insulation the two areas of specific importance are:

i) determination of the voltage stresses which the insulation must withstand, and

ii) determination of the response of the insulation when subjected to these voltage stresses.

This, in turn, is possible only through a thorough understanding of the properties of insulating materials, and knowledge of electric fields and methods of controlling electric stress.

3.1 Electrical field distribution and breakdown strength of insulating materials

It is often assumed that a voltage V between two electrodes may be adequately insulated by placing a homogeneous insulating material of breakdown field strength E_b which is considered as a characteristic constant of the material, between these electrodes. The necessary separation d may then simply be calculated as $d = V/E_\mathrm{b}$. Although the electrodes are usually well defined and limited in size, the experienced designer will be able to take care of the entire field distribution between the electrodes and will realize that in many cases only a small portion of the material is stressed to a particular maximum value E_max.

One may conclude that the condition $E_\mathrm{max} = E_\mathrm{b}$ would provide the optimal solution for the insulation problem, which thus could be solved merely by field analysis. This is only true when E_b has a very specific value directly related to the actual field distribution, and can be calculated for very well-known insulating materials, such as gaseous dielectric. However, for most solid and liquid dielectrics such values are only approximately known. Hence a special approach is necessary to solve the insulation problem with fair accuracy.

These statements will be elucidated and confirmed by considering the simple example of an insulation system shown in Figure 3.1, which represents a rod–plane electrode configuration insulated by atmospheric air at atmospheric pressure. Whereas the gap length and the air density are assumed to remain constant, the diameter ∅ of the hemispherical-shaped rod will change over a very wide range as indicated by the dashed lines $\varnothing_1 < \varnothing_2 < \varnothing_3$.

Two field quantities may be defined for rods of any diameter: the maximum field strength E_max at the rod tip (hemispherical heads) and the mean value of the field strength $E_\mathrm{mean} = V/d$. With these two quantities an '*electric field factor*' η is defined as Equation (3.1) originally proposed by Schwaiger [23].

$$Electric\ field\ factor,\ \ \eta\ =\ \frac{E_{\mathrm{mean}}}{E_{\mathrm{max}}}\ =\ \frac{V}{d\ E_{\mathrm{max}}} \tag{3.1}$$

This factor is clearly a pure quantity related to electrostatic field analysis only. In a more complex electrode arrangement, E_{max} may appear at any point on an electrode, not necessarily coinciding with the points providing the shortest gap distance d. Electric field factor η equals unity or 100 % for a uniform field and it approaches zero for an electrode with an edge of zero radius or needle-point electrode.

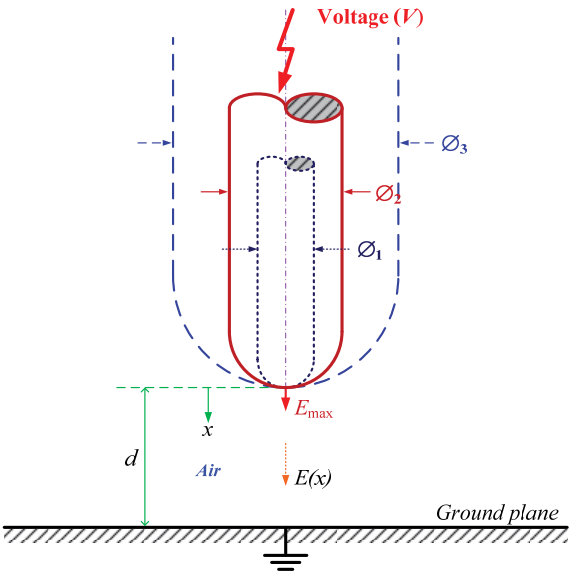

Figure 3.1: Rod-to-plane electrode configuration with different electric field factor η

If the breakdown of the gap is only caused by E_{max} ($E_{\mathrm{b}} = E_{\mathrm{max}}$), then the breakdown voltage V_{b} is obtained from Equation (3.1) as:

$$V_{\mathrm{b}}\ =\ E_{\mathrm{max}} \times d \times \eta\ =\ E_{\mathrm{b}} \times d \times \eta\quad (\text{with } E_{\mathrm{b}} = E_{\mathrm{max}}). \tag{3.2}$$

Equation (3.2) illustrates the concept of the electric field factor η. The electric field factor η can explain the electric field distribution between the electrode configurations [23]. As $0 < \eta \leq 1$ for any field distribution, it is obvious that field non-uniformities ($\eta < 1$) reduce the breakdown voltage of electrical insulation.

It is necessary to check the validity of Equation (3.2) with experimental results [23]. In Figure 3.2 the DC breakdown voltage V_{b} in atmospheric air is shown for the electrode arrangement of Figure 3.1 for gap length d = 10 cm as function of electric field factor η. The dashed straight line corresponds to Equation (3.2) with E_{b} = 26.6 kV/cm, a value which agrees well with measured breakdown field intensities in atmospheric air under normal conditions (temperature 20 °C; pressure 101.3 kPa; humidity 11 g/m^3). The highest breakdown voltage of the gap can be calculated from $V_{\mathrm{b}} = 26.6 \times 10 = 266$ kV for a uniform field (η = 1). This can also be found in the calibration tables for measuring sphere gaps

discussed in the standard IEC 60052 [70], for spheres of large diameters, i.e. ∅ ≥ 100 cm. With small gaps, the field distribution is uniform in the highly stressed regions. The measured breakdown voltages, obtained with positive and negative DC voltages, are also shown over wide ranges of η or diameter ∅. The differences are remarkable. The lowest measured V_b values are polarity dependent due to the influence of space charges. Except when η = 100 %, the breakdown voltages are always higher than those predicted by Equation (3.2). For $\eta > 0.3$ for negative and about 0.1 for positive polarity, the breakdown is not preceded by any noticeable pre-discharge phenomenon, i.e. corona, partial discharges. Thus it is obvious that E_b in Equation (3.2) is not a constant value for a given gap length. A calculation of breakdown field strength in atmospheric air using the streamer breakdown criterion and the relevant field distribution within the gap would confirm the dependence of the breakdown strength E_b upon rod or sphere diameter ∅ or – *more accurately* – upon the actual field distribution. In reality, the lowest breakdown voltage is not reached with the smallest values of electric field factor η. Below the minimum breakdown voltages, the sparkover of the gap is influenced by pre-discharges, which, for lower voltages, partially bridge the gap and thus produce charged particles, completely altering the field distribution due to space charges. Computation of the breakdown voltages in this region based upon physical parameters only is inaccurate due to a lack of precise knowledge of the physical data and complications introduced due to the moving space charge [23].

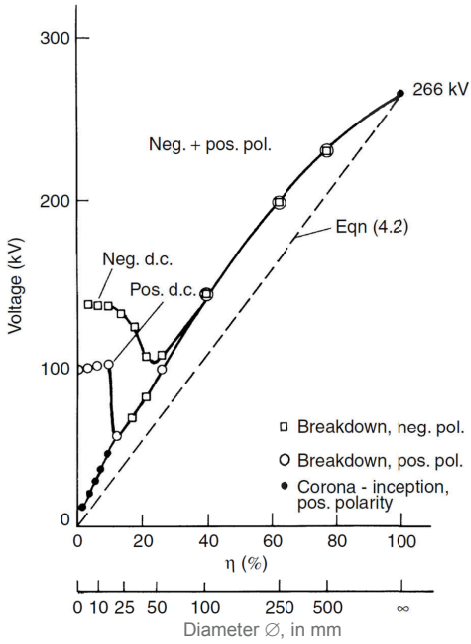

Figure 3.2: Breakdown and corona inception voltage for the electrode arrangement of Figure 3.1 in atmospheric air (normal conditions) with d = 10 cm, for positive and negative DC voltage (η see Equation (3.1)) [23]

This example, which is typical for most insulation media, demonstrates the complexity of the problems, i.e. the interaction between the static field distribution, field changes due to discharge development, and parameters related to the insulation materials.

Further complications arise from differences in behaviour with direct, alternating and impulse voltages. For any other material, the results would be different even for the same electrode configuration. The proper design of insulation systems is therefore very difficult. Nevertheless, the maximum field intensity $E_{\max}$ within any insulation system may be considered as a significant quantity even though it only serves as a guide.

In practice, data on the dielectric stresses in the insulation materials used in HV equipment obtained by field analysis must be validated by extensive tests in which the breakdown stresses are experimentally determined for similar insulation arrangements. Computations of the stresses are most advanced in gaseous dielectrics. Tests necessary for most of the other materials need not, however, to involve complete experimental models which precisely simulate the actual equipment. In general, breakdown stresses are dependent upon the field distribution within high field regions. Thus, models representing only those regions in which high stresses occur are, in general, sufficient; this offers definite advantages. Apart from saving time and costs by simplifying the experimental insulation assemblies, the required voltage levels may also often be reduced significantly, as the models can be reduced in size using electrode configurations in which the low field regions are absent.

3.2 Fields in homogeneous, isotropic materials

Many electrical insulation systems contain only one type of dielectric material. Most materials may be considered as isotropic, i.e., the electric field vector $\boldsymbol{E}$ and the displacement vector $\boldsymbol{D}$ are parallel. At least on the macroscopic scale many materials at uniform temperature may also be assumed to be homogeneous. The homogeneity is well-confirmed in insulating gases and purified liquids. Solid dielectrics are often composed of large molecular structures forming crystalline and amorphous regions so that the homogeneity of the electrical material properties may not be assured within microscopic structures. The materials will also be assumed to be linear; that means, the electric susceptibility is not a function of electric field strength. On a macroscopic basis, the permittivity ε will then simply be a scalar quantity correlating $\boldsymbol{D}$ and $\boldsymbol{E}$, with $\boldsymbol{D} = \varepsilon \boldsymbol{E}$ or $\boldsymbol{D} = \varepsilon_0 \varepsilon_\mathrm{r} \boldsymbol{E}$.

At this stage, it is assumed here that the influence of electrical conductivity σ on the field distribution may be ignored; this is justified for most insulating materials when they are stressed by alternating voltages at frequencies above about 1 Hz. Thus, simple electrostatic field theory may be applied to most of the practical applications concerned with power frequency or impulse voltages. In case of direct or slowly alternating voltages the use of simple electrostatic field theory would be impeded by conduction phenomena. In the limiting case, the field is purely given by conduction and the correlation between field strength $\boldsymbol{E}$ and current density $\boldsymbol{J}$ is $\boldsymbol{J} = \sigma \boldsymbol{E}$, where σ is electrical conductivity (or the complex conductivity).

The electrical conductivity σ is dependent upon time due to relaxation phenomena, upon temperature and often also upon field intensity. This problem is only mentioned here to emphasize the difficulties encountered with DC voltage applications. The following examples for electrostatic field distributions are typical for HV power cables and the electrodes for dielectric strength testing.

3.2.1 Coaxial cylindrical fields

Electrode configurations providing two-dimensional cylindrical shape is used in high-voltage equipment, i.e. coaxial power cables, busbars for SF_6-insulated switchgears (GIS), as well as in laboratories for fundamental research or field stress control. Cross-section of coaxial cylinders is sketched in Figure 3.3 a) with cylindrical conductors of the inner and outer radii r_1 and r_2, respectively. The electrical field distribution is symmetrical with respect to the cylinder axis. The lines of force are radial and the field strength E is only a function of the distance x from the centre. The cylinders are then uniformly charged over their surface with a charge per unit length Q/l, when a voltage V is applied to the electrode. Using Gauss's law, the field strength $E(x)$ at x is derived from the following:

$$E(x) = \frac{Q/l}{2\pi\varepsilon_0\varepsilon_r}\frac{1}{x} = \frac{V}{x\ln(\frac{r_2}{r_1})} \tag{3.3}$$

where $\varepsilon_0 = 8.854 \times 10^{-12}$ F/m and ε_r is the relative permittivity or dielectric constant of the insulation. The electric field in a coaxial cable varies only in the radial direction as the field magnitude decreases with increasing distance from the conductor center (see Figure 3.3 b) and c)). Its value is maximum at $x = r_1$ and minimum at $x = r_2$. The capacitance C per unit length (in F/m) of such a cable is given as:

$$C = \frac{2\pi\varepsilon_0\varepsilon_r}{\ln(\frac{r_2}{r_1})} \quad \text{F/m.} \tag{3.4}$$

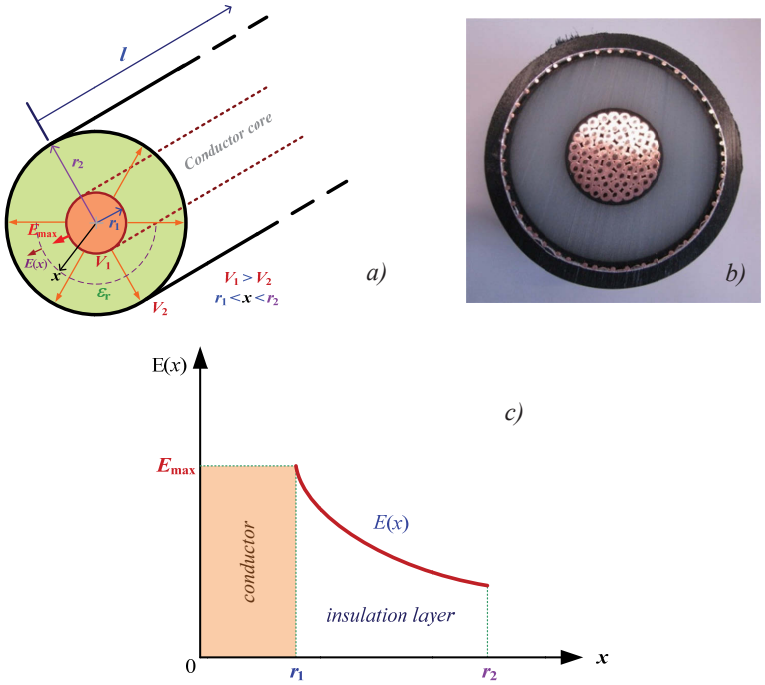

Figure 3.3: Cross-sections of coaxial cylinders a), and an XLPE coaxial cable b); the electric field varies in the radial direction of the coaxial cable c)

The maximum stress $E_{\max}$ is usually near the inner conductor area at $x = r_1$, therefore, $E_{\max}$ is obtained from Equation (3.3) as shown in Equation (3.5).

$$E_{\max} = \frac{V}{r_1 \ln\left(\frac{r_2}{r_1}\right)} \tag{3.5}$$

High degree of electrical stress is behind many of the aging mechanisms in the insulation of electrical power cables. It has been widely known that the use of multiple insulation layers of differing permittivity can be used to reduce the levels of electrical stress at the centre of the cable. However this theory relies on the use of a discrete method of stress grading [23]. The insulation medium used in modern power cables is typically XLPE which has a high dielectric strength and is capable of withstanding large value of imposed electrical stress. However, when a cable end is terminated for testing and other purposes, the field at such an end region is no longer purely radial and a tangential component is also introduced. Such a tangential field component can cause partial and surface discharges which consequently can lead to breakdown of the cable insulation. Therefore HV cable terminations are needed.

3.2.2 Sphere-to-plane electrode configuration

In practice, the sphere-to-plane electrode configuration is widely used in many investigations of dielectrics at fields approaching the breakdown value. This geometry permits a single well-defined point of maximum field and gradual reduction of the field far from the point. The field lines are not accurately parallel to the axis of symmetry, but for a sufficiently large sphere radius and small gap, the approximation may be sufficiently accurate as a uniform field ($\eta = 1$) and the field intensity can be calculated like the case of parallel-plane geometry $E = V/d$. A schematic representation of the sphere-to-plane electrode system is presented in Figure 3.4.

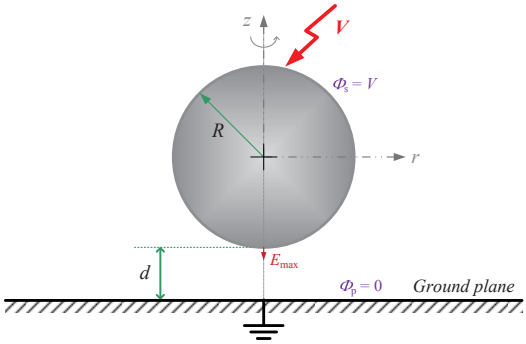

Figure 3.4: The sphere-to-plane electrode system

The electrostatic field, potential and capacitance of a sphere-to-plane electrode system have been analysed theoretically in several works [71-72]. The field distribution can analytically be calculated based upon the method of image charges [23]. The field pattern, and consequently, the potential distribution for the real electrodes system is equivalent to one generated by two point charges. The approximation for the maximum field strength $E_{\max}$ is derived from the image charge technique shown in Equation (3.6).

$$E_{\max} \cong 0.9 \frac{V}{d} \frac{R+d}{R} , \tag{3.6}$$

where d is the shortest gap distance between the electrodes, R is the radius of sphere electrode and V is the applied voltage.

3.3 Breakdown in solid dielectrics

Solid insulation forms an integral part of high-voltage equipment. The solid materials provide the mechanical support for conducting parts, and at the same time, insulate the conductors from one another. Practical insulation structures frequently consist of combinations of solids with liquid and/or gaseous media. A good dielectric should have low dielectric loss, high mechanical strength, should be free of gaseous inclusions and moisture, and shall be resistant to thermal and chemical deterioration. Therefore the knowledge of failure mechanisms of solid dielectrics under electric stress is of great importance. In gases the transport of electricity is limited to positive and negative charge carriers, and the destruction of insulating properties involves a rapid growth of current by the formation of electron avalanches. The mechanism of electrical failure in gases is now understood reasonably clearly. This is, however, not the case for solid insulation. Although numerous investigators have studied the breakdown of solids for almost a century, and a number of detailed theories have been put forward which aim to explain quantitatively the breakdown processes in solids, the state of knowledge in this area is still very crude and inconclusive.

Studies on electrical conduction studies in solids are obscured by the fact that the transport phenomena besides electronic and ionic carriers include also currents due to the slower polarisation processes such as slow moving dipoles (orientation polarisation) and interfacial polarisation [23]. Electrical methods are unable to distinguish between the conduction currents and the currents due to polarisation that have a longer time constant than the duration of a particular experiment. At low stresses and normal temperatures, conduction by free electrons and ions in solids is the exception. Examples in which the conduction is believed to be of the simple electrolytic type at room temperature and above are glasses. In this case the conduction–temperature relation is found to be of the form shown in equation (3.7), where A and u are empirical constants, and k is the Boltzmann's constant.

$$\sigma = A\, e^{\left(-\frac{u}{kT}\right)} \tag{3.7}$$

As the stress in solids increases and approaches the breakdown stress, the current is found to increase exponentially, but does not vary so markedly with time for steady voltage. This increased current at high stresses is generally believed to result from the injection of carriers from an electrode or from electron multiplication in the bulk material or both. In addition, if impurities or structural defects are present, they may cause local allowed energy levels (traps) in the forbidden band, and electrons may pass through the insulator by jumping from one trap to another (hopping effect).

From the electrodes, the electrons are believed to be ejected by either the '*Schottky's emission effect*' or the '*field emission effect*' (tunnelling) [23]. Once injected into the material, the electron multiplication is thought to be analogous to that in a gas discharge. Under certain strictly controlled experimental conditions, the breakdown of solids may therefore be accomplished by a process similar to gas breakdown. Under normal industrial

conditions, however, the same solid materials are found to exhibit a wide range of dielectric strength, depending upon the conditions of the environment and the method of testing. The measured breakdown voltage is influenced by a large number of external factors such as temperature, humidity, duration of test, whether AC, DC, or Impulse voltage is applied, whether pressure is applied to the electrodes, by discharges in the ambient or surrounding medium, by discharges in cavities and many other factors. The fundamental mechanisms of breakdown in solids are understood much less clearly than those in gases; nevertheless, several distinct mechanisms have been identified and treated theoretically [23, 73-76].

The mechanism of breakdown in solid dielectrics is a complex phenomenon. The breakdown of solid dielectrics does not only depend upon the magnitude of voltage applied but it is also a function of time for which the voltage is applied. The product of the breakdown voltage and the logarithm of the time required for breakdown is almost a constant. The dielectric strength of solid materials is affected by many factors, e.g. ambient temperature, humidity, duration of test, impurities or structural defects, whether AC, DC or Impulse voltages are being used, whether pressure is applied to test electrodes etc. The mechanism of breakdown in solids is again less understood. However, as said earlier, the time of application plays an important role in breakdown process. For discussion purposes, it is convenient to divide the time scale of voltage application into regions in which different mechanisms operate as shown in Figure 3.5.

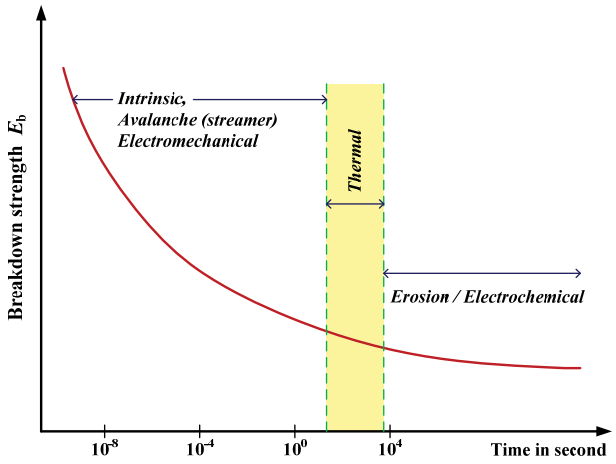

Figure 3.5: Mechanisms of failure and variation of breakdown strength in solids with time of stressing [23, 74]

The various breakdown mechanisms can be classified as follows:

a) intrinsic or ionic breakdown,
b) electromechanical breakdown,
c) failure due to treeing and tracking,
d) thermal breakdown,
e) electrochemical breakdown, and
f) breakdown due to internal discharges.

The mechanisms are briefly described in a qualitative manner.

3.3.1 Intrinsic breakdown

If the dielectric material under test is pure and homogeneous, the temperature and environmental conditions are carefully controlled and the sample is so stressed that there are no external discharges. Under voltages applied for a short time of the order of 10^{-8} seconds, the electric strength increases rapidly up to an upper limit known as *intrinsic electric strength*. The intrinsic strength of the dielectric material depends mainly upon the material and temperature conditions. Experimentally, this highest dielectric strength can be obtained only under the best experimental conditions when all extraneous influences have been isolated. To achieve the highest strength, the sample has to be so designed that there is a high stress in the centre of the solid under test and very low stress at the edges which cause discharge in the medium as shown in Figure 3.6.

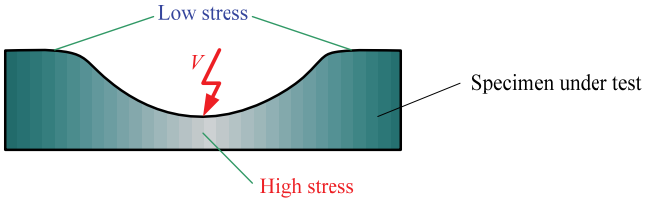

Figure 3.6: Electrode arrangement used for measuring intrinsic breakdown in solids

The stresses required for an intrinsic breakdown are quite over 10^6 V/cm. The intrinsic strength is generally assumed to be reached when electrons in the insulator gain sufficient energy from the applied field to cross the forbidden energy gap from the valence to the conduction band. The criterion is formulated by solving an equation for the energy balance between the gain of energy by conduction electrons from the applied field and its loss to the lattice. Several models have been proposed in an attempt to predict the critical value of the field which causes intrinsic breakdown, but no completely satisfactory solution has been obtained yet [23, 74].

In pure homogeneous dielectric materials the conduction and the valence bands are separated by a large energy gap, and at room temperature the electrons cannot acquire sufficient thermal energy to make transitions from valence to conduction band. The conductivity in perfect dielectrics should therefore be zero. In practice, however, all crystals contain some imperfections in their structures due to missing atoms, and more frequently due to the presence of foreign atoms (impurities). The impurity atoms may act as traps for free electrons in energy levels that lie just below the conduction band, as illustrated schematically in Figure 3.7. At low temperatures the trap levels will be mostly filled with electrons caught there as the crystal was cooled down during its manufacture. At room temperature some of the trapped electrons will be excited thermally into the conduction band, because of the small energy gap between the trapping levels and the conduction level. An amorphous crystal will therefore have some free conduction electrons.

When a field is applied to a crystal, the conduction electrons gain energy from it, and due to collisions between them the energy is shared by all electrons. For a stable condition this energy must be somehow dissipated. If there are relatively few electrons such as in pure crystals, most of the energy will be transferred to the lattice by electron-lattice interaction. In steady state conditions the electron temperature T_e will be nearly equal to the lattice temperature T_L.

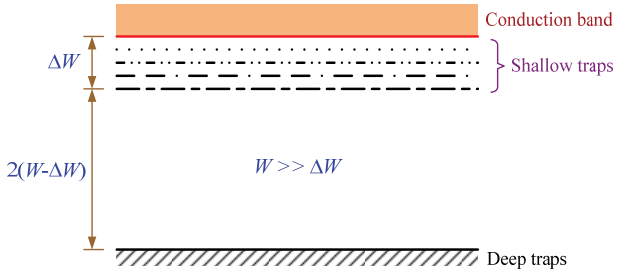

Figure 3.7: Schematic energy level diagram for an amorphous

In amorphous dielectrics the electron interactions predominate, the field raises the energy of the electrons more rapidly than they can transfer it to the lattice, and the electron temperature T_e will exceed the lattice temperature T. The effect of the increased electron temperature will be a rise in the number of trapped electrons reaching the conduction band. This increases the material's conduction and as the electron temperature continues to increase, a complete breakdown is eventually reached known as '*high-temperature breakdown*' [23].

Neglecting for the moment the details of the mechanism of energy transfer and assuming electronic conduction in solids, for an applied field the rate of energy gained by electrons from the field will be a function of the field strength E and the lattice temperature T. The rate at which this energy is transferred to the lattice will depend only on T. In addition, both rates will depend on parameters describing the conduction electrons. If we denote these parameters collectively by a, then for steady-state conditions the energy equation for conduction electrons may be written as

$$A(E,T,a) = B(T,a)\,, \tag{3.8}$$

where the left-hand side represents the rate of energy gain by electrons from the applied electric field, and the right-hand side is the rate of energy transfer from electrons to lattice. Equation (3.8) can be physically satisfied for values of electrical field E below a certain critical value E_c, and this value has been considered as the *intrinsic critical field* [23]. The value of E_c can be found by identifying correctly the parameters a and then solving equation (3.8) for the *critical field strength* E_c. The relationship between the parameters in equation (3.8) is illustrated in Figure 3.8, which shows the average rate of energy gain from the field for various field strengths and the rate of energy loss to the lattice. For the *critical field criterion*, equation (3.8) becomes

$$A(E_c,T,i) = B(T,i) \tag{3.9}$$

where i is the ionization energy corresponding to the transition of an electron from a valence band to a conduction band. From Figure 3.8 it is seen that for an electron to remain accelerated and thus lead to instability at any given field, it should find itself with an energy which brings it above the curve B so that it gains energy more rapidly than it loses. Equation (3.9) enables to determine the critical field strength E_c that is required to cause collision ionization from valence to conduction band. For field strength exceeding E_c the electrons gain energy more rapidly from the field than they lose to the lattice and breakdown will result. The above mechanism applies to pure solids in which the equilibrium is controlled by collisions between electrons and the lattice vibrations.

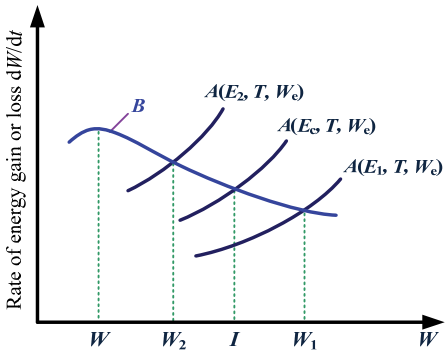

Figure 3.8: The average rate of energy gain $A(E, T, W_e)$ from an applied field for various field strengths and the average rate of energy loss to lattice $B(W_L, T)$ [23]

Fröhlich and Paranjape [76] have extended this model to amorphous materials in which the concentration of conduction (or trapped) electrons is high enough to make electron–electron collisions the dominant factor. In this case it is necessary to calculate the electron temperature T_e which will be higher than the lattice temperature T. The energy balance equation (3.8) has then the form

$$A(E, T_e, T) = B(T_e, T). \tag{3.10}$$

This relationship is plotted schematically in Figure 3.9 in which the family of curves plotted for various values of E represents the left-hand side of the equation and the single curve $E = E_2$ represents the right-hand side. The intersections give possible solutions for the various electron temperatures.

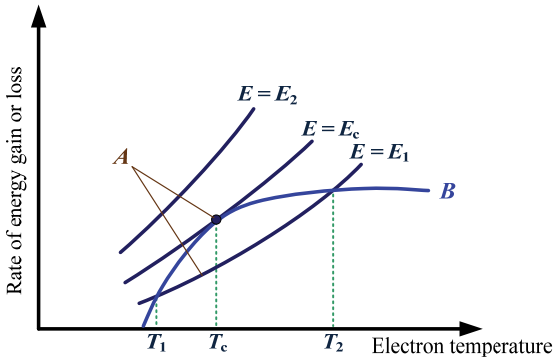

Figure 3.9: Rate of energy gain and loss for high temperature intrinsic breakdown model [23]

To date, there has been no direct experimental proof to show whether an observed breakdown is intrinsic or not, except for plastic materials such as polyethylene, and so conceptually it remains an ideal mechanism identified as the highest value obtainable after all secondary effects have been eliminated [23].

3.3.2 Streamer breakdown

This is similar to breakdown in gases due to cumulative ionization. The concept is similar to the streamer theory developed by Raether (positive streamer theory), Meek and Loeb (negative streamer theory) for gases discussed earlier [23, 74]. Conduction electrons gain sufficient energy above a certain critical electric field and cause liberation of electrons from the lattice atoms by collisions. Under uniform field conditions, if the electrodes are embedded in the specimen, breakdown will occur when an electron avalanche bridges the electrode gap. An electron within the dielectric, starting from the cathode will drift towards the anode and during this motion gains energy from the field and loses it during collisions. Occasionally, the free path may be long enough for the energy gain to exceed the lattice ionization energy and an additional electron is produced on collision.

We know that the strength of a chain is given by the strength of the weakest link in the chain. The covalent bond, typical of polymeric materials, is very sensitive to ionizing radiations. When the energy gained by an electron exceeds the lattice ionization potential, an additional electron will be liberated due to collision of the first electron. This process repeats itself resulting in the formation of an electron avalanche. Breakdown will occur, when the avalanche exceeds a certain critical size. In practice, breakdown does not occur by the formation of a single avalanche itself, but occurs as a result of many avalanches formed within the dielectric and is extending step by step through the entire thickness of the dielectric material as shown in Figure 3.10. This can be demonstrated in a laboratory by applying a high-frequency and high-voltage waveform between point-plane electrodes with a needle embedded in the transparent silicone rubbers. An obvious carbonization path is originated from the tree tip to the grounded electrode.

Figure 3.10: Breakdown channels in transparent polymer between point-plane electrodes

3.3.3 Electromechanical breakdown

Substances which can deform without fracture may collapse when the electrostatic compression forces on the test specimen exceed its mechanical compressive strength. The compression forces arise from the electrostatic attraction between surface charges which appear when the voltage is applied. The pressure exerted when the field reaches about 1.0 MV/cm may be several kN/m^2. If the initial thickness of the specimen is d_0 and is

compressed to a thickness d under an applied voltage V, then the electrically developed compressive stress F_E is in equilibrium with the mechanical compressive strength F_m if

$$\frac{1}{2}\varepsilon_0\varepsilon_r\frac{V^2}{d^2} = Y\ln\left(\frac{d_0}{d}\right)$$

or

$$V^2 = \frac{2Y}{\varepsilon_0\varepsilon_r}d^2\ln\left(\frac{d_0}{d}\right), \tag{3.11}$$

where ε_0 and ε_r are the permittivity of free space and the relative permittivity of the dielectric respectively, and Y is the Young's modulus of the dielectric. Differentiating with respect to d, then we get

$$2V\frac{dV}{dd} = \frac{2Y}{\varepsilon_0\varepsilon_r}\left[2d\ln\frac{d_0}{d} - d^2.\frac{d}{d_0}.\frac{d_0}{d^2}\right] = 0$$

or $$2d\ln\frac{d_0}{d} = d$$

or $$\ln\frac{d_0}{d} = 0.5\ .$$

We find that expression (3.11) has a maximum when d/d_0 = exp[-1/2] = 0.6. Therefore, no real value of V can produce a stable value of d/d_0 less than 0.6 (or the reduction in thickness of the specimen cannot be more than 40 %). If the intrinsic strength is not reached at this value, a further increase in V makes the thickness unstable and the specimen collapses. The highest apparent strength is then given by

$$E_b = \frac{V}{d_0} = 0.6\sqrt{\frac{Y}{\varepsilon_0\varepsilon_r}}\ . \tag{3.12}$$

This treatment ignores the possibility of instabilities occurring in the lower average field because of stress concentrations at irregularities, furthermore the dependence of Y on time and stress. Also when the material is subjected to high mechanical stresses, the theory of elasticity cannot be used to estimate plastic deformation that have to be considered here.

3.3.4 Edge breakdown and treeing

In practical insulation systems, which use solid material, it is stressed together with other surrounding materials, e.g. oil, air or gas. If one of the materials is, for example, a gas or a liquid, then the measured breakdown voltage will be influenced more by the weak medium than by the solid. A cross-section of a simplified example is shown in Figure 3.11 which represents testing of a dielectric sheet between sphere-plane electrodes. Ignoring the field distribution, i.e. assuming a homogeneous field, if we consider an elementary cylindrical volume with the area dA spanning the electrodes at distance x as shown in Figure 3.11, then on applying the voltage V between the electrodes, a fraction V_1 of the voltage appears

$$V_1 = \frac{Vd_1}{d_1 + \left(\frac{\varepsilon_1}{\varepsilon_2}\right)d_2}\ . \tag{3.13}$$

d_1 and d_2 represent the thickness of the media 1 and 2 in Figure 3.11, and ε_1 and ε_2 are their respective permittivities.

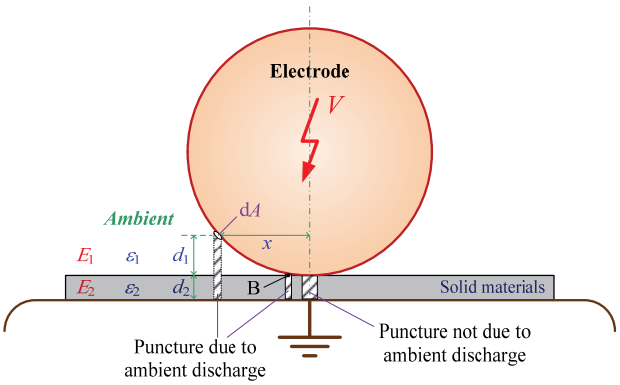

Figure 3.11: Breakdown of solid specimen due to ambient discharge-edge effect

For the simple case that a gaseous dielectric is in series with a solid dielectric stressed between two parallel plate electrodes, the stress in the gaseous part will exceed that of the solid by the ratio of permittivities $\varepsilon_s = \varepsilon_2/\varepsilon_1$ or $E_1 = \varepsilon_s E_2$. For the case shown in Figure 3.11, the stress in the gaseous part increases further as x decreases, and reaches very high values as d_1 becomes very small (point B in Figure 3.11). Consequently, the surrounding medium breaks down at a relatively low applied voltage. The charge at the tip of the discharge will further disturb the applied local field and transform the arrangement to a highly non-uniform system. The charge concentration at the tip of a discharge channel has been estimated to be sufficient to give a local field of the order of 10 MV/cm, which is higher than the intrinsic breakdown field. A local breakdown at the tips of the discharge is likely, and as a the result of many such breakdown channels formed in the solid and extending step by step through the whole thickness, a complete breakdown occurs.

The breakdown event in solids in general is not accomplished by the formation of a single discharge channel, but assumes a *tree-like* structure as shown in Figure 3.12. This can readily be demonstrated in a laboratory by applying an impulse voltage between point-plane electrodes with the point embedded in a transparent solid, e.g., plexiglass, transparent silicone rubbers. The tree pattern shown in Figure 3.12 was recorded by Cooper [23] with a waveshape of 1/30 µs impulse voltage at the same amplitude (radius of point = 0.01 inches; thickness of specimen = 0.19 inches; total number of impulses = 190; number of channels produced = 16; (n) point indicates end of n –th channel; and radii of circles increase in units of 10^{-2} inches). After application of each impulse the channels were observed with a microscope, and new channels were recorded. Not every impulse will produce a channel. The time required for this type of breakdown under alternating voltage will vary from a few seconds to a few minutes. The tree-like pattern discharge is not specifically limited to the edge effect but may be observed in other dielectric failure mechanisms in which nonuniform field stresses predominate.

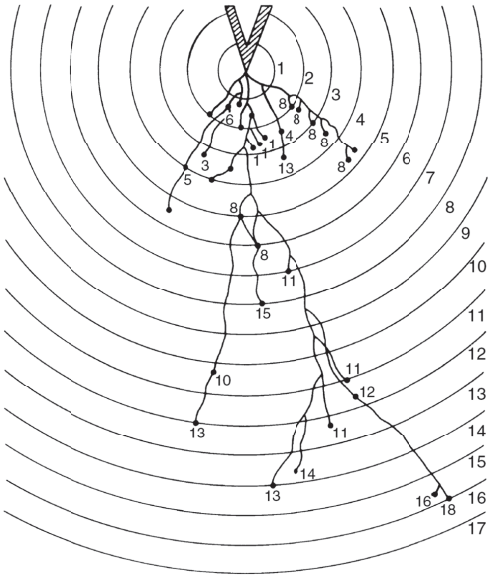

Figure 3.12: Breakdown channels in plexiglass between point-plane electrodes. Radius of point = 0.01 inches; thickness 0.19 inches. Total number of impulses = 190. Number of channels produced = 16; (*n*) point indicates end of *n* –th channel. Radii of circles increase in units of 10^{-2} inches [23]

3.3.5 Thermal breakdown

When an insulating material is subjected to an electric field $\boldsymbol{E}$, the material gets heated up because of conduction currents and dielectric losses due to polarisation. Heat is continuously generated within the dielectric. In general, the conductivity σ increases with temperature and the conditions of instability are reached when the rate of heating exceeds the rate of cooling and the specimen may undergo thermal breakdown. The situation is illustrated in Figure 3.13.

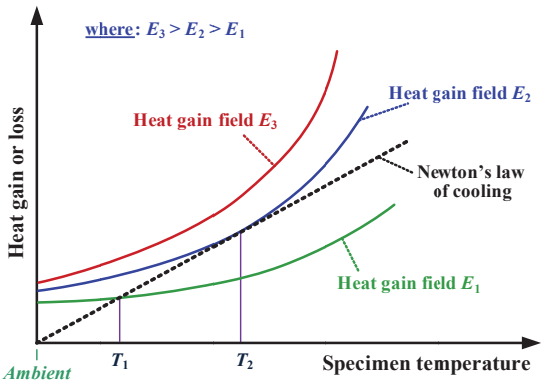

Figure 3.13: Thermal stability or instability under different applied fields [23]

The cooling of a specimen is represented by the straight line and the heating at various field strengths by curves of increasing slope. The test specimen is at thermal equilibrium corresponding to field E_1 at temperature T_1 as beyond that heat generated is less than heat lost. Unstable equilibrium exists for field E_2 at T_2, and for field E_3 the state of equilibrium is never reached and hence the specimen breaks down thermally.

In order to obtain the basic equation for studying thermal breakdown, a small cube of face area A (m^2) with side Δx within the dielectrics is considered. Assuming that the heat flow in the x-direction is shown in Figure 3.14, then the

$$\textit{heat flow across face}\ (1) = KA\frac{dT}{dx}\ ,$$

$$\textit{heat flow across face}\ (2) = KA\frac{dT}{dx} + KA\frac{d}{dx}\left(\frac{dT}{dx}\right)\Delta x\ ,$$

where K is thermal conductivity.

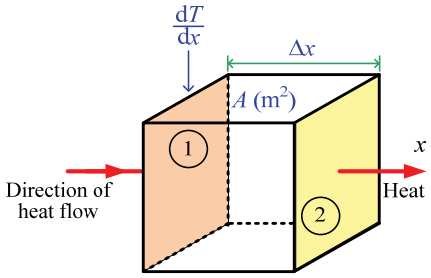

Figure 3.14: Cubical specimen – Heat flow

The second term represents the heat input into the differential element. The heat flow per volume absorbed by the differential cube volume,

$$K\frac{d}{dx}\left(\frac{dT}{dx}\right) = \text{div}\ (K\ \text{grad}\ T).$$

The heat generated by the electric field is σE^2 and supposes that the rise in temperature of the dielectric block is ΔT, in time dt. The conservation of energy requires that heat input into the element must be equal to the heat conducted away, plus the heat used to raise the temperature T of the block or

$$\text{heat generated} = \text{heat absorbed} + \text{heat lost to surroundings},$$

that is;

$$\sigma E^2 = C_\text{v}\frac{dT}{dt} + \text{div}\ (K\ \text{grad}\ T) \qquad (3.14)$$

where C_v is the thermal capacity of the dielectric, σ is the electrical conductivity, and in the case of alternating voltage the heat is generated primarily as a result of dipole relaxation, and the conductivity is replaced by $\omega\varepsilon_0\varepsilon_\text{r}''$ where ε_0 represents permittivity of free space and ε_r'' is the imaginary component of the complex relative permittivity of the material [23].

To consider the critical thermal situation, equation (3.14) provides a solution. To solve it, one assumes that a critical condition arises and the insulation properties are lost, when at some points in the dielectric the temperature exceeds a critical temperature T_c. The solution gives the time required to reach T_c for a given field and boundary condition. The equation cannot be solved analytically for the general case since C_v, K and σ may be all functions of temperature T and σ may also depend upon the applied field E. We consider two extreme cases for the solution of equation (3.14) [23].

Case I. This assumes a rapid build-up of heat so that heat lost to surroundings can be neglected and all heat generated is used in raising the temperature of the solid dielectric. We obtain an expression for 'impulse thermal breakdown' and equation (3.14) reduces to

$$\sigma E^2 = C_v \frac{dT}{dt}.$$

The objective now is to obtain the critical field strength E_c which will generate sufficient heat very fast so that requirement above is met. Assuming that a ramp function field, that is $E = \left(\frac{E_c}{t_c}\right) t$, where t_c is the critical time is applied, then is valid

$$\sigma E^2 = C_v \frac{dT}{dE}\frac{dE}{dt}.$$

For the conductivity, can be assumed

$$\sigma = \sigma_0 e^{\left(-\frac{u}{kT}\right)},$$

where σ_0 is the conductivity at ambient temperature T_0 and k is the Boltzmann's constant. Substituting for σ and rearranging, we get

$$\int_0^{E_c} \frac{t_c}{E_c}\frac{\sigma_0}{C_v} E^2\, dE = \int_{T_o}^{T_c} \exp\left[-\frac{u}{kT}\right] dT.$$

For the case when $u \gg kT$ and $T_c \gg T_0$ (T_c is critical temperature), the solution of the equation above is

$$\int_0^{E_c} \frac{t_c}{E_c}\frac{\sigma_0}{C_v} E^2\, dE = \int_{T_o}^{T_c} \exp\left[-\frac{u}{kT}\right] dT$$

$$\frac{1}{3} t_c \frac{\varepsilon_0}{C_v} E_c^2 = T_0^2 \frac{k}{u} \exp\left[\frac{u}{kT_0}\right]$$

Therefore

$$E_c = \left[\frac{3C_v k T_0^2}{\sigma_0 u t_c}\right]^{0.5} \exp\left(\frac{u}{2kT_0}\right)$$

From the expression above follows that the critical condition requires a combination of critical time t_c and critical field. However, the critical field E_c is independent of the critical temperature T_c due to the fast rise in temperature.

Case II. It concerns minimum thermal voltage, i.e., the lowest voltage for thermal breakdown. For this case, a thick dielectric slab is assumed that is constrained to ambient temperature at its surfaces by using sufficiently large electrodes as shown in Figure 3.15 [23].

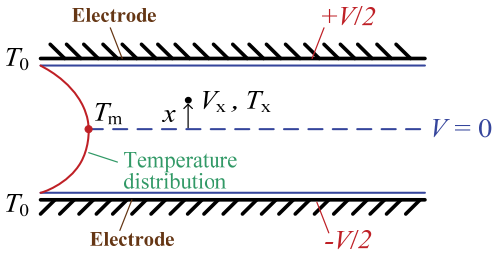

Figure 3.15: Arrangement for testing a dielectric for minimum thermal breakdown voltage

Applying a voltage, a temperature distribution within the dielectric will be established after some time with the highest temperature at the centre T_1, whereas the surface remains at ambient temperature. Increasing the voltage further, an equilibrium will be established at a higher central temperature T_2. If the process is continued, a thermal runaway will eventually result as shown in Figure 3.16.

In order to calculate the minimum thermal voltage, a point inside the dielectric with a distance x from the centre is considered. The voltage and temperature at that point is V_x and T_x respectively. For this case can be assumed that all the heat generated in the dielectric will be carried away to its surroundings through the electrodes. Neglecting the term $C_v(dT/dt)$, eqn (3.14) becomes

$$\sigma E^2 = \frac{d}{dx}\left(K\frac{dT}{dx}\right) .$$

Using the relations $\sigma E = J$ and $E = -\partial V/\partial x$ (where J is current density), and inserting them into the equation above, we obtain

$$-J\frac{\partial V}{\partial x} = \frac{d}{dx}\left(K\frac{dT}{dx}\right).$$

Integrating it to an arbitrary point x in the dielectric

$$-J\int_0^{V_x} dV = \int_0^x \frac{d}{dx}\left(K\frac{dT}{dx}\right)dx$$

$$-JV_x = K\frac{dT}{dx}$$

or

$$V_x\sigma\frac{dV}{dx} = K\frac{dT}{dx}.$$

Substituting it for $\sigma = \sigma_0 \exp[-u/kT]$, and integrating it from the centre of the dielectric to the electrode, we get

$$\int_0^{V_c/2} V_x dV = \frac{K}{\sigma_0}\int_{T_0}^{T_c} \exp\left[\frac{u}{kT}\right] dT$$

$$V_c^2 = 8\frac{K}{\sigma_0}\int_{T_0}^{T_c} \exp\left[\frac{u}{kT}\right] dT. \quad (3.15)$$

Equation (3.15) gives the critical thermal breakdown voltage V_c, where T_c is the critical temperature at which the material decomposes and the calculation assumes that T_c corresponds to the centre of the slab. The voltage V_c is independent of the thickness of the specimen, but for thin specimens the thermal breakdown voltage becomes thickness dependent and is proportional to the square root of the thickness tending asymptotically to a constant value for thick specimens.

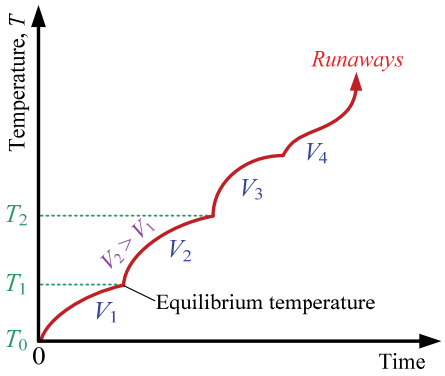

Figure 3.16: Temperature–time relationship for slow thermal stressing under various applied voltages [23]

Under alternating fields the losses ($\sigma E^2 + V^2\omega C \tan\delta$) are much greater than under direct fields. Consequently, the thermal breakdown strength is generally lower for alternating fields, and it decreases with increasing frequency of the supply voltage. These results correspond to a thick slab of material.

The thermal breakdown is a well-established mechanism; therefore the magnitude of the product $\varepsilon \tan\delta$ which represents the loss is a very essential parameter for the application of insulation material.

3.3.6 Erosion and electrochemical breakdown

Practical insulation systems often contain cavities or voids within the dielectric materials or on boundaries between the solid dielectric and the electrodes. These cavities are usually filled with a medium (gas or liquid) of lower breakdown strength than the solid dielectric. Moreover, the permittivity of the filling medium is frequently lower than that of the solid insulation, which causes that the field intensity in the cavity is higher than in the dielectric. Accordingly, under normal working stress of the insulation system the voltage across the cavity may exceed the breakdown value and may initiate breakdown in the void.

Figure 3.17 shows a cross-section of a dielectric of thickness d containing a cavity in the form of a disc of thickness t, together with an analogue circuit. In the analogue circuit the capacitance C_c corresponds to the cavity, C_b corresponds to the capacitance of the dielectric which is in series with C_c, and C_a is the capacitance of the rest of the dielectric. For $t \ll d$, which is usually the case, and assuming that the cavity is filled with gas, the field strength across C_c is given by the expression

$$E_c = \varepsilon_r E_a \ ,$$

where ε_r is the relative permittivity of the dielectric.

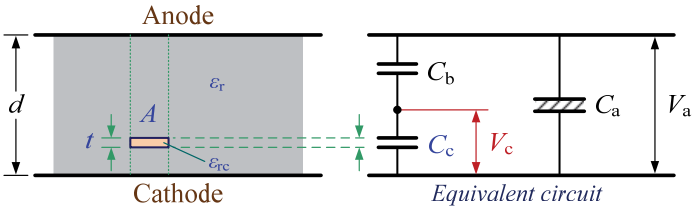

Figure 3.17: Electrical discharge in cavity and its equivalent circuit [23]

For the simple case of a disc-shaped dielectric in solid insulation shown in Fig. 3.17, the discharge inception voltage applied across the dielectric can be expressed in terms of the cavity breakdown stress. Assuming that the gas-filled cavity breakdown stress is E_{cb}, then treating the cavity as series capacitance with the healthy part of the dielectric can be written as

$$C_b = \frac{\varepsilon_0 \varepsilon_r A}{d - t}$$

and

$$C_c = \frac{\varepsilon_0 A}{t} \ .$$

The voltage across the cavity is

$$V_c = \frac{C_b}{C_c + C_b} V_a = \frac{V_a}{1 + \frac{1}{\varepsilon_r}\left(\frac{d}{t} - 1\right)} .$$

Therefore the voltage across the dielectric which will initiate discharge V_{ai} in the cavity is given by

$$V_{ai} = E_{cb} t \left\{1 + \frac{1}{\varepsilon_r}\left(\frac{d}{t} - 1\right)\right\} . \tag{3.16}$$

In practice a cavity in a material is often nearly spherical, and for such a case the internal field strength for $\varepsilon_r \gg \varepsilon_{rc}$ is

$$E_c = \frac{3\varepsilon_r E}{\varepsilon_{rc} + 2\varepsilon_r} = \frac{3E}{2} \ , \tag{3.17}$$

where E is the average stress in the dielectric under an applied voltage V_a. When V_c reaches breakdown value V^+ of the gap t, the cavity may break down then. The sequence of breakdowns under sinusoidal alternating voltage is illustrated in Figure 3.18. The dotted curve shows qualitatively the voltage that would appear across the cavity if it did not break down. As V_c reaches the value V^+, a discharge takes place, the voltage V_c collapses and the gap extinguishes. The voltage across the cavity then starts increasing again until it reaches V^+, when a new discharge occurs. Thus several discharges may take place during the rising part of the applied voltage V_a. Similarly, on the negative half-cycle of AC applied voltage, the cavity discharges as the voltage across it reaches V^-. In this way, groups of discharges originate from a single cavity and give rise to positive and negative current pulses when increasing and decreasing the voltage, respectively.

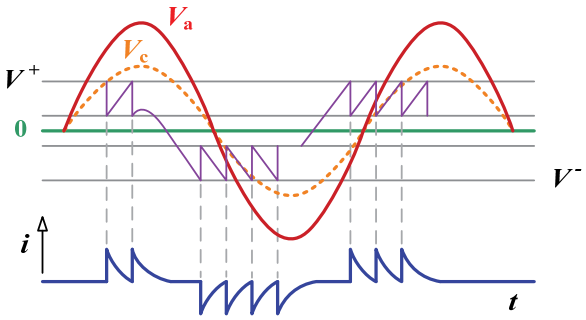

Figure 3.18: Sequence of cavity breakdown under alternating voltages [23]

When the gas in the cavity breaks down, the surfaces of the specimen provide instantaneous anode and cathode. Some of the electrons dashing against the anode with sufficient energy shall break the chemical bonds of the insulation surface. Similarly, positive ions bombarding against the cathode may increase the surface temperature and produce local thermal instability. Also channels and pits are formed which elongate through the insulation by the '*edge mechanism*'. Additional chemical degradation may result from the active discharge products, e.g. O_3 or NO_2, formed in air which may cause deterioration. The net effect of all these processes is a slow erosion of the material and a consequent reduction in the thickness of the specimen.

In case of outdoor environment insulation, physically, when the discharges occur on the insulation surface, the erosion takes place initially over a comparatively large area. The erosion roughens the surface and slowly penetrates into the insulation, and at some stage will again give rise to channel propagation and '*tree-like*' growth through the insulation.

Normally for practical application it is important that the dielectric strength of a system does not deteriorate significantly over a long period of time (years). In practice, however, because of imperfect manufacture and sometimes poor design, the dielectric strength (e.g. in cables and their accessories) decreases with the life time and in many cases the decrease in dielectric strength E_b with time t follows the empirical relationship

$$tE_b^n = constant\,, \tag{3.18}$$

where the exponent 'n' depends upon the dielectric material, the ambient conditions, and the quality of manufacture.

Figure 3.19 illustrates the case for several medium-voltage polyethylene cables produced by different manufacturers [23]. The breakdown strength has been plotted against time on a log–log scale. This is the main reason why high AC voltage testing is not recommended for on-site testing of cables. In fact, these days very low frequency (VLF) testing is being suggested (0.1 Hz) which simulates the effects of both AC 50 Hz and DC voltages and the dielectric strength of the specimen is not yet much affected by VLF voltage application.

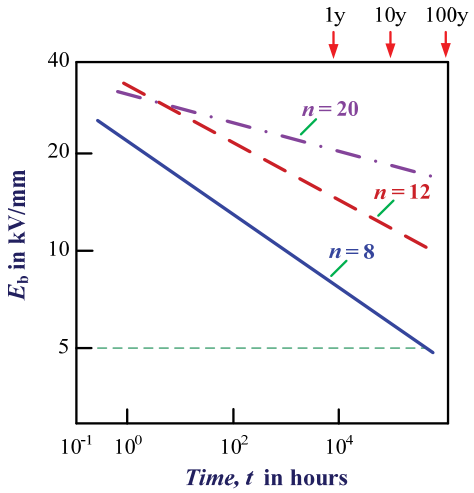

Figure 3.19: Lifetime (*t*) versus stress relationship of polyethylene medium-voltage cables determined by different manufacturers [23]

3.3.7 Tracking

Tracking is the formation of a permanent conducting path, usually carbon, across a surface of insulation and in most cases the conduction path results from degradation of the insulation. In an outdoor environment, the insulation becomes covered with industrial or coastal contaminant over time. If tracking occurs, inside the insulation organic substances are developed. The contamination layer gives rise to leakage current in the presence of moisture, which heats the surface and causes interruption in the moisture film; small sparks are drawn between the separating moisture films. This process acts effectively as an extension to the electrodes. The heat resulting from the small sparks causes carbonization and volatilization of the insulation and leads to formation of permanent '*carbon track*' on the surface. The phenomenon of tracking severely limits the use of organic insulation in the outdoor environment. The rate of tracking depends upon the structure of the polymers and it can be drastically slowed down by adding appropriate fillers to the polymer which inhibit carbonization.

Moisture is not essential to initiate tracking. The conducting path may arise from metallic dust; for example, in oil-immersed equipment with moving parts which gradually wear and deposit on the surface.

3.4 Mechanism of electrical degradation and breakdown in polymers

Polymeric materials, such as polyethylene (PE) and polypropylene (PP), are widely used as insulating materials in the field of high-voltage engineering. For this reason, a considerable amount of attention has been paid in recent years to the problem of polymer aging in the electric field (deterioration of the electrical strength properties) and elucidation of the mechanisms responsible for a breakdown in polymers. However, these issues are not yet completely understood. This is partly due to special properties of polymers as molecular solids. Polymers are characterized by a weak intermolecular interaction (*macromolecules* with saturated bonds preserve their individuality in the condensed phase). Calculations of the electron spectrum of polymers – or molecular crystals – yielded band widths of ~ 0.01 eV. In such narrow bands charge transport is hindered. At the same time, the notions of the band structure of the electron spectrum are applicable to an individual (isolated) macromolecule, which is a many-atom many-electron system similar to a one-dimensional crystal. The bandwidths in macromolecules are estimated at several electronvolts [77].

It is important to emphasize that, as experimental evidence indicates, the electrical breakdown of the polymer is not a critical event occurring at a certain electric field intensity characteristic of this polymer sample. The electrical breakdown of polymers is a kinetic process that develops over the time. It is characterized by the damage accumulation rate and the inverse value, i.e. the lifetime of a polymer sample in the electric field. The breakdown itself – *formation of a conducting channel* – is a final stage of polymer degradation in the electric field which is prepared by the damage accumulation process whose rate depends on the electric field intensity. The dependence of the electrical lifetime on the electric field intensity can be assumed to be nearly exponential [77].

Mechanisms of electrical breakdown in polymers can be helpful to explain how degradation processes influence the dielectric strength of polymeric insulation materials. It can be represented by the following models [78]:

i) Low-level degradation models, in which the insulating system's characteristics are deleteriously affected by the electric field, possibly in conjunction with other agents.

ii) Deterministic models, in which the ultimate breakdown event is the direct effect of some earlier causal events or conditions produced by exceeding a critical electric field value.

iii) Stochastic models in which either local physical conditions are considered to be continuously changing, or there are local electric field variations caused by inhomogeneities so that there is a finite probability at any time that breakdown may occur.

In this section, low-level degradation models, electrical treeing, electroluminescence under electric field conditions and deterministic breakdown models are discussed.

3.4.1 Low level degradation in polymers

Mechanisms of low-level degradation in polymers are categorized by Dissado and Fothergill [78] as physical aging, chemical aging or electrical aging. Physical and chemical aging are considered to be important as they can influence the probability of breakdown and they may also be accompanied with electrical degradation when driven by an electrical field

during service. Although introduced separately, all three models may be responsible for polymer degradation in practice.

1) Physical aging

Physical aging is caused by decreasing segmental motions of polymer chains in amorphous regions. A physical description of the aging is usually given in terms of reduction of free volume. All polymers contain amorphous structure, and free volume is the unoccupied part of volume of the amorphous phase. The length of the free path depends on the size of the unoccupied part in the amorphous phase.

Arbauer [79] has developed a free volume breakdown model in which electrons (either intrinsic or injected) gain kinetic energy by field acceleration in long free volume regions where the distance between scattering events is large. In a given applied electric field the electrons surmount the barriers to their motion in the polymer when the free volume is large enough to give a rapid increase in current density, and an increase in temperature sufficient to damage the polymer and cause instant failure.

According to the breakdown criterion [79], the probability that all electrons will be accelerated sufficiently on the free path to gain the energy necessary to overcome the barrier and start the breakdown will be attained when the voltage drop xE_b attains the value

$$xE_\mathrm{b} \;=\; U_\mu \;=\; \frac{W_\mu}{e}\,, \tag{3.19}$$

where U_μ is an intrinsic property of the polymer dielectric, which depends only on its structure; W_μ is the barrier energy; E_b is the breakdown electric field; and x is the longest free path which depends on the sample size, temperature and crystallinity. Generally, x is not a constant.

Distribution of the characteristic largest value x_n in a sample of size *n* is:

$$G(x) \;=\; \exp\left\{-e^{-\left(\frac{x-x_\mathrm{n}}{s}\right)+\ln N}\right\}, \tag{3.20}$$

where N is a factor which describes the sample size increase; and s is a scale parameter.

Both the longest free path and the breakdown field are dependent on temperature. When the frequency *f* of thermal movements of molecules equals zero (only at zero absolute temperature), x has its lowest value x_0 and consequently the breakdown field has the highest value F_0, which only depends on the structure of the dielectric. At temperatures satisfying $f = f\,(T) > 0$, x increases but the breakdown strength decreases with temperature and time, during which the polymer has been stressed by the applied field.

2) Chemical aging

Chemical aging usually proceeds via the formation of polymer free radicals R^* following an initiation step X, i.e.:

$$X \;+\; R_{(\mathrm{a+b})} \;\;\rightarrow\;\; R_\mathrm{a}^* + R_\mathrm{b}^*\,.$$

Free radicals are chemically very active and lead to propagating chain scission or cross-linking network formation via chain reactions [78]. Two types of chain scission may occur. Either the bond breaking is random in space with free radical transfer between chains or it unzips a chain by the ejection of volatile monomers or side group products. The former case produces degradation products containing large molecular weight fragments and is favoured by polyethylene, whereas the latter case is typical of poly (∞ – methylstyrene) where it results in a large monomer fraction and poly (vinyl chloride) which dehydrochlorinates producing hydrogen chloride. The initiating mechanism may be thermal, oxidation, caused by UV absorption or ionizing radiation, or mechanical.

3) Electrical aging

Electric fields, especially DC, lead to dissociation and transport of ionized and ionizable by-products that could cause a deterioration of the insulation's performance due to increased losses and local stress enhancements [78].

According to Kao's theoretical model [80] of electrical discharge and breakdown in condensed insulating materials, charge carrier injection and recombination play a decisive role in breaking of polymer chains and the creation of free radicals, macromolecules, and traps. The mechanism of the dissociation of macromolecules, the central point of which is the assumption of the formation of hot electrons capable of initiating a rupture of chemical bonds was suggested. Thus, Kao [80] considered a multistage process involving electron injection from the cathode into the polymer, the capture of injected electrons by traps accompanied by the release of the energy approximately equal to the trap depth at every event, and the transfer of this energy to another electron. In other words, the appearance of hot electrons, their interaction with macromolecules, the dissociation of macromolecules into free radicals, the trapping of the electrons that have lost energy (cold electrons), etc. are described. The last stages were illustrated by the following scheme:

$$AB + e_{(\mathrm{hot})} \xrightarrow{dissociation} \dot{A} + \dot{B} + e_{(\mathrm{cold})} \longrightarrow \dot{A} + \dot{B} + e_{(\mathrm{trapped})} + energy\ release\ ,$$

where AB denotes the macromolecule, $\dot{A}$ and $\dot{B}$ indicate free macro-radicals, and e represents the electron. It was assumed that the energy released at the trapping of a cold electron is transferred to another injected electron, etc. Thus, the process has a chain character.

Unfortunately, no quantitative data on the rates of the separate stages of the chain reaction (and on the rate of the process as a whole) were given in Kao's model [80] to confirm the considerations. Kao also did not consider the probability with which the entire energy released during electron trapping is transferred to another electron, did not estimate the probability that this energy can be dissipated through molecular vibrations without being transferred to an electron, did not discuss the mechanisms responsible for energy transfer to an electron and how the probability of energy transfer depends on the trap-electron distance, and did not consider the probability of bond rupture when they are excited by relatively low-energy electrons. Note that the thermal depth of traps in polyethylene (PE) is evidently not more than 2 eV, and the energy for rupture of the $\mathrm{C-C}$ bonds can be higher than 3 eV [77]. Finally, one more fact should be pointed out. Kao [80] considered the chain reaction due to successive energy release during electron trapping. However, it could not yet find examples of chain energy reactions in polymers. Typically, the chain reactions of the transformation of chemical bonds in polymers proceed by the free-radical mechanism, i.e. with the participation

of chemically active particles. This is the mechanism for the reactions of the thermal destruction of polymers, oxidation of polymers, etc.

The above discussion relates to the situation when the negative electrode in the needle-plane system is the needle and electrons are injected into a polymer. The analysis of Kao's attempts to treat the dissociation of macromolecules as resulting from the injection of holes from the positive needle raises even more questions. Typically only mono-polar injection from the needle is taken into account in the needle-plane system. Nevertheless, it is supposed that hot electrons capable of initiating the dissociation of macro- molecules are formed (due to a complicated six-stage process) in the case of the positive needle as well. The probability of the realization of such a multistage process was not estimated. All these facts indicate that the scheme discussed by Kao's model cannot be thought of as a realistic model of the dissociation of macromolecules in the electric field.

The model described in [81], in which the dissociation of macromolecules is regarded as a consequence of the charge recombination in a polymer seems more realistic. Recombination of charges (a free electron and a positive macro-ion hole) gives rise to the release of energy $\Delta E = I_g - P - |V_0|$, where I_g is the energy for ionization of a macromolecule in the gaseous phase, and P is the energy for polarisation of the polymer by a unit charge. If we take I_g = 8 eV, P = 1.5 eV, and $|V_0|$ = 0.5 eV [77], we obtain $\Delta E \approx 6$ eV. This energy is higher that the energy of rupture of covalent chemical bonds. Therefore, the reaction of the dissociation of macromolecules can proceed according to the scheme

$$AB^+ + e \longrightarrow (AB)^* \longrightarrow \dot{A} + \dot{B},$$

where AB^+ indicates the macro-ion, and $(AB)^*$ represents the excited macromolecule. The rupture of chemical bonds in polymers (dissociation of macromolecules) initiated by the electric field was described in [82] and [83].

Liufu and coworkers [82], who believe that electrical aging is due to this gradual degradation process, carried out a series of experiments which indicated that electrical aging phenomena in polypropylene can be well interpreted on the basis of Kao's model [80]. They also discovered that the degree of electrical aging can be determined by the rate of increase in the concentration of stress-created traps. It has been proved that polyolefin degradation in the electric field under discharge conditions is due to the formation of free radicals, especially initiated by accelerated electrons with energy higher than 3.8 eV [84].

3.4.2 Electrical treeing

In dry environment the degradation gives rise to electrical treeing which has two distinct time periods. The first is the initiation or the incubation phase during which partial discharge (PD) do not occur, and the second is the propagation period during which PD occur and the tree grows. Once an electrical tree starts, its growth cannot be stopped. Treeing could be slowed down or retarded, but sooner or later it will lead to the breakdown of the insulation. For insulation operating in a wet environment, especially in underground power distribution cables, the degradation of the insulation gives rise to water treeing, but even when a water tree bridges the entire insulation between the conductors breakdown does not occur immediately. However, prior to breakdown an electrical tree, which could be initiated by transient voltages and other factors, grows from the water treed region, and it is the electrical tree that causes the breakdown. Hence, in both wet and dry environment it is always

the electrical tree that is responsible for the insulation breakdown. Lee [85] has shown in a recent paper that large stress enhancement factors can be induced in small asperities or defects at the semicon/dielectric interface of an extruded cable. Therefore electrical treeing is usually considered as a principal form of electrical degradation distinct from the low-level degradation mechanisms discussed in the former section. It is well established that electrical tree shapes can be roughly characterized as branch and/or bush-shaped structures.

Electrical trees found in polymeric insulation grow in regions of high electrical stress, such as metallic asperities, conducting contaminant and structural irregularities [78]. Electrical treeing occurs in all high voltage polymeric insulation and is the principal aging process that leads directly to breakdown failure.

According to the model for electrical tree initiation developed by Wu and Dissado [86], the generation of new charge traps by the recombination of injected charges of opposite polarity from a divergent field stress point, is sufficient to continuously drive the system to the initiation of an electrical tree. They also showed that this is achieved by the increase of trap density to the point where shallow traps can connect together in the form of a percolation cluster under the application of an electric field. Bamji *et al*. [87] discovered that certain type or polarity of charge is required to initiate electrical treeing in LDPE (low density polyethylene). For example, it is impossible for the unipolar injected charge to gain sufficient energy to cause impact ionization or break bonds of the polymer chain.

Propagation of electrical trees was described as 3-stage tree growth model which was based on partial discharge measurements [88]. **Stage 1** is considered to be the tree inception which is detectable only by very sensitive measurements. **Stage 2** is considered to be the growth of the first small branches to the opposite electrode. It starts at tree inception and it ends when the first branch has reached the opposite electrode without causing specimen breakdown. The branches are characterised by a size $L < 10$ μm in the trunk and $L < 1$ μm in the tip. **Stage 3** is considered to be the stage where the small branches will be widened up to a pipe-shaped structure. It starts when the first branch has reached the opposite electrode and it ends with the final breakdown. The channels are characterised by a size of $L > 10$ μm having typical values between 60 μm and 150 μm. Propagation states of electrical treeing until breakdown is shown in Figure 3.20.

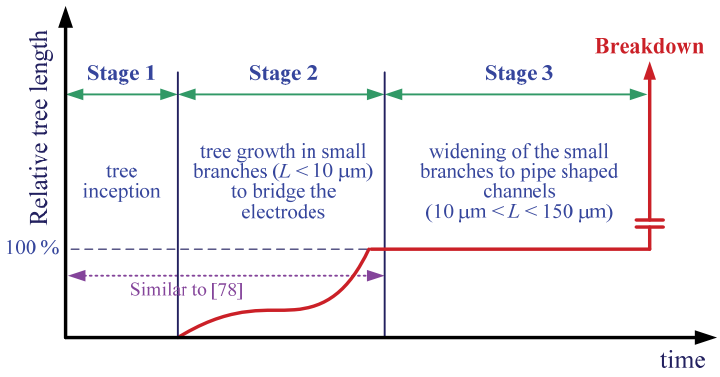

Figure 3.20: Propagation states of electrical treeing until breakdown [88]

Two alternative theoretical approaches to electrical tree propagation exist. Stochastic models [89-90] attribute tree structures to random probabilistic factors. On the other hand, in the discharge-valance model [91-92], field fluctuation due to non-uniformly distributed regions of trapped space charge is responsible.

A kinetic [93] electrical tree growth rate formula was developed. This formula is based on a quantitative physical model [87] in which the propagation is considered to arise from the formation of electrodamage that precedes and surrounds the tree tip during the tree propagation process.

$$X = (L/L_{\mathrm{b}})^{d_{\mathrm{f}}} \tag{3.21}$$

$$\frac{\mathrm{d}L}{\mathrm{d}t} = \frac{\mathrm{k}TL_{\mathrm{b}}^{d_{\mathrm{f}}}}{\mathrm{h}d_{\mathrm{f}}} L^{(1-d_{\mathrm{f}})} \exp\left(\frac{\pi\varepsilon\alpha_{\mathrm{m}}E^2S_0 - U_0}{\mathrm{k}T}\right), \tag{3.22}$$

where X is the number of submicroscopic trees that have formed the electrical tree; L is electrical tree length; L_{b} is unit increment in electrical tree length due to the jointing of a secondary tree and is approximately equal to the average length of the secondary tree; d_{f} is the fractal dimension of the electrical tree; k and h are the Boltzmann's and Planck's constants, respectively; T is the absolute temperature; S_0 is the size of the submicroscopic void; U_0 is the activation energy of the breakdown process in physics; ε is the dielectric permittivity. E is electric field strength and α_{m} is a property of the material, which represents the activation area in the direction of the applied electric field.

3.4.3 Electroluminescence under electric field

It has been established [94-103] that electroluminescence (EL), the emission of light in dielectrics subjected to high electric stress, occurs in most polymers, such as PE, PP, PVC and epoxy, under AC, DC and Impulse voltages. EL is emitted prior to electrical tree inception and even before the first partial discharge occurs in the polymeric insulation. Unlike the light of partial discharges, EL occurs continuously above a certain threshold field and has been attributed to the injection of electric charge from the electrodes. The injected charge accumulates in the insulating material to form a space charge, which plays a major role in DC voltage applications [102]. Although, the role of space charges is less significant under AC field, it cannot be completely ignored. Space charges can cause field distortions and give rise to dissipative energetic processes which can affect the onset of electrical aging, decrease the withstand voltage and lead to insulation failure. Hence, the determination of space charge injection and distribution in the polymer is not only helpful for developing better insulating materials but also for improving the existing designs of high voltage apparatus.

Authors of [103] suppose that, under the action of this radiation, the dissociation of macromolecules and the formation of low-density regions take place in the AC field. It is known that EL in the DC field is not observed or its intensity is low [94-95]. It is likely that the recombination mechanism of the dissociation of macromolecules should be taken into consideration only in the case of the AC field.

EL spectrum is short-wave (ultraviolet: UV) radiation. The UV light of EL can enhance chemical reactions and lead to degradation of the polymeric insulation. Saturated

polyolefins (PO), in the pure form, do not absorb light of wavelength > 190 nm. However, photodegradation of polymers is known to occur with light in the UV range due to the presence of chromophores which are accidently introduced into the polymer during the processing and synthesis of the material. The UV light causes photodegradation due to photochemical reactions, creates free radicals, and breaks bonds leading to the formation of a microcavity and subsequently an electrical tree. The combination of these modes will finally lead to ultimate failure of the polymeric insulation. The physical ageing model of polymeric insulating materials is shown in Figure 3.21.

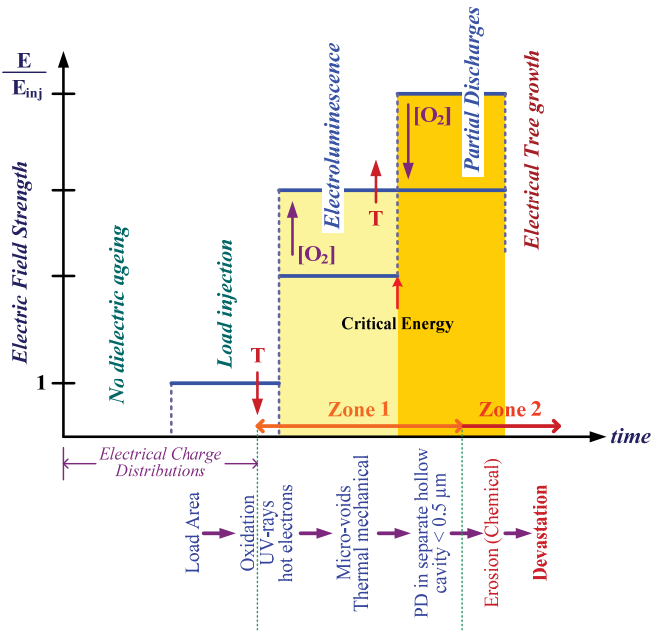

Figure 3.21: Physical ageing model of polymeric insulating materials. **Zone 1**: optical detection can be applied, **Zone 2**: electrical, optical and acoustical detection can be used. *Carrier detection* (i.e. electrical charge distributions) can be measured only in the laboratory experiment but cannot be measured in the field test

A possible mechanism as to how and why light emission occurs when AC high voltage is applied to the polymer is shown in Figure 3.22 [102]. A polymeric insulation can be represented by the band-gap model where E_{con} stands for the conduction band and E_{val} stands for the valence band. An insulator such as XLPE has a wide band gap > 8 eV [104]. Due to imperfections, crystalline amorphous boundaries, additives etc., there are many states in the band gap. Antioxidants and the complex products that are formed by reactions with oxygen during processing of the polymer provide non-volatile species which also act as trapping centers [105]. The various trapping states can be represented as shallow and deep traps below the conduction band for electrons and shallow and deep traps above the valence band for holes. In polyethylene the shallow traps are due to physical defects such as molecular weight distribution and conformational defects in the amorphous phase. The deep traps are associated with defects such as chain branching, chain ends, chemical irregularities, additives and crosslinking by-products [102].

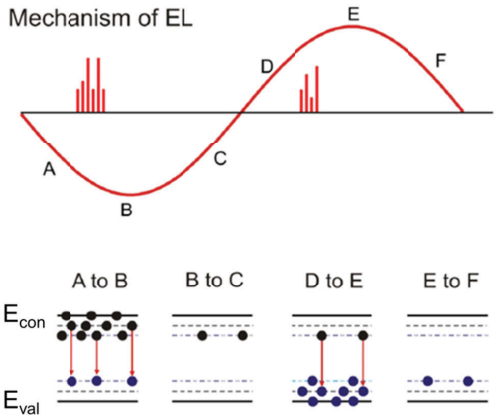

Figure 3.22: Mechanism of EL during each cycle of the AC voltage [102]

When AC voltage is applied to the specimen, during the negative half cycle, at a certain threshold voltage level denoted by A in Figure 3.22, electrons are injected into the polymer. These electrons get trapped in the shallow and deep traps of the polymer. Some of these electrons recombine with the holes, which were injected into the polymer during the previous positive half cycle and which could not de-trap when the polarity is reversed. Holes are produced by removal of electrons that form neutral states involved in the covalent bonding of the polymer. The recombination of the electrons and the holes gives rise to light emission [105]. During the portion B to C of the negative half cycle the electrons in the shallow traps de-trap but those in the deep traps remain trapped.

When the polarity reverses, above a certain threshold voltage level denoted by D, holes are injected into the polymer and are trapped in the shallow and deep traps of the polymer. Some of these holes will recombine with the electrons in the deep electron traps of the polymer and light is again emitted. When the voltage decreases from E to F the holes in the shallow traps will de-trap but those in the deep traps cannot do so they remain in the insulation. Some of these trapped holes will recombine with the electrons emitted during the next negative half-cycle to give rise to EL. This process is repeated every cycle of the AC voltage and since the light is caused by the application of a high electric field, this phenomenon of light emission is called electroluminescence.

It has been argued that EL emission can be caused by hot electrons. Hot electron emission was proposed [106] for fields greater than 60 % of the breakdown value of the polymer. Other than this opinion, it is important to note that, light emission can be caused by other sources such as partial discharges, surface plasmons, thermoluminescence etc. [102].

3.4.4 Deterministic models of breakdown in polymeric materials

Breakdown in polymeric insulations is always ‘catastrophic’ in the sense that it is irreversible and destructive resulting in a narrow breakdown channel between the electrodes [78]. All catastrophic breakdowns in polymeric insulations are electrically power driven and ultimately thermal in the sense that the discharge track involves at least the melting and probably carbonization or vaporization of the dielectric. Deterministic models of breakdown can therefore be categorized according to the processes leading up to its final breakdown

stage, which is subdivided into: electric, thermal, electromechanical (introduced in section 3.3.3), and partial discharge breakdowns.

1) Electric breakdown in polymeric materials

The main classical models of electron-driven breakdown in polymeric materials include [78]:

a) Avalanche breakdown due to field-induced impact ionization. A high energy electron collides with a bound electron and thereby produces a pair of free electrons which can acquire sufficient energy in the presence of high field to produce two more pairs of free electrons. The density of free electrons rapidly increases in this process and the avalanche can lead to a very high local energy dissipation causing local lattice disruption after a sufficient number of generations. Two parts of avalanche breakdown are described: firstly, the number of generations of ionizing collisions required to cause damage must be estimated, and secondly, the corresponding field must be evaluated.

b) Intrinsic breakdown due to the transfer of the energy of free electrons to the lattice so as to increase the lattice temperature to a critical value. A recent paper [107] presents a percolation model for intrinsic breakdown in insulating polymers. The model starts with the premise that charges are present in the polymers in traps with a variable range of trap depth. It is shown that the trap barrier can decrease to zero for a set of sites forming a 3-D percolation cluster when the field becomes high enough. This will result in an abrupt increase in charge mobility and electron mean free path, and an irreversible breakdown via current multiplication and impact ionization is possible.

c) Zener breakdown associating with the direct excitation from valence to conduction band. It is nondestructive breakdown in semiconductor, occurring when the electric field across the barrier region becomes high enough to produce a form of field emission that suddenly increases the number of carriers in this region.

2) Thermal breakdown in polymeric materials

In thermal breakdown models [23, 78], electrical power dissipation causes heating up of at least a part of the polymeric insulation to temperatures above a critical temperature, which results directly or indirectly in catastrophic failure. The general power balance equation governing thermal breakdown is:

$$\frac{dT}{dt} = \frac{1}{\rho C_{\mathrm{h}}}(\sigma E^2 + K\nabla^2 T)\,, \tag{3.23}$$

where C_{h} is the specific heat of the polymer dielectric; ρ is the density of dielectric; σ is the electrical conductivity; E is the electric field; and K is the thermal conductivity.

Assuming that there is a solution such that $dT = dt = 0$; below the critical temperature, thermal breakdown will not take place. This general equation can be transferred to different forms for different thermal conditions. If thermal equilibrium is assumed ($dT = dt = 0$), the general equation simplifies to

$$\sigma(T, E)E^2 + K\nabla^2 T = 0\,. \tag{3.24}$$

This is called steady-state breakdown, which is a limiting case where the heat generated by the applied electrical stress is in balance with the thermal dissipation. In case of temperature rise is so slow that the thermal capacity term can be ignored.

The opposite extreme is impulse breakdown, in which the temperature rise can be considered to be so fast that thermal conductivity may be ignored. This simplifies the analysis as the temperature of the whole slab can always be considered uniform. In this case the insulator is considered to break down at the end of the impulse, i.e. the time to breakdown is the length of the impulse. The general equation therefore becomes:

$$\rho C_{\mathrm{v}} \frac{dT}{dt} = \sigma(T,E)E^2 , \tag{3.25}$$

where C_{v} is the thermal capacity of the polymeric dielectric material at constant volume.

Breakdown does not usually occur on a broad front across the insulation area but at weak points. The temperature of a weak spot reaches the critical temperature before the rest of the insulation. Such behaviour is difficult to analyse in a general manner as different assumptions give rise to a wide variety of boundary conditions. Filamentary thermal breakdown can be applied in this case, which is illustrated with reference to specific experimental results. Two experimental methods have been used to investigate filamentary breakdown: pre-breakdown current measurement and direct observation of the spatial and temporal evolution of specimen temperature. Based on result for the pre-breakdown current on several small-area specimens, the general equation above is rearranged to

$$\frac{1}{\sigma_0}\int_T^{\infty} \exp\left(\frac{\tau}{\mathrm{k}T}\right) = \frac{E^2}{\rho C_{\mathrm{v}}}\int_t^{t_{\mathrm{b}}} dt \tag{3.26}$$

where σ_0 and τ are experimentally determined values which are found to be constant over a given range of temperature; ρ is the density; t_{b} is the time of breakdown; and k is the Boltzmann's constant.

Various attempts have been made to monitor the spatial and temporal evolution of the temperature of thin polymer films after the application to an electric field. Although existence of hot spots has been proved [78], it has not yet conclusively demonstrated that the initiating breakdown mechanism is thermal.

3) Partial discharge breakdown

In partial discharge (PD) breakdown [78], sparks occur within voids in the insulation causing degradation of the void walls and progressive deterioration of the dielectric. It is difficult to eliminate voids in polymeric materials [105, 108]. They may result simply from non-uniform contraction produced in the slow chemical reactions of thermosetting occurring after the main manufacturing process.

The influencing parameters in the initiation and the propagation of PD are numerous. For example, the temperature gradient changes the volume conductivity of the insulating material and affects the discharge location. It is stated in [109] that inception discharge voltage decreases with gas pressure in the cavity if its depth is larger than 6 μm, which corresponds to the Paschen minimum [23, 74]. For smaller cavities, the decrease of pressure arises in a very short time and it can consider that the inception discharge voltage increases

rapidly and the repetition rate may decrease. The nature of the material plays a role on the equilibrium process following the increase of pressure, since the diffusion of gaseous products into the bulk polymer leads to a decrease of pressure within the cavity. The partial discharges break the bonds of the polymer to give rise to hydrogen and carbon and the evolution of hydrogen gas and carbon dioxide [109]. The chemical reactions caused by the interaction between PD and solid dielectric are complicated processes. The evolution of the chemical by-products (i.e. gaseous, liquid and solid by-products) from the start of PD activity is accelerated insulation aging and leads to ultimate failure.

3.5 Partial discharges

Partial discharge (PD) is defined as localised discharge process, in which the distance between conductors is only partially bridged, i.e. the insulation between the electrodes is partially punctured. Partial discharges may originate directly at one of the electrodes or occur in a cavity in the dielectric. In general, PDs are restricted to a part of the dielectric materials used, and thus only partially bridging the electrodes between which the voltage is applied. Various types of partial discharge phenomena are shown in Figure 3.23.

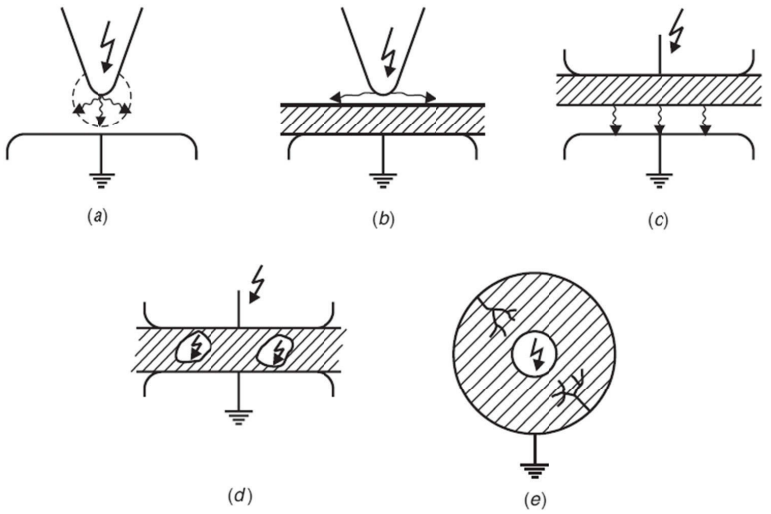

Figure 3.23: Various partial discharge phenomena

The term "*partial discharge*" includes a wide group of discharge phenomena:

i) Corona or gas discharge; this occurs due to a non-uniform field on sharp edges of the conductor subjected to high voltage especially when the insulation provided is air or gas as shown in Fig. 3.23 (a);

ii) Surface discharges and discharges in laminated materials on the interfaces of different dielectric material such as gas/solid interface as gas; they get overstressed ε_r times the stress on the solid material (where ε_r is the relative permittivity of solid material) and ionization of gas results as shown in Fig. 3.23 (b) and (c);

iii) Cavity discharges (Fig. 3.23 (d)), when cavities are formed in solid or liquid insulating materials; the gas in the cavity is overstressed and discharges are formed;

iv) Treeing Channels; high intensity fields are produced in an insulating material at its sharp edges and this deteriorates the insulating material. The continuous partial discharges so produced are known as Treeing Channels in Fig. 3.23 (e).

The importance of partial discharges for the life of insulation has long been recognized. Every discharge event causes a deterioration of the material by the energy impact of high energy electrons or accelerated ions, causing chemical transformations of many types. It is also obvious that the actual deterioration is dependent upon the material used. Corona discharges in air will have no influence on the life expectancy of an overhead line; but PDs within a polymeric dielectric (e.g. PE, silicone rubbers) may cause breakdown within a few days. It is still the aim of many investigations to relate partial discharge to the lifetime of specified materials. Such a quantitatively defined relationship is, however, difficult to ensure. PD measurements have nevertheless gained great importance during the last five decades and a large number of publications are concerned with either the measuring techniques involved or the deterioration effects of the insulation.

The detection and measurement of discharges is based on the exchange of energy taking place during the discharges. These exchanges are manifested as [110-114]:

i) electrical pulse currents (with some exceptions, i.e. some types of glow discharges);

ii) dielectric losses;

iii) electromagnetic (EM) radiation (i.e. light emitted);

iv) sounds (i.e. noise, acoustic wave);

v) increased gas pressure; chemical reactions.

Therefore discharge detection and measuring techniques may be based on the observation of any of the above phenomena. The oldest and simplest method relies on listening to the acoustic noise from the discharge, the '*hissing test*' [23]. The sensitivity is, however, often low and difficulties arise in distinguishing between discharges and extraneous noise sources, particularly when tests are carried out on factory premises. The use of optical techniques is limited to discharges within transparent media and thus not applicable in most cases [115]. Only modern acoustical detection methods utilizing ultrasonic transducers can successfully be used to localize the discharges [116-119]. Summaries of older methods can be found in the book of Kreuger [120]. More recent developments may be found in [15-18, 68].

However, the light caused by partial discharges (PDs) is different from the light of electroluminescence (EL), which occurs prior to tree inception [102]. EL emission occurs continuously above a certain threshold voltage and will only stop when the voltage is reduced below that level. On the other hand, PD can occur inside a micro-cavity or a tree channel and can be intermittent depending on the gas pressure in the cavity or the tree channel. Also, the intensity of EL is at least two orders of magnitude smaller than the intensity of the light generated by very small (<1 pC) partial discharges. The phase relationship of the light of EL and PD is also different with respect to the applied voltage. These criteria should be used to differentiate between the light of PD and that due to EL.

The most frequently used and established detection methods (conventional methods) are the electrical ones, to which the new IEC Standard is also related [110]. These methods aim to separate the impulse currents linked with partial discharges from any other phenomena. The adequate application of different PD detectors which became now quite well

defined and standardized, pre-supposes a fundamental knowledge about the electrical phenomena within the test samples and the test circuits. However, non-conventional methods for PD measurement can be found in the report [121] and these techniques will be standardized in the near future by IEC 62478. Different non-conventional PD detection methods and their specific features are summarized in Table 3.1. Even though the conventional and non-conventional method measure different physical quantities, there has been some research regarding comparison and correlation of their measurement results. Those studies include the PD pattern, linearity of measuring quantity [122-123]. However so far, finding solid correlation between the two methods seems to be very difficult due to the fact that the results from both methods largely depend on the condition, sensor type, sensor location, manufacturer of test object, test engineer and so on. Some questions have arisen regarding the correlation between the two different methods and interpretation of results [121]. The general comparison is shown below in Table 3.2.

Table 3.1: The specific features of non-conventional PD detection methods

	Electrical	**Acoustical**	**Optical**	**Chemical**
Advantage	• Applicable for all kinds of HV equipment • Intensity, source, type, location of PD is assessable • Most suitable for continuous on-line PD monitoring	• High sensitivity • Immunity against electrical noise • Very efficient for localization of PD • Relatively low cost	• Immunity against electrical noise • High sensitivity • Location of PD is assessable (in some case) • Test is possible for impulse voltage condition	• Immunity against electrical noise • Easy to measure • Provide critical information for Go/No Go decision
Disadvantage	• High electromagnetic interference • Relative expensive	• Low signal intensity • Not good for continuous PD measurement	• No information about magnitude of PD • Night vision needed	• No information about location, source, intensity, and type of PD
Possible Sensors	• Capacitive • Inductive	• Piezo-electric transducers • Condenser microphones • Acousto-optic sensors based on interferometric methods	• Optical fibre • Fluorescent fibre • Fluorescent probe • UV detector • Photomultiplier tube	• DGA[1)] Sensors • SF_6 Sensors
Main applicative area	• All HV equipment	• Transformer • GIS • Cable accessories	• Cables and their accessories, • GIS • Transformer	• Transformer • GIS • Cables

Note:

[1)] DGA – Dissolved Gas Analysis method, it is a technology for essential on-line monitoring of transformer oil.

Table 3.2: Comparison of conventional and non-conventional methods

	Conventional	Non-conventional
Main Standard	IEC 60270	IEC 62478 (will be standardized in the near future)
Sensor type	• Measuring impedance (the sensor for conventional method can be capacitive, inductive-HFCT or Rogowski coil)	• Electric sensors • Acoustic sensors • Optical Sensors • Chemical Sensors
Frequency band	• Wide band (30 kHz to 500 kHz) or Δf = 100 kHz to 400 kHz • Narrow band (50 kHz to 1MHz) or Δf = 9 kHz to 30 kHz	• HF (3 MHz to 30 MHz)[a] • VHF (30 MHz to 300 MHz)[b] • UHF (300 MHz to 3 GHz)[c] • AE (20 kHz to 250 kHz, and 100 Hz to 3 kHz)
Calibration	• Must be calibrated	• Sensitivity check • Performance check
Measuring unit	• Usually pC, μV	• Amps, mV, V/mm or dB
Measuring quantity	• Apparent charge	• Transient earth voltage or current pulse (Electromagnetic wave) • Acoustic, Chemical by products, Optical spectrum
Measuring system	• Coupling device, transmission system, measuring instrument	• Sensing components, transmission path, data acquisition unit
Noise Level	• Relatively high	• Relatively low
Application type	• Mostly Off-line (Laboratory, On-site) • On-line (Transformer)	• Off-line and on-line • On-line (Electrical, Chemical)

Note:

a: Typical narrow band width for HF/VHF is 2 MHz

b: Typical wide band range is 50 MHz or higher

c: Zero span mode for individual frequencies or for specific frequency range between 4 MHz and 6 MHz or higher

3.6 Dielectric polarisation and permittivity

The primary role of electrical insulation is to maintain a continuous and specified value of dielectric permittivity over a specified electromagnetic field, in order to resist current flow between conductors. Due to the presence of insulating medium, the capacitance is increased by a factor of the dielectric permittivity ε. The increase in capacitance is attributed with polarisation of the dielectrics where charge distribution is distorted by the applied electrical field.

3.6.1 Polarisation mechanisms

Due to the various kinds of charge carriers existing within dielectric materials which are able to be displaced and polarized by an electric field, there are several types of polarisation mechanisms that tend to dominate certain frequency ranges. When an external electric field is applied, the charge distribution realign in materials. This phenomenon is called dielectric polarisation or polarisation. Polarisation arises due to the existence of atomic and molecular forces, and appears whenever charges in a material are somewhat displaced with respect to one another under the influence of an electric field. The number of charges per unit of volume multiplied by the average displacement is the polarizability of the dielectric. The magnitude of polarizability of a material is reflected by the dielectric constant. Four basic kinds of polarisation mechanisms are illustrated in Figure 3.24.

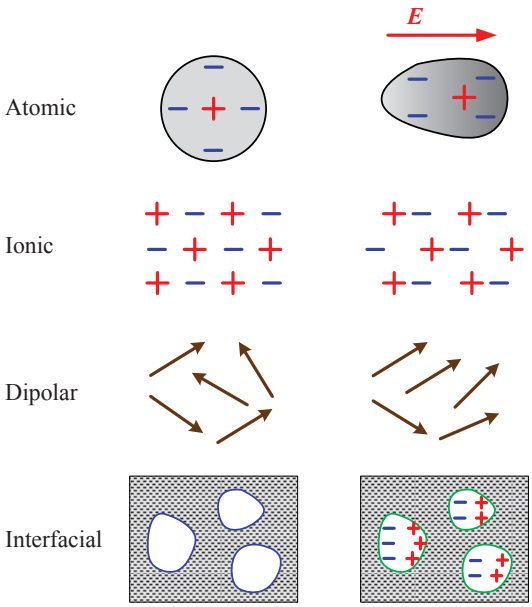

Figure 3.24: Mechanisms of dielectric polarisation

From Figure 3.24, four basic kinds of polarisation mechanisms are:

i) *Atomic (electronic) polarisation* results from shift of the electron clouds within each atom due to application of an electric field. This type of polarisation is quite small compared with the polarisation due to the valence

electrons in the covalent bonds within the solid dielectrics. This polarisation is evident in most materials.

ii) *Ionic polarisation* occurs in ionic crystals, which have distinctly identified ions located at well-defined lattice sites. Each pair of oppositely charged neighboring ions has a dipole moment in the presence of an electrical field.

iii) *Dipolar (orientational) polarisation* is a phenomenon involving rotation of permanent dipoles under an applied field. Dipolar polarisation is more common in polymers, which permit re-orientation by virtue of their atomic structure. This mechanism of permanent dipoles is different from that of induced dipoles of ionic polarisation. This polarisation loses the response to electric fields at the lowest frequency in polarisations because the rotation is not instantaneous.

iv) *Interfacial (space charge or diffusional) polarisation* occurs whenever there is an accumulation of charge at an interface between two different materials or between regions within a material. A typical interfacial polarisation is the trapping of electrons or holes at defects at a crystal surface, at the interface of crystal and the electrode. Dipoles between the trapped charges can increase the polarisation vector. Interfaces also arise in heterogeneous dielectric materials, such as semi-crystalline polymers.

Polarisation is responsible for the refractive index and dielectric constant of materials. If there is no polarisation, the refractive index and dielectric constant are unity. This occurs only with a vacuum. The magnitude of each type of polarisation depends primarily on the density of the participating species and the resistance against motion presented by the medium in the case of ionic-interfacial and dipolar types. In general, a dielectric medium exhibits more than one polarisation mechanism. Thus, the average induced dipole moment per molecule will be the sum of all polarisation contributions depending on which that determines the dielectric permittivity of the material.

Atomic-ionic polarisation is the predominant form of polarisation in inorganic crystals, glasses and ceramics. It is the principle contributing mechanism to their dielectric constant at a uniform level up to infrared frequencies [124]. A special form of this polarisation, namely "*ferroelectric*" (where polarisation occurs collectively in domains), results in very high effective dielectric constants, in analogy to ferromagnetic polarisation. The high dielectric constant titanate ceramics are examples of this. Dipolar polarisation occurs from DC up to microwave frequencies, depending on the presence of dipolar molecules and the resistance to molecular rotation presented by the material's internal structure. Interfacial polarisation, involving a longer range ion movement, is observed usually only at lower frequencies [124].

3.6.2 Dielectric permittivity

In the presence of an electric field $\boldsymbol{E}$ originally equal by distributed positive and negative charges ($\pm q$) in dielectrics are displaced from their equilibrium positions to form local electric dipoles; the dielectric is said to be polarized. According to the principle of superposition, this distorted charge distribution is equivalent to the original distribution plus a dipole moment $\boldsymbol{p}$ is

$$\boldsymbol{p} = q\boldsymbol{d}\,, \tag{3.27}$$

where $\boldsymbol{d}$ is the distance vector from charge *-q* to *+q* of the dipole. The total dipole moment $\boldsymbol{p}_{\mathrm{t}}$ of a material is obtained by summation the dipole moments of all the orientational polarisation dipoles, each of which is represented by Equation (3.27). For a volume Δv where there are N_{d} electric dipoles per unit of volume, or a total of $N\Delta v$ electric dipoles, we can write that

$$\boldsymbol{p}_{\mathrm{t}} = \sum_{i=1}^{N_{\mathrm{d}}\Delta v} d\boldsymbol{p}_i \,. \tag{3.28}$$

The *electric polarisation vector* $\boldsymbol{P}$ can then be defined as the *dipole moment per unit of volume* and is given by

$$\boldsymbol{P} = \lim_{\Delta v \to 0}\left[\frac{1}{\Delta v}\boldsymbol{p}_t\right] = \lim_{\Delta v \to 0}\left[\frac{1}{\Delta v}\sum_{i=1}^{N\Delta v} d\boldsymbol{p}_i\right] \quad \left(\frac{\mathrm{C}}{\mathrm{m}^2}\right). \tag{3.29}$$

When all dipoles are aligned in the same direction, the electric polarisation vector can be written, as

$$\boldsymbol{P} = N_{\mathrm{d}}\boldsymbol{p}_{\mathrm{av}} \,, \tag{3.30}$$

where $\boldsymbol{p}_{\mathrm{av}}$ is the average electric dipole moment per polarized entity (e.g. molecule, ion, etc.), with N_{d} of those per unit of volume.

Whereas the applied electric field $\boldsymbol{E}$ maintains its value, the electric flux density inside the dielectric material differs from what would exist were the dielectric material replaced by free-space. In the free-space part of the parallel capacitive electrodes where the electric field is applied, the electric flux density $\boldsymbol{D}_0$ is given by

$$\boldsymbol{D}_0 = \varepsilon_0 \boldsymbol{E} \,, \tag{3.31}$$

where ε_0 is the permittivity of free-space. In the dielectric portion, the electric flux density $\boldsymbol{D}$ is related to that in free space $\boldsymbol{D}_0$ by

$$\boldsymbol{D} = \varepsilon_0 \boldsymbol{E} + \boldsymbol{P} \,. \tag{3.32}$$

The electric flux density $\boldsymbol{D}$ can also be related to the applied electric field intensity $\boldsymbol{E}$ by the static permittivity ε of the dielectric materials. In this thesis, however, ε is considered as a scalar. So that,

$$\boldsymbol{D} = \varepsilon \boldsymbol{E} \,. \tag{3.33}$$

It is apparent that $\boldsymbol{P}$ can be related to $\boldsymbol{E}$ by another parameter, χ, which is called "*electric susceptibility*" (dimensionless quantity). The dielectric susceptibility (χ) of a material measures the extent of polarisation $\boldsymbol{P}$ within the dielectric in response to an external electric field $\boldsymbol{E}$. This relationship is represented in vector form as follows:

$$\boldsymbol{P} = \varepsilon_0 \chi \boldsymbol{E} \tag{3.34}$$

Finally, from equations (3.32), (3.33) and (3.34) we can write that

$$\boldsymbol{D} = \varepsilon_0 \boldsymbol{E} + \varepsilon_0 \chi \boldsymbol{E} = \varepsilon_0 (1 + \chi) \boldsymbol{E} = \varepsilon \boldsymbol{E} \ . \tag{3.35}$$

The relative value of ε and ε_r is given by

$$\varepsilon_r = \frac{\varepsilon}{\varepsilon_0} = 1 + \chi \ , \tag{3.36}$$

where ε_r is the relative permittivity of dielectric materials.

Traditionally, it is also called the dielectric constant, because in the linear regime it is independent of the field strength. However, it can be a function of many other variables. For example, for time variable fields it is dependent on the frequency of the applied electric field, sample temperature, sample density (or pressure applied to the sample), sample chemical composition. In free- space, the susceptibility is zero ($\chi = 0$) so that $\varepsilon_r = 1$ and the permittivity is that of free-space $\varepsilon = \varepsilon_0$. The relative permittivity is a parameter that indicates the relative charge storage (energy storage) capability of dielectric materials compared with those in free-space. The larger its value, the greater its ability to store charge (energy).

3.6.3 Complex permittivity and dielectric loss ($\tan \delta$)

The static permittivity is an effect of polarisation under DC conditions. However, if a sinusoidal electrical field is applied, the polarisation of the medium under these AC conditions differs from that of the static case. Polarisation of a dielectric always fails to respond instantaneously to variations of an applied field due to thermal agitations which randomizes the dipole orientations and rotation of molecules in a viscous medium by virtue of their interactions with neighbours. This response of dielectric materials to external fields depends on the frequency of the field, which can be represented by a phase difference. Consequently, dielectric permittivity is often treated as a complex function of the frequency of the applied field:

$$D_0 e^{-j\omega t} = \hat{\varepsilon}(\omega) E_0 e^{-j\omega t} \ , \tag{3.37}$$

where D_0 and E_0 are the amplitudes of the displacement and electrical field, ω is the angular frequency of the electromagnetic field, t is time and j is the imaginary unit, respectively. By convention, we always write the *relative complex permittivity* of the materials as

$$\varepsilon_r = \frac{\varepsilon}{\varepsilon_0} = \varepsilon_r' - j\varepsilon_r'' \ , \tag{3.38}$$

where ε_r' is the real part of dielectric constant (or the common relative permittivity) of the material and ε_r'' is imaginary part of dielectric constant. The real part of dielectric constant represents the capacitive behaviour or polarizability of the dielectric material, while the imaginary part represents the energy losses due to polarisation and conduction.

For linear dielectric response, the relation between the real and imaginary parts of the *relative complex permittivity* is expressed by the Kramers-Kronig relations [125],

$$\varepsilon_r'(\omega) = 1 + \frac{2}{\pi} \int_0^\infty \frac{\omega' \varepsilon_r''(\omega')}{(\omega')^2 - \omega^2} d\omega' \quad \text{and} \tag{3.39a}$$

$$\varepsilon_r''(\omega) = \frac{2\omega}{\pi}\int_0^{\infty}\frac{1-\varepsilon_r'(\omega')}{(\omega')^2-\omega^2}d\omega' \quad . \tag{3.39b}$$

The general features of the frequency dependence of the real and imaginary parts of permittivity for the four polarisation mechanisms are illustrated in Figure 3.25. Although it shows distinctive peaks in ε_r'' and transition features in ε_r', in real materials these peaks and various features are often broader. For polycrystalline materials, glasses, plastics and some crystals (e.g. with cubic crystallographic structure) all diagonal elements become identical and the complex permittivity becomes a scalar quantity [126].

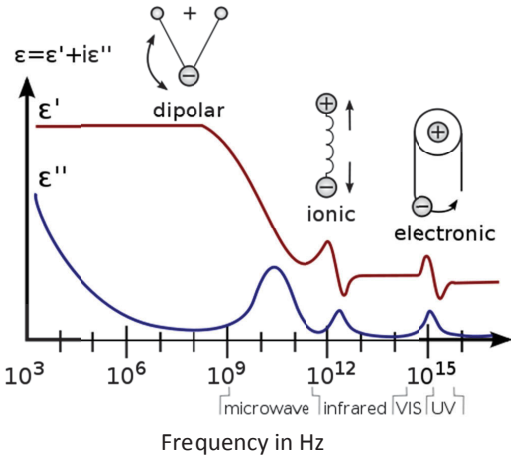

Figure 3.25: Dielectric permittivity spectrum over a wide range of frequencies; ε′ and ε″ denote the real and the imaginary part of the permittivity. Various polarisation mechanisms are labelled on the image

When an alternating electric field is applied, a polarisation is produced. That polarisation can be measured in terms of capacitance. Measuring the dielectric constant, a basic understanding of capacitance theory is beneficial. Capacitance C is defined as the ability of two electrodes to store a charge Q when a potential V is applied across them. If the region between the two parallel electrodes is a vacuum at parallel plate capacitor, then the capacitance C_0 is

$$C_0 = \frac{Q}{V} = \varepsilon_0\frac{A}{d} \ , \tag{3.40}$$

where ε_0 is the permittivity of free space, A is the area of the electrodes and d is the distance between the two electrodes.

If a material with a permittivity of ε is inserted between the plates, the capacitance is given by:

$$C = \varepsilon\frac{A}{d} = C_0\frac{\varepsilon}{\varepsilon_0} = C_0\varepsilon_r \ . \tag{3.41}$$

The ε_r of the material that is a real part of the relative complex permittivity ($\varepsilon_r = \varepsilon_r'$) and is defined as the ratio of the permittivity of the material to the permittivity of free-space and dimensionless [127].

If there is some energy dissipation mechanism inherent in a capacitor, there will be a loss current I_1 that lags the charging current I_c and is separated from the charging current by a loss angle δ. Dissipation factor (DF) or *dielectric loss* (tan δ) factor can be expressed by the ratio of loss current to charging current as shown in Equation (3.42).

$$DF = \tan\delta = \frac{I_1}{I_c} = \frac{\varepsilon_r''}{\varepsilon_r'} = \frac{1}{\omega R_p C_p} \tag{3.42}$$

where $\omega = 2\pi f$, R_p is resistance (in Ω) and C_p is capacitance (in F) in the equivalent parallel circuit as shown in Figure 3.26, which is defined by IEC 60250 standard [127]. The parallel representation of an insulating material having a dielectric loss is usually the more proper representation (Figure 3.26 a)), while it is always possible and occasionally desirable to represent a capacitor at a single frequency by a capacitance C_s in series with a resistance R_s (Figure 3.26 b)).

Therefore the imaginary part of the complex permittivity can be written as

$$\varepsilon_r'' = \varepsilon_r' \tan\delta = \frac{\varepsilon_r'}{\omega R_p C_p}. \tag{3.43}$$

By measuring the real and imaginary parts of the dielectric constant for frequency, the dielectric behaviour of a material could give information on the characteristics of the material.

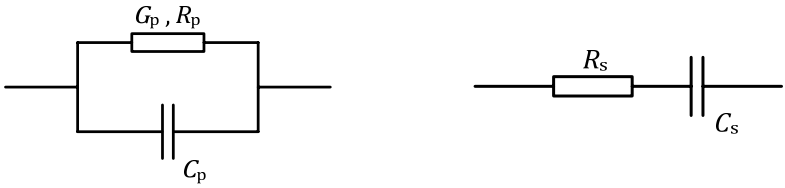

$$\tan\delta = \frac{1}{\omega C_p R_p} = \frac{G_p}{\omega C_p} \qquad \tan\delta = \omega C_s R_s$$

a) Equivalent parallel circuit *b) Equivalent series circuit*

Figure 3.26: A capacitor with losses can be represented at any given frequency either by capacitance C_s and resistance R_s in series, or by capacitance C_p and resistance R_p (or conductance G_p) in parallel

The dielectric loss (tan δ) of any material describes quantitatively dissipation of the electric energy due to different physical processes such as electrical conduction, dielectric relaxation or polarisation, dielectric resonance and loss from nonlinear processes (such as hysteresis) [126]. When we measure the loss of a dielectric at a single frequency we cannot, in general, distinguish between them. Phenomenologically, they all give rise to just one

measurable quantity, namely, the total measured loss tangent. As only a few materials, such as fused silica, polystyrene, or polyethylene, have ε_r and tan δ practically constant over the wide frequency range through which dielectric materials are used for technical purposes, it is necessary to measure the dielectric loss factor and the permittivity at those frequencies at which the dielectric material will be used [127].

3.6.4 Factors influencing dielectric properties

Frequency *f*: Changes in permittivity and in dielectric loss factor are produced by the dielectric polarisation and conductivity. The most important changes are caused by diploe polarization due to polar molecular and interfacial polarization caused by inhomogeneities in the material.

Temperature *T*: The loss index may show a maximum at a frequency which depends upon the temperature of the dielectric material. The temperature coefficients of dielectric loss factor and permittivity can be positive or negative depending on the position of the loss index maximum with respect to the measuring temperature.

Field strength ***E***: When interfacial polarization exists, the number of free ions increases with the field strength, and the magnitude and the position of the loss index maximum is altered (only in the low frequency range).

Moisture: The degree of polarization is increased by absorption of water or by the formation of a water film on the surface of the dielectric material, thus raising the permittivity, the dielectric loss factor and the DC conductivity. Conditioning of test specimens is, therefore, of decisive importance and control of the moisture content, both before and during testing, is imperative if test results are to be interpreted correctly. Therefore, the moisture content in the test chamber must be kept constant for all experiments.

4 Development of the breakdown test facility for silicone rubbers

Silicone rubbers have been extensively used as electrical insulation in power cable accessories (i.e. joints and terminations) and silicone insulators for power lines because of their excellent electrical and mechanical capabilities, chemical stability over a wide range of temperatures, hydrophobic nature, flexibility, easy handling and easy application. These advantages can result in lower assembly and maintenance costs whilst being economically attractive. Silicones make good elastomers because the backbone chain is very flexible. The bonds between a silicon atom and the two oxygen atoms attached to it are very flexible. The inorganic siloxane backbone is the most available flexible polymer backbone. The increasing ease of engineering polymers with selected additives makes silicone polymers an ideal basis for the development of novel dielectric materials with specific properties for application in high-voltage engineering. One of the most common concerns in industry is the reliability of materials. The breakdown field strength or dielectric strength E_b value of dielectric materials is a key of interest for the current state of dielectric application where an electric field stress is present. In most cases, the dielectric strength of an insulation material is the determining factor when characterizing it for use in high-voltage facilities. Thus, in order to expand the application to higher voltages, the study of breakdown of silicone dielectrics is extremely important in industrial applications as well as in material research laboratories. The increasing demands for the modification of silicone polymers for high-voltage insulation require the investigation of the dielectric strength value of the modified material. These investigations require a large number of breakdown tests. The use of a complicated testing methodology causes widely scattered breakdown data points that affect the accuracy of the measured results. The lack of accurate data on dielectric strength could lead to design shortcomings: excessive insulation could lead to more expensive equipment, while inadequate insulation could lead to premature failure. Therefore the appropriate testing method should be considered in order to match technical and economic demands. This chapter deals with the development of a new methodology to measure dielectric strength of silicone rubbers.

4.1 State-of-the-art review of dielectric breakdown testing methods for silicone rubbers

It is well known that the breakdown voltage of solid material is not a definite value because it is a statistical probability whether the material will fail at a given voltage or electric field stress. When a dielectric strength value is given, it is usually the mean breakdown value of a large number of samples. The dielectric breakdown value of silicone elastomers depends on various parameters such as electrode configuration, preparation processes of the test specimen, impurities or structural defects, type of voltage stress (AC, DC or impulses), voltage rate-of-rise, the stressed volume or thickness of specimens and surrounding medium. Therefore the absolute dielectric strength value is meaningless. Practically, the dielectric breakdown value is measured under the best experimental conditions when all external influences are isolated. A good statistical evaluation of the dielectric breakdown values is obtained when a suitable electrode and a proper specimen are selected for the breakdown test. Likewise, the unknown factors, which are caused by the preparation processes of the test specimen, should be reduced to the minimum.

There is a universal methodology for the measurement of electrical strength of general solid insulating materials at commercial power frequencies. Test procedures for that are described in the IEC 60243-1 standard [24] and ASTM D149 [128]. Because IEC standards are more popular for research and industry in high-voltage engineering, the IEC standard 60243-1 was critically checked. Unfortunately, it does not give recommendations for the measurement of the dielectric strength value of elastomeric materials, i.e. silicone rubbers. Specific recommendations for cast and moulded materials, e.g. fiberglass, thermosets and thermoplastics, are provided in sub-clause 4.1.6 of this standard. Because of missing recommendations for silicone rubbers, often the procedure according to sub-clause 4.6.1 of IEC 60243-1 is used and the sheet specimen with thickness of 1.0 mm ± 0.1 mm is usually selected. Electrode arrangements with unequal- or equal-diameter opposing-cylinders can be applied for dielectric breakdown test. The test arrangements are shown in Figure 4.1 a) and b). The advantage of these test arrangements is their use with a silicone sheet specimen, which can easily be prepared and its quality can be controlled. The setup is typically immersed in a liquid surrounding medium, e.g. silicone oil or insulating oils, to prevent surface discharges around the electrode edges.

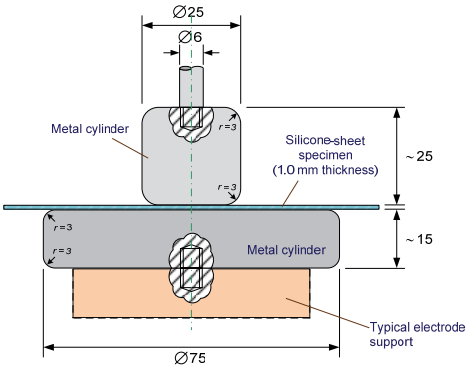

a) Unequal-diameter opposing cylinders (unit: in mm)

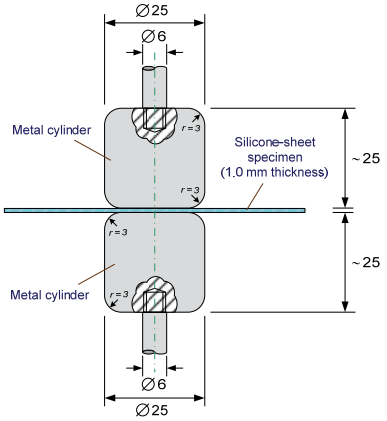

b) Equal-diameter opposing cylinders (unit: in mm)

Figure 4.1: Electrode arrangements for tests on silicone sheet perpendicularly to the surface

For these experiments, it is allowed to use embedded electrodes or cast-in electrodes to avoid discharges around the electrode edges, which may occur before breakdown and cause unwanted stress of the specimen. The metal electrodes shall be maintained smooth, clean and free from defects at all times. The electric field can be considered to be uniform and the breakdown field strength E_b can be calculated from $E_b = V_b/d$, where V_b the electrical breakdown voltage under the prescribed conditions and d the thickness of silicone sheet specimen are.

Measurements of the breakdown voltage of the silicone elastomers under AC conditions are usually done under increasing voltage control. The mode of voltage increase shall be selected for the elastomeric material under test, which is recommended in clause 9 of IEC 60243-1 [24]. For short-term breakdown test, the continuously rising voltage with the raise rate of 1 kV/s and the 60 s step-by-step test procedures are typically selected for the determination of dielectric strength of silicone rubbers.

The equal-diameter electrode configuration has the decisive advantage over the unequal-diameter arrangement, of providing a lower stress intensification factor at the edges. The field intensification factor at the edge depends on the radius of curvature at the electrode edges. Therefore for preliminary study, this electrode arrangement was tested to examine the appropriate methodology for the breakdown test of transparent silicone rubbers. The brass electrodes with 25 mm in diameter and 25 mm thick with edges rounded to 3 mm according to the standard IEC 60243-1 were used. The electrodes were embedded into a silicone rubber cube by using a special mould made from brass. The dimensions of test specimen were 80 (L) × 80 (W) × 80 (H) mm^3. The distance between the electrodes was adjusted to 1.0 mm. Example of the test sample is shown Figure 4.2.

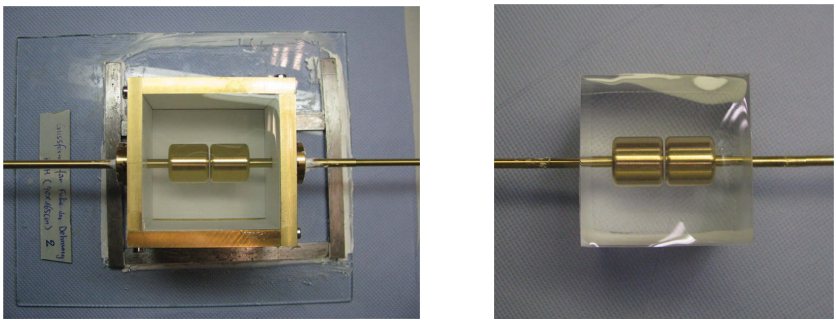

a) Electrodes after casting the mixed silicone *b) Completed test specimen*

Figure 4.2: Test sample embedded with the equal-diameter opposing cylinder electrodes

The sample embedded with the equal-diameter opposing cylinder electrodes can be used for the breakdown voltage test of silicone elastomers. It is easy to fix the electrodes in the mould and to cast the liquid silicone rubber. The curing process typically takes about one hour. It was found that the specific breakdown strength values of silicone rubbers are in the range from 20 kV/mm to 40 kV/mm and depend on variable factors such as sample parameters (e.g. type of silicone rubber under test, molecular structure, degree of cross-linking, micro-voids), electrical stress parameters (e.g. mode of increasing voltage) and electrode parameters (e.g. surface roughness of the electrodes). The test results are consistent with those of other investigations, e.g. [22] and [129]. Unfortunately, this method is not

suitable for routine tests especially for the material research laboratories when a large number of breakdown tests are needed for a good statistical evaluation. It doesn't match the economic reality because the test sample requires a big volume of materials. Moreover, the impact of other parameters usually affecting the breakdown field strength of polymers is also a technical problem. It is difficult to

a) adjust an exact distance between the embedded electrodes,

b) control the quality of the test samples; only one of the test sample can be used for one breakdown test. A good statistical evaluation of the result requires a certain number of samples. The lack of quality control of each sample resulted in a large dispersion of the values because for every test a new sample was needed. In such cases, the use of a simple Weibull statistics does not deliver reliable results because some data points lie outside the upper and lower bounds of 90 % confidence intervals. It is clear that these are due to a breakdown event at an external defect.

c) control the electrode parameters during the test; electrode parameters, i.e. the surface roughness of the electrodes and the removal of sharp edges, influence the breakdown voltage of the material under test and reduce the reliability of the measured results. Non-smooth areas in the electrode surface initiate a location of concentrated electric stress with high and divergent electric field. This electric stress concentration is a result of the redistribution of electric potential field at a sharp protrusion point on the interface between a surface of embedded electrode and silicone specimen. Because of a higher local field gradient, the electric stress at the peaks of the electrode surface profile increases from a base level. Thus, the dielectric breakdown voltage is reduced. On the other hand, a poor removal of sharp edges lead to an increase of the stress intensification factor at the edges, and eventually causes breakdown outside the electrode active surface (see Figure 4.3 a) and b)). After several breakdown tests, the visual examination of the electrodes denotes a local surface deterioration as shown in Figure 4.3 b). In practice, the electrodes require a good polishing process, e.g. electro-polishing technology or sputtering technique, after breakdowns to maintain their surface smooth, clean and free from defects, hence, this is an expensive experiment.

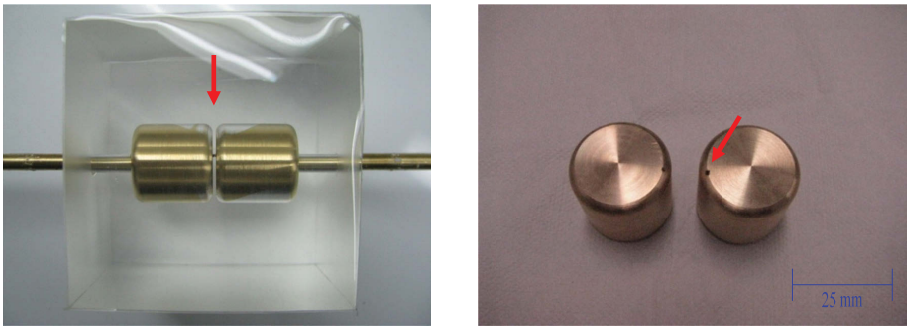

a) Breakdown channel outside the active area *b) Electrode damage at breakdown*

Figure 4.3: Problems with electrodes in dielectric breakdown tests of silicone rubbers

In such cases mentioned above, all the information on the dielectric material itself is lost and a simple Weibull distribution cannot describe the results. Uncontrolled samples or electrode parameters may result in a complete loss of the information for the population being investigated. The information is not generally known, and the analysis is more difficult by the limited number of data points in the low probability regions.

Danikas [19, 21], Österheld [20] and Winter [22] have proposed technical methods to measure dielectric strength of RTV-2 silicones. The AC 50 Hz dielectric strength value of a special grade silicone rubber for electrical insulation has been investigated under different test methodologies and electrical stress conditions. The test methods and results are summarized in Table 4.1. A sketch of the test cells, which were used by them, is illustrated in Figure 4.4.

Table 4.1: Review of E_b measurement techniques for silicone rubbers

	Generally [24, 128-129]	**Winter [22]**	**Österheld [20]**	**Danikas [19, 21]**
Electrode arrangement	IEC 60243-1 (sub-clause 4.1.6)	Hemispherical shaped rod-to-plate (R = 10 mm)	Sphere-to-plate (R = 7 mm)	Rogowski
Test-specimen	Sheet-specimen under surrounding medium	Sheet-specimen embedded	Sheet-specimen embedded	Electrodes embedded
Test thickness d in mm	1.0	1.0	0.5	5, 10 and 20
Cast-in electrode	No	Yes (with 4 electrodes per test cell)	Yes (with 4 electrodes per test cell)	Yes
Mode of voltage increase	IEC 60243-1 (clause 9)	1 kV/s	2 kV/s	5 kV / 6 min
Type of silicone rubber	Typical elastomeric materials	RTV-2	RTV-2 (PowerSil 600)	RTV-2
Approx. E_b in kV/mm	**20 – 40**	**> 100**	**> 100**	**12.8 – 29.3** (depending on the thickness)

Considering the test results and the test cell characteristics that are illustrated in Table 4.1 and Figure 4.4, we cannot compare the results because there are quite different test conditions. For example, considering the same material, the test cells embedded with electrode curvature and very thin thickness show very high breakdown results. On the other hand, test cells embedded with Rogowski's electrodes and higher thickness show very low breakdown results. This is due to the size effect of specimen and the different electric stress conditions.

The test cell with embedded test electrode seems to be usable for measurement of dielectric strength of elastomeric materials because this configuration is similar to the real insulation. Unfortunately, it is very complex in structure. The complicated method for specimen preparation makes, however, a good quality control difficult.

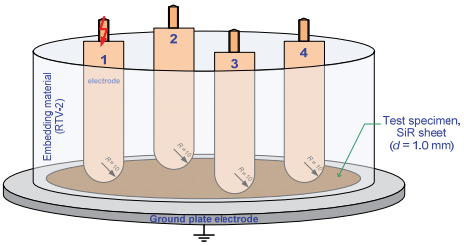

a) Test cell after Winter et al. [22]

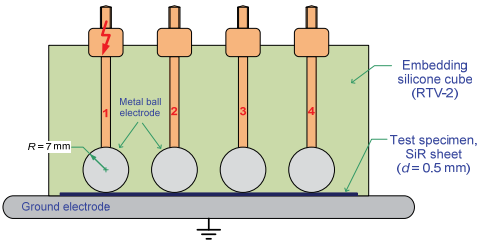

b) Test cell after Österheld [20]

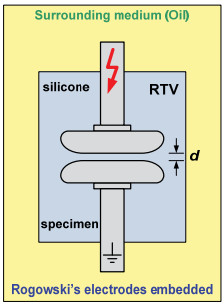

c) Test cell after Danikas et al. [19, 21]

Figure 4.4: Various types of the test cells used for the measurement of dielectric strength in silicone rubbers

The test cell embedded with multi-electrodes requires a big volume of the embedding material as electrical insulation to separate the electrodes during the breakdown test. That is an expensive work. It does not match the economic reality because it is waste of materials, particularly when a large number of breakdown tests are needed for a good statistical evaluation. There are time-consuming steps at every stage of the process. Moreover, this technique is not applicable for highly viscous silicone rubbers because it requires more complex pre-treatment to get rid of all defects inside, e.g. micro-voids or air bubbles occurring during the cross-linking process. Therefore the preparation process may affect the accuracy of dielectric breakdown measurements. Due to all these reasons, an appropriate and cost-efficient test cell as well as a methodology for breakdown test of silicone rubbers need to be developed to cover issues related to both the technical and economic demands.

From a practical point of view, Rogowski's electrodes provide a uniform electric field in the active region under test but the manufacturing of the Rogowski profile electrodes is difficult and very expensive. While the electrode curvature (e.g. sphere-to-plate and hemispherical shaped rod-to-plate configurations) permits a single well-defined point of maximum field at the centre, away from it, the field intensity is gradually reduced. For sufficiently large sphere radius and small gap the approximation of the field lines can be considered as a uniform electric field (see chapter 3.2) and the magnitude of the electric field strength is defined in terms of $E = V/d$. The electrode has more advantage than the opposing cylinders arrangement (Fig. 4.1) for the dielectric breakdown test of elastomeric materials, because it is easy to maintain their surface smooth, clean and free from defects. These can reduce the influence of electrode parameters on the breakdown data. Moreover, it does not require an extensive polishing process so that the maintenance costs can be held low.

4.2 Steps in test cell construction for dielectric breakdown test of silicone rubbers

Because the IEC standard 60243-1 [24] does not define the specific test method for the determination of the short-time dielectric strength value of elastomeric materials, and current approaches do not provide the solution to meet the current challenge, especially, when a large number of breakdown tests are needed, different types of the test cells based on sphere-to-plate electrode configuration have been constructed and investigated. Going this way, the appropriate approach for the AC dielectric strength measurement of silicone elastomers could be found. Important steps on this way are briefly described below.

4.2.1 The test cell configuration with five embedded sphere electrodes

This test cell configuration follows those proposed by Winter *et al.* [22]. But the size of the test cell has been reduced to a reasonable size (about half of its original size) in order to minimize the amount of silicone material. Sphere electrodes were used instead of the hemispherical shaped rod electrodes to reduce the pressure contact caused by the electrode weight. The main concept of this test cell is the reduction of time taken per unit by embedding five electrodes in each preparation process. Well-polished stainless steel balls of 20 mm in diameter were used as sphere electrodes. The electrode arm was made from brass for the high-voltage connection. The specimen (silicone sheet) with a thickness of 0.5 mm (± 0.02 mm) was placed at the bottom of the test cell. The electrodes were mounted in a special insulating holder onto the silicone sheet specimen. The whole configuration was embedded by using a moulded type RTV-2 silicone polymer as shown in Figure 4.5. The breakdown tests were carried out one by one. Five breakdown test results could be obtained from one test cell.

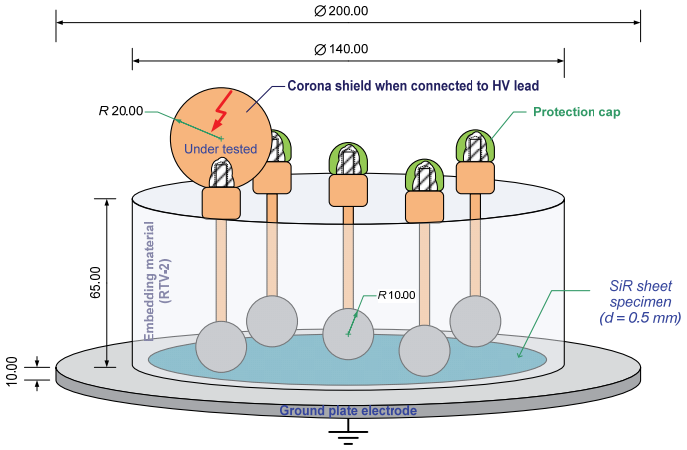

Figure 4.5: The test cell configuration using five embedded sphere electrodes (*unit: in mm*)

Unfortunately, this method is a bit complicated in practice. It is difficult to control the quality of the whole test cell during the preparation process that influences the breakdown test of each specimen in the same test cell. Beside these, there were side effects caused by unwanted electrical stress (capacitive coupling) when high voltage is applied to the electrode under test. In this case, other virgin specimens in the same test cell were damaged. Therefore the sample condition has changed. In such a case, all the information on the dielectric material itself is lost.

4.2.2 The test cell configuration with single embedded sphere electrode

A big test cell has been resized in order to minimize again the volume of embedding material and to reduce the weight of the test cell. The test cell with embedded single sphere electrode has been designed as shown in Figure 4.6. A stainless steel ball was used as sphere electrode and connected to the electrode arm made from brass. The dimension of the test electrode is shown in Figure 4.7. It is essential to get an optimum size of the test cell for high-voltage testing as well as to keep the material used to a minimum. Therefore the test cell configuration and its dimensions were reasonable designed. The test cell was modelled and the electric field distribution in the focused area was simulated using the special software (ANSOFT_Maxwell - 2D student version). The simulation result is shown in Figure 4.8. It could be confirmed that the designed dimensions provide a uniform electric field in the active region under test.

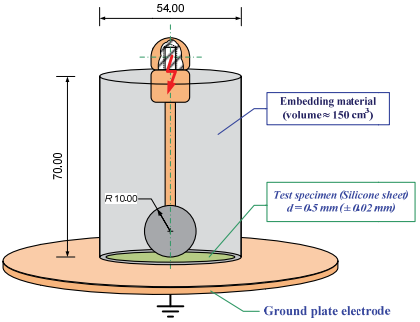

a) Dimensions of the test cell

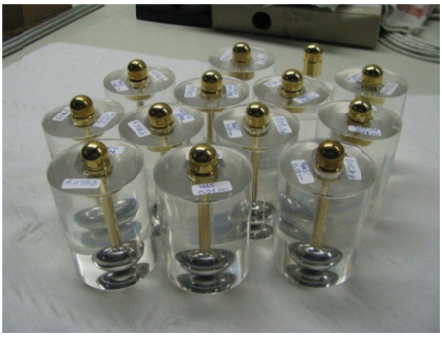

b) Examples of the test cell

Figure 4.6: The test cell configuration with embedded single sphere electrode (*unit: in mm*)

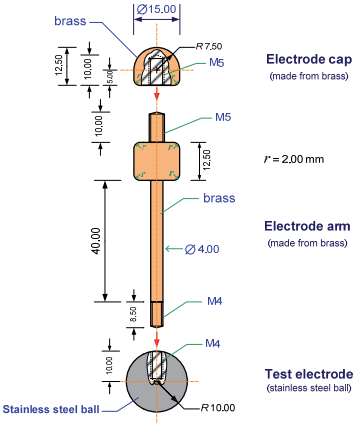

a) Dimensions of the sphere electrode

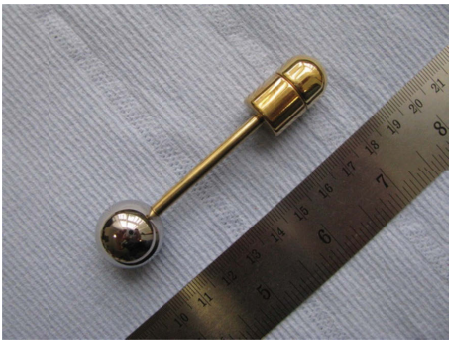

b) Real electrode

Figure 4.7: Sphere electrode and accessories (*unit: in mm*)

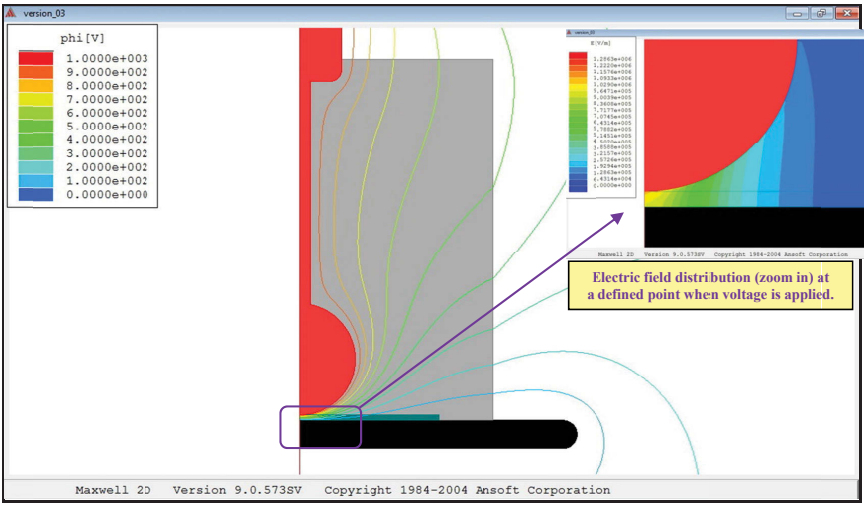

Figure 4.8: Voltage distribution (equi-potential lines) between test electrodes (*R-Z* plane)

This test cell provides conditions similar to real application environment in HV equipment. It is possible to use this test cell for the specific measurement of dielectric strength of silicone elastomers, i.e. intrinsic breakdown measurements. But the preparation process of each test cell is quite complicated and time consuming. In some cases problems can arise, if, for example, the degree of cross-linking of silicone sheet specimen needs to be controlled, and the RTV silicone is used as the embedding material, and if a longer period of curing time is needed to be sure that the curing process of embedding silicone at room temperature is completed and stable without any impact on the specimen under test.

The curing time of silicone rubbers depends on volume and/or size of the test cell. Curing process can be accelerated by heating but it may influences the characteristic changes of specimen parameters. The difference of each sample's quality results in scattering breakdown voltage values that lead to inaccuracies in measuring the dielectric strength of the investigated material.

Last but not least, a preliminary investigation revealed that uncured liquid silicone polymer, which is used as embedding material, could flow between the electrode and specimen (silicone rubber sheet). This results in a higher breakdown voltage level and a longer time to breakdown (in case of constant stress tests). It is surprising that this issue has never been considered in the previously published papers.

4.2.3 Summary

All the problems mentioned above, reveal disadvantages when using both types of the test cell. It is not reasonable to use them when performing extensive test series in material research laboratories. The preparation process of each test cell has become very time consuming. The lack of quality control of a sample parameter may result in a loss of the information from the silicone rubbers being investigated. This leads to misinterpretation of the dielectric strength behaviour of modified silicone polymers or all information on the modified silicone itself can be lost.

4.3 Development of a new efficient methodology to measure dielectric strength of silicone rubbers

Knowing that the dielectric strength of an insulating material can only be determined with a certain probability, the mean breakdown value of a number of samples is measured. The dielectric strength of silicone rubbers (SiRs) varies depending on three parameters:

- *Sample parameters*: e.g. material type, molecular structure, degree of cross-linking, impurities or micro-voids,
- *Electrode parameters*: e.g. electrode configuration, surface roughness of the electrodes, and
- *Electrical stress parameters*: e.g. mode of increasing voltage.

A good statistical evaluation of the dielectric breakdown values requires a suitable electrode and a proper specimen. Likewise, inaccuracies in measuring by imponderability in the specimen preparation must be reduced to a minimum.

In order to meet both technical and economic demands, an efficient methodology for basic investigations of the dielectric strength behaviour of silicone rubbers has been designed and developed. The core element of this methodology - *the new test facility* - allows easy preparing and handling of a silicone-sheet specimen. The technique is optimized for liquid silicone rubbers with very high viscosity as used in high-power cables accessories. Moreover, the new test facility can optimally be used for dielectric breakdown tests in some other cases, such as testing with embedded electrode. The developed technique is also reasonable for routine tests in materials research laboratories. The electrode arrangement is shown in Figure 4.9.

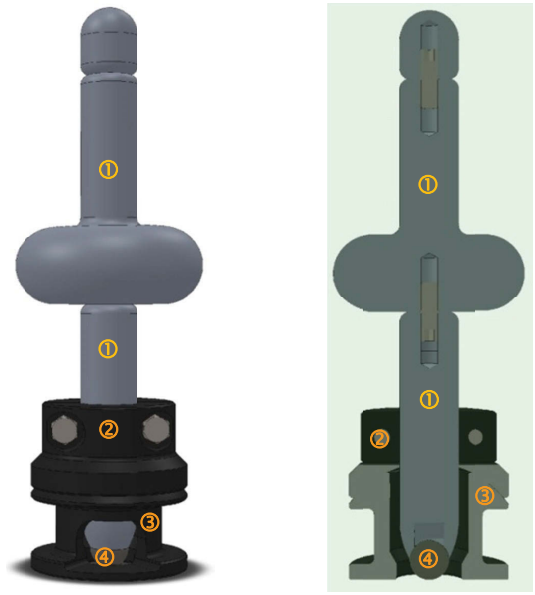

a) 3-dimentional body *b) Cross-sectional view*

Notations show in Figure:

① Main electrode to apply the high voltage;

② Electrode clamping (insulating material) to adjust and fix the test electrode;

③ Standing ring (insulating material) to fix the test electrode (to avoid tilt) and to limit the surface pressure acting from the electrode to the specimen;

④ Test electrode made by the standard stainless-steel ball-bearing.

Figure 4.9: The efficient electrode arrangement to measure the dielectric strength of SiRs

The electrode arrangement (Figure 4.9) provides basic information about characteristic changes in the dielectric strength behaviour resulting from modification (e.g. fluorescent modification and nano-fillers addition) of transparent or translucent silicone rubbers with regard to optical compatibility. The high advantage of the developed methodology is the use of only one silicone-sheet specimen, which is enough for breakdown tests under the same condition. Thus, a large number of breakdown data points can be recorded. This minimises the expense to produce test specimens and reduces the amount of embedding material. The effect of unknown parameters from the process of highly viscous liquid silicone rubber specimen preparation can be limited. It is also very useful for testing HTV (high temperature vulcanisation) types of silicone rubbers when the degree of cross-linking needs to be controlled. The new test arrangement with silicone sheet specimen is shown in Figure 4.10 [25].

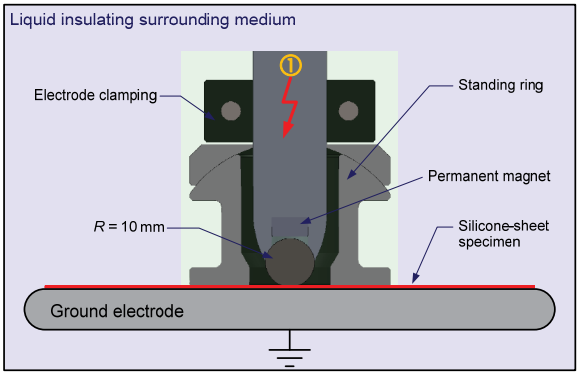

Figure 4.10: Test arrangement with silicone sheet specimen

The sphere-to-plane geometry permits a single well-defined point of maximum field and gradual reduction of the field away from the point. For a sufficiently large sphere radius and a small thickness of silicone sheet specimen, the electric field can be considered as uniform (or homogenous). A standard ball-bearing, made from well-polished stainless steel with a diameter of 20 mm and 32.6 g weight, are used as the sphere electrode to minimise electrode damage at breakdown and to reduce the manufacturing costs as well as maintenance costs. The sphere electrode is connected to the main electrode (number ① in Figure 4.9) by using magnetic force. The main electrode has been designed with sufficient dimension to avoid surface discharges (or corona discharges) that could have environmental impacts during the test. The advantage of this design is the removal or the rotation of the metal ball to new positions when the previous position was damaged at breakdown. Using this technique, a smooth, clean and defects-free surface of the sphere electrode can be maintained. Only a basic polishing process is required for cleaning of electrode surface before each test. One metal ball can be used at least for six breakdown tests before it has to be exchanged. This technique reduces the influence of electrode parameters (shape deformation) on the breakdown test as well as the expensive electrode.

The standing ring made from insulating material is used to limit the contact pressure between the test electrode and the surface of the silicone sheet specimen (Figure 4.10). Thus, the sphere electrode only touches the specimen surface. The position of the touching point shall be calibrated before every test. The real electrode and the standing ring are shown in Figure 4.11.

a) Test electrode and its installation

b) Adjustment of electrode position before test

Figure 4.11: The new accessories for breakdown test of elastomeric materials

Practically, the basic requirements for silicone rubbers used as an insulating material for HV power cable accessories are their electrical and mechanical properties. Mechanical elongation usually occurs in cable accessories when a rubber is loaded (stressed) in tension. Thus, the dielectric strength behaviour of silicone elastomers under the condition of loaded in tension should be investigated. The concept of this test is shown in Figure 4.12. Therefore, the tool was specially designed for such test (see Figure 4.13).

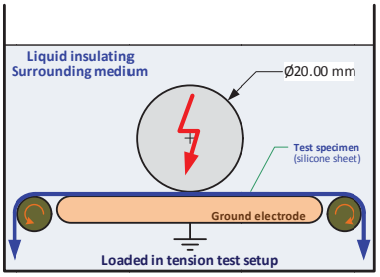

Figure 4.12: Schematic test diagram for investigation of the dielectric strength behaviour of silicone elastomers when loaded in tension

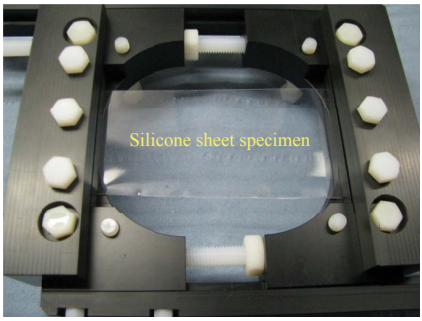

a) Specimen holding and taking tension force

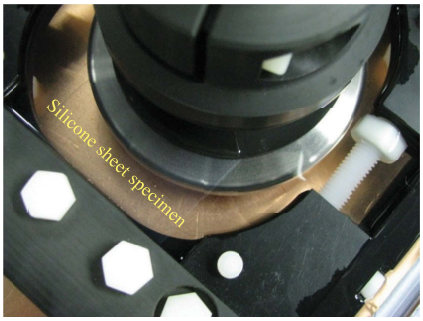

b) Example of the test setup

Figure 4.13: Special tool for loading silicone rubber sheets in tension

Furthermore, the new test accessories can easily be used for the measurements of dielectric strength in some other cases, such as testing with embedded sphere electrode or with cast-in electrode. Such tests can be complemented by *the new test facility* when the measurement of dielectric strength of silicone rubbers requires better test conditions, e.g. intrinsic breakdown test and thermal accelerated aging test [130]. The test cell with embedded sphere electrode gives a high stress in the centre area of the specimen and low stress at the edges, that all external influences are then controlled. Another new test cell with sufficient dimensions was developed (see Figure 4.14). It is suitable for such an application. The volume of embedding material is about 5.5 cm^3 and the weight of the test cell is only 38.0 g. It avoids the waste of material and provides a reasonable structure.

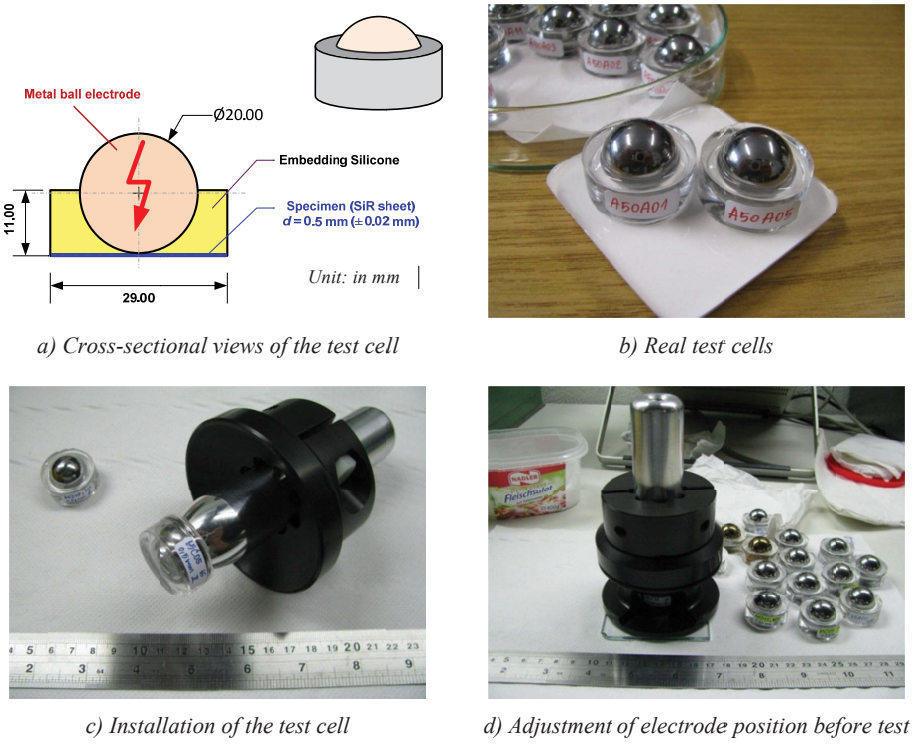

a) Cross-sectional views of the test cell

b) Real test cells

c) Installation of the test cell

d) Adjustment of electrode position before test

Figure 4.14: A small test cell with embedded sphere electrode for the specific breakdown test

In all dielectric strength measurements of silicone rubbers, thus, partial discharges and thermal effects during the test period must be avoided. The whole setup shall be immersed in surrounding liquid insulating medium, e.g. silicone oil or castor oil. The test chamber was designed to maximise the testing capabilities for high-voltage breakdown test. The developed apparatus is reliable in its mechanical structure and can be used for the dielectric breakdown test of silicone rubbers under AC, DC as well as impulse voltages. The complete test system is shown in Figure 4.15.

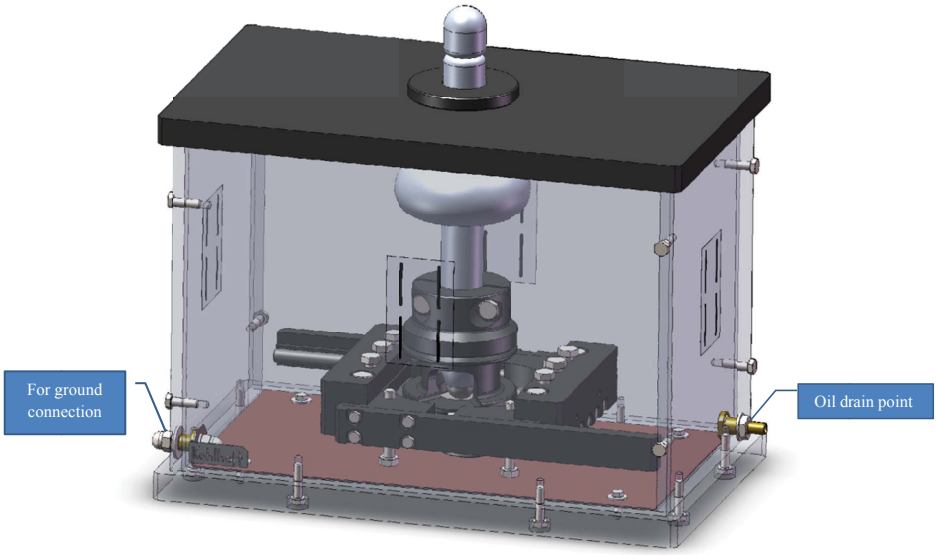

Figure 4.15: New apparatus for the dielectric breakdown test of silicone rubbers

4.4 Conclusions

Because the IEC standard 60243-1 [24] does not define the specific test method for the determination of the short-time dielectric strength value of elastomeric materials, particularly silicone rubbers, an efficient methodology for a basic investigation of the dielectric strength behaviour of silicone rubbers has been developed. It is optimised to satisfy the technical and economic demands. The core element of this methodology - *the new test facility* - has the following advantages [25]:

- Only one sheet specimen is needed for breakdown test, a large number of breakdown data points can be recorded, with this only sheet; the effect of unknown parameters can be limited.
- This method enables the investigation of highly viscous silicone rubber, which was not yet possible by traditional approaches.
- The breakdown test facility can be used for a high-temperature curing (HTV) type of silicone rubbers when the degree of cross-linking needs to be controlled.
- The quality of the test specimen and the electrode parameter can be controlled; this possibility can enhance the statistical significance of the test results, so that a valid estimation of the needed variables of such silicone elastomers is now possible.
- The material input is minimised and the process of specimen preparation is less then time-consuming; this low-cost experimental method provides dielectric strength values for silicone rubbers with low uncertainty.
- This technique is also reasonable for routine tests in materials research laboratories.

The developed methodology is used to evaluate the dielectric strength of silicone rubbers where especially thin silicone sheet specimens are in the focus. The dielectric strength behaviour of the virgin and modified silicone elastomers for optical compatibility was investigated. Experimental work, results and conclusion will be shown in the following chapters of this thesis.

5 Experimental details

This chapter deals with the details of the materials, the preparation of test specimen, experimental setup and the statistical methodology used for analysis of the results. The process of specimen preparation is of utmost importance because it has the power to be the most rigid type of research. The best approach is to control as many interacting variables as possible to eliminate or reduce errors in the measurement of dielectric strength of silicone rubbers. They will be discussed below in the order of effectiveness.

5.1 Description of the materials used

The optical PD detection requires optically-transparent insulating materials [15, 17-18]. Thus, the modification of transparent or translucent types of silicone rubber (SiR) for highly efficient optical PD detection is needed. In order to expand their application to higher voltages, the dielectric strength of such silicone rubbers before and after modifications should be evaluated. These investigations require a large number of breakdown tests in the high-voltage laboratory**.**

Silicone polymers are extensively used as an insulating part of high-voltage cable accessories. Hence, silicone polymers are ideal for modification or the development of novel specific-dielectric material for high-voltage insulation. For the reason mentioned above, the main purpose of this work is to give an overview on the dielectric strength behaviour of the optically compatible types of silicone rubbers. Four types of two-component liquid silicone rubber were selected for investigation of the strength behaviour:

- Two transparent types with different mixing ratio,
- One translucent type, and
- Electrical grade silicone rubber (RTV-2).

Transparent and translucent types to be used as basic silicone polymers have similar properties compared with currently used polymeric insulation materials in high-voltage engineering. Transparent polymers have excellent optical but worse mechanical properties. Translucent materials should be avoided when optical detection methods should be used but has excellent mechanical properties. To make use of the optical properties of the transparent materials, the mechanical properties must be improved by modification. On the other hand, the optical properties of translucent materials should be improved to take advantages from the excellent mechanical properties. When these materials are modified, their electrical properties must be investigated and approved for their use in high-voltage engineering.

It is worth noting that the materials investigated were bought from commercially available sources. The electrical grade silicone rubber (RTV-2) was also investigated in this work and is here considered as the reference rubber material to which all important properties of the others are compared. The selected silicone rubbers and values of some physical properties are shown in Table 5.1.

Table 5.1: The values of some physical properties of the selected silicone rubbers

Silicone Name	Type of silicone	Mixing ratio A:B (by weight)	Conditions for cross-linking process	Viscosity (mPa.s)	Density (g/cm^3)	Appearance
ESA 7250	LSR - 2	**10:1**	at room temperature *or* accelerated by heating	4,000	1.02	Transparent
LSR 7665	LSR - 2	**1:1**	at room temperature *or* accelerated by heating	20,000	1.01	Transparent
LSR 3003/30	LSR - 2	**1:1**	by heating	213,000	1.1	Translucent
PowerSil 600	LSR - 2	**9:1**	at room temperature	15,000	1.13	Light grey

Note: 1) LSR - 2 is two-component liquid silicone rubber

ESA 7250 is a two component, optically clear and low-viscous silicone elastomer with good pourability. The mixing ratio is 10:1 by weight. Therefore, this is more flexible and suitable to add nanoparticles or fillers. This silicone elastomer cures by a polyaddition reaction and the elastomer can be removed from the curing form after 24 to 48 hours at room temperature. Curing can also be accelerated by heating; the curing temperatures recommended by producer are 4 hours at 60 °C, or 2 hours at 100 °C, or 1 hour at 150 °C. This grade is suitable for casting or mould filling process.

LSR 7665 is a highly transparent two-component liquid silicone rubber. This grade is possible for modification, i.e. fluorescent modification and nano-fillers addition. It can be cured at room temperature or accelerated by heating. This silicone elastomer has excellent optical properties. When heat stabilizers (post curing) are added, the products can be used within a temperature range of -55 °C to +230 °C, for a short time up to +300 °C. It is also suitable for casting or mould filling process.

LSR 3003/30 is a very highly viscous (paste-like) silicone polymer. This grade is a translucent type; fluorescent pigments can easily be mixed into the two component compound. Short curing times can be achieved by heating. It has excellent mechanical and electrical properties which are appropriate for cable accessories and insulators. When heat stabilizer (post curing) is added, the product can be used within a temperature range from - 55 °C to +230 °C, and for a short time up to +300 °C. These grades are suitable for an economical manufacturing of large series of injection moulding processes. Therefore the cable industry is interested to know electrical properties of this silicone rubber.

PowerSil 600 is a special grade for electrical insulation. It has a light grey colour; it is a pourable, addition-curing, two-component silicone rubber that cures at room temperature (RT) to form soft products with high mechanical strength. The platinum catalyst is in component B. It has excellent hydrophobic properties, outstanding dielectric properties (high resistivity and low loss factor), high tracking and arc resistance. Presently, the PowerSil 600 silicone rubber is mostly used for electrical insulation in power systems equipment particularly in power cable joints and accessories.

The values of some mechanical and electrical properties are shown in Table 5.2 and Table 5.3, and are found in the technical data sheets of the silicone producers [131-134]. It is important to note that these data are only intended as the guidance and should not be used in preparing specifications.

Table 5.2: Mechanical properties of the selected silicone rubbers, which are guided by the silicone producers

Silicone Name	Processing (for industrial process)	Hardness Shore A	Tear strength (N/mm)	Tensile strength (N/mm^2)	Elongation at break (%)
ESA 7250	Casting, mould filling	52	4	6.2	115
LSR 7665	Casting, mould filling	54	8.3	7.5	180
LSR 3003/30	Injection moulding	31	23	7.5	610
PowerSil 600	Casting, mould filling	30	25	6.5	500

Table 5.3: Electrical properties of the selected silicone rubbers, which are guided by the silicone producers

Silicone Name	Volume resistivity (Ω cm)	Dielectric constant (ε_r) at 50 Hz	Dielectric strength (kV/mm)	Dissipation factor (tan δ) at 50 Hz
ESA 7250	1×10^{15}	2.7	~ 20 [1)]	1×10^{-3}
LSR 7665	4×10^{15}	2.8	27 [2)]	2×10^{-4}
LSR 3003/30	5×10^{15}	2.8	23 [2)]	20×10^{-4}
PowerSil 600	~ 10^{15}	2.9	> 23 [1)]	3×10^{-4}

Note:

[1)] Dielectric strength values were determined in accordance with IEC60243-1 [24]

[2)] Dielectric strength values were determined in accordance with IEC60243-2 [135]

5.2 Preparation of the test specimen

The developed test facility as described in chapter 4 was used for dielectric breakdown tests of silicone rubbers. Two types of test specimens, i.e. a silicone sheet specimen for the basic breakdown test and a small test cell with sphere electrode embedded for the specific breakdown test were used in the same facility. The main objective of this research effort is the analysis of the characteristic changes in the dielectric strength behaviour of the virgin and the modified silicone rubbers. The dielectric breakdown test with a silicone sheet specimen can provide basic information about such characteristic changes in silicone materials. Therefore breakdown test on a silicone sheet is in the focus of the research work.

5.2.1 A silicone sheet specimen

When carrying out dielectric breakdown measurements, the insulating materials must not have obvious defects or discontinuities in the material. The test specimen shall be large enough to permit making as many individual tests as required for the particular material. The silicone sheets shall be of sufficient size to prevent flashover under conditions. The surfaces of the silicone sheet specimens, which will be in contact with the electrodes, shall be parallel planes as smooth as possible. A thin sheet is often convenient for the use as the specimen because it can reduce the breakdown voltage as well as the size of HV testing transformer.

After mixing A and B parts, it was preferable to degas the product to eliminate the air bubbles that would be visible in the finished part. Silicone sheet specimens with a minimum size of 8 cm (width) × 11 cm (length) and a thickness of 0.5 mm ± 0.02 mm were carefully prepared. The special casting form made from the heat resistant glass plate has been developed for the production of a silicone sheet. For the transparent and translucent types of the investigated silicones, the cross-linking (curing) process was carried out by heating under vacuum using a vacuum bag to remove air bubbles (micro-voids). Such micro-voids could reduce the mechanical and dielectric properties. The cross-linking process of the RTV-2 silicone was conducted at room temperature under low-pressure condition (approximately 20 mbars) that was placed inside the vacuum chamber. Examples of the transparent silicone sheet specimens are shown in Figure 5.1, while the translucent and the RTV-2 silicone sheet specimens are show in Figure 5.2, respectively.

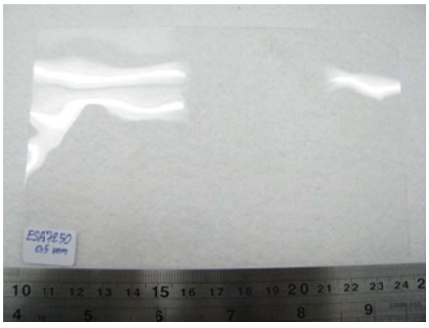

a) ESA 7250 silicone sheet specimen

b) LSR 7665 silicone sheet specimen

Figure 5.1: Examples of the transparent silicone sheet specimens

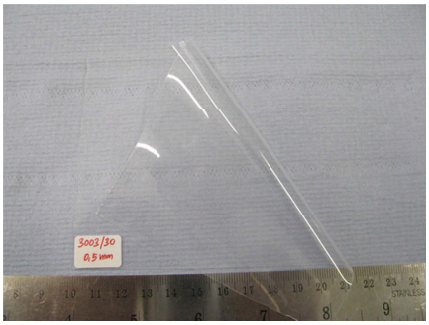

a) LSR 3003/30 silicone sheet specimen

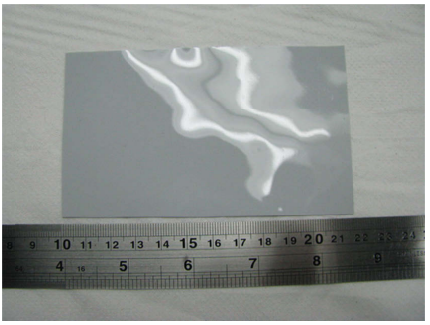

b) PowerSil 600 silicone sheet specimen

Figure 5.2: Examples of the translucent and the RTV-2 silicone sheet specimens

5.2.2 A small test cell with embedded sphere electrode

In some other cases, e.g. intrinsic breakdown test and thermally accelerated ageing test, the measurement of dielectric strength of silicone rubber requires better test conditions. These can be obtained from a small test cell with embedded sphere electrode. All external influences are then controlled. The preparation of such test cells is very easy by using the casting mould as shown in Figure 5.3 a). The circular shaped specimen with a diameter of about 36 mm and a thickness *d* of 0.5 mm (± 0.02 mm) was cut from a silicone sheet that was prepared in accordance to the process mentioned in section 5.2.1. The specimen was placed onto the bottom part of the mould (segment ③ in Fig. 5.3 a)) and then fixed by screw-down the plastic hollow cylinder (segment ①). After that, a well-polished stainless-steel ball electrode was mounted on the centre area of the specimen. The whole arrangement was embedded using a castable RTV-2 silicone elastomer and then cured at room temperature. The sphere electrode was fixed at the centre using the plastic cap holder (segment②). After vacuum-casting and curing of the embedded silicone rubber, the test cell was carefully demoulded and finally a satisfying test sample as shown in Figure 5.4 could be achieved. Ten sets of the casting mould were applied to reduce the time used for the preparation of test cells.

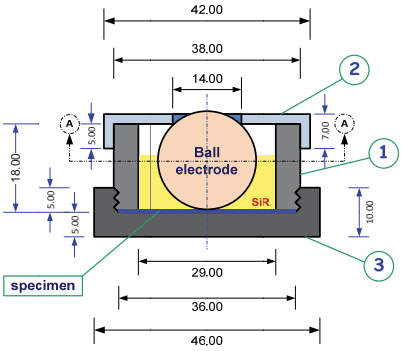

a) Casting mould made from PVC

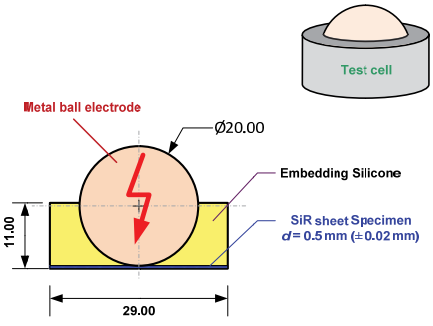

b) Cell with sphere electrode embedded

Figure 5.3: Cross-sectional views of the casting mould and the small test cell with embedded sphere electrode (*unit: in mm*)

a) ESA 7250 test specimens

b) LSR 7665 test specimens

Figure 5.4: Test cells with embedded sphere electrodes for specific breakdown test

The test cell was designed with sufficient dimension. The volume of the embedded silicone is about 5.5 cm^3 and the weight of the whole test cell is only 38.0 g. These test cells will be used to measure the specific breakdown field strength of virgin silicone rubbers. Several of these new applications will be discussed in the next chapter.

5.3 Experimental setup

A short-term dielectric breakdown test of the focused silicone rubbers was conducted with AC voltage and the 60 s step-by-step test procedure according to IEC 60243-1 [24]. The whole setup was immersed in liquid surrounding medium in order to minimise the effects of surface discharges prior to breakdown. Castor oil ($C_{18}H_{34}O_3$) [136] with high permittivity ($\varepsilon_r \approx 4.5$) is a suitable surrounding medium for the test with a silicone-sheet specimen. However, for the test with the embedded electrode, the high grade silicone oil ($\varepsilon_r = 2.9$) can be used. Figure 5.5 shows schematically the experimental setup; its use in the high-voltage laboratory is shown in Figure 5.6.

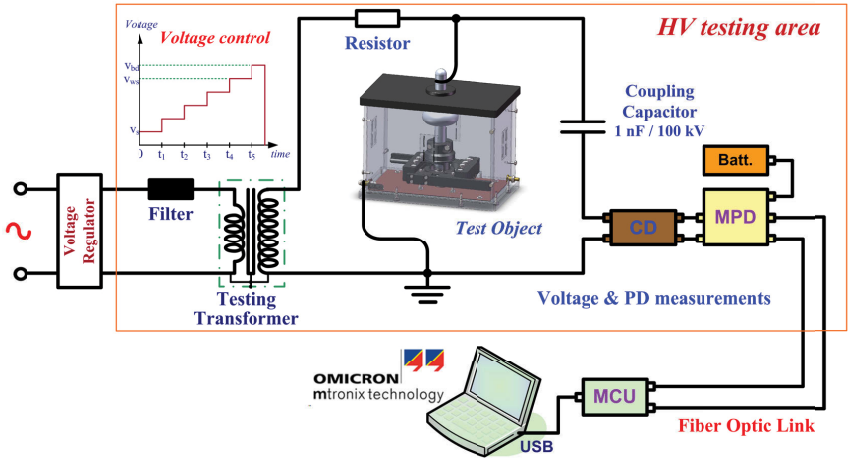

Figure 5.5: Experimental setup

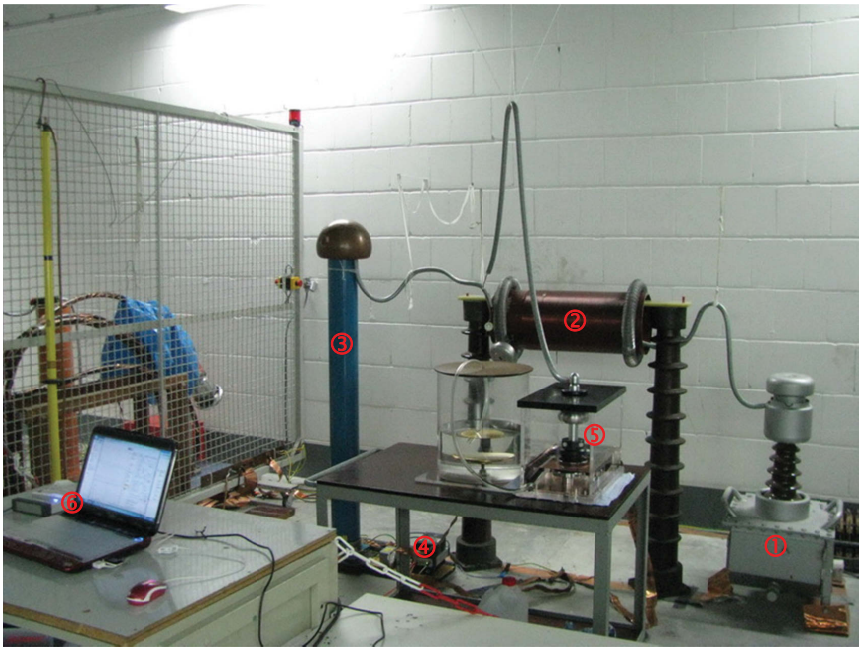

Figure 5.6: Experimental setup in the high-voltage laboratory (CESI-IPH Berlin); Notations:

① HV testing transformer; 220 V / 50 kV, 3 kVA, 50 Hz

② Current limiting resistor (HV resistor)

③ HV coupling capacitor, 1 nF / 100 kV

④ LV part of the measuring system (MPD and MI system by OMICRON electronics GmbH)

⑤ Test object (test chamber)

⑥ USB box and the computer software to record the voltage and partial discharge activity (PD) during the test.

Electric breakdown is accompanied by an increase of current flowing in the circuit and by a decrease of voltage across the specimen. The increased current may trip a circuit-breaker or blow a protection fuse. However, tripping of a circuit-breaker may sometimes be influenced by flashover, specimen charging current, leakage or partial discharge currents, equipment magnetizing current or malfunctioning. It is therefore essential that the circuit-breaker is well co-ordinated with the characteristics of the test equipment and the material under test; otherwise the circuit-breaker may operate without breakdown of the specimen, or fail to operate when breakdown has occurred and thus not provide a positive criterion of breakdown. Even under the best conditions, premature breakdowns in the ambient medium may occur, and observations shall be made to detect them during tests.

5.3.1 Calibration of partial discharge measuring system

In order to investigate the electrical breakdown mechanism only, any partial discharges and thermal effects during the test period must be avoided. For that purpose, a short-term breakdown test procedure and a homogeneous structure of the stressed material is required. A level of partial discharge (PD) activity occurring during the test period shall be recorded. Before starting the experiments, calibration of the PD measuring system by a reference impulse charge generator (Figure 5.7) is necessary to ensure accurate measurement results.

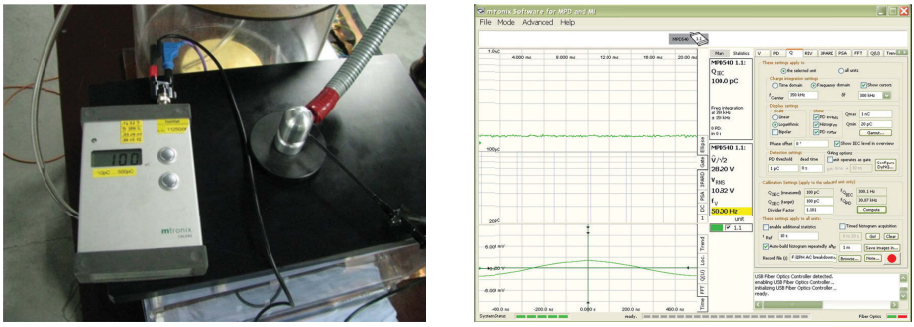

a) PD calibration at 100 pC *b) Real-time measuring software display*

Figure 5.7: Calibration of PD measuring system before every test

5.3.2 Method of voltage application

AC voltage was applied to the test specimen and increased stepwise until breakdown. The 60 s step-by-step test procedure was carried out according to sub-clause 9.4 in IEC standard [24]. The increases of voltage shall be made as quickly as possible and without any transient overvoltage, and the time spent in raising the voltage shall be included in the period of 60 s at the higher voltage level. In some cases it would be necessary to run one or two preliminary tests in order to determine the expected breakdown voltage of the silicone specimen being investigated; such data is then referred as the test guideline criteria. The electric strength is based on the highest nominal voltage, which withstood for 60 s without breakdown. The highest nominal voltage is to be used to calculate dielectric breakdown strength of the material under test. An example of voltage profile is shown in Figure 5.8.

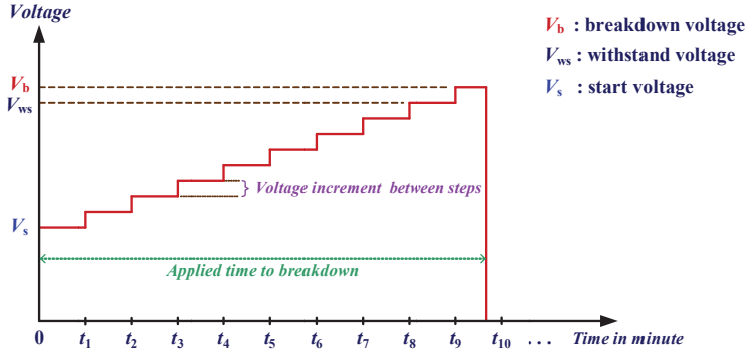

Figure 5.8: Voltage profile of the 60 s step-by-step test procedure

5.4 Methodology for statistical analysis of dielectric breakdown results

When assessing the breakdown test results for polymeric materials or polymeric insulations, the use of a statistical method is often required. A number of statistical functions have been applied to describe general properties of a data population. It is often of interest to find out what is "typical" for the population or to predict a probable outcome of the behaviour of the population being investigated. Generally, the failure data set of an electrical insulation may be represented in the normal distribution from numbers of specimens failed in consecutive periods. The mean value and standard deviation of the data set are easily calculated using a scientific calculator. Unfortunately, it is not usually appropriate to electrical breakdown data of polymeric insulation because the specimen will not break at its average strength but at its weakest point, which is dependent on its polymeric structure. Therefore, an important step in analysing breakdown data of silicone rubbers is the selection of an appropriate distribution.

In fact, the breakdown field strength in elastomeric materials shows much larger dispersion than in liquids and gasses. It is a type of *extreme value distribution*, in which the material fails when the weakest structural element fails. The failure of solid insulation can mostly be described by *extreme-value statistics*, such as the Weibull, Gumbel and lognormal distributions, but the most commonly used is the Weibull statistics [137]. The extreme values are linked to phenomena that have small probability of occurrence and as such they have no or very limited effect on the average behaviour of the whole population. In this method the properties of the weakest extremes are controlling the behaviour of the whole material. The nature of various phenomena to a breakdown in an electrical insulation is characterized by extreme values. The guide for the Weibull distribution includes methods for determining whether the data is a well fit to the distribution, graphical and computer-based techniques for estimating the most likely parameters of the Weibull function, computer-based techniques for estimating statistical confidence intervals, and techniques for comparing data sets as well as some case studies, are addressed in the IEC 62539 standard [138] or IEEE standard 930 [139].

The Weibull distributions may be described in terms of two parameters. To give more generality, however, a third parameter may be included which corresponds to a lower voltage level (or a shorter time), for which the specimen will not break down. In some cases two or more mechanisms may be acting; this may need the combination of two or more distributions functions. The effect of the specimen size (i.e. thickness, area, volume) on life or breakdown voltage can be modelled using extreme value distributions. The lognormal distribution may be useful where specimens breakdown due to unrelated causes or mechanisms. The lognormal distribution may be closely approximated by the Weibull distribution.

5.4.1 The Weibull distribution for dielectric breakdown data

Waloddi Weibull (18 June 1887 – 12 October 1979) was a Swedish engineer, scientist, and mathematician well-known for his work on strength of materials and fatigue analysis. The Weibull distribution [137], also known as the Extreme Value Type III distribution, first appeared in his papers in 1939. It is flexible and adaptable to a wide range of data. The Weibull statistic is used to model data regardless of whether the failure rate is increasing, decreasing or constant. The breakdown voltage, time to failure, cycles to failure, mileage to failure, mechanical stress or similar continuous parameters need to be recorded for all items. The Weibull distribution has wide applicability, especially in representing failure data, and its use is by no means confined to electrical breakdown [140-151]. The expression

for the cumulative density function for the *two-parameter* Weibull distribution is shown in equation (5.1).

$$F(x;\alpha,\beta) = 1 - exp\left\{-\left(\frac{x}{\alpha}\right)^{\beta}\right\}, \tag{5.1}$$

where

- x is the measured variable, usually the breakdown voltage or time to breakdown,
- $F(x)$ is the cumulative probability of failure at a voltage or time less than or equal to x. For tests with large numbers of specimens, this is approximately the proportion of specimens broken down by voltage or time, x,
- α is the scale parameter and is positive, and
- β is the shape (or slope) parameter and is positive.

The cumulative probability of failure $F(x)$ equal to zero at $x = 0$, is $F(0) = 0$. The probability of failure rises continuously as x increases. As the voltage or time increases, the probability of failure approaches certainty is $F(\infty) = 1$.

The scale parameter α represents characteristic voltage (or time to breakdown) for which the failure probability is 0.632. In this case is the expected variable $x = \alpha$, and therefore

$$F(\alpha) = 1 - exp\left\{-\left(\frac{\alpha}{\alpha}\right)^{\beta}\right\} = 1 - \frac{1}{e} = 0.632 \;\; or \;\; 63.2\,\% \;\; .$$

The scale parameter α is analogous to the mean value of the normal distribution. The units of α are the same as x, that is, voltage, electric stress, time, number of cycles to failure etc. [138-139].

The shape parameter β is a measure of the range of the failure times or voltages. The larger β is, the smaller is the range of breakdown voltages or times. It is analogous to the inverse of the standard deviation (SD) of the normal distribution ($\beta \propto \frac{1}{\mathrm{SD}}$).

The Weibull distribution is also used to represent breakdown voltages in tests, in which the test voltage is "*raised up*" at a constant rate until breakdown occurs, i.e. progressive stress tests. In this case, much higher values of β are expected. A very high value of β would indicate a very narrow distribution of breakdown voltages, i.e. all systems suffer breakdown at about the same voltage [152].

The *two-parameter* Weibull distribution of Equation (5.1) is a special case of the *three-parameter* Weibull distribution that has the cumulative distribution function as shown in equation (5.2):

$$F(x) = \begin{cases} 1 - exp\left\{-\left(\frac{x-\gamma}{\alpha}\right)^{\beta}\right\} & ;\; x \geq \gamma \\ 0 & ;\; x < \gamma \end{cases} \tag{5.2}$$

The additional term γ is called *the location parameter*. $F(x) = 0$ for $x = \gamma$ is the probability of failure for $x < \gamma$ is zero.

If the γ-parameter is set to zero, the expression "*two-parameter*" Weibull distribution is then used. The frequency distribution function $f(x)$ is obtained from $\frac{dF(x)}{dx}$. Therefore equation (5.1) can be written as

$$f(x) = \frac{dF(x)}{dx} = \frac{\beta}{\alpha}\left(\frac{x}{\alpha}\right)^{\beta-1} e^{\left(\frac{x}{\alpha}\right)^{\beta}} . \tag{5.3}$$

Typical examples of the Weibull distribution function with different values for the α- and β-parameters are shown in Figure 5.9 a) and b), representing the cumulative and frequency distribution functions, respectively. For clarity, in the following text "the Weibull distribution" or "the Weibull function", refers always to the cumulative distribution function unless stated otherwise.

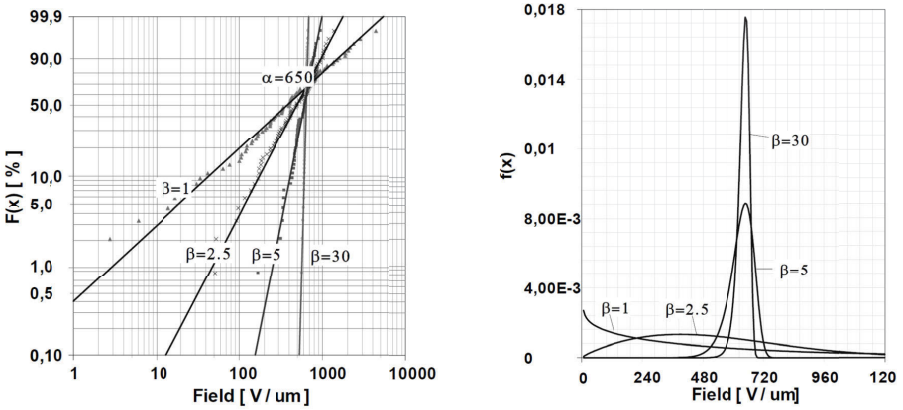

a) Cumulative distribution function F(x) *b) Frequency distribution function f(x)*

Figure 5.9: Examples of the *two-parameter* Weibull distribution functions with α = 650 and β = 1, 2.5, 5 and 30. Note that β =1 equals to exponential distribution function [153]

5.4.2 Plotting of the Weibull function

Data distributed according to the *two-parameter* Weibull function should form a reasonably straight line when plotted in a Weibull probability diagram. The measured data is plotted on the horizontal axis, which is scaled logarithmically $\ln x$. The cumulative probability of breakdown is plotted on the vertical axis, which is also highly non-linear $y = \ln\left(-\ln\left(1 - F(x)\right)\right)$. The reason for this change of variables is the cumulative distribution function and can be linearized. From equation (5.1) follows

$$F(x) = 1 - e^{-(x/\alpha)^{\beta}}$$

$$1 - F(x) = e^{-(x/\alpha)^{\beta}}$$

$$-\ln\left(1 - F(x)\right) = \left(\frac{x}{\alpha}\right)^{\beta}$$

$$\ln\left(-\ln\left(1 - F(x)\right)\right) = \beta \ln x - \beta \ln \alpha$$

or $$\ln \ln\left[\frac{1}{1-F(x)}\right] = \beta \ln x - \beta \ln \alpha \ , \tag{5.4}$$

which can be seen to be in the standard form of a straight line ($y = \mathrm{m}x + \mathrm{C}$). Therefore, if the data came from a Weibull distribution, a straight line is then expected in the Weibull plot.

As the left side of the equation (5.4) is inconvenient for the reader, a help scale giving the label of $F(x)$ is normally used. In Weibull chart the vertical axis is scaled in term of $F(x)$. When the logarithmic scale for the x-axis is used, the different β-parameter values are easily visualised as different slopes. The values for the α- and β-parameters are obtained by using the maximum likelihood estimation technique as described in [138-139].

5.4.3 Plotting the experimental data into the Weibull probability diagram

Endurance and strength of insulation systems and materials subjected to electrical stress may be tested using constant stress tests, in which times to breakdown are measured for a number of test specimens, and progressive stress tests, in which breakdown voltages may be measured. In either case it will be found that a different result is obtained for each specimen and that, for given test conditions, the data obtained can be represented by a statistical distribution.

When plotting the experimental data, the first step is to sort the data in increasing order from smallest to largest and assign them a rank from $i = 1$ to $i = n$, where n is the total number of data. Therefore, appropriate approximation for plotting positions is needed.

The linear regression using least squares would be expected to give similar results to a best fit plotted by eye in a Weibull plot. Linear regression is the simplest of the techniques to implement. The technique requires pairs of coordinates. For a large number of specimens ($n \geq 50$), the cumulative probability of failure coordinate for each data point x_i, is close to the proportion of specimens failed [152]. For the calculation of the i-th cumulative probability (P_i) corresponding to the i-th failure event, the most accurate technique is the incomplete beta function [154-155]. A good median rank approximation, the Bernard estimator, is given by

$$P_i = \frac{i - 0.3}{n + 0.4} \ . \tag{5.5}$$

The Bernard rank estimator is the most popular approximation for plotted positions in a Weibull graph. It is suitable for a large sample size ($n \geq 50$). But, unfortunately, it has been found that this technique gives unreliable results in some cases, especially when a small sample size and a complete (uncensored test) data set are used for the analysis of electrical insulation breakdown [152, 156-157].

The appropriate approximation for the most likely probability of failure data for a small sample size is found in Ross [146, 158]. In case of a complete test (uncensored data) and a small size of the samples ($n < 20$), a superior approximation recommended by the IEC 62539 standard [138] for the calculation of the i-th cumulative probability (P_i) corresponding to the i-th failure event is provided as

$$P_i = \frac{i - 0.44}{n + 0.25} , \quad (5.6)$$

where n the size of the specimens and i the rank of the measured data ($i = 1$ to n) are. These can be used for Weibull probability plots of the experimental data in the research.

5.4.4 Parameter estimation for the Weibull distributed data

When the data follows a straight line, it can be assumed that they are distributed according to the two-parameter Weibull function. For given breakdown data, the values of α and β need to be found, which correspond to the distribution most likely to represent them. Constructing the "best straight line" through data points in a Weibull plot or using statistical techniques to find the most appropriate values of α and β, it is not a trivial procedure. The estimation of the Weibull function parameters for the Weibull distributed measurement data can be performed in many different techniques [146, 152, 155-159]. The most commonly used estimation techniques are simple linear regression using the least squares technique, or "by eyes" fitting in a Weibull plot, or the maximum likelihood estimation, which is computationally simple and has been widely used. The most convenient techniques, depending upon the number of specimens available in each sample and the values of shape and scale parameters, are recommended in standard methods [138-139]. With modern computing the Weibull papers as such are not used any longer but a least square fit or more accurate linear regression can be applied for the parameter estimation. However, the above methods require the use of an approximate rank function, as seen in the previous chapter. The maximum likelihood (ML) method has been found to give biased estimates of the parameters, especially for small data sets [152, 156-157], then it should be avoided.

Graphical and computational techniques are available for estimating the Weibull parameters. Universally, for large data sets, typically with more than 20 breakdowns, the least-squares linear regression technique is adequate. But, for small data sets, typically with less than 15-20 breakdowns, it can be inaccurate to use the standard least-squares regression technique since different points plotted in the Weibull plot need to be allocated different weightings, and these are recommended in standard methods [138-139]. For very small data sets, typically with less than 5 breakdowns, it can give rise to erroneous parameter estimates and the best approach, wherever possible, is to obtain more data. Only if more data cannot be obtained, such an analysis, using the White method [160] should be carried out with very small data sets [157].

The number of data points required depends upon the number of parameters that describes the distribution and the confidence demanded in the experimental results. In this research work, the breakdown data on at least ten specimens is obtained and all test specimens broke down so the data is "*complete data*". The breakdown field strength (E_b) of each specimen could be calculated using the relationship between breakdown voltage (V_b) and thickness (d) of specimen. To check for the appropriateness of a set of breakdown data, they are placed in the order from the smallest to the largest and assign them a breakdown probability (P_i) using equation (5.6) as described in section 5.4.3. For each breakdown field strength data, $E_{\mathrm{b},i}$, assign a value

$$Y_i = \ln(E_{\mathrm{b},i}) , \quad (5.7)$$

where $\ln(E_{\mathrm{b},i})$ is the natural logarithm or $\log_{\mathrm{e}}\{E_{\mathrm{b},i}\}$. For each probability of failure, P_i, expressed as a percentage, assign a value

$$X_i = \ln\left(-\ln\left(1-\frac{P_i}{100}\right)\right) . \tag{5.8}$$

Using the least squares regression technique the correlation coefficient is found [138-139]. For complete test (uncensored data) and ten specimens broke down ($n = r = 10$), it is found that the value of correlation coefficient, which is recommended by IEC 62539 [138] for well fit to the two-parameter Weibull, is must be greater than 0.92.

Looking up the weightings for each data point, w_i, given in standards [138] and [139], the weighted averages of X_i and Y_i as shown in Equation (5.9) and Equation (5.10) can be calculated:

$$\bar{X} = \frac{\sum_{i=1}^{n}[w_i X_i]}{\sum_{i=1}^{n}[w_i]} \tag{5.9}$$

$$\bar{Y} = \frac{\sum_{i=1}^{n}[w_i Y_i]}{\sum_{i=1}^{n}[w_i]} . \tag{5.10}$$

Using Equation (5.11) and Equation (5.12), the shape parameter β and the scale parameter α can be estimated:

$$\hat{\beta} = \frac{\sum_{i=1}^{n}[w_i(X_i-\bar{X})^2]}{\sum_{i=1}^{n} w_i(X_i-\bar{X})(Y_i-\bar{Y})} \tag{5.11}$$

$$\hat{\alpha} = \exp\left\{\bar{Y}-\frac{\bar{X}}{\hat{\beta}}\right\} . \tag{5.12}$$

It is important to note that, the α- and β-parameters are normally available on commercial spreadsheet programs, e.g. ReliaSoft Weibull++8, Weibull Analysis module of AvSim+ by Isograph, ReliaSoft Weibull++ MT 6.0.

Estimation of Weibull percentiles is often useful to estimate the breakdown field strength, for which there is a given probability of failure (p %); this is known as the p-th percentile. The breakdown p-th percentile ($E_{\mathrm{b},p\,\%}$) may be estimated by using Equation (5.13):

$$\hat{E}_{\mathrm{b},p\,\%} = \hat{\alpha}\left[-\ln\left(1-\frac{p}{100}\right)\right]^{1/\hat{\beta}} , \tag{5.13}$$

where p is expressed as a percentage.

5.4.5 Estimation of confidence intervals for the Weibull function

If the same experimental tests with many specimens are performed several times, the values of the parameters and percentile estimated from each experiment differ. The variation in estimates results from different methods applicable by different authors, e.g. by Dissado *et al.* [141], Chauvet *et al.* [142] and Cacciari *et al.* [143]. Therefore any parameter estimated differs from the true parameter value that is obtained from an experiment involving an infinitely large number of specimens. Hence, it is common to give with each parameter estimate a confidence interval that encloses the true parameter value with high probability. In general, the more specimens are tested, the narrower the confidence interval is.

There are various methods of estimating confidence intervals for Weibull parameters [161]. Many computer programs are available although some of these may not be accurate if used with small sample sizes. The exact values of the statistical confidence intervals depend on the method used to estimate the parameters. The graphical procedure for estimating the bilateral 90 % confidence intervals for sample sizes from $n = 4$ *to* $n = 100$ can be found in the standard guide method [138-139]. The technique is applicable to complete and singly-censored data. The lower and upper factors for calculation of the 90 % confidence intervals for the Weibull function are represented by the curves. They assume that

a) the data adequately fits the two-parameter Weibull distribution using the simple test described in sub-clause 5.4 in such standard [138], and
b) the least squares regression has been used for larger data sets with $n > 20$ and the White method has been used for smaller data sets with $n \leq 20$.

The standard curves have been calculated using a Monte-Carlo method and are estimated to be accurate in the range of 1 % for $4 \leq n \leq 20$ and 4 % for $20 < n \leq 100$.

In this thesis, the determination of the 90 % confidence intervals for the Weibull parameters (α and β) is carried out according to sub-clause 9.1 of IEC 62539 [138]. Ten samples (n = 10) are used for every test series in order to get a sufficient statistical confidence level.

5.4.6 Tests with increasing voltage

Practically, the voltage is increased linearly (ramp with a uniform rate of rise) or by small steps until breakdown occurs. As the same thickness and the same test conditions were given, each test provides a value of the breakdown gradient which constitutes the random variable E_{b}. The Weibull distribution for the breakdown gradients can be written as

$$P(E) = 1 - \exp\left[-\left(\frac{E}{\alpha}\right)^{\beta}\right], \tag{5.14}$$

where α is the breakdown gradient with 63.2 % probability.

Electric strength (ES) tests and progressive stress tests belong to this test type. For different rise rates, different breakdown strength values are obtained. If the voltage rise rate is rather high, the breakdown occurs typically in a few tens of seconds. Otherwise, breakdown could take longer.

For the ES tests, Equation (5.14) becomes

$$P(ES) \;=\; 1 - \exp\left[-\left(\frac{ES}{ES'}\right)^{\beta_{\mathrm{ES}}}\right] , \tag{5.15}$$

where ES' is the breakdown field strength at 63.2 % probability. The shape parameter β_{ES} is usually rather large, e.g. 10 or more. This corresponds to a scatter of the breakdown gradients of a few per cents.

It is well-known that Equation (5.15) is used to derive the ratio between the breakdown gradients of specimens having *different size*, because the scale parameter of the Weibull distribution is proportional to the dimensional coefficient, N. This ratio is given by

$$\frac{ES_1}{ES_2} \;=\; N^{1/\beta_{\mathrm{ES}}} \;, \tag{5.16}$$

where ES_2 is the electric strength of specimens N times larger than the smaller specimens having electric strength equal to ES_1. If $N > 1$ then the ratio ES_1/ES_2 is > 1, becoming 1 for β_{ES} tending to ∞. Thus, the larger β_{ES} is the smaller the scatter of the breakdown data, the lower is the ratio of ES_1 to ES_2.

6 Experimental results and discussions

Two major criteria in selecting the silicone rubbers for a rubber stress cone of the HV cable accessories are their electrical and mechanical performances. Dielectric strength E_b and mechanical properties (i.e. tensile strength and elongation at break) are the key important factors for HV cable accessories. The specific elastic properties of a rubber stress cone are important for its functional capability of stabilizing interfaces. In this chapter, electrical and mechanical properties of commercially available silicone rubbers are presented. The dielectric strength value as well as tensile strength and elongation at break of three types of the optically compatible silicone rubbers are evaluated. The obtained test results were verified by statistical analysis based on the 2-parameter Weibull distribution function. Suggestions for transfer of the results into the cable industry are discussed as well.

6.1 Mechanical properties of the optically compatible silicone rubbers

The transparent and translucent types of commercially available silicone rubbers were selected for investigation of their properties which are related to the capability for optical and high-voltage applications. Three types of a two-component liquid silicone rubber, i.e. ESA 7250, LSR 7665, and LSR 3003/30, are in the focus based on the requirements of the power cable industry to investigate their basic properties. Unfortunately, from a critical reading in the recommended datasheets [131-133], there are several curing processes that can be applied to produce a silicone rubber, as listed in Table 6.1 below.

Table 6.1: Recommended curing conditions for the silicone rubber samples

Silicone Samples	Appearance	Mixing ratio A:B (by weight)	Curing conditions of silicone rubbers	
			Normal curing (NC)	Post curing (PC)
ESA 7250	Transparent	10:1	1) 72 hours at RT 2) 4 hours at 60 °C or 3) 2 hours at 100 °C or 4) 1 hour at 150 °C	+ 2 hours at 200 °C
LSR 7665	Transparent	1:1	1 hour at 80 °C	+ 2 hours at 200 °C
LSR 3003/30	Translucent	1:1	2 hours at 80 °C	+ 4 hours at 200 °C

Note: a) Normal curing of the ESA 7250 can be performed in different temperatures as recommended in [131]
b) Post curing (PC) process is carried out after normal curing (NC) process

The mechanical and electrical properties of silicone rubbers depend on their chemical structure, particularly on the degree of cross-linking in polymer matrices. The degree of cross-linking in elastomers is related to their curing processes. Therefore, in the beginning, the appropriate curing method of each silicone should be defined. Following curing process of each silicone will be used for all cases of investigation in this research such as dielectric strength measurements and consequently use as the curing procedure for the modification of silicone rubbers (i.e. fluorescent modification and nano fillers addition) in the future research. A simple method to determine the appropriate curing process is the measurement of their mechanical properties, so, tensile strength and elongation at break were measured. The normal curing (NC) and the additional post curing (PC) conditions are the main focus of this review. The test procedure will be briefly described below.

The measurements of tensile strength and elongation at break of the silicone rubbers were carried out according to the ISO 37:2011 standard [162]. The dumb-bells test pieces (Type 2) with the dimensions shown in Figure 6.1 were used as a test specimen. The thickness of the test pieces is 2.0 mm ± 0.2 mm and the test length is 20 mm ± 0.5 mm. A cutting machine was used to cut the dumb-bells test pieces from a bigger silicone sheet perpendicularly to the grain of materials. Ten specimens were cut from three different silicone sheets, which were prepared in the same process to have a truly random sample from the target population. The test pieces were marked with two reference marks to define the test length as specified in Figure 6.1. A tensile testing machine produced by Zwick Roell AG was used. The speed of load application was set to 250 mm/min with the initial load of 0.1 N. Examples of test pieces and the experimental setup are shown in Figure 6.2 and Figure 6.3.

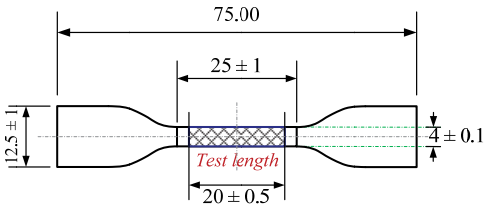

Figure 6.1: Dimensions of a dumb-bell test pieces Type 2 according to ISO 37:2011 [162]

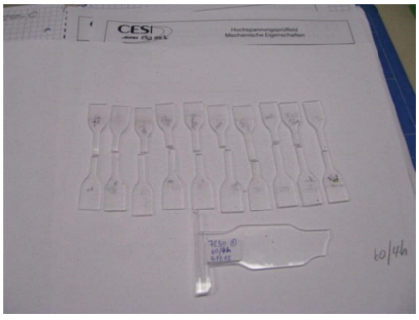

a) Specimen cured at 60 °C for 4 hours

b) Specimen cured with post curing condition

Figure 6.2: Examples of the transparent silicone test pieces

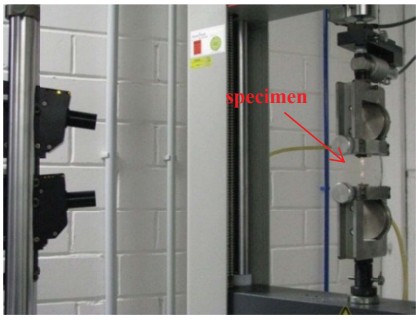

a) Installation of the test piece

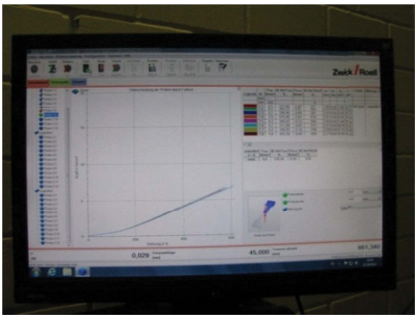

b) TestXpert II testing software by Zwick

Figure 6.3: Examples of the experimental setup in the testing laboratory of CESI-IPH Berlin

6.1.1 Mechanical properties of ESA 7250 silicone rubber

The commercially available liquid silicone rubber (2-component) – ESA 7250 silicone can be cured in several conditions, i.e. at room temperature (RT) or accelerated by heating, which are recommended by the silicone producer. The influences of curing processes on the mechanical properties of ESA 7250 were investigated to define the appropriate curing method for further investigations. The silicone sheet specimens were cured under five curing procedures: (*a*) RT for 72 hours, (*b*) 60 °C for 4 hours, (*c*) 100 °C for 2 hours, (*d*) 100 °C for 2 hours + 200 °C for 2 hours; so-called "*post curing*", and (*e*) 150 °C for 1 hour. The two-parameter Weibull distribution function was fitted to the experimental data and it was used for a statistical evaluation of the results. The results for tensile strength at break TS_b of the ESA 7250 under different curing processes are shown in Figure 6.4; the estimated Weibull parameters α and β as well as the correlation coefficient r are illustrated in Table 6.2.

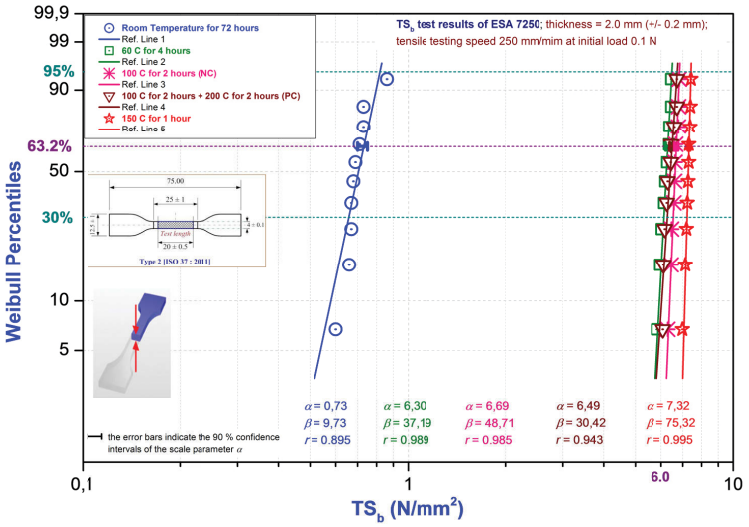

Figure 6.4: Tensile strength TS_b test results for ESA 7250 silicone rubber under different curing processes

Table 6.2: Estimates of the 90 % confidence intervals of the Weibull parameters for tensile strength at break results of ESA 7250 from Figure 6.4

Curing conditions	90 % confidence intervals of Weibull parameters						Correlation coefficient r
	Scale α, in N/mm²			Shape β			
	α_{lower}	α	α_{upper}	β_{lower}	β	β_{upper}	
Room temperature for 72 hours	0.70	**0.73**	0.75	9.38	**9.73**	23.55	**0.895**
60 °C for 4 hours	6.20	**6.30**	6.40	22.58	**37.19**	56.68	**0.989**
100 °C for 2 hours (NC)	6.61	**6.69**	6.77	30.63	**48.71**	76.89	**0.985**
100 °C for 2 hours + 200 °C for 2 hours (PC)	6.38	**6.49**	6.59	22.19	**30.42**	55.70	**0.943**
150 °C for 1 hour	7.26	**7.32**	7.38	42.38	**75.32**	106.40	**0.995**

The results for tensile strength at break TS_b as shown in Figure 6.4 and Table 6.2 reveal that a high-temperature curing provides better mechanical strength. The value of TS_b is increasing when the curing temperature is increased. But there is no significant difference in the value of tensile strength when they cured at high temperatures above 60 °C. This means that the ESA 7250 silicone rubber should be cured at high temperature to achieve good cross-linking reaction between the polymer chains, and thus good tensile strength. The additional post-curing process, however, does not improve tensile strength of the rubber whereas it tends to decrease as shown by the scale parameter α in Table 6.2.

Likewise, the elongation at break (in %) of ESA 7250 obtained under different curing processes are shown in Figure 6.5 and the estimated Weibull parameters α and β as well as the correlation coefficient r are illustrated in Table 6.3.

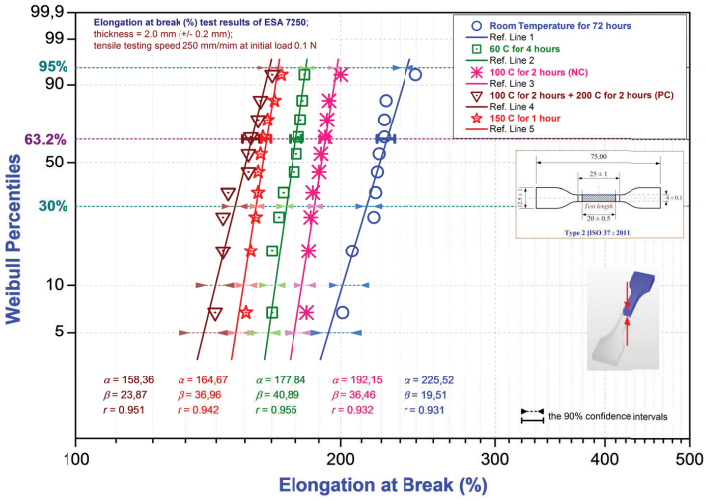

Figure 6.5: Elongation at break of ESA 7250 under different curing conditions; the error bars (⊢⊣) represent the 90 % confidence intervals of data for the *i*-th Weibull percentiles

Table 6.3: Estimates of the 90 % confidence intervals of the Weibull parameters for the elongation at break results of ESA 7250 from Figure 6.5

Curing conditions	90 % confidence intervals of Weibull parameters						Correlation coefficient r
	Scale α, in %			Shape β			
	α_{lower}	α	α_{upper}	β_{lower}	β	β_{upper}	
Room temperature for 72 hours	219.71	**225.52**	230.10	16.10	**19.51**	40.43	**0.931**
60 °C for 4 hours	175.10	**177.84**	180.45	24.70	**40.89**	62.02	**0.955**
100 °C for 2 hours (NC)	189.43	**192.15**	194.17	30.11	**36.46**	75.58	**0.932**
100 °C for 2 hours + 200 °C for 2 hours (PC)	154.58	**158.36**	161.69	16.55	**23.87**	41.54	**0.951**
150 °C for 1 hour	162.36	**164.67**	166.42	31.14	**36.96**	75.66	**0.942**

The results for elongation at break of ESA 7250 show that they are significantly different in their elastic properties because there is no essential overlap between the 90 % confidence intervals of each data set. The ESA 7250 silicone rubber cures by a polyaddition

reaction at room temperature (RT) and the elastomer can be handled after 72 hours, but it is a soft elastomer. It has relatively low tensile strength but high elasticity as shown in the results. The high temperature curing reduces the time consuming process and increases the degree of cross-linking in the elastomer matrix; thus, it has higher hardness and stronger molecular bonds, and consequently reduced elongation ability as shown in the experimental results.

Considering Figure 6.5, it was found that the elasticity (elongation) of this silicone rubber is limited when the curing temperature was increased up to 100 °C. This condition was defined as a reference condition. The scale parameter α decreased by -14.3 % when curing at 150 °C for 1 hour was applied and, likewise, it decreased by -17.6 % when the additional post-curing process was applied. These results are compared to the reference condition. Therefore, the additional post-curing (PC) procedure does not give a positive impact on their mechanical properties.

For reasons mentioned above, curing at 100 °C for 2 hours is suitable for ESA 7250. This condition was used for normal-curing preparation of silicone sheet specimens in further investigations which are presented in the next section.

6.1.2 Mechanical properties of LSR 7665 silicone rubber

The normal curing (NC) and the additional post-curing (PC) procedures can be applied for the 2-component liquid silicone rubber LSR 7665 as recommended by the silicone producer. Specimens cured with and without the additional post-curing process were tested to investigate the impact of post-curing condition. The tensile strengths at break TS_b for LSR 7665 with and without the post-curing process are shown in Figure 6.6 and Table 6.4. The error bars (⊢⊣) shown in the graphs represent the 90 % confidence intervals of data for the *i*-th Weibull percentiles.

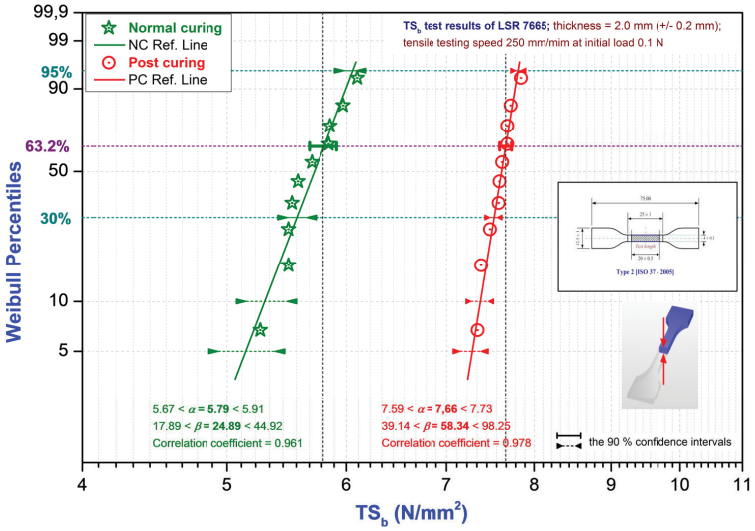

Figure 6.6: Tensile strength TS_b test results for LSR 7665 silicone rubber in case of normal- and post-curing conditions

Table 6.4: Estimates of the 90 % confidence intervals of the Weibull parameters for tensile strengths at break results of LSR 7665 from Figure 6.6

Curing conditions	90 % confidence intervals of Weibull parameters						Correlation coefficient (r)
	Scale α, in N/mm^2			Shape β			
	α_{lower}	α	α_{upper}	β_{lower}	β	β_{upper}	
Normal curing (NC) ***at 80 °C for 1 hour***	5.67	**5.79**	5.91	17.89	**24.89**	44.92	**0.961**
Post curing (PC) ***+ 200 °C for 2 hours***	7.59	**7.66**	7.73	39.14	**58.34**	98.25	**0.978**

Likewise, the results for elongation at break of LSR 7665 specimens with and without post-curing are shown in Figure 6.7 and the estimated Weibull parameters α and β as well as the correlation coefficient r are illustrated in Table 6.5. The error bars (⊢⊣) shown in the graphs represent the 90 % confidence intervals of data for the i-th Weibull percentiles.

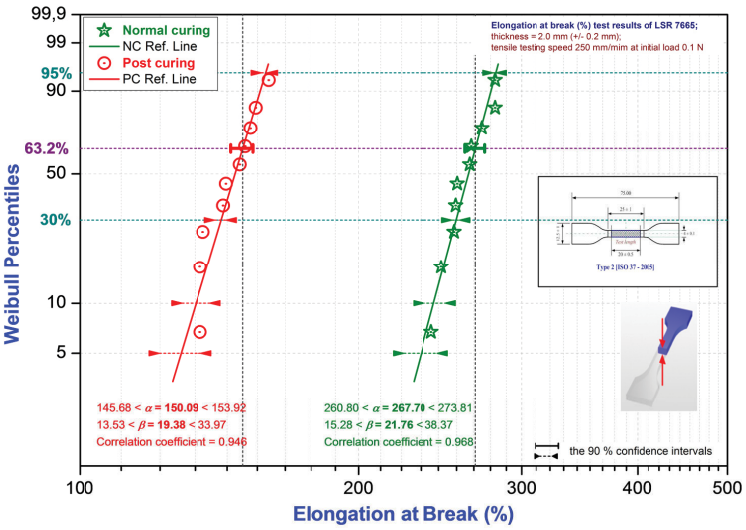

Figure 6.7: Elongation at break of LSR 7665 in case of normal- and post-curing conditions

Table 6.5: Estimates of the 90 % confidence intervals of the Weibull parameters for the elongation at break results of LSR 7665 from Figure 6.7

Curing conditions	90 % confidence intervals of Weibull parameters						Correlation coefficient r
	Scale α, in %			Shape β			
	α_{lower}	α	α_{upper}	β_{lower}	β	β_{upper}	
Normal curing (NC) ***at 80 °C for 1 hour***	260.80	**267.70**	273.81	15.28	**21.76**	38.37	**0.968**
Post curing (PC) ***+ 200 °C for 2 hours***	145.68	**150.09**	153.92	13.53	**19.38**	33.97	**0.946**

The results show that the curing processes can influence the mechanical properties of LSR 7665 silicone rubber. The additional post-curing process can enhance the degree of cross-linking in the rubber materials and then makes stronger molecular bonds. Thus, a

significantly higher tensile strength than for normal curing can be achieved. But unfortunately, the elongation behaviour is in contrast to these results.

The experimental results show that when the post-curing procedure was applied, the tensile strength value of LSR 7665 silicone rubber increases by about +32 %, whereas the elongation at break decreased by approximately -44 %, compared with the normal-curing case. This is particularly advantageous since the elongation at break property of the elastomer is also able to withstand strong tensile force.

In practice, a rubber stress-cone component of the high-voltage cable accessories requires the elastic property of elastomeric materials rather than the tensile strength property. The experimental results for normally cured specimens show sufficient high tensile strength that can be exploited for cable accessories. The additional post-curing procedure does not provide a positive impact on their elongation abilities. Therefore, the normal-curing process is suitable for LSR 7665. This process was used for the preparation of silicone sheet specimens in further investigations which are presented in the next section.

6.1.3 Mechanical properties of LSR 3003/30 silicone rubber

It is important to note that the 2-component liquid silicone rubber LSR 3003/30 in the uncured state is a very highly viscous (approx. 213,000 mPa.s) with translucent appearance. One limitation of this silicone is the difficulty in obtaining qualitative test specimens. Normally, for the cross-linking process, the normal curing (NC) and the additional post curing (PC) can be applied. Specimens cured with and without post-curing process were tested to investigate the effect of post-curing procedure. The results for tensile strength of LSR 3003/30 silicone rubber are shown in Figure 6.8 and Table 6.6. Again, the results for elongation at break of such silicone rubber with and without post-curing process are shown in Figure 6.9 and Table 6.7.

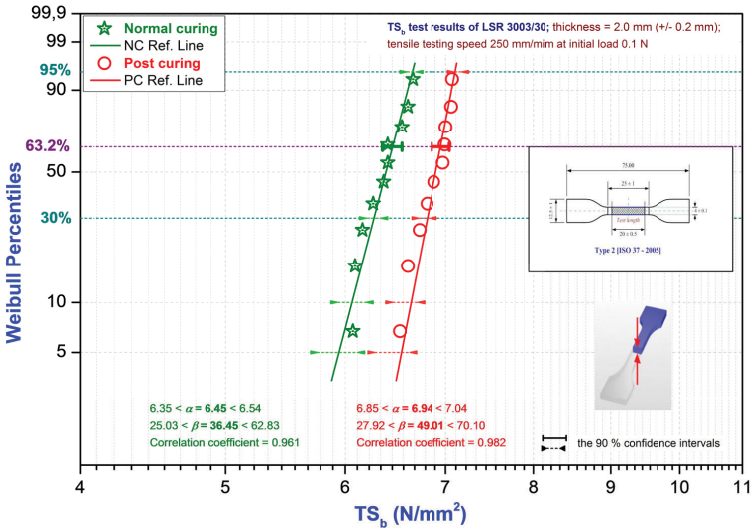

Figure 6.8: Tensile strength TS_b test results for LSR 3003/30 silicone rubber in case of normal- and post-curing conditions

Table 6.6: Estimates of the 90 % confidence intervals of Weibull parameters for tensile strength at break results of LSR 3003/30 from Figure 6.8

Curing conditions	90 % confidence intervals of Weibull parameters						Correlation coefficient r
	Scale α, in N/mm^2			Shape β			
	α_{lower}	α	α_{upper}	β_{lower}	β	β_{upper}	
Normal curing (NC) ***at 80 °C for 2 hours***	6.35	**6.45**	6.54	25.03	**36.45**	62.83	**0.961**
Post curing (PC) ***+ 200 °C for 4 hours***	6.85	**6.94**	7.04	27.92	**49.01**	70.10	**0.982**

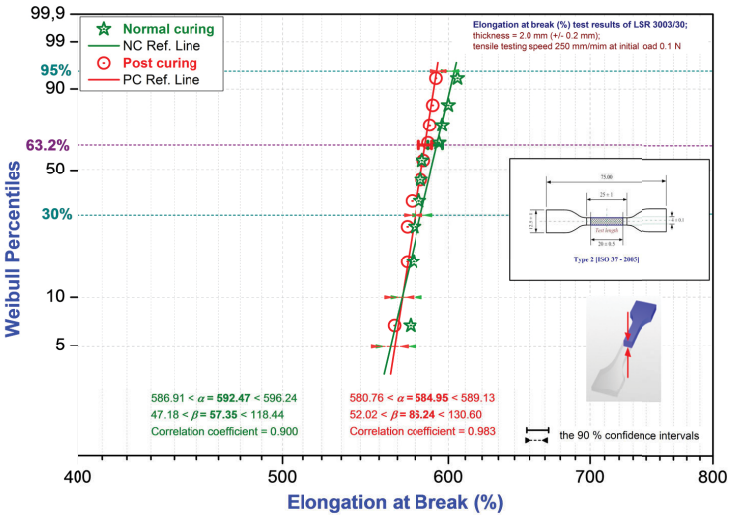

Figure 6.9: Elongation at break of LSR 3003/30 in case of normal- and post-curing conditions

Table 6.7: Estimates of the 90 % confidence intervals of Weibull parameters for the elongation at break results of LSR 3003/30 from Figure 6.9

Curing conditions	90 % confidence intervals of Weibull parameters						Correlation coefficient r
	Scale α, in %			Shape β			
	α_{lower}	α	α_{upper}	β_{lower}	β	β_{upper}	
Normal curing (NC) ***at 80 °C for 2 hours***	586.91	**592.47**	596.24	47.18	**57.35**	118.44	**0.900**
Post curing (PC) ***+ 200 °C for 4 hours***	580.76	**584.95**	589.13	52.02	**86.24**	130.60	**0.983**

The results show that the stress-strain characteristic (in tension) for LSR 3003/30 silicone rubber is excellent. It has high tensile strength property and good elasticity. The additional post-curing procedure does not have significant impact on its tensile strength. Further improvement of the elongation ability for this silicone rubber may not be necessary.

The tensile strength value of the LSR 3003/30 was increased by about +8 % when the additional post-curing procedure was applied. But in case of the elongation at break, the 90 % confidence intervals of two data sets are overlapping along the edges of both graphs as shown

in Figure 6.9. Thus, the additional post-curing process does not improve on its elasticity. Therefore, only the normal-curing procedure is reasonable to use for preparation of the LSR 3003/30 silicone sheet specimen for further investigations.

6.1.4 Discussion and conclusion

This section states briefly the mechanical behaviour of the optically compatible silicone rubber materials to provide a context for the appropriate curing conditions for each silicone type as well as shows further possibilities of modification.

As a result, the reasonable curing process parameters for each type of the silicone samples are as follows:

- ESA 7250 should be cured at 100 °C for 2 hours,
- LSR 7665 should be cured at 80 °C for 1 hour,
- LSR 3003/30 should be cured at 80 °C for 2 hours.

By the way, the mechanical properties of the electrical grade RTV 2 – PowerSil 600 – silicone rubber was investigated in order to compare the results with those optically compatible silicone rubbers under the appropriate curing conditions as mentioned above. The comparison of their tensile properties is shown in Figure 6.10.

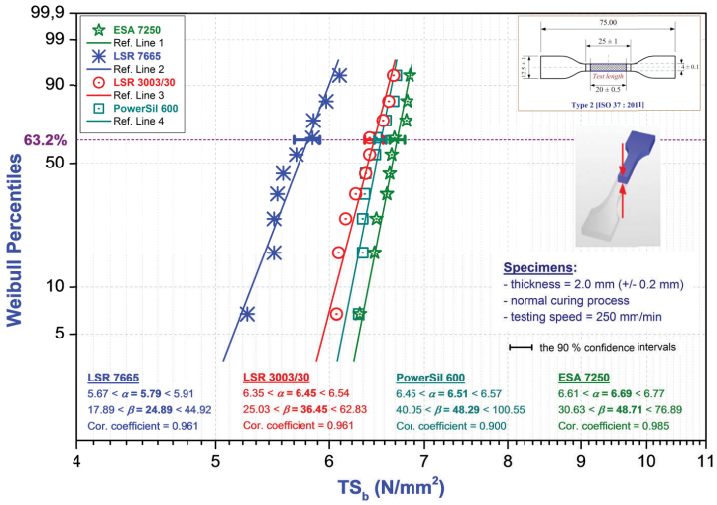

Figure 6.10: Comparison of tensile strength properties of the optically compatible silicone rubbers (ESA 7250, LSR 7665 and LSR 3003/30) and the electrical grade silicone rubber (PowerSil 600)

From the experimental results as shown in Figure 6.10, the transparent ESA 7250 provides the highest value of tensile strength. On the other hand, the transparent LSR 7665 provides the lowest value. The tensile strength properties of LSR 3003/30, ESA 7250 and PowerSil 600 are quite similar, because their 90 % confidence intervals do overlap.

The comparison of elongation at break is shown in Figure 6.11. The experimental results show that the transparent types of silicone rubbers have a very low percent elongation at break, and ESA 7250 has the lowest. A combined evaluation of all experimental results from this study

shows that the tensile strength properties and the percentage of elongation at break of the translucent LSR 3003/30 are quite the same as the properties of the electrical grade silicone rubber. Therefore, from an engineering point of view, the LSR 3003/30 silicone rubber has good mechanical properties, i.e. high tensile strength and high percent elongation at break, which are sufficiently good for use as a rubber stress cone of the high-voltage cable accessories.

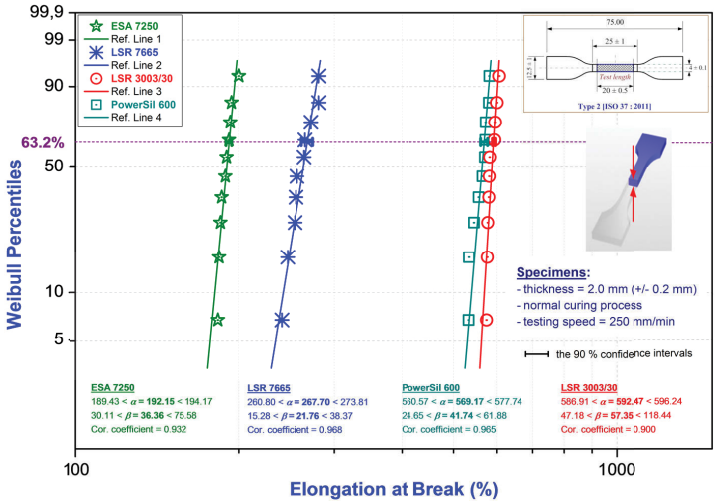

Figure 6.11: Comparison of elongation at break of the transparent types (ESA 7250 and LSR 7665), the translucent type (LSR 3003/30) and the electrical grade (PowerSil 600) silicone rubbers

The experimental evaluations of tensile strength and elongation at break for silicone rubbers, i.e. ESA 7250, LSR 7665, LSR 3003/30 and PowerSil 600 are shown in Figure 6.12 and Figure 6.13. They are compared to reference values which can be found in the data sheets given by silicone producers [131-134]. The tensile strength values of the optically compatible silicone rubbers are in the range from 5.7 N/mm² to 6.7 N/mm², which is sufficient for cable accessories.

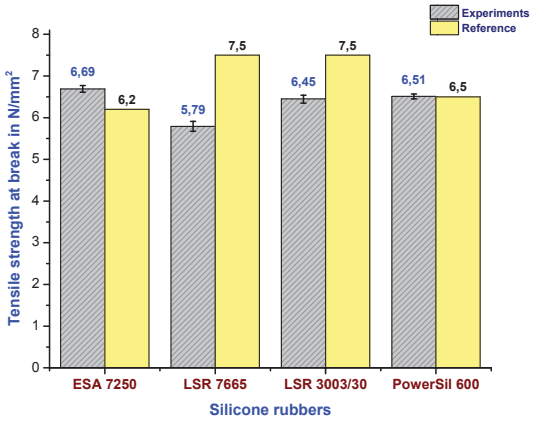

Figure 6.12: Experimental evaluation of tensile strength at break for silicone rubbers compared to reference values from silicone producers

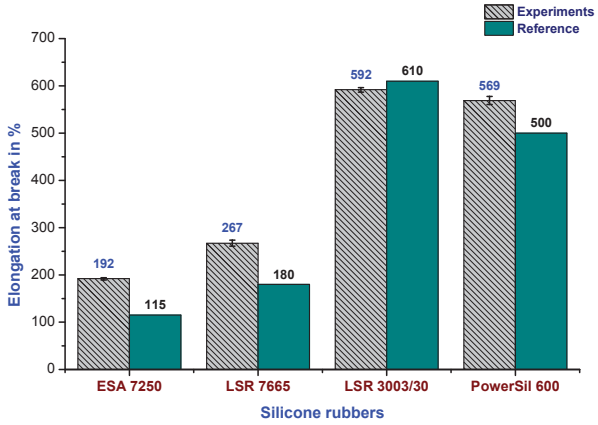

Figure 6.13: Experimental evaluation of elongation at break for silicone rubbers compared to reference values from silicone producers

However, results show that the elongation at break (in %) for transparent silicone rubbers are higher than the expected level but not sufficiently high for power cable accessories. The transparent silicone rubbers are compatible with optical sensors for optical PD detection but they have very low elongation ability. Thus further improvement of their elasticity is necessary if used as a rubber stress cone of HV cable accessories.

The relationship between tensile stress and strain (stress-strain curves) of all silicone samples sketched in the same scale are shown in Figure 6.14.

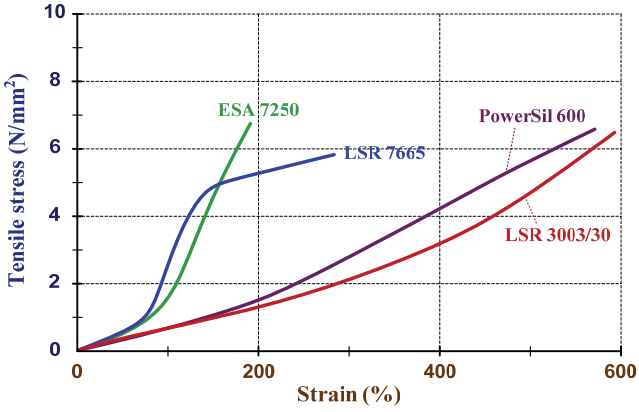

Figure 6.14: Stress-strain characteristics of the investigated silicone rubbers

The stress-strain characteristics of the transparent silicone rubbers are different: ESA 7250 shows a *J*-shaped curve, but the LSR 7665 shows an *S*-shaped curve with 2 yield points. The elastic region of the LSR 7665 elastomer is limited to small strain. In the context of material behaviour, during loading/unloading, their deformation is irreversible. Therefore it is difficult to improve the elongation ability of the LSR 7665 silicone rubber while maintaining its transparency. On the other hand, in case of the ESA 7250, there has little change in shape

for a small load, until a certain force is applied. It may be possible to improve their elongation ability by modification of its polymer matrix using nano-fillers addition or chemical bonding enhancement.

From Figure 6.14, the translucent silicone rubber (LSR 3003/30) and the electrical grade silicone rubber (PowerSil 600) have a large elastic region with an acceptable plastic deformation. The translucent silicone rubber has good mechanical properties, which are sufficiently enough for use as a rubber stress cone of HV cable accessories. Unfortunately, the translucent silicone rubber does not have such an excellent transparency like the transparent silicone rubbers.

6.2 Dielectric strength of silicone rubbers

Dielectric strength E_b is the most important property for high-voltage electrical insulations. In order to modify the characteristics of the optically compatible silicone rubbers and to improve some of their properties regarding the optical and mechanical characteristics, the effects of modification on the dielectric strength behaviour of such materials must be investigated to ensure that they meet minimum requirement specifications for high-voltage insulation of cable accessories. Therefore, the dielectric strength value of virgin silicone rubbers before its modification must be correctly evaluated, since it will serve as a reference for the further investigations.

In this section, the evaluation of dielectric strength values of the optically compatible silicone rubbers as well as the electrical grade silicone rubber is presented. As the same objectives, four types of silicone rubbers that is, ESA 7250, LSR 7665, LSR 3003/30 and PowerSil 600, are in the focus.

6.2.1 The reliability of measurements

Generally, in any dielectric breakdown measurements, one of the principal characteristics of an outcome measure is its reliability. Reliability refers to the reproducibility of measurements when repeated at random in the same subject or the same material sample. Reliability is often confused with validity but reliability of the measurements does not imply validity. However, a reliable experiment may provide useful valid or dependable results, while an experiment that is not reliable cannot possibly be valid. The reliability of dielectric breakdown measurements is an important consideration in the choice of the primary outcome measures for the evaluation of dielectric strength value of elastomeric materials. Therefore, the reliability of measurements for the developed methodology to measure dielectric strength of silicone rubbers was checked.

The most common form of reliability is retest reliability, which refers to the reproducibility of values of a variable when the same subject is measured twice or more. It is not only a good statistical evaluation which can give reliable results. In practice, testing measures are never perfectly consistent. Hence, five LSR 7665 silicone sheet specimens with the thickness of 0.5 mm (± 0.02 mm) were tested to compare their breakdown results from one specimen to another. All silicone sheets were cured under the same curing procedure as defined in chapter 6.1.4. The high-voltage AC breakdown tests at 50 Hz frequency were carried out under identical conditions. The 60 s step-by-step test procedure was applied. Ten breakdown data points were measured in series for each silicone rubber sheet. The two-

parameter Weibull distribution function was fitted to the experimental data and it was used for a statistical evaluation of dielectric strength value of all samples. The evaluation of AC dielectric strength E_b value for each silicone sheets is shown in Figure 6.15. The estimated Weibull parameters α and β as well as the correlation coefficient r are illustrated in Table 6.8.

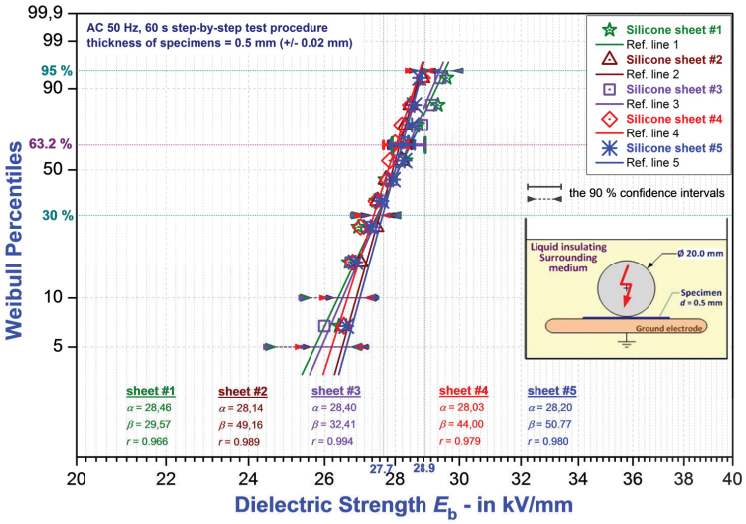

Figure 6.15: Comparison of the AC 50 Hz dielectric strength values measured from five different silicone sheets made from the same type of silicone rubber

Table 6.8: Estimates of the 90 % confidence intervals of the Weibull parameters for AC dielectric strength measurements from five silicone sheets as shown in Figure 6.15

LSR 7665 silicone rubber	Sample size n	90 % confidence intervals of the Weibull parameters						Correlation coefficient r
		Scale α, in kV/mm			Shape β			
		α_{lower}	α	α_{upper}	β_{lower}	β	β_{upper}	
Silicone sheet #1	10	27.91	**28.46**	28.94	20.58	**29.57**	51.66	**0.966**
Silicone sheet #2	10	27.80	**28.14**	28.48	30.67	**49.16**	76.99	**0.989**
Silicone sheet #3	10	27.89	**28.40**	28.92	20.40	**32.41**	51.20	**0.994**
Silicone sheet #4	10	27.66	**28.03**	28.37	29.51	**44.00**	74.09	**0.979**
Silicone sheet #5	10	27.85	**28.20**	28.57	29.29	**50.77**	73.54	**0.980**

A slight downward curvature of the experimental data points can be observed from Figure 6.15. This plot resembles qualitatively the results reported in [20] and [22] under the designation of 2-parameter Weibull population distribution characteristic "*type 1*" as described in [149]. But in this case, all data points lie inside the tolerance bounds. The correlation coefficient r values of all data sets (Table 6.8) are greater than the critical value recommended by IEC 62539 [138] for a small sample size ($n = 10$) and a complete data set. Therefore, the data is a good fit to the 2-parameter Weibull distribution. The 2-parameter Weibull function proves that the samples can be considered as belonging to the same population at a significance level of the 30th percentiles.

The values for shape parameter β shown in Table 6.8 from each 2-parameter Weibull fit were noted as a general indication of result reliability. It is generally considered that β values greater than 10 are acceptable [143, 145, 163].

Notice that the breakdown tests of only one silicone sheet reduce the complexity of the specimen preparation processes. The unknown factors, which are caused by the preparation processes, could be reduced to the minimum. Therefore, a good statistical evaluation of the test results can be achieved. Comparing the E_b values for the breakdown tests performed from different sheets of the same silicone material, the obtained values show a good consistency. The E_b value obtained from the breakdown tests with five silicone sheets is in the range of about 27 kV/mm to 29 kV/mm. Since the 90 % confidence intervals overlap each other, especially at the 63.2 percentile of the Weibull cumulative probability as shown in Figure 6.15. It is accepted that there is no significant difference for the scale parameter α between their experimental; this is due to the fact that the variability of the individual measurements was minimized. Therefore, this testing methodology provides the necessary degree of reproducibility of measurements.

Additionally, a larger silicone sheet of LSR 7665 of similar thickness was prepared following the same curing procedure as mentioned before. The 60 electrical breakdown data points were measured from such specimen under the same test conditions to compare the results with the cases of smaller sample sizes. The 2-parameter Weibull distribution function was fitted to the experimental data. The statistical evaluation of AC dielectric strength value for larger sample size ($n = 60$) is illustrated in Figure 6.16.

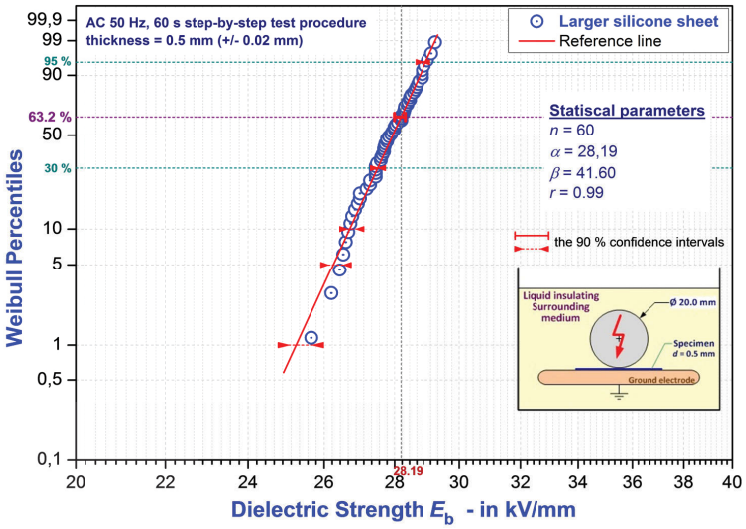

Figure 6.16: The results of statistical evaluation of the AC 50 Hz dielectric strength value of LSR 7665 silicone rubber sheet when tested with larger sample size ($n = 60$)

It is obvious from Figure 6.16 that the Weibull plots of the AC dielectric breakdown data points for larger sample size are very well approximated by a straight line as confirmed by the very good fit with a 2-parameter Weibull distribution, as shown in Table 6.9.

Moreover, the Weibull scale parameter α is likely similar to that for a smaller sample size ($n = 10$), as shown in Figure 6.15.

Table 6.9: Estimates of the 90 % confidence intervals of the Weibull parameters for experimental results with larger sample size ($n = 60$) as shown in Figure 6.16

LSR 7665 rubber sheet with large sample size	90 % confidence intervals of the Weibull parameters						Correlation coefficient r
	Scale α, in kV/mm			Shape β			
	α_{lower}	α	α_{upper}	β_{lower}	β	β_{upper}	
n = **60**	28.00	**28.19**	28.32	36.11	**41.60**	56.56	**0.992**

The results from larger sample size confirm that the newly developed test methodology for dielectric breakdown measurements of silicone rubbers can give reliable results for a small sample size. They provide a similar result for the same material under the same test conditions. A measurement method is considered to have a high reliability when it produces similar results under consistent conditions. Therefore ten breakdown data points are adequate for every test series in order to obtain a sufficient statistical evaluation for E_{b} value of elastomeric materials. However, when experiments are being made for purposes other than routine test, larger numbers of breakdown tests will be necessary depending on the variability of the polymeric materials and the statistical analysis to be applied.

6.2.2 The dielectric strength values of optically compatible silicone rubbers

This section deals with the evaluation of AC 50 Hz dielectric strength value for the virgin optically compatible types of silicone rubber (SiR) which are used as a basic material for development of the novel silicone optical fibre and the optical sensor elements for optical PD detection in HV cable terminations [15, 18]. The E_{b} values of two transparent types and one translucent type of silicone samples (i.e. ESA 7250, LSR 7665 and LSR 3003/30) were investigated and evaluated using the newly developed methodology for breakdown test of elastomeric materials. The results are compared with the E_{b} value of the electrical grade RTV-2 silicone rubber (PowerSil 600), which was also examined under the same test conditions. The silicone-sheet specimens with a thickness of 0.5 mm (±0.02 mm) were tested. Ten breakdown data points were measured in series from each test specimen. The Weibull plots of AC 50 Hz dielectric breakdown strength for the selected silicone polymers compared to the RTV-2 are shown in Figure 6.17. The estimated Weibull parameters α and β as well as the correlation coefficient r for each type of silicone rubbers are illustrated in Table 6.10.

In Figure 6.17, the solid lines are the regression line of the experimental data points. The error bars (►◄) represent the 90 % confidence intervals of data for the i-th Weibull percentiles. The results show that the 2-parameter Weibull distribution function fits the experimental data very well. There is no data point lies outside the 90 % confidence bounds. The E_{b} values of the virgin transparent silicone rubbers (28.11 kV/mm and 29.27 kV/mm) are higher than that of the virgin translucent type (24.53 kV/mm), whereas, they are lower than, of course, the electrical grade RTV-2 silicone rubber (33.56 kV/mm). The translucent silicone type has great mechanical properties but it provides low dielectric breakdown strength. The translucent silicone rubbers generally contain a filler to enhance their mechanical characteristics; however, it may influence the dielectric strength property of the silicone polymer itself.

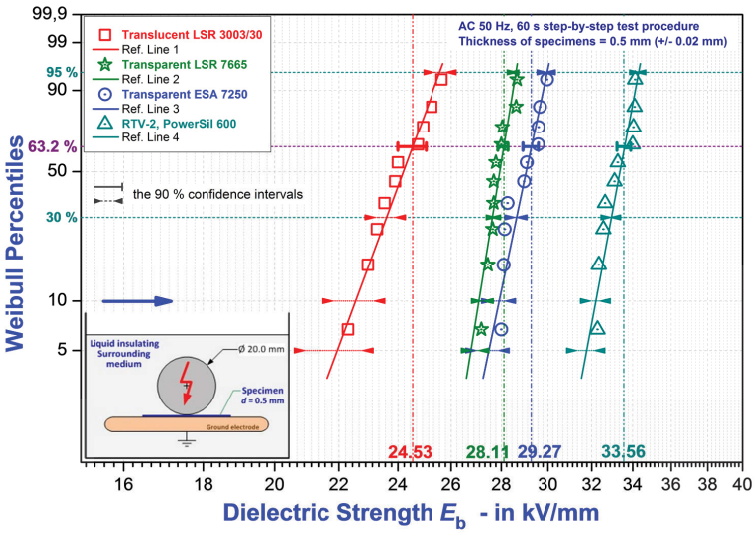

Figure 6.17: AC 50 Hz dielectric strength values of the optically compatible silicone rubbers compared to the E_b value of the electrical grade RTV-2 silicone rubber

Table 6.10: Estimates of the 90 % confidence intervals of the Weibull parameters for AC dielectric strength values of the investigated silicone sheets as shown in Figure 6.17

Silicone rubbers	Sample size *n*	90 % confidence intervals of the Weibull parameters						Correlation coefficient *r*
		Scale α, in kV/mm			Shape β			
		α_{lower}	α	α_{upper}	β_{lower}	β	β_{upper}	
LSR 3003/30	10	24.00	**24.53**	25.02	17.88	**26.73**	44.89	**0.982**
LSR 7665	10	27.86	**28.11**	28.28	50.30	**61.15**	126.28	**0.925**
ESA 7250	10	28.91	**29.27**	29.58	32.50	**47.23**	81.60	**0.926**
PowerSil 600	10	33.22	**33.56**	33.90	36.69	**52.89**	92.11	**0.923**

The two-component transparent silicone rubbers have good optical properties in terms of low light absorption and low scattering. It is the products from the different companies. They have a different mixing ratio, i.e. 10:1 and 1:1 for A:B component by weight (see chapter 5). But, however the results reveal that it is no significant difference between the E_b values of them. A statistical difference between the both distribution functions cannot be detected. Their E_b values are sufficient for cable accessories but, unfortunately, they provide low elongation at break, particularly for the ESA 7250 silicone rubber as mentioned in section 6.1.4.

Electrical grade RTV-2 silicone rubber provides the highest E_b value when compared to the transparent and translucent types. Moreover, its dielectric strength value is higher than that the value declared by the silicone producer [134].

It is worth noting that the evaluation results are different from the breakdown strength values given in the industry manuals which are declared by the manufacturers [131-134], as is shown in Figure 6.18. The E_b values evaluated by new test methodology are greater than that

the E_b value given in such manuals, which is usually based on relatively standardized tests for solid insulating materials with a specimen of 1.0 mm thickness, for examples: IEC 60243-1 [24], ASTM D149 [128]. Therefore, the breakdown strength of silicone rubbers from the present investigation may give an indication as to the suitability of the insulating material (i.e. high or low breakdown strength) but not necessarily information about its dielectric strength behaviours in a complicated system in real insulation cases.

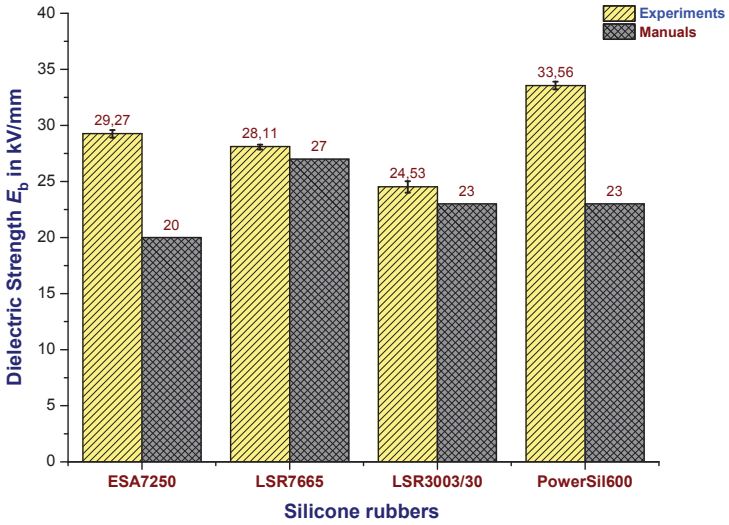

Figure 6.18: Comparison of the dielectric strength values of silicone rubbers evaluated from experimental data and the values given in the data-sheets from silicone producers

An inspection of a breakdown point on the silicone rubber specimens revealed mostly a carbonized channel containing at that point. Since, pure silicone rubbers usually have poor thermal conductivity [164-166]. Thus, it seems that the breakdown process depends on the energy localised in a breakdown initiation point and on the morphological properties of the silicone polymer in the neighbourhood of the deterioration source, confirming the investigations of Danikas [21]. Such a property naturally depends on the elastomer formulation such as the type of chemical reactions for the cross-linking process, the nature of fillers incorporated and the possible presence of impurities or micro-cavities.

The measured values of the breakdown voltage V_b of solid dielectrics are greatly influenced by the experimental conditions. Several factors affect the breakdown strength of silicone rubbers. The dielectric strength values of silicone rubbers found in the literatures [19], [20], [21] and [22], which were reviewed in chapter 4, show that they are varying with different experimental parameters. The influence of different parameters is not clearly identified when compared to another one. Therefore, in the present study, the influence of basic parameters on dielectric breakdown measurements of silicone rubbers was investigated. The focus is on two important parameters: the thickness of test specimen and the voltage increase rate, which have not been done before. The results are discussed in the next section.

6.2.3 The influence of specimen thickness on dielectric breakdown measurements

Several studies have already reported the relationships between the high electric field conduction and the breakdown processes in polymers [78, 167-170]. Theories on the breakdown mechanisms are usually divided into three categories: electronic (or intrinsic), thermal and mechanical processes [78, 169-170]. However, the measured dielectric breakdown strength could sometimes be influenced by secondary effects such as field distortion due to space charge, temperature increase due to local heating and thickness deformation due to Maxwell stress [168-169]. The impact of other parameters usually affecting the breakdown field of polymeric materials such as geometrical parameters (i.e. thickness and area) has been investigated [171-173]. The study of their influence is of primary importance since this allows predicting the dielectric breakdown strength for wide range of geometries. Thus the technical standard ASTM D149 gives a significant remark that the dielectric strength of solid electrical insulating materials is greatly dependent upon a thickness of test specimens: for solid and semi-solid materials, the dielectric strength varies inversely as a fractional power of the sample thickness [128]. In case of silicone rubbers, Danikas *et al.* [19, 21] have reported the variation of breakdown strength with the gap spacing (i.e. 5.0 mm, 10.0 mm and 20.0 mm) for the electrical grade RTV-2 silicone rubber. They reported that the breakdown strength of RTV silicone rubber decreases exponentially with increasing gap spacing. Unfortunately, there is no report regarding the influences of a small thickness (less than 1.0 mm) of test specimens and the different types of silicone elastomers in particular the optically compatible silicone rubbers. So, in this section, the influence of smaller specimen thicknesses on dielectric breakdown measurements for the optically compatible silicone rubber is presented.

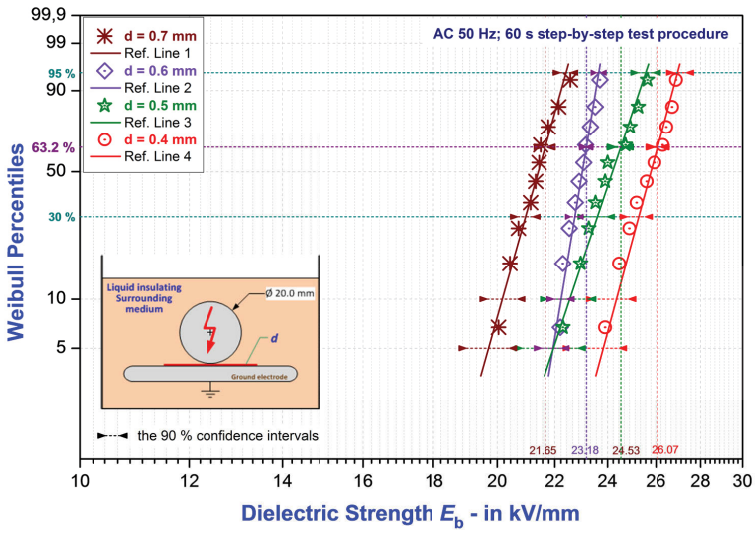

Figure 6.19: Effect of specimen thickness on AC 50 Hz dielectric breakdown measurements of silicone rubber sheets

AC 50 Hz dielectric strength of the translucent silicone rubber was measured. Four rubber sheets with different thicknesses d, i.e. 0.4 mm, 0.5 mm, 0.6 mm, and 0.7 mm, were tested. The variation of thickness was within ± 0.02 mm. The 60 s step-by-step test procedure

was applied. Ten breakdown data points were recorded in series for each silicone rubber sheet. The 2-parameter Weibull plots for each data set are shown in Figure 6.19. The estimated Weibull parameters α and β as well as the correlation coefficient r for the distribution functions in Figure 6.19 are illustrated in Table 6.11.

Table 6.11: Estimates of the 90 % confidence intervals of the Weibull parameters for the distribution functions of the results in Figure 6.19

Thickness of test specimen *d* in mm	**Sample size *n***	**90 % confidence intervals of the Weibull parameters**						**Correlation coefficient *r***
		Scale α, in kV/mm			**Shape β**			
		α_{lower}	**α**	α_{upper}	β_{lower}	**β**	β_{upper}	
0.7 (± 0.02)	10	21.27	**21.65**	22.00	22.01	**31.73**	55.24	**0.983**
0.6 (± 0.02)	10	22.93	**23.18**	23.41	36.32	**53.91**	91.18	**0.976**
0.5 (± 0.02)	10	24.00	**24.53**	25.02	17.88	**26.73**	44.89	**0.982**
0.4 (± 0.02)	10	25.59	**26.07**	26.56	20.02	**33.06**	50.27	**0.990**

The results indicate that the measured E_b value of silicone rubber varies with thickness d of test specimens as shown in Figure 6.19 and Table 6.11. The observed downward trend of the breakdown strength with increasing thickness of silicone rubbers cautions us for the use of dielectric strength values directly from the technical data sheets [131-134]. Such tests refer mostly to experiments done in laboratory conditions under the technical standard recommendations for solid insulating materials, e.g. IEC 60243, ASTM D149. They do not take into account the variation of the breakdown strength with sample thicknesses. It simply shows that in order to draw realistic conclusions one should bear in mind the insulating system under consideration and not the ideal laboratory test. Since the dielectric strength is so dependent upon thickness it is meaningless to report dielectric strength data for a material without stating the thickness of the test specimens used.

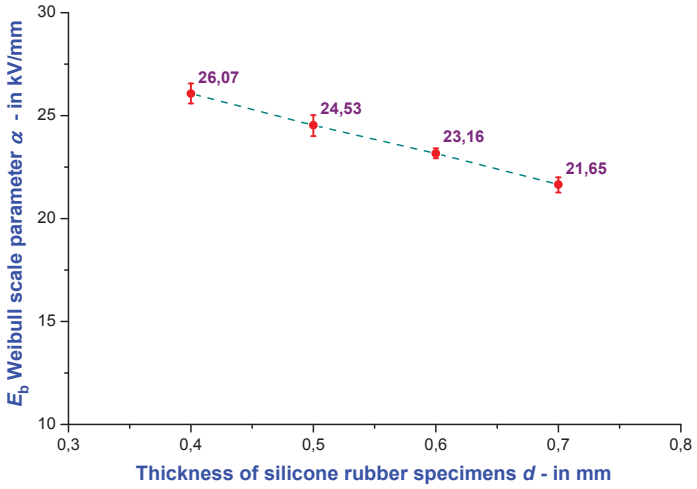

Figure 6.20: Variation of the AC 50 Hz dielectric strength of silicone rubber as a function of the thickness of test specimens in the range of small thickness (less than 1.0 mm)

Figure 6.20 shows the variation of the AC 50 Hz dielectric strength behaviours of the translucent silicone rubber as a function of the thickness of test specimens. The results reveal that dielectric strength of this silicone material also decreases with the increasing of specimen thickness. This experimental result is consistent with those of RTV silicone rubber and larger thicknesses that have reported by Danikas *et al.* [19, 21]. But the difference for smaller scale of thicknesses (0.4 mm to 0.7 mm) is it tends to decrease slightly as a linear function of increasing thicknesses (see Figure 6.20). These results agree with the known "*size effect*" or "*volume effect*". It must be taken into account in designing insulation systems with silicone rubber as insulating material for HV equipment.

Electrical breakdown of silicone rubbers may involve thermal, electrical and mechanical mechanisms. From the electrical point of view, irrespective of whether one subscribes to the theory that the electrical breakdown is initiated by collision ionization of conduction electrons or field emission from the cathode. It is important to note here that, for relatively homogeneous polymeric materials and non-electrical defects inside; a critical number of ionizations by collision are required to produce breakdown mechanisms. The number of ionizations by collision decreased with decreasing the thickness of materials. Hence, in case of smaller thicknesses, the number of ionizations could be increased by higher electric field. Thus, the dielectric strength increases with decreasing thickness of test specimen. The dielectric strength of RTV silicone varies approximately as the reciprocal of the square root of the thickness is confirmed by the results reported in [21] for the range of larger thicknesses, i.e. 5 mm, 10 mm and 20 mm.

In the range of smaller thicknesses, based on the experimental results, there is a significant difference. The dielectric strength of silicone rubber does not change very much, as is shown by the results in Figure 6.20. Therefore it should be noted that, for a small scale of thicknesses (d < 1.0 mm) and applied by 60 s step-by-step test procedure under liquid insulating surrounding medium, the AC dielectric breakdown strength of silicone rubber could be mainly influenced by secondary effects due to thermal instability. This may be caused by temperature increase due to localised heating in regions of the highest electrical stress. However, for the improvement of theoretical breakdown mechanisms in silicone rubbers, more investigations under better experimental conditions are required, and it is beyond the scope of this research work to cover such matter.

6.2.4 The influence of voltage increase rate on breakdown test results of silicone rubber

Because no specific standard test method is available for the determination of the short-term electric strength of elastomeric insulation materials, i.e. silicone rubbers. Typically, the test procedures that are described in the presently available standard test methods for the determination of electric strength of solid insulating materials are often applied [24,128]. For the traditional approaches, the step-by-step test procedure [19, 21] and the short-time (rapid-rise) test procedure [20, 22] are commonly used for the dielectric breakdown test of silicone rubbers. In the mode of rapid-rise test, the applied voltage is raised from zero at a uniform rate (e.g. 200 V/s, 500 V/s, 1 kV/s, 2 kV/s) until breakdown occurs. But, in fact, the modes of increase of voltage can affect the breakdown voltage V_b of the material under test. The breakdown voltage will tend to increase with increasing rate of voltage application. Unfortunately, there are inconsistencies in the traditional methods regarding the time limitation of breakdown mechanisms and the rate of voltage rise for some thicknesses of silicone rubbers that lead to differences in the experimental results. The tolerance range of results according to those standards should define to meet precision

otherwise accuracy of the test results could lead to dispute between the silicone suppliers and the users. Therefore future study and a critical review of the standard test methods for E_b measurements of elastomeric materials seem to be inevitable in order to propose correct and reliable data for many electrical insulation applications particularly for HV/EHV cable accessories. For this purpose, in this thesis, the influence of voltage increase rate on breakdown test results of silicone rubber is presented.

A translucent silicone rubber sheet with a thickness of 0.4 mm (± 0.02 mm) was selected as a test specimen for this experiment in order to investigate the effect of various rates of voltage rise on AC 50 Hz electric strength behaviours of silicone rubbers. The 60 s step-by-step and the rapid rise of voltage, i.e. 200 V/s and 1 kV/s, test procedures were carried out to examine the E_b behaviours of such elastomeric material. Ten breakdown data points were recorded for each test procedure. The 2-parameter Weibull plots for each data set show in Figure 6.21. The estimated Weibull parameters α and β as well as the correlation coefficient r for the distribution functions in Figure 6.21 are illustrated in Table 6.12.

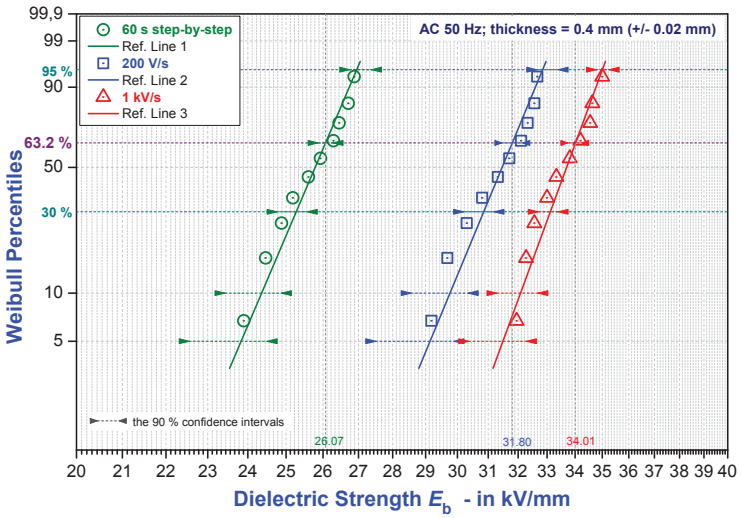

Figure 6.21: The influence of voltage increase rate on dielectric strength measurements of silicone rubber

Table 6.12: Estimates of the 90 % confidence intervals of the Weibull parameters for the distribution functions of the results in Figure 6.21

Modes of increase voltage	Sample size n	90 % confidence intervals of the Weibull parameters						Correlation coefficient r
		Scale α, in kV/mm			Shape β			
		α_{lower}	α	α_{upper}	β_{lower}	β	β_{upper}	
60 s step-by-step	10	25.59	**26.07**	26.56	20.02	**33.06**	50.27	**0.990**
200 V/s	10	31.22	**31.80**	32.40	19.98	**33.95**	50.15	**0.985**
1 kV/s	10	33.49	**34.01**	34.50	25.20	**38.44**	63.27	**0.971**

It is indicated that the modes of increasing voltage influence the measured results of dielectric breakdown measurements for silicone rubbers, as is shown by the experimental

data in Figure 6.21 and Table 6.12 above. As mentioned in chapter 3.4, there are mechanisms related to the short-term breakdown of polymeric materials. The relative importance of these mechanisms is dependent on the modes of voltage increase used in the dielectric breakdown strength measurements. The 60 s step-by-step test procedure results in lower breakdown strength compared to the rapid rise test methods. This is due to long-time existence of the applied electric field. The material under test was broken down at higher voltage level when the rapid rise of voltage was applied, and therefore the greater breakdown strength value is obtained. However, the E_b test result obtained by the 60 s step-by-step test procedure is more reasonable than the others for safety margin in designing of a complex insulation system. The 60 s step-by-step test seems to be the efficient method for the determination of dielectric strength performance of the solid insulating materials [24, 128]. Thus, the results from this test method are widely accepted.

In a case of rapid-rise test method, it is demonstrated clearly that a faster rate of voltage rise results in greater measured breakdown voltage V_b as confirmed by experimental results shown in Figure 6.22 and Table 6.13 below. The E_b value obtained from the slow rate-of-rise test (i.e. 200 V/s) increased by approximately +22 % compared to the results from 60 s step-by-step test procedure. However, the electrical breakdown strength of silicone rubber didn't change too much when the 5 times faster rate-of-rise test (i.e. 1 kV/s) was applied; the measured E_b value increased again by about +7 % compared to the results from 200 V/s test procedure. This difference is a result of the fact that the breakdown voltage and the applied time to breakdown are mutually dependent on each other. The occurrence of breakdown in shorter time duration requires applying of higher voltage level. That is, when increasing the rate of voltage rise, the occurrence of breakdown will occur after a few seconds with high V_b level; on the other hand, when applying a voltage with a slow rate-of-rise, a longer period of time for the occurrence of breakdown is needed, and lower V_b level is obtained. Thus, time to breakdown occurrence from each the rapid-rise test procedures is totally different. Moreover, the measured breakdown voltages are also different, as is illustrated by the experimental data in Table 6.13.

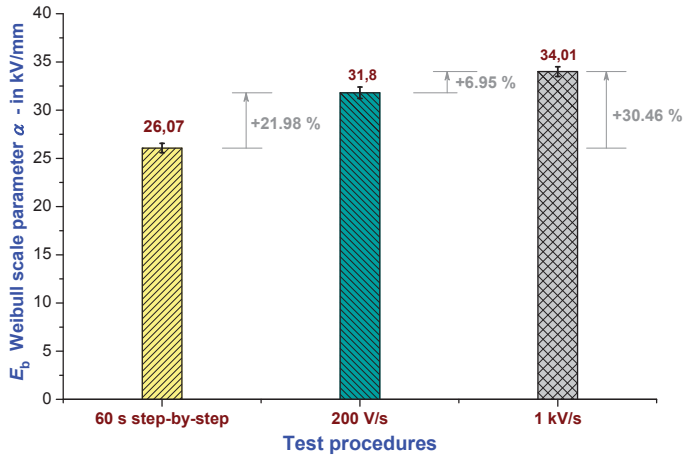

Figure 6.22: The influences of modes of increasing voltage on AC 50 Hz dielectric strength measurements of the silicone rubber

Table 6.13: AC 50 Hz dielectric strength and time to breakdown for the translucent silicone rubber measured with different test procedures

Silicone rubbers	Test procedures	Thickness of specimens in mm	Experimental results					
			V_b [(1)] in kV		E_b [(2)] in kV/mm	App. time to breakdown in seconds (s)		
			Avg.	SD		t_{min}	t_{avg}	t_{max}
Translucent type	60 s step-by-step	0.4 ± 0.02	10.51	0.46	26.07	600.00	654.00	720.00
	200 V/s	0.4 ± 0.02	12.70	0.68	31.80	58.35	63.5	67.90
	1 kV/s	0.4 ± 0.02	13.85	0.58	34.01	13.10	13.85	14.70

Note: [(1)] the average value from the group of ten breakdown data points
[(2)] the scale parameter α from 2-parameter Weibull distribution fit to the experimental data points

In addition, when considering only the rapid-rise test method, the results show that an electrical breakdown process in silicone rubbers is likely limited when they are subjected to high electrical stress by rapidly rise rate of the applied voltage, i.e. 31.8 kV/mm for 200 V/s test and 34.01 kV/mm for 1 kV/s test. This result corresponds with the assumption that the possible breakdown processes in silicone rubber specimens may depend on the energy localised in a breakdown initiation point in the neighbourhood of the deterioration source as discussed in the previous section. Generally, under steady-state applied field stress, the electro-thermal breakdown mechanisms in polymers are usually time-dependent [169-170]. But, since pure silicone rubbers typically have poor thermal conductivity in between 0.165 W/m K and 0.2 W/m K [164-166]. Therefore, under high and sufficient electrical stress, the latter mechanisms may cause rapid failure by producing critically high localised heating in regions of the highest electrical stress. This phenomena lead to the idea that it would be possible to define the criterion for time limitation of breakdown mechanism and the rate of voltage rise for some thicknesses (a thin thickness) of silicone rubbers. In order to avoid a problem due to a large tolerance range as well as the accuracy of the test results, the acceptance criteria for time limitation of breakdown occurrence in test samples should be defined. It is probably essential for future developments of specific standard test methods for silicone rubbers. Furthermore, an inter-laboratory study to determine the precision of a test method as well as the minimum permitted E_b value for silicone insulating materials would be necessary in the future.

In accordance with clause 9.1 of IEC 60243-1 [24] for the rapid-rise test of solid insulating materials, the occurrence of breakdown in test specimens shall be within the time range of 10 s to 20 s. Regarding to this criterion, it seems that the result obtained by 1 kV/s test procedure is able to satisfy the commitments of breakdown time criterion as shown in Table 6.13. Therefore, in this case, the E_b value of 34.01 kV/mm could be accepted for the rapid-rise test result. So in order to get consistent results for the comparison of electrical breakdown performance of silicone rubbers using the rapid-rise test procedure, a rate of voltage rise shall be selected for the material under test to achieve the occurrence of breakdown in test specimens within the time range of 10 s to 20 s. This criterion would also be appropriate for the determination of dielectric strength of elastomeric materials.

So, it should be pointed out again that the new test methodology enables the large number of individual tests, which are necessary to precisely measure the dielectric strength value of silicone rubbers. This low-cost and time-saving experimental method provides a reasonable result with low uncertainty. Various advantages could be achieved.

6.3 Dielectric strength behaviour of silicone rubber under mechanical tensile stress

Basic requirements for rubber materials used as an electrical insulation for HV cable accessories are their electrical and mechanical performances. The specific elastic properties of a rubber stress cone are important for its functional capability of stabilizing interfaces. When a rubber stress cone is mounted to a slightly oversized XLPE insulated cable core, the resulting radial stress ensures a tight fitting to the cable insulation. This is due to avoid the interface problems between two solid insulators, which can influence the whole capability of HV cable terminations and joints. Practically, the maximum elongation of a rubber stress cone after installation is up to 30 % [20]. Therefore, such devices normally operate under combined electrical and mechanical stresses for long-term service. Then, the rubber material with good stress-stain characteristics and excellent dielectric strength is required.

In this section, a preliminary study of the influence of mechanical tensile stress on dielectric strength behaviour of the optically compatible silicone rubber is presented. The applied tensile stress is represented as a percentage of elongation of silicone rubber sheet. For this special investigation, a mechanical tool was specially designed as described in chapter 4.3. The virgin translucent silicone rubber was selected as a test sample because it has excellent stress-strain characteristics, i.e. high tensile strength at break with good elastic properties. A silicone sheet specimen with a thickness of 0.7 mm (± 0.02 mm) was carefully prepared. The normal curing procedure at 80 °C for 2 hours was applied for the preparation of a good silicone rubber sheet. The AC 50 Hz dielectric breakdown measurements were carried out using the 60 s step-by-step test method. Two conditions of mechanical tensile stress, i.e. 15 % elongation and 30 % elongation, were applied to the specimen during the dielectric breakdown measurements. Ten breakdown data points were recorded in series for each elongation condition. The 2-parameter Weibull plots for each breakdown data set show in Figure 6.23. The estimated Weibull parameters α and β as well as the correlation coefficient r for the distribution functions in Figure 6.23 are illustrated in Table 6.14.

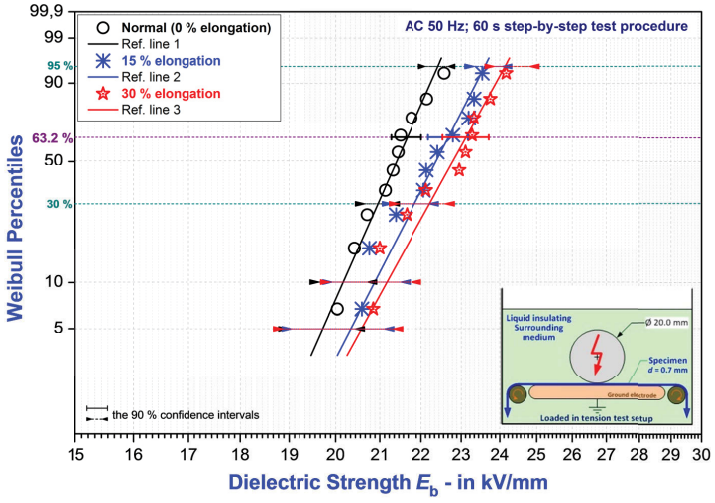

Figure 6.23: AC 50 Hz dielectric strength behaviour of silicone rubber under the influence of mechanical tensile stresses

Table 6.14: Estimates of the 90 % confidence intervals of the Weibull parameters for the distribution functions of the results in Figure 6.23

Applied elongation on specimens [%]	Sample size n	90 % confidence intervals of the Weibull parameters						Correlation coefficient r
		Scale α, in kV/mm			Shape β			
		α_{lower}	α	α_{upper}	β_{lower}	β	β_{upper}	
0	10	21.27	**21.65**	22.00	22.01	**31.73**	55.24	**0.983**
15	10	22.17	**22.67**	23.17	16.89	**27.30**	42.39	**0,978**
30	10	22,53	**23.12**	23,71	14.60	**25.50**	36.65	**0.983**

Figure 6.24 shows the variation of the dielectric strength values and the thicknesses of silicone rubber sheet under the influence of mechanical tensile stress. The results illustrate that the dielectric strength values of silicone rubber tend to increase slightly with increasing the percentage of elongation applied to the specimen under test. This is due to the reduction of thickness of silicone rubber sheet caused by the elongation strain in one direction.

As mentioned in the previous section, the reduction of insulation thickness can enhance dielectric strength of insulating material. However, there is no significant difference between the E_b results of 15 % and 30 % elongations. The 90 % confidence intervals of two such data sets are obviously overlapping along the edges of both E_b distribution graphs as shown in Figure 6.23. Hence, pointing out that the mechanical tensile stress does not influence on the dielectric strength behaviour of silicone rubber. This conclusion is confirmed by similar results for RTV-2 silicone rubber which reported by Österheld [20].

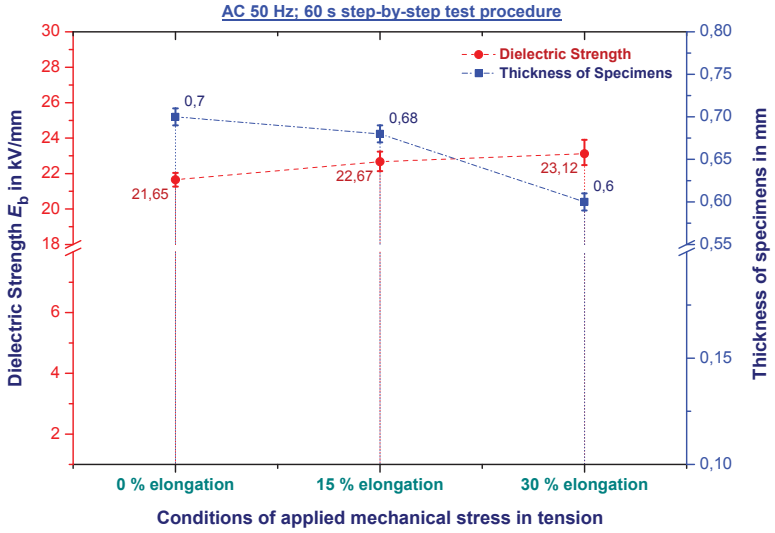

Figure 6.24: Variation of the dielectric strength values and the thicknesses of silicone rubber sheet under the influence of elongation strains

6.4 Dielectric strength behaviour of fluorescent silicone rubbers

A novel optical sensor and sensing elements for PD on-line monitoring in HV cable terminations are being developed as an innovation project at the Federal Institute for Materials Research and Testing (BAM) in Berlin [15, 18]. A fluorescent polymer optical fibre used as sensing elements for early detection of PD activities is the main focus. The siloxane ($R_3Si-[O-SiR_2]_n-O-SiR_2$) material is a flexible polymer with good properties for the application as elastomeric optical-fibre sensor and as transparent elastomer insulation. Siloxane polymers are highly transparent, have low optical attenuation, good mechanical properties and the refractive index can be tuned within a relatively wide range [69]. The fluorescent silicone rubbers (FlSiRs) are beneficial for effective coupling of light into the sensing elements. The fluorescent dyes absorb optical light independently of the angle of incidence, and the fluorescent light is emitted in all directions. Consequently, a higher percentage of light fulfils the requirements relating to total reflection, and is guided to the detector. The FlSiR used as a sensing element has a key advantage that it can be integrated into a rubber stress cone of HV cable accessories, which is made from the optically compatible silicone rubbers. As the embedment into the transparent elastomer insulation plays an important role, the sensor element must not weaken the dielectric strength performance of the main insulation structure. Furthermore, it must not be the cause of PD initiation in HV equipment. Therefore dielectric strength behaviour of the fluorescent silicone rubber was investigated.

The 2-component liquid silicone polymer was mixed with different commercially available fluorescent dyes by 0.02 wt. %. The mixing process was carried out using a triple roller mill machine to disperse fluorescent particles in silicone polymer. This is due to their small size and high surface area-to-volume ratio, high shear force mixing is an effective method to achieve good dispersion of such particles. After that, both silicone components were mixed together at a ratio of 1:1 by weight and degas it applying vacuum. The normal curing procedure at 80 °C for 2 hours was used for curing the rubber matrix. The fluorescent silicone rubber (FlSiR) sheets with a thickness of 0.6 mm (± 0.02 mm) were prepared under identical conditions. Examples of the FlSiR sheets are shown in Figure 6.25.

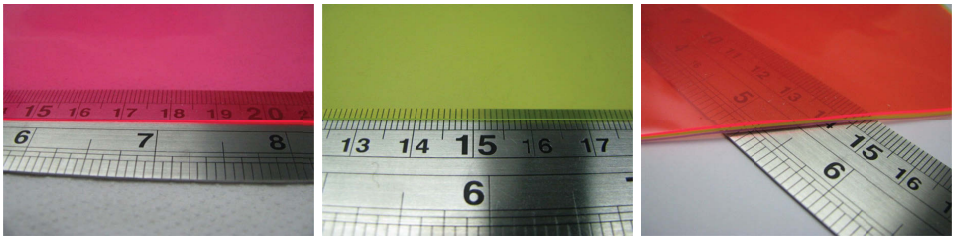

a) FlSiR red *b) FlSiR yellow* *c) FlSiR pink, yellow and blue*

Figure 6.25: Examples of the fluorescent silicone rubber (FlSiR) sheets with different commercially available dyes by 0.02 wt. %

The uniformity of fluorescent particles in silicone rubber sheets was inspected using digital microscope (1000x) to ensure that it is homogeneous. Some inspected results show in Figure 6.26.

a) Virgin silicone rubber, translucent type *b) Fluorescent red silicone rubber*

Figure 6.26: Examples of the inspected results to see uniformity of fluorescent particles in silicone rubber sheet using 2D digital microscope (1000x); there were no perceivable inhomogeneities

AC 50 Hz dielectric strength measurements for the florescent silicone sheet specimens were performed using the 60 s step-by-step test method. Ten breakdown data points were recorded in series for each specimen. The 2-parameter Weibull distribution function was fitted to the experimental results as shown in Figure 6.27. The estimated Weibull parameters α and β as well as the correlation coefficient r for the distribution functions in Figure 6.27 are illustrated in Table 6.15. Translucent silicone polymer mixed with different commercially available dyes by 0.02 wt. % shows the same breakdown strength as the undoped virgin polymer within the statistical 90 % confidence intervals (Figure 6.27). The E_b values within 90 % confidence intervals for all the different fluorescent dyes compared to that of the virgin silicone rubber are obviously overlapping as shown in Figure 6.28.

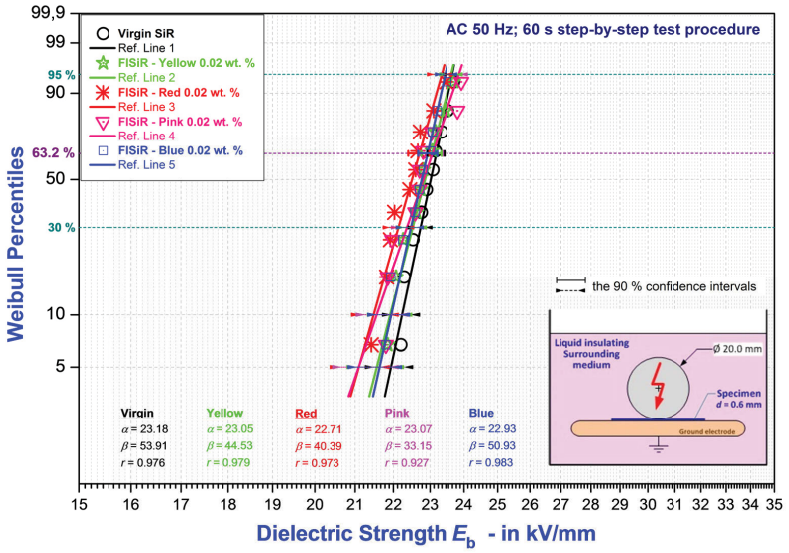

Figure 6.27: AC 50 Hz dielectric strength behaviour of the fluorescent silicone rubbers with different commercially available dyes by 0.02 wt. %

Table 6.15: Estimates of the 90 % confidence intervals of the Weibull parameters for the distribution functions of the results in Figure 6.27

Type of silicone rubbers	Breakdown data points	90 % confidence intervals of the Weibull parameters						Correlation coefficient r
		Scale α, in kV/mm			Shape β			
		α_{lower}	α	α_{upper}	β_{lower}	β	β_{upper}	
Virgin silicone	10	22.93	**23.18**	23.41	36.32	**53.91**	91.18	**0.976**
Fluorescent yellow	10	22.76	**23.05**	23.32	30.43	**44.53**	76.40	**0.979**
Fluorescent red	10	22.40	**22.71**	22.93	28.87	**40.39**	72.47	**0.973**
Fluorescent pink	10	22.70	**23.07**	23.35	26.02	**33.15**	65.31	**0.927**
Fluorescent blue	10	22.67	**22.93**	23.20	32.47	**50.93**	81.52	**0.983**

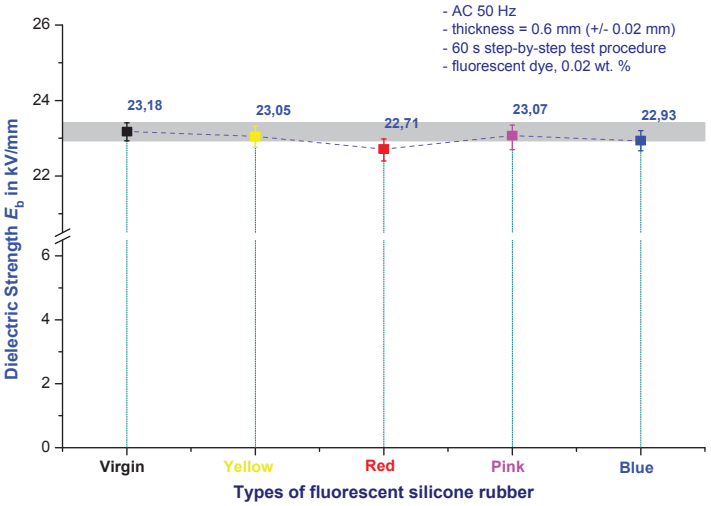

Figure 6.28: Influence of fluorescent dye on dielectric strength behaviour of the optically compatible silicone rubber

Based on the results, hence, it can be concluded that the fluorescent dyes do not seem to negatively influence the dielectric strength of the optically compatible silicone rubber. It is possible to apply such modified materials in a region of moderate to high electric field stress near the critical interface area of HV cable accessories, where PDs most likely occur.

It is important to note here that the fluorescent dyes in silicone polymer by using a triple roller mill machine is not suitable because they are not chemical bonds. The fluorescent particles in silicone polymer are not stable, particularly at elevated temperature. Colour bleeding is an unacceptable phenomenon for the optical element that has to have the expected long lifetime (25 years or more). To prevent dye migration, our new strategy is to covalently link the dye to the siloxane network by taking advantage of the cross-coupling reaction during the curing process of the siloxane network, as described in chapter 2.5.2.

So the optically compatible silicone rubbers are perfectly suitable for the fabrication of Fluorescent Silicone Optical Fibre (FSiOF). Recently, the new FlSiOF models based on

silicone polymer modification have been proposed. Several coumarin dyes were functionalized with unsaturated hydrocarbon groups. The optical properties of the dyes in the siloxane polymer matrices were reported in the literature [69]. An additional way to further improve the level of optical PD detection is the replacement of an opaque elastomer that is currently used for a rubber stress cone of HV cable accessories with a new transparent silicone rubber. To further enhance the transparency, one possibility is to use hydrophobic nanoparticles as fillers. These fillers are much smaller than the wavelength of visible light and reduce the proportion of light being scattered at the interfaces of the nanoparticles and the siloxane polymer matrices. The ongoing development of novel functionalized silicone rubbers at BAM involves a growing number of different modifications that have to be tested for their dielectric strength. Therefore, the research work presented here is essential for reliable, economic and high-throughput dielectric strength testing and will certainly boost future research and facilitate new discoveries.

6.5 Dielectric strength behaviour of silicone rubber with embedded sphere electrode

The dielectric strength E_b values of the optically compatible silicone rubber as presented in chapter 6.2.2 were evaluated from the experimental data obtained by the electric breakdown tests using a silicone rubber sheet under liquid insulating medium. Those results provide the necessary E_b information to indicate the suitability of an insulating material but not the information about its E_b behaviours in complete insulation. However, in some cases such as for the economic design of cable insulation thickness, the information of E_b behaviour of dielectric materials in complete insulation is needed. In such a case, the dielectric strength test requires better test conditions. This can be obtained using a test setup with an embedded sphere electrode and all extraneous influences are then controlled [25]. Therefore, in this section, the E_b behaviour of the silicone samples tested with embedded sphere electrode is presented. The E_b test results will be compared with those results of testing performed using a silicone rubber sheet.

The new type of test specimen with embedded ball electrode was developed, as described in chapter 4.3. It is fully suitable for dielectric breakdown test of silicone rubbers [25, 130]. The embedded sphere to plane electrode arrangement gives a high electric stress in the centre area of the specimen and low stress at the edges. The specimen dimension was minimised in order to enable economic use of sample materials. The test specimen can be mounted on the main electrode of the same test facility, which was used for a silicone rubber sheet specimen (see Figure 4.14 in chapter 4). The standard ball-bearing, made from stainless-steel with a diameter of 20.0 mm and 32.6 g weight, was used as the sphere electrodes to minimise electrode damage at breakdown and to reduce the manufacturing costs. The ball electrode was mirror surface finish polished by a mechanical/chemical polishing process before embedded into the silicone samples. The thickness of test specimens was controlled as 0.5 mm (± 0.02 mm). The normal curing procedure was applied to obtain the complete specimens.

The whole setup was immersed in the electrical grade silicone oil (ε_r = 2.9) in order to avoid surface discharges prior to breakdown. The AC 50 Hz dielectric breakdown tests for the E_b evaluation of the virgin silicone samples, i.e. ESA 7250, LSR 7665 and LSR 3003/30, were performed using the 60 s step-by-step test procedure. Ten specimens were tested for each type of the silicone samples. The 2-parameter Weibull distribution function was fitted to

the experimental data sets and the E_b values were estimated. Figure 6.29 shows the Weibull plots of the breakdown test results for virgin LSR 7665 silicone rubber, comparing the case of an embedded ball electrode with the case of a ball electrode in contact to a silicone sheet specimen. The results indicate that the 2-parameter Weibull distribution fits the new group of breakdown data points for the embedded ball electrode very well. The comparison of estimated E_b results for each type of the silicone samples is shown in Figure 6.30.

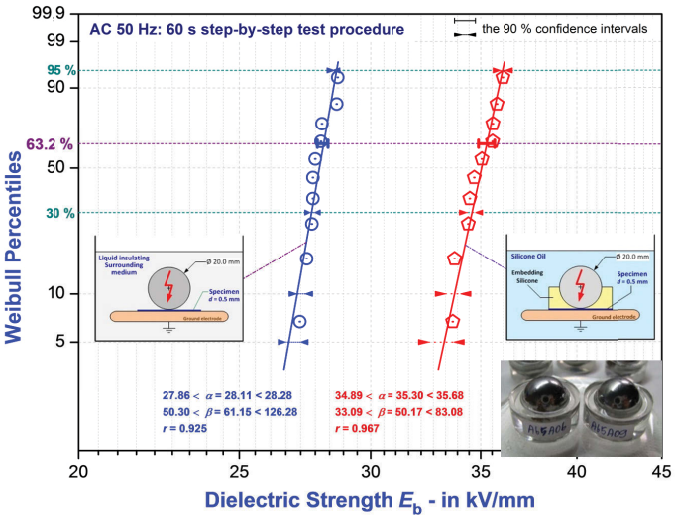

Figure 6.29: Statistical evaluations for AC 50 Hz dielectric strength of the virgin LSR 7665 silicone rubber tested with and without embedded sphere electrode

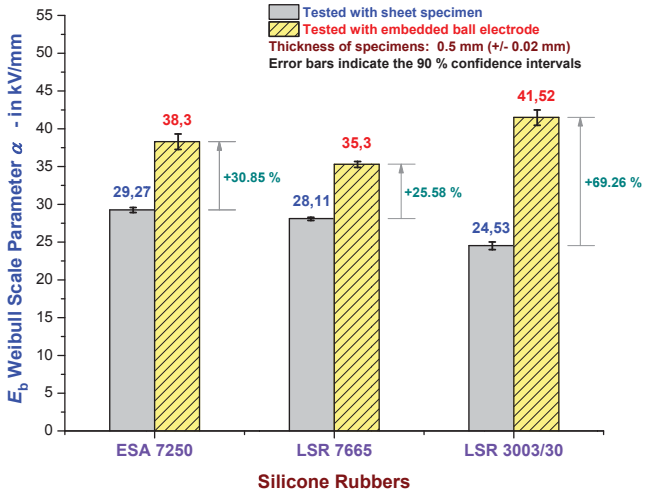

Figure 6.30: AC 50 Hz dielectric strength behaviour of the ESA 7250, LSR 7665 and LSR 3003/30 silicone samples tested with and without embedded sphere electrode (specimen thickness d = 0.5 mm and 60 s step-by-step test)

The experimental results reveal that the dielectric strength value of LSR 7665 silicone sample is approximately increased by 26 % compared to those results obtained from the breakdown test with a silicone rubber sheet (see Figure 6.17) under the same thickness 0.5 mm (± 0.02 mm). Likewise, the dielectric strength values of ESA 7250 and LSR 3003/30 silicone samples are also increased as shown in Figure 6.30. The dielectric strength value is increased by about 31 % for ESA 7250 and by about 69 % for LSR 3003/30. The estimated Weibull parameters for the distribution functions of the E_b results for each type of the silicone samples tested with and without embedded sphere electrode are shown in Table 6.16. Statistical analysis of experimental data shows a good fit with Weibull distribution. The correlation coefficient r of all data sets was greater than 0.92 [138].

Table 6.16: The estimated Weibull parameters for the E_b test results of the silicone samples with and without embedded sphere electrode

Type of silicone rubbers	Type of test specimens	Sample size n	90 % confidence intervals of the Weibull parameters						Correlation coefficient r
			Scale α, in kV/mm			Shape β			
			α_{lower}	α	α_{upper}	β_{lower}	β	β_{upper}	
ESA 7250	**Silicone sheet**	10	28.91	**29.27**	29.58	32.50	**47.23**	81.60	**0.926**
	Embedded	10	37.27	**38.30**	39.31	13.93	**22.14**	34.97	**0.977**
LSR 7665	**Silicone sheet**	10	27.86	**28.11**	28.28	50.30	**61.15**	126.28	**0.925**
	Embedded	10	34.89	**35.30**	35.68	33.09	**50.17**	83.08	**0.967**
LSR 3003/30	**Silicone sheet**	10	24.00	**24.53**	25.02	17.88	**26.73**	44.89	**0.982**
	Embedded	10	40.46	**41.52**	42.49	15.25	**23.14**	38.28	**0.966**

The apparent discrepancy between the two different testing methods is due to the fact that the specimens with embedded ball electrode have more completed insulation between the testing electrode and the grounding electrode, which is completed by the embedding silicone material. There is no material interface at the junction so that losses due to interface states can be avoided, resulting in higher breakdown voltage. This means that the silicone specimens can be able to withstand higher electric stress under the same thickness condition. However, the critical E_b values obtained by, both, different testing methods for the same silicone material do not differ by more than 100 % or by many times. The lower E_b value obtained from testing with using silicone rubber sheet gives sufficient information for safety margin in designing of complex insulations. Therefore, this investigation confirmed that the E_b measurements using a silicone rubber sheet provide the fundamental quantity E_b results with economic experiments. Such method is appropriate for efficient routine tests in material research laboratories.

In addition, presently, manufacturers of polymer-based electrical insulation materials are increasingly asked for assurance of product lifetime, which cannot be easily inspected. The use of silicone rubber in long-term or critical applications requires a far better understanding of the failure mechanisms and the use of accelerated ageing conditions in order to enable reliable lifetime predictions. Thermal degradation refers to the chemical and physical processes in silicone polymers that occur at elevated temperatures. The induction period of the degradation process can normally be regarded as the serviceable lifetime of the polymer. Hence, dielectric strength behaviour of silicone rubbers after thermo-cycling aging should additionally be investigated in further research. The embedded ball electrode

specimen is a greatly appropriate test cell to simulate the effect of a thermally-accelerated aging in silicone rubber which is not yet investigated in this work.

Finally, this research work will be useful for future revision of a standard test method for the determination of AC dielectric strength of elastomeric materials.

7 Conclusions

Modern rubber stress cones of HV cable accessories use transparent silicone insulating materials. To monitor such accessories with an integrated optical PD detection system, it is necessary to examine the important properties of such materials. Unfortunately, IEC standard 60243-1 does not define a specific method for short-term dielectric breakdown tests of silicone rubbers, and current approaches do not provide the solution to meet the challenges of those requirements as described in chapter 4. Therefore an efficient methodology to investigate dielectric strength of elastomeric materials was developed. Following, the important outcomes of this research work are summarised.

7.1 A novel methodology for dielectric breakdown test of silicone rubbers

The main contribution of the developed novel methodology is the efficient test facility that allows easily preparing and handling a silicone-sheet specimen. It is greatly satisfactory to meet both technical and economic demands. With this test methodology, various advantages could be achieved:

- This method enables investigations of a high-viscosity liquid silicone rubber, which was not yet possible by traditional approaches.
- Only one silicone sheet specimen is needed for one breakdown test series; large number of breakdown data points can be recorded as well as the effect of unknown parameters or defects resulting from the specimen preparation process can be limited.
- This low-cost and time-saving experimental method provides E_b values for silicone polymers with low uncertainty.
- This methodology can be applied for high-temperature cured (HTV) silicone rubbers; the degree of cross-linking can be controlled.
- The quality of test specimens and electrode parameters can be optimised; statistical significance of the test results can be enhanced; a reasonable reproducibility of measurements could be achieved.
- The test method allows estimating the influence of any modifications of such silicone elastomers onto their E_b behaviour.
- This facility enables efficient routine tests in materials research laboratories.

The reliability of measurements was examined by using different sample sizes. Sixty breakdown data points ($n = 60$) and ten breakdown data points ($n = 10$) were applied. The experimental results were very well fitted on the basis of 2-parameter Weibull distribution function. The results confirmed that the developed methodology provides a reliable result for a small sample size. Ten breakdown data points are adequate for every test series in order to obtain a sufficient statistic result. However, when experiments are made for purposes other than routine test, larger numbers of breakdown tests will be necessary depending on the variability of the polymeric materials and the statistical analysis to be applied.

Based on the experimental results, some recommendations could be made below for the improvement of a standard test method in the future.

- The dielectric strength of silicone rubbers is dependent upon the thickness of test specimens even in the range of small thickness (less than 1.0 mm). It is meaningless to report dielectric strength data for an elastomeric material without stating the thickness of the test specimen used. These results agree with the known "*size effect*" and it must be taken into account in designing a real insulation system.

- For AC 50 Hz, the modes of increase of voltage have an effect to the breakdown voltage of the specimen under test. The E_b result obtained from 60 s step-by-step test procedure was lower than that from the rapid-rise test methods. Such breakdown value could be considered for safety margin in designing of a complex insulation system. Hence, the 60 s step-by-step test would be a reasonable method for determination of E_b performance of silicone rubbers.

- In case of rapid-rise test procedures, the result obtained from this method may give an indication as to the suitability of the insulating material. To compare such a performance of different types of elastomeric material, the criterion for time limitation of breakdown mechanism must be defined in order to avoid a problem due to a large tolerance range and a less accuracy of the test results. It was found that the time range of 10 s to 20 s is also suitable as a limitation of breakdown criterion in silicone rubbers. So in order to get consistent results, a rate of voltage rise (e.g. 500 V/s, 1 kV/s, 2 kV/s) shall be selected for the sample material under test to achieve the occurrence of breakdown in test specimens within the time range of 10 s to 20 s.

The results will be useful for future revision of IEC standard 60243-1, especially the chapter dealing with the determination of AC dielectric strength of silicone rubbers.

7.2 Mechanical properties and dielectric strength behaviour of optically compatible silicone rubbers

7.2.1 Mechanical properties

Based on the experimental results and discussions described in chapter 6.1, the virgin translucent LSR 3003/30 silicone rubber provides an excellent stress-strain characteristic close to those for the electrical grade PowerSil 600 silicone. They have a large elastic region with an acceptable plastic deformation (Figure 7.1). Therefore, from an engineering point of view, the translucent silicone rubber has good mechanical properties, which are sufficiently good for use as a rubber stress cone of HV/EHV cable accessories. Unfortunately, its optical transmittance is poor compared to optically clear transparent silicone rubbers.

Nevertheless the transparent silicone rubbers are different: the transparent LSR 7665 shows an *S*-shaped curve with 2 yield points while the transparent ESA 7250 shows a *J*-shaped curve. The mechanical properties of virgin transparent silicone rubbers do not comply with those demanded from push-on stress cones. In particular, their elongation at break is considered too low for that application. Hence, the elongation at break of virgin transparent silicone rubbers must be improved before they can be used as insulating material for a rubber stress cone of power cable accessories. However, the elastic region of the virgin LSR 7665 is

limited to small strain (Figure 7.1). In the context of material behaviour, during loading/unloading, their deformation is irreversible. Therefore it is difficult to improve the elongation at break value of such silicone rubber while maintaining its transparency. On the other hand, in case of the virgin ESA 7250, there has little change in shape for a small load, until a certain force is applied. Hence it will be possible to improve the elongation at break value of this silicone rubber by modification of its polymer matrices using silica-based nanofillers surface treatment in conjunction with a covalent bonding technique as mentioned in chapter 2.

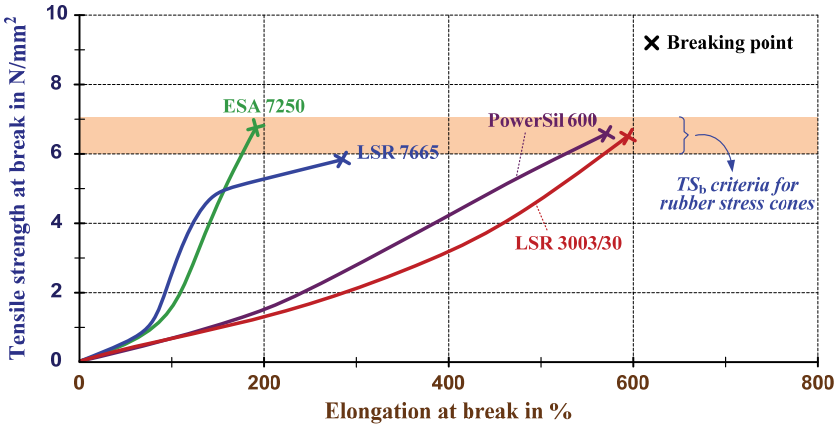

Figure 7.1: Definition of breaking point in stress-strain characteristics of the optically compatible silicone rubbers compared to the electrical grade silicone rubber, according to results shown in Figure 6.14

When optically compatible silicone rubbers are to be modified and used as optical sensor element and as elastomeric insulation material, it is important to define the appropriate curing condition for each silicone type. Mechanical investigations revealed that the post-curing procedure does not provide a positive impact on their elongation ability. Therefore, the reasonable curing condition for each elastomer should be based on their normal curing condition as discussed in chapter 6.1.4. Manufacturers of a modern rubber stress cone of HV/EHV cable accessories should take that into account when using such silicone rubbers as a basic material for the fabrication of a fluorescent silicone optical fibre as well as a new transparency dielectric elastomer.

7.2.2 AC 50 Hz dielectric strength behaviour

Based on the experimental results and discussions described in chapter 6.2, it is worth noting that all measured E_b values are slightly higher than the values given in the technical data sheets. The translucent silicone rubber was provided the lowest breakdown strength compared to the others. On the other hand, the transparent types that have a poor elongation at break value offered the better dielectric strength value. However, all of them have a sufficient E_b performance that can be used as insulating material for a rubber stress cone of HV cable accessories.

The effect of applied mechanical tensile stress on the E_b behaviour of the virgin translucent silicone rubber has been investigated. The results illustrated that E_b values of such

silicone rubber tend to increase slightly with increasing applied extension. This is due to the reduction of the thickness of the silicone rubber sheet caused by applied tensile stress. It could clearly be seen that mechanical tensile stress does not negatively influence on the dielectric strength of silicone rubber. Silicone rubber can be well operated under combined electrical and mechanical stresses.

An inspection of a breakdown point on the silicone rubber sheets revealed mostly a carbonized channel uniting at that point. It seems that the breakdown process depends on the energy localized in a breakdown initiation point and on the morphological properties of the silicone polymer in the neighbourhood of the deterioration source. Such a property naturally depends on the elastomer formulation such as the type of chemical reactions for the cross-linking process, the nature of fillers incorporated and the possible presence of catalysts. Therefore, such an investigated silicone rubbers provide a different dielectric breakdown performance.

Dielectric strength behaviour of the fluorescent silicone rubbers has been examined. The translucent silicone polymer modified with different commercially available dyes by 0.02 wt. % (200 ppm) shows the same breakdown strength as the undoped virgin polymer within the statistical 90 % confidence intervals (Figure 6.27 and Figure 6.28). Hence fluorescent dyes do not seem to negatively influence the dielectric strength of silicone rubber. It is possible to apply such a modified silicone polymer in a region of moderate to high electric field stress near the critical interface area of HV cable accessories. So the optically compatible silicone rubber is perfectly suitable for the fabrication of a novel fluorescent silicone optical fibre. Such a new fibre is compatible for integration into a rubber stress cone of HV cable accessories.

7.3 Observations

From the fabrication of a new fluorescent silicone rubber, it was experienced that the fluorescent dyes in silicone polymer are not stable, particularly at elevated temperatures. Colour bleeding is an unacceptable phenomenon for the optical sensing element that has to have the expected long lifetime (25 years or more). To prevent dye migration, our new strategy is to covalently link the dye to the siloxane network by taking advantage of the cross-coupling reaction during the curing process of the siloxane network. Therefore fluorescent dyes need to be synthesized carrying reactive groups to functionalize the siloxane polymer matrix.

An additional way to improve the level of PD light detection further is improvement of the transparency of a rubber stress cone of HV/EHV cable accessories. To enhance the transparency further, one possibility is to use hydrophobic nanoparticles as fillers. These fillers must be smaller than the wavelength of the visible light and reduce the proportion of the light being scattered at the interface of particle and polymer matrix. Thus, dielectric strength behaviour of the modified silicone polymers needs to be investigated.

References

[1] T. Kubota, Y. Takahashi, S. Sakuma, M. Watanabe, M. Kanaoka and H. Yamanouchi, "*Development of 500-kV XLPE cables and accessories for long distance underground transmission line. Part 1. Insulation design of cables*", IEEE Transactions on Power Delivery, Vol. 9, pp. 1738-1749, October 1994.

[2] T. Kubota, Y. Takahashi, T. Hasegawa, H. Noda, M. Yamaguchi, and M. Tan, "*Development of 500-kV XLPE cables and accessories for long distance underground transmission lines-Part II: jointing techniques*", IEEE Transactions on Power Delivery, Vol. 9, No. 4, pp. 1750-1759, October 1994.

[3] T. Tanaka, T. Okamoto, N. Hozumi, and K. Suzuki, "*Interfacial Improvement of XLPE Cable Insulation at Reduced Thickness*", IEEE Transactions on Dielectrics and Electrical Insulation, Vol. 3, No. 3, pp. 345-350, June 2996.

[4] K. Uchida, S. Kobayashi, T. Kawashima, H. Tanaka, S. Sakuma, K. Hirotsu and H. Inoue, "*Study on detection for the defects of XLPE cable lines*", IEEE Transactions on Power Delivery, Vol. 11, No. 2, pp. 663-668, April 1996.

[5] R. Ross, "*Dealing with Interface Problems in Polymer Cable Terminations*", IEEE - Electrical Insulation Magazine, Vol. 15, No. 4, pp. 5-9, July/August 1999.

[6] T.R. Blackburn, R.E. James, B.T. Phung and Z. Liu, "*Partial discharge characteristics in polymeric cable accessories*", International Symposium on Electrical Insulating Materials (ISEIM 2001), pp. 532-535, 2001.

[7] P.N. Bosworth and H.K. Farr, "*Cable Accessory Design Utilizing New Laboratory Techniques*", Transactions of the American Institute of Electrical Engineers, Vol. 68, No. 2, pp. 1268-1274, July 1949.

[8] B.J. Harrison, "*Cable accessories. Accessory failures*", IEE Colloquium on Ensuring the Reliability of 11-132 kV Cable Accessories, pp. 7/1 - 7/6, 1998.

[9] F.J. Wester, "*Condition Assessment of Power Cables Using PD Diagnosis at Damped AC Voltages*", Ph.D. thesis, ISBN 90-8559-019-1, TU Delft, Nederland, 2004.

[10] C.Q. Su, "*Case study: lessons learned from the failure of a new 230-kV transformer-cable termination*", Electrical Insulation Magazine, IEEE-DEIS, Vol. 26, No. 1, pp. 15-19, Jan/Feb 2010.

[11] Chengwei Chen, Gang Liu, Guojun Lu, Wang Jin, "*Influence of cable terminal stress cone install incorrectly*", IEEE 9th International Conference on the Properties and Applications of Dielectric Materials (ICPADM 2009), pp. 63-65, 2009.

[12] Chang-Hsing Lee, Lin Yu-Chih, Min-Yen Chiu, Huang Chih-Hsien, Shih-Shong Yen and Chiang Haeng, "*Recognition of partial discharge defects in cable terminations*", International Conference on Condition Monitoring and Diagnosis, Beijing, China, pp. 1242-1245, April 21-24, 2008.

[13] Yuao Jiang, Peng Liu, Zongren Peng and Naikui Gao, "*Electric Field Calculation of 500 kV Cable Terminal and Structural Optimization of Stress Cone*", 8th International Conference on Properties and applications of Dielectric Materials, pp. 836-839, 2006.

[14] D. Weida et al., "*Design of ZnO Microvaristor Material Stress-cone For Cable Accessories*", IEEE Transactions on Dielectrics and Electrical Insulation, Vol. 18, No. 4, pp. 1262-1267, August 2011.

[15] W.R. Habel, U. Buchholz, G. Heidmann, M. Hoehse and C. Lothongkam, "*Fibre-optic Sensors for Early Damage Detection in Plastic Insulations of High Voltage Facilities*", 17th International Symposium on High Voltage Engineering, Hannover, Germany, August, 2011.

[16] M. Habel, K. Vaterrodt, G. Heidmann, W. Habel, R. Vogelsang, W. Weissenberg, O. Sekula, D. Pepper and R. Plath. "*Optical PD Detection in Stress Cones of HV Cable Accessories*", 8th International conference on insulated power Cables, Versailles, France, Paper B 8.4, June 2011.

[17] P. Rohwetter, T. Kielau, C. Lothongkam, G. Heidmann and W. Habel, "*All fibre-optic simultaneous detection of optical and acoustic emission from partial discharges in silicone elastomer*", 22nd International Conference on Optical Fiber Sensors (OFS-22), Beijing, China, October 2012.

[18] P. Rohwetter, C. Lothongkam, D. Siebler and W. R. Habel, "*Fibre optic sensors for the detection of partial discharge in high voltage facilities and equipment*", VDE (ETG) 2012.

[19] T. Onodi, M.G. Danikas and A.M. Bruning, "*A study of factors affecting the breakdown strength of silicone rubber*", Annual Report - Conference on Electrical Insulation and Dielectric Phenomena, pp. 811-816, 1992.

[20] J. Österheld, "*The Dielectric Behaviour of Silicone Elastomer Insulation under High Electrical Field Strength*", PhD thesis, ISBN 3-18-319621-2, TU-Dresden, 1995 (in German)

[21] M.G. Danikas, "*On the breakdown strength of silicone rubber*", IEEE Transactions on Dielectrics and Electrical Insulation, Vol. 1, No. 6, pp. 1196-1200, December 1994.

[22] H. Winter, J. Lambrecht and R. Bärsch, "*On the measurement of the dielectric strength of silicone elastomers*", 45th International Universities Power Engineering Conference (UPEC), pp. 1-5, August/September 2010.

[23] E. Kuffel, W.S. Zaengl and J. Kuffel, "*High Voltage Engineering Fundamental*", 2nd edition, ISBN 0 7506 3634 3, Butterworth-Heinemann, Oxford, 2000.

[24] IEC 60243-1, "*Electrical strength of insulating materials - Test methods - Part 1: Tests at power frequencies*", 3rd edition, International Electrotechnical Commission (IEC), Geneva, 2013.

[25] C. Lothongkam, W. R. Habel, G. Heidmann and E. Gockenbach, "*Development of A New Methodology to Measure Dielectric Strength of Elastomeric Materials*", 18th International Symposium on High Voltage Engineering, Hanyang University, Seoul, Republic of Korea, August 2013.

[26] *Silicone rubber*, http://en.wikipedia.org/wiki/Silicone_rubber

[27] J.H. Davis and D.E.W. Rees, "*Silicone rubbers: their present place in electrical insulation*", Proceedings of the Institution of Electrical Engineers, Vol. 112, No. 8, pp. 1607-1613, August 1965.

[28] Wacker Chemie AG, "*Solid and Liquid Silicone Rubber - Material and Processing Guidelines*", Wacker technical brochure, 2011, http://www.wacker.com

[29] Shin-Etsu Chemical, "*Characteristic properties of Silicone Cone Rubber Compounds*", Shin-Etsu Silicone brochure, Tokyo, Japan, 2012, http://www.silicone.jp

[30] P. Jerschow, "*Silicone Elastomers*", Rapra review report 137, ISBN 1-85957-297-9, Vol. 12, November 2001.

[31] Cai Dengke, Yu Jian Hui, Wen Xishan and Lan Lei1, "*Research on characterization of RTV silicone rubber/LS(layered silicate) electrical insulation nanocomposites*", International Conference on Solid Dielectrics, Toulouse, France, Vol. 2, pp. 796-799, July 2004.

[32] L.H. Meyer, S.H. Jayaram, and E.A. Cherney, "*The Role of Inorganic Fillers in Silicone Rubber for Outdoor Insulation Alumina Tri-Hydrate or Silica*", IEEE Electrical Insulation Magazine, Vol. 20, No.4, pp. 13-21, Jul-Aug 2004.

[33] A.H. El-Hag, S.H. Jayaram and E.A. Cherney, "*Comparison between silicone rubber containing micro- and nano- size silica fillers*", Annual Report Conference on Electrical Insulation and Dielectric Phenomena, Boulder, pp. 385-388, October 2004.

[34] E.A. Cherney, "*Silicone Rubber Dielectrics Modified by Inorganic Fillers for Outdoor High Voltage Insulation Applications*", Conference on Electrical Insulation and Dielectric Phenomena, Nashville, pp.1-9, Oct 2005.

[35] N. Andrés Pérez, A. Sylvestre, J.L. Augé, M.T. Do and S. Rowe, "*Dielectric spectroscopy in Silicone Rubber Incorporating Nanofillers*", Annual Report Conference on Electrical Insulation and Dielectric Phenomena, Kansas City, pp. 453-456, October 2006.

[36] A.H. El-Hag, L.C. Simon, S.H. Jayaram, and E.A. Cherney, "*Erosion resistance of nano-filled silicone rubber*", IEEE Transactions on Dielectrics and Electrical Insulation, Vol. 13, No. 1, pp. 122-128, February 2006.

[37] I. Ramirez et al, "*Nanofilled Silicone Dielectrics Prepared with Surfactant for Outdoor Insulation Applications*", IEEE Transactions on Dielectrics and Electrical Insulation, Vol. 15, No. 1, pp. 228-235, February 2008.

[38] S. Raetzke and J. Kindersberger, "*Role of interphase on the resistance to high-voltage arcing, on tracking and erosion of silicone/SiO_2 nanocomposites*", IEEE Transactions on Dielectrics and Electrical Insulation, Vol. 17, No. 2, pp. 607-614, April 2010.

[39] F. Madidi, G.Momen and M. Farzaneh, "*Effect of filler concentration on dielectric properties of RTV silicone rubber / TiO_2 nanocomposite*", Electrical Insulation Conference, Ottawa, Ontario, Canada, pp. 273-275, June 2013.

[40] G. Momen and M. Farzaneh, "*Survey of micro/nano filler use to improve silicone rubber for outdoor insulators*", Reviews on advanced materials science, Vol. 27, No. 1, pp. 1-13, 2011.

[41] J.F. Dexter and P.C. Servais, "*Silicone rubber as cable insulation*", Dow Corning Corporation, Midland, Michigan, USA, 1953.

[42] T.J. Lewis, ‘‘*Nanometric Dielectrics*’’, IEEE Transactions on Dielectrics and Electrical Insulation, Vol. 1, No. 5, pp. 812-825, October 1994.

[43] K.S. Zhao and K.J. He, “*Dielectric relaxation of suspensions of nanoscale particles surrounded by a thick electric double layer*”, Physical Review B: condensed matter and materials physics, Vol. 74, pp. 205319-1-205319-10, November 2006.

[44] P. Kim, N. M. Doss, J.P. Tillotson, P.J. Hotchkiss, M.J. Pan, S.R. Marder, J.Y. Li, J.P. Calame and J.W. Perrty, “*High energy density nanocomposites based on surface-modified $BaTiO_3$ and a ferroelectric polymer*”, Journal of the American Chemical Society - Nano, Vol. 3, pp. 2581-2592, 2009.

[45] L. Chen and G.H. Chen, “*Relaxation behavior study of silicone rubber crosslinked network under static and dynamic compression by electric response*”, Polymer Composite, Vol. 30, pp. 101-106, 2009.

[46] H. Tan and W. Yang, “*Toughening mechanisms of nano-composite ceramics”,* Mechanics of Materials, Vol. 30, pp. 111-123, 1998.

[47] H. Awaji, Y. Nishimura, S.M. Choi, Y. Takahashi, T. Goto and S. Hashimoto, “*Toughening mechanism and frontal process zone size of ceramics*”, Journal of Ceramic Soc. of Japan, Vol. 117, pp. 623-629, 2009.

[48] G.X. Zeng, H.Y. Zhang, L.C. Hu and Y.M. Chen, “*Research on complex permittivity spectrum and microwave absorption of anti-infrared $In(Sn)_2O_3$(ITO) painting*”, Journal of Aeronautical Materials, Vol. 28, pp. 87-90, 2008.

[49] M.Z. Rong, M.Q. Zhang and W.H. Ruan, “*Surface modification of nanoscale fillers for improving properties of polymer nanocomposites: a review*”, Materials Science and Technology, Vol. 22, pp. 787-796, July 2006.

[50] C. Calebrese, L. Hui, L.S. Schadler and J.K. Nelson, “*A Review on the Importance of Nanocomposite Processing to Enhance Electrical Insulation*”, IEEE Transactions on Dielectrics and Electrical Insulation, Vol. 18, No. 4, pp. 938-945, August 2011.

[51] Lijin Xia, Zhonghua Xu, Leming Sun, P.M. Caveney and Mingjun Zhang, “*Nano-fillers to tune Young’s modulus of silicone matrix*”, Journal of Nanoparticle Research, Vol. 15, No. 4, Article: 1570, April 2013.

[52] Y. Cao, P.C. Irwin, and K. Younsi, “*The future of nanodielectrics in the electrical power industry*”, IEEE Transactions on Dielectrics and Electrical Insulation, Vol. 11, No. 5, pp. 797-807, October 2004.

[53] F.P. Espino-Cortes, S. Jayaram and E.A. Cherney, “*Stress grading materials for cable terminations under fast rise time pulses*”, IEEE Transactions on Dielectrics and Electrical Insulation, Vol. 13, No. 2, pp. 430-435, April 2006.

[54] E.G. Rochow, “*Silicon and Silicones*”, Springer-Verlag: Berlin, Heidelberg, New York, 1987.

[55] W. Noll “*Chemistry and Technology of Silicones*”, Academic Press, New York, 1968.

[56] T.L. Cottrell, “*The Strengths of Chemical Bonds*”, 2nd edition, Butterworths, London, 1958.

[57] J.L. Goudie, M.J. Owen and T. Orbeck, "*A review of possible degradation mechanisms of silicone elastomers in high voltage insulation applications*", Annual Report Conference on Electrical Insulation and Dielectric Phenomena, Vol. 1, pp. 120-127, 1998.

[58] M. Andriot *et al.*, "*Silicones in Industrial Applications*", Dow Corning Corporation, Midland, Michigan, USA, 2007. [Originally released in 2007 as a chapter in "Inorganic Polymers", an advanced research book by Nova Science Publishers]

[59] E.B. Baker, A.J. Barry and M.J. Hunter, "*Dielectric constants of dimethyl siloxane polymers*", Industrial Engineering Chemistry, Vol. 39, No. 11, pp. 1117-1120, 1946.

[60] Wacker Chemie AG, "*Silicone for the electronics industry*", Wacker technical brochure, 2006. http://www.wacker.com

[61] C. Johansson and M. Robertsson, "*Broadband Dielectric Characterization of a Silicone Elastomer*", Journal of Electronics Materials, Vol. 36, No. 9, 2007.

[62] R.R. Buch, "*Rates of heat release and related fire parameters for silicones*", Fire Safety Journal, Vol. 17, No. 1, pp.1-12, 1991.

[63] F.Y. Hsieh and R.R. Buch, "*Controlled atmosphere cone calorimeter studies of silicones*", Fire and Materials, vol. 21, No. 6, pp. 265-270, November/December 1997.

[64] A. Bacher, "*Silicone Rubber used for Fire Safety and Fire Retardant Cables*", 45th International Universities Power Engineering Conference (UPEC), pp. 1-2, 2010.

[65] Wacker Chemie AG, "*Silicone Solutions for the Transmission and Distribution Technology*", Wacker technical brochure, 2009, http://www.wacker.com.

[66] IEC 60587, "*Electrical insulating materials used under severe ambient conditions – Test methods for evaluating resistance to tracking and erosion*", International Electrotechnical Commission (IEC), 3rd Edition, Geneva, May 2007.

[67] S. Behrend, W. Kalkner, G. Heidmann, H. Emanuel and R. Plath, "*Synchronous optical and electrical PD measurements*", 17th International Symposium on High Voltage Engineering (ISH 2011), Leibniz University of Hannover, Germany, pp. 1027-1032, August 2011.

[68] W.R. Habel and G. Heidmann, "*Chapter 24: Electric Power Stations and Transmission Networks*", Handbook of Technical Diagnostics (Editor by H. Czichos), ISBN 978-3-642-25849-7, Springer-Verlag Berlin Heidelberg, pp. 471-504, 2013.

[69] D. Siebler, C. Lothongkam, P. Rohwetter, W. Habel and G. Heidmann, "*Fluorescent Fibre Optical Partial Discharge Sensor in High Voltage Cable Facilities*", 22nd International Conference on Plastic Optical Fibers - POF2013, Buzios, Rio de Janeio, Brasil, September 2013.

[70] IEC 60052, "*Voltage measurement by means of standard air gaps*", Third edition, International Electrotechnical Commission (IEC), Geneva, 2002.

[71] F.F. Dall'Agnol and V.P. Mammana, "*Solution for the electric potential distribution produced by sphere-plane electrodes using the method of images*", Revista Brasileira de Ensino de Fisica, Vol. 31, No. 3, Article No. 3503, September 2009.

[72] M.A. Shallal and J.A. Harrison, "*Electric, field potential and capacitance of a sphere-plane electrode system*", Proceedings of The Institution of Electrical Engineers, Vol. 116, No. 6, pp. 1115-1118, June 1969.

[73] M.S. Naidu and V. Kamaraju, "*High Voltage Engineering*", Second Edition, ISBN 0-07-462286-2, McGraw-Hill Publishing Co., Ltd., 1996.

[74] C.L. Wadhwa, "*High Voltage Engineering*", Second Edition, New Age International (P) Ltd., Publishers, New Delhi, 2007.

[75] J.J. O'Dwyer, "*The Theory of Electrical Conduction and Breakdown in Solid Dielectrics*", Clarendon Press, Oxford, 1973.

[76] H. Fröhlich and B.V. Paranjape, "*Dielectric Breakdown in Solids*", Proceedings of the Physical Society, Section B, Vol. 69, No. 1, p. 21, January 1956.

[77] V.A. Zakrevskii, N.T. Sudar, A. Zaopo and Yu. A. Dubitskya, "*Mechanism of electrical degradation and breakdown of insulating polymers*", Journal of applied physics, Vol. 93, No. 4, pp. 2135-2139, February 2003.

[78] L.A. Dissado and J.C. Fothergill, "*Electrical degradation and breakdown in polymers*", IEE materials and devices series 9, Peter Peregrinus Ltd, London, UK, 1992.

[79] J. Artbauer, "*Electrical strength of polymers*", Journal of Physics D: Applied Physics, Vol. 29, pp. 446-456, 1996.

[80] K.C. Kao, "*New theory of electric discharge and breakdown in low-mobility condensed insulator*", Journal of Applied Physics, Vol. 55, No. 3, pp. 752-755, 1984.

[81] T. Lebey and C. Laurent, "*Charge injection and electroluminescence as a prelude to dielectric breakdown*", Journal of Applied Physics, Vol. 68, No. 1, pp. 275-282, July 1990.

[82] D. Liufu, X.S. Wang, D.M. Tu and K.C. Kao, "*High-field induced electrical aging in polypropylene films*", Journal of Applied Physics, Vol. 83, No. 4, pp. 2209-2214, February 1998.

[83] N. Shimizu, H. Katsukawa, M. Miyauchi, M. Kosaki, and K. Hirii, "*The Space Charge Behavior and Luminescence Phenomena in Polymers at 77 K*", IEEE Transactions on Electrical Insulation, Vol. 14, No. 5, pp. 256-263, October 1979.

[84] G. Mazzanti and G. C. Montanari, "*Electrical aging and life models: the role of space charge*", IEEE Transactions on Dielectrics and Electrical Insulation, Vol. 12, No. 5, pp. 876-890, 2005.

[85] W.K. Lee, "*A study of electric stress enhancement: Part 1 - Implication in power cable design*", IEEE transactions on dielectrics and electrical insulation, Vol. 11, No. 6, pp. 976-982, 2004.

[86] K. Wu and L.A. Dissado, "*Model for electrical tree initiation in epoxy resin*", IEEE Transactions on Dielectrics and Electrical Insulation, Vol. 12, No. 4, pp. 655-668, 2005.

[87] S.S. Bamji, A.T. Bulinski, and R.J. Densley, "*Degradation of polymeric insulation due to photoemission caused by high electric field*", IEEE Transactions on Electrical Insulation, Vol. 24, No. 1, pp. 91-98, 1989.

[88] R. Vofelsang, B. Fruth, T. Farr, and K. Fröhlich, "*Detection of electrical tree propagation by partial discharge measurements*", European Transactions on Electrical Power, Vol. 15, pp. 271-284, 2005.

[89] H.J. Wiesmann and H.R. Zeller, "*A fractal model of dielectric breakdown and prebreakdown in solid dielectrics*", Journal of Applied Physics, Vol. 60, pp. 1770-1773, 1983.

[90] M.D. Noskov, V.R. Kukhta, and V.V. Lopatin, "*Simulation of the electrical discharge development in inhomogeneous insulators*", Journal of Physics D: Applied Physics, Vol. 28, pp. 1187-1194, 1995.

[91] L.A. Dissado and P.J.J. Sweeney, "*Physical model for breakdown structures in solid dielectrics*", Physical Review B: condensed matter and materials physics, Vol. 48, pp. 16261-16268, December 1993.

[92] L.A. Dissado, "*Fractal processes and Weibull statistics*", Proceedings of the 3rd International Conference on Conduction and Breakdown in Solid Dielectrics (ICSD), pp. 528-532, July 1989.

[93] H.Z. Ding and X.S. Xing, "*A kinetic model of time-dependent dielectric breakdown for polymers*", Journal of Physics D: Applied Physics, Vol. 27, pp. 591-595, 1994.

[94] N. Shimizu, H. Katsukawa, M. Miyauchi and M. Kosaki, "*The Space Charge Behavior and Luminescence Phenomena in Polymers at 77 K*", IEEE Transactions on Electrical Insulation, Vol. 14, No. 5, pp. 256-263, 1979.

[95] I. Kitani, T. Hirano and K. Arii, "*Very Faint Light Emission in LDPE Films under dc Field*", Journal of Applied Physics, Vol. 26, pp. 639-640, 1987.

[96] J. Jonsson, B. Ranby, D. Mary, C. Laurent and C. Mayoux, "*Electroluminescence from Polyolefins Subjected to a Homogeneous AC Field*", IEEE transactions on dielectrics and electrical insulation, Vol. 2, pp. 107-113, 1995.

[97] S.S. Bamji, A.T. Bulinski, H. Suzuki, M. Matsuki and Z. Iwata, "*Light and Tree Inception Characteristics of XLPE at Elevated Temperatures*", IEEE Conf. Electr. Insul. Dielectr. Phenomena (CEIDP), Pocono Manor, Pa, USA, pp. 688-694, 1993.

[98] A. Ishibashi, T. Kawai, S. Nakagawa, H. Muto, S. Katakai, K. Hirotsu and T. Nakatsuka, "*A Study of Treeing Phenomena in the Development of Insulation for 500 kV XLPE cables*", IEEE Trans. Dielectr. Electr. Insul., Vol. 5, pp. 695-712, 1998.

[99] K. Tohyama, S.S. Bamji and A.T. Bulinski, "*Spectra of EL in XLPE due to Impulse Voltage*", IEEE Conf. Electr. Insul. Dielectr. Phenomena (CEIDP), Atlanta, Georgia, USA, pp. 601-604, 1998.

[100] G. Teyssedre, G. Tardieu, D. Mary and C. Laurent, "*AC and DC Electroluminescence in Insulating Polymers and Implication for Electrical Aging*", Journal of Physics D: Applied Physics, Vol. 34, pp. 2220-2229, 2001.

[101] S.S. Bamji and A.T. Bulinski, "*Luminescence in XLPE of HV cables*", IEEE International Conference on Properties and Applications of Dielectric Materials (ICPADM), Seoul, Korea, pp. 11-15, 1997.

[102] S.S. Bamji, A.T. Bulinski and M. Abou-Dakka, "*Luminescence and Space Charge in Polymeric Dielectrics*", IEEE Transactions on Dielectrics and Electrical Insulation, Vol. 16, No. 5, pp. 1376-1392, October 2009.

[103] S.S. Bamji, A.T. Bulinski, and R.J. Densley, "*Evidence of near-ultraviolet emission during electrical-tree initiation in polyethylene*", Journal of Applied Physics, Vol. 61, No. 2, pp. 694-699, January 1987.

[104] G. Teyssedre and C. Laurent, "*Charge Transport Modeling in Insulating Polymers: from Molecular to Macroscopic Scale*", IEEE Transactions on Dielectrics and Electrical Insulation, Vol. 12, pp. 857-875, 2005.

[105] G.C. Montanari, C. Laurent, G. Teyssedre, A. Campus and U.H. Nilsson, "*From LDPE to XLPE: Investigating the Change of Electrical Properties – Part I and II*", IEEE Transactions on Dielectrics and Electrical Insulation, Vol. 12, pp. 438-454, 2005.

[106] H.R. Zeller, P. Pfluger and J. Bernasconi, "*High-Mobility States and Dielectric Breakdown in Polymeric Dielectrics*", IEEE Transactions on Electrical Insulation, Vol. EI-19, pp. 200-204, 1984.

[107] K. Wu and L.A. Dissado, "*Percolation model for electrical breakdown in insulating polymers*", Conference on Electrical Insulating and Dielectric Phenomena, pp. 514-518, 17-20 October 2004.

[108] G.C. Stevens, E Perkins, and J.V. Champion, "*Microvoid formation and growth in epoxy resins under mechanical and electrical stress by laser light scattering*", IEEE Conference on Dielectric Materials, pp. 234-237, 1988.

[109] C. Mayoux and C. Laurent, "*Contribution of partial discharge to electrical breakdown of solid insulating materials*", IEEE Transactions on Dielectrics and Electrical Insulation, Vol. 2, pp. 641-652, 1995.

[110] IEC 60270, "*Partial Discharge Measurements*", 3rd edition, March 2001.

[111] CIGRE Working Group D1.02, "*Sensors and Sensing Used For Non-conventional PD Detection*", CIGRE 2006.

[112] M. Muhr, R. Schwarz, S. Pack and B. Koerbler, "*Unconventional partial discharge measurement*", Annual Report Conference on Electrical Insulation and Dielectric Phenomena (CEIDP '04), pp. 430-433, 2004.

[113] R. Schwarz, T. Judendorfer and M. Muhr, "*Review of Partial Discharge Monitoring techniques used in High Voltage Equipment*", Conference on Electrical Insulation and Dielectric Phenomena (CEIDP 2008), pp. 400-403. 2008.

[114] R. Bartnikas, "*Partial discharges: Their mechanism, detection and measurement*", IEEE Transactions on Dielectrics and Electrical Insulation, Vol. 9, No. 5, pp. 763-808, October 2002.

[115] Y. Tian, P.L. Lewin, J.S. Wilkinson, G. Schroeder, S.J. Sutton and S.G. Swingler, "*An Improved Optically Based PD Detection System for Continuous On-line Monitoring of HV Cables*", IEEE Transactions on Dielectrics and Electrical Insulation, Vol. 12, No. 6, pp. 1222-1234, December 2005.

[116] D. Zhu, A.J. McGrail, S. Swinglei, D.W. Auckland and B.R. Varlow, "*Partial Discharge Detection in Cable Termination Using Acoustic Emission Techniques and Adaptive Signal Processing*", IEEE International Symposium on Electrical Insulation, Pittsburgh, USA, pp. 74-76, June 1994.

[117] M. Ekberg, A. Gustafsson, M. Leijon, T. Bengtsson, T. Eriksson, C. Tornkvist, K. Johansson, and L. Ming, "*Recent Results in HV Measurement Techniques*", IEEE Transactions on Dielectrics and Electrical Insulation, Vol. 2, No. 5, pp. 906-914, October 1995.

[118] L.E. Lundgaard and W. Hansen, "*Acoustic method for quality control and in-service periodic monitoring of medium voltage cable terminations*", IEEE International Symposium on Electrical Insulation, Vol. 1, pp. 130-133, June 1998.

[119] R, Cselkó, Z.A. Tamus, A. Szabó, and I. Berta, "*Comparison of acoustic and electrical partial discharge measurements on cable terminations*", IEEE International Symposium on Electrical Insulation (ISEI), pp. 1-5, 2010.

[120] F.H. Kreuger, "*Partial Discharge Detection in High-Voltage Equipment*", ISBN 0-408-02063-6, Butterworth & Co. (Publishers) Ltd, 1989.

[121] CIGRE Working group D1.33, "*Guidelines for Unconventional Partial Discharge Measurements*", Cigre Technical Brochure, DEC, 2010.

[122] A. Reid, M. Judd, B. Stewart and R. Fouracre, "*Comparing IEC60270 and RF partial discharge patterns*", International Conference on Condition Monitoring and Diagnosis 2008 (CMD 2008), pp. 89-92, 2008.

[123] A.J. Reid, M.D. Judd, R.A. Fouracre, B.G. Stewart, and D.M. Hepburn, "*Simultaneous measurement of partial discharges using IEC60270 and radio-frequency techniques*", IEEE Transactions on Dielectrics and Electrical Insulation, Vol. 18, No. 2, pp. 444-455, 2011.

[124] T.W. Dakin, "*Conduction and Polarisation Mechanisms and Trends in Dielectrics*", IEEE Electrical Insulation Magazine, Vol. 22, No. 5, September-October 2006.

[125] C.A. Balanis, "*Advanced engineering electromagnetics*", 2nd edition, John Wiley & Sons, Inc., USA, Copyright © 2012.

[126] J. Krupka, "*Frequency domain complex permittivity measurements at microwave frequencies*", Institute of Physics Publishing, Measurement Science and Technology, Vol. 17, No. 6, R55, 2006.

[127] IEC 60250, "*Recommended methods for the determination of the permittivity and dielectric dissipation factor of electrical insulating materials at power, audio and radio frequencies including metre wavelengths*", First edition, International Electrotechnical Commission (IEC), Geneva, 1996.

[128] ASTM D149, "*Standard Test Method for Dielectric Breakdown Voltage and Dielectric Strength of Solid Electrical Insulating Materials at Commercial Power Frequencies*", An American National Standard, USA, 2009.

[129] J. Lambrecht, "*Accelerating Tests for Insulating Materials in Daily Use at Wacker*", 2. Burghauser Isolierstoff Kolloquium, June 2009, Wacker Chemie AG, 2009. (in German.)

[130] C. Lothongkam, D. Siebler, G. Heidmann, R. Plath and E. Gockenbach, "*The Influence of Thermal Aging on AC Dielectric Strength of Transparent Silicone Rubbers for HV Insulation*", 2014 International Symposium on Electrical Insulating Materials (ISEIM 2014) Toki Messe, Niigata City, Japan, June 2014. (in press)

[131] Bluestar Silicones, "*Technical data sheet for BLUESIL™ ESA 7250 A & B*", Technical Data Sheet No. SIL 11 547 3, December 2011.

[132] Wacker Chemie AG, "*Technical data sheet for ELASTOSIL® LR 7665 A/B*", Version: 1.5, 15 April 2011.

[133] Wacker Chemie AG, "*Technical data sheet for ELASTOSIL® LR 3003/30 A/B*", Version: 1.5, 6 April 2011.

[134] Wacker Chemie AG, "*Technical data sheet for POWERSIL® 600 A/B*", Version: 1.2, 26 July 2010.

[135] IEC 60243-2, "*Electrical strength of insulating materials - Test methods - Part 2: Additional requirements for tests using direct voltage*", 3rd edition, International Electrotechnical Commission (IEC), Geneva, 2013.

[136] G.R. Paranjpe and P.Y. Deshpande, "*Dielectric properties of some vegetable oils*", Proceedings of the Indian Academy of Sciences - Section A, Vol. 1, No. 12, pp. 880-886, June 1935.

[137] W. Weibull, "*A Statistical Distribution Function of Wide Applicability*", J. Appl. Mech., Vol. 18, pp. 293-297, September 1951.

[138] IEC 62539, "*Guide for the statistical analysis of electrical insulation breakdown data*", First edition: 2007-07, International Electrotechnical Commission (IEC), Geneva, 2007.

[139] IEEE Std 930™ - 2004, "*IEEE Guide for the Statistical Analysis of Electrical Insulation Breakdown Data*", IEEE Dielectrics and Electrical Insulation Society, Now York, USA, April 2005.

[140] R.M. Hill and L.A. Dissado, "*Theoretical basis for the statistics of dielectric breakdown*", Journal of Physics C: Solid State Physics, Vol. 16, pp. 2145-2156, 1983.

[141] L.A. Dissado, J.C. Fothergill, S.V. Wolfe and R.M. Hill, "*Weibull Statistics in Dielectric Breakdown; Theoretical Basis, Applications and Implications*", IEEE Transactions on Electrical Insulation, Vol. EI-19, No.3, pp. 227-233, June 1984.

[142] C. Chauvet and C. Laurent, "*Weibull statistics in short-term dielectric breakdown of thin polyethylene films*", IEEE Transactions on Electrical Insulation, Vol. 28, No. 1, pp. 18-29, February 1993.

[143] M. Cacciari, G. Mazzanti and G.C. Montanari, "*Communication: Weibull statistics in short-term dielectric breakdown of thin polyethylene films*", IEEE Transactions on Electrical Insulation, Vol. 1, No. 1, pp. 153-159, February 1994.

[144] C. Chauvet and C. Laurent, "*Discussion: Weibull statistics in short-term dielectric breakdown of thin polyethylene films*", IEEE Transactions on Electrical Insulation, Vol. 1, No. 1, pp. 163, February 1994.

[145] L. Pierrat, G.C. Montanari, G. Mazzanti and M. Cacciari, "*Weibull statistics in short-term dielectric breakdown of thin polyethylene films [comments and reply]*", IEEE Transactions on Dielectrics and Electrical Insulation, Vol. 2, No. 2, pp. 321-326, April 1995.

[146] R. Ross, "*Bias and standard deviation due to Weibull parameter estimation for small data sets*", IEEE Transactions on Dielectrics and Electrical Insulation, Vol. 3, No. 1, pp. 28-42, February 1996.

[147] E.Y. Wu and R.P. Vollertsen, "*On the Weibull Shape Factor of Intrinsic Breakdown of Dielectric Films and Its Accurate Experimental Determination – Part I: Theory, Methodology, Experimental Techniques*", IEEE Transactions on Electron Devices, Vol. 49, No. 12, pp. 2131-2140, December 2002.

[148] E.Y. Wu and R.P. Vollertsen, "*On the Weibull Shape Factor of Intrinsic Breakdown of Dielectric Films and Its Accurate Experimental Determination – Part II: Experimental Results and the Effects of Stress Conditions*", IEEE Transactions on Electron Devices, Vol. 49, No. 12, pp. 2141-2150, December 2002.

[149] D. Fabiani and L. Simoni, "*Discussion on Application of the Weibull Distribution to Electrical Breakdown of Insulating Materials*", IEEE Transactions on Dielectrics and Electrical Insulation, Vol. 12, No. 1, pp. 11-16, February 2005.

[150] T. Tsuboi, J. Takami, S. Okabe, H. Hirose and K. Tsuru, "*Analytical Evaluation of Dielectric Breakdown Test Based on One-minute Step-up Method*", IEEE Transactions on Dielectrics and Electrical Insulation, Vol. 16, No. 5, pp. 1393-1396, October 2009.

[151] L. Li, N. Bowler, P.R. Hondred and M.R. Kessler, "*Statistical Analysis of Electrical Breakdown Behavior of Polyimide Following Degrading Processes*", IEEE Transactions on Dielectrics and Electrical Insulation, Vol. 18, No. 6, pp. 1955-1962, December 2011.

[152] G.C. Montanari, G. Mazzanti, M. Cacciari and J.C. Fothergill, "*In Search of Convenient Techniques for Reducing Bias in the Estimation of Weibull Parameters for Uncensored Tests*", IEEE Transactions on Dielectrics and Electrical Insulation, Vol. 4, No. 3, pp. 306-313, June 1997.

[153] S.J. Laihonen, "*Polypropylene: Morphology, Defects and Electrical Breakdown*", PhD thesis, ISBN-91-7178-091-2, The Royal Institute of Technology, Stockholm, Sweden, 2005.

[154] J. Jacquelin, "*A Reliable Algorithm for the Exact Median Rank Function*", IEEE Trans. EI, Vol. 28, part 2, April 1993 (and Erratum: IEEE Transactions on Electrical Insulation, Vol. 28, Part 5, p. 892, October 1993).

[155] J.C. Fothergill, "*Estimating the Cumulative Probability of Failure Data Points to be Plotted on Weibull and other Probability Paper*", IEEE Transactions on Electrical Insulation, Vol. 25, part 3, pp. 489-492, June 1990.

[156] G.C. Montanari, G. Mazzanti, M. Cacciari and J.C. Fothergill, "*Optimum Estimators for the Weibull Distribution from Censored Test Data: Singly-censored Tests*", IEEE Transactions on Dielectrics and Electrical Insulation, Vol. 4, No. 4, pp. 462-469, August 1997.

[157] G.C. Montanari, G. Mazzanti, M. Cacciari and J.C. Fothergill, "*Optimum Estimators for the Weibull Distribution from Censored Test Data: Progressively-censored Tests*", IEEE Transactions on Dielectrics and Electrical Insulation, Vol. 5, No. 2, pp. 157-164, April 1998.

[158] R. Ross, "*Graphical methods for plotting and evaluating Weibull distributed data*", Proceedings of the IEEE International Conference on Properties and Applications of Dielectric Materials, 1, pp. 250-253, July 1994.

[159] J. Jacquelin, "*Generalization of the Method of Maximum Likelihood*", IEEE Transactions on Electrical Insulation, Vol. 28, part 1, pp. 65-72, February 1993.

[160] J.S. White, "*The Moments of Log-Weibull Order Statistics*", Technometrics, 11(2), pp. 373-386, 1969.

[161] H. Rinne, "*The Weibull Distribution - A Handbook*", ISBN: 978-1-4200-8743-7, Taylor & Francis Group, Florida, USA, 2009.

[162] ISO 37, "*Rubber, vulcanized or thermoplastic – Determination of tensile stress-strain properties*", 5th edition, International Organization for Standardization (ISO), Geneva, Switzerland, 2011.

[163] A.F. Holt, A.C. Topley, R.C.D. Brown, P.L. Lewin, A.S. Vaughan and P. Lang, "*Towards Intelligent Insulation Technologies*", 10th IEEE International Conference on Solid Dielectrics, Potsdam, Germany, pp. 1-4, July 2010.

[164] L. Meyer, S. Jayaram and E.A. Cherney, "*Thermal Conductivity of Filled Silicone Rubber and its Relationship to Erosion Resistance in the Inclined Plane Test*", IEEE Transactions on Dielectrics and Electrical Insulation, Vol. 11, No. 4, pp. 620-630, August 2004.

[165] Qiuhong Mu, Shengyu Feng and Guangzhao Diao, "*Thermal Conductivity of Silicone Rubber Filled With ZnO*", Polymer Composites, Vol. 28, No. 2, pp. 125-130, April 2007.

[166] Wenying Zhou, Caifeng Wang, Qunli An and Haiyan Ou, "*Thermal Properties of Heat Conductive Silicone Rubber Filled with Hybrid Fillers*", Journal of COMPOSITE MATERIALS, Vol. 42, No. 2, pp. 173-187, January 2008.

[167] J.J. O' Dwyer, "*Breakdown in Solid Dielectrics*", IEEE Transactions on Electrical Insulation, Vol. 17, No. 6, pp. 484-487, 1982.

[168] M. Ieda, M. Nagao, and M. Hikita, "*High-field Conduction and Breakdown in Insulating Polymers: Present Situation and Future Prospects*", IEEE Transactions on Dielectrics and Electrical Insulation, Vol. 1, pp. 934-945, 1994.

[169] M. Ieda, "*Dielectric Breakdown Process of Polymers*", IEEE Transactions on Electric Insulation, Vol. 15, pp. 206-224, 1980.

[170] G. Sawa, "*Dielectric Breakdown in Solid Dielectrics*", IEEE Transactions on Electrical Insulation, Vol. EI-21, No. 6, pp. 841-846, December 1986.

[171] S. Ul-Haq and G.R. Govinda Raju, "*Weibull Statistical Analysis of Area Effect on the Breakdown Strength in Polymer Films*", IEEE Conference on Electrical Insulation and Dielectric Phenomena (CEIDP), pp. 518-521, 2002.

[172] P. Bjellheim and B. Helgee, "*AC breakdown strength of aromatic polymers under partial discharge reducing conditions*", IEEE Transactions on Dielectrics and Electrical Insulation, Vol.1, No. 1, pp. 89-96, February 1994.

[173] G. Yilmaz and O. Kalenderli, "*Dielectric behavior and electric strength of polymer films in varying thermal conditions for 5 Hz to 1 MHz frequency range*", Electrical Insulation Conference and Electrical Manufacturing & Coil Winding Conference, pp. 269-271, 1997.

LIST OF PUBLICATIONS 2011-2014:

1. **C. Lothongkam**, P. Rohwetter, W. Habel and E. Gockenbach, "*Dielectric Strength Behavior and Mechanical Properties of Transparent Silicone Rubbers for HV Cable Accessories*", 2014 International Symposium on Electrical Insulating Materials (ISEIM 2014) Toki Messe, Niigata City, Japan, June 2014.

2. **C. Lothongkam**, D. Siebler, G. Heidmann, R. Plath and E. Gockenbach, "*The Influence of Thermal Aging on AC Dielectric Strength of Transparent Silicone Rubbers for HV Insulation*", 2014 International Symposium on Electrical Insulating Materials (ISEIM 2014) Toki Messe, Niigata City, Japan, June 2014.

3. P. Rohwetter, **C. Lothongkam**, W. Habel, G. Heidmann and D. Pepper, "*Improved fibre-optic acoustic sensors for partial discharge in elastomeric insulations*", 23rd International Conference on Optical Fiber Sensors (OFS23), Santander, Spain, June 2014.

4. **C. Lothongkam**, W. R. Habel, G. Heidmann and E. Gockenbach, "*Development of A New Methodology to Measure Dielectric Strength of Elastomeric Materials*", 18th International Symposium on High Voltage Engineering, Hanyang University, Seoul, Republic of Korea, August 2013.

5. D. Siebler, **C. Lothongkam**, P. Rohwetter, W. Habel and G. Heidmann, "*Fluorescent Fibre Optical Partial Discharge Sensor in High Voltage Cable Facilities*", 22nd International Conference on Plastic Optical Fibers - POF2013, Buzios, Rio de Janeio, Brasil, September 2013.

6. P. Rohwetter, T. Kielau, **C. Lothongkam**, G. Heidmann and W. Habel, "*All fibre-optic simultaneous detection of optical and acoustic emission from partial discharges in silicone elastomer*", 22nd International Conference on Optical Fiber Sensors (OFS-22), Beijing, China, October 2012.

7. P. Rohwetter, **C. Lothongkam**, D. Siebler and W. R. Habel, "*Fibre optic sensors for the detection of partial discharge in high voltage facilities and equipment*", VDE-ETG Kongress 2012, Stuttgart, Germany, November 2012.

8. W. R. Habel, U. Buchholz, G. Heidmann, M. Hoehse and **C. Lothongkam**, "*Fibre-optic Sensors for Early Damage Detection in Plastic Insulations of High Voltage Facilities*", 17th International Symposium on High Voltage Engineering, Hannover, Germany, August, 2011.